

Lawrence Berkeley National Laboratory

Recent Work

Title

THEORETICAL STUDIES OF SOME NONLINEAR LASER-PLASMA INTERACTIONS

Permalink

<https://escholarship.org/uc/item/797221gz>

Author

Cohen, Bruce Ira.

Publication Date

1975-08-01

0 0 0 0 4 2 0 3 3 2 5

LBL-3291

c.1

THEORETICAL STUDIES OF SOME NONLINEAR
LASER-PLASMA INTERACTIONS

Bruce Ira Cohen
(Ph.D. thesis)

August 15, 1975

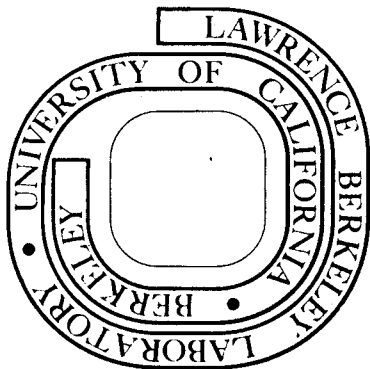
RECEIVED
PHYSICS
BERKELEY LABORATORY

JAN 15 1976

LIBRARY AND
DOCUMENTS SECTION

Prepared for the U.S. Energy Research and
Development Administration under Contract W-7405-ENG-48

For Reference
Not to be taken from this room



LBL-3291
c.1

DISCLAIMER

This document was prepared as an account of work sponsored by the United States Government. While this document is believed to contain correct information, neither the United States Government nor any agency thereof, nor the Regents of the University of California, nor any of their employees, makes any warranty, express or implied, or assumes any legal responsibility for the accuracy, completeness, or usefulness of any information, apparatus, product, or process disclosed, or represents that its use would not infringe privately owned rights. Reference herein to any specific commercial product, process, or service by its trade name, trademark, manufacturer, or otherwise, does not necessarily constitute or imply its endorsement, recommendation, or favoring by the United States Government or any agency thereof, or the Regents of the University of California. The views and opinions of authors expressed herein do not necessarily state or reflect those of the United States Government or any agency thereof or the Regents of the University of California.

THEORETICAL STUDIES OF SOME NONLINEAR LASER-PLASMA INTERACTIONS

Contents

Abstract	vii
Preface	viii
I. Introduction	1
A. Overview of Three-Wave Interactions	1
B. Thesis Synopsis	5
C. Coupling of High Frequency Transverse Waves to Unmagnetized Plasma	10
II. Beat Heating of a Plasma	20
A. Introduction to the Coupling of Transverse Waves to Electron Plasma Waves	20
B. Electromagnetic Simulation Code	24
C. Beat Heating of Opposed Lasers	28
1. Theory of Beat Heating for Small Amplitude Electron Plasma Waves	28
2. Space-time Interaction of Opposed Transverse Waves in a Plasma	40
3. Three-wave Analysis of Beat Heating Coupled Mode Equations	42
4. Introduction to Nonlinear Beat-Wave Effects	48
a. Onset of trapping in beat heating simulations	49
b. Simulations of nonlinear beat heating: electromagnetic code	52
c. Competition of beat heating and beat-wave trapping with other effects	54
d. Motivation for a model problem	58

5.	Resonant Excitation of Nonlinear Plasma Waves	59
a.	Introduction	59
b.	General formulation of the model problem	60
c.	Application to the excitation of electron plasma waves	63
d.	Equilibrium response	65
e.	Energy and momentum conservation laws	66
f.	Stability of equilibria	72
g.	Simulations with constant-amplitude ponderomotive potential	75
6.	Beat Heating with Trapped Electrons	79
a.	General consideration of the coupled mode equations	79
b.	Quasi-steady nonlinear plasma response	81
c.	Simulations with self-consistent ponderomotive potential and coupled mode equations	82
d.	Removal of trapping effects by plasma inhomogeneity	87
D.	Cascading	89
III.	Filamentation and Stimulated Brillouin Scattering	96
A.	Introduction to the Coupling of Transverse Waves to Ion Modes	96
B.	General Formulation of Brillouin and Filamentation	97
C.	Filamentation Dispersion Relation	98
D.	Brillouin Scattering	100
1.	Introduction to Brillouin Weak and Strong Coupling	100
2.	Generalization of Brillouin Analysis to Three Dimensions	101

3. Brillouin Dispersion Relations	102
4. Absolute Instability of Brillouin	108
5. Plasma and Laser Parameters for Brillouin Strong Coupling and Filamentation	120
Appendix 1: Linear Susceptibilities	123
Appendix 2: Electromagnetic Code	126
List of Symbols	149
References	157
Figure Captions	164

THEORETICAL STUDIES OF SOME NONLINEAR LASER-PLASMA INTERACTIONS

Bruce Ira Cohen

Lawrence Berkeley Laboratory
University of California
Berkeley, California 94720

August 15, 1975

ABSTRACT

The nonlinear coupling of intense, monochromatic, electromagnetic radiation with plasma is considered in a number of special cases. The first part of the thesis serves as an introduction to three-wave interactions. A general formulation of the stimulated scattering of transverse waves by longitudinal modes in a warm, unmagnetized, uniform plasma is constructed. We derive a general dispersion relation that describes Raman and Brillouin scattering, modulational instability, and induced Thomson scattering.

In the second part Raman scattering (the scattering of a photon into another photon and an electron plasma wave) is investigated as a possible plasma heating scheme. Analytic theory complemented by computer simulation is presented describing the nonlinear mode coupling of laser light with small and large amplitude, resonantly excited electron plasma waves. Trapping of electrons in the electron plasma wave is found to be an important nonlinear feature. We formally analyze the nonlinear, time-dependent response for a resonantly excited longitudinal wave and demonstrate our construction in simulation. Trapping influences the nonlinear dispersion relation of the plasma wave, whose back-reaction on the beating of the lasers

plays a significant role in the transfer of energy from the transverse waves to the plasma.

The third part investigates the stimulated scattering of a coherent electromagnetic wave by low frequency density perturbations in homogeneous plasma. A composite picture of the linear dispersion relations for filamentation and Brillouin scattering is constructed. Finally we describe in detail the absolute instability of Brillouin weak and strong coupling by analytic and numerical means.

PREFACE

This thesis presents work completed in partial fulfillment of requirements for a Ph.D. in physics at the University of California, Berkeley. The author expresses his gratitude to various people for their invaluable assistance: Professor Allan Kaufman for his infinite patience, his painstaking conscientious job of teaching and advising, his helpful criticisms, and his many personal contributions to this research; fellow graduate students Mike Mostrom, Dwight Nicholson, and Gary Smith for their many helpful discussions, their substantial contributions to the research and the computer effort, and their daily support; Professor C. K. Birdsall and Dr. A. Bruce Langdon for supplying a very thorough and patient course of instruction in plasma simulation, and for their excellent computer codes, research support, and wise counsel; Dr. C. E. Max and Professor W. B. Kunkel for their contributions to the research, numerous informative discussions, and moral support; and Georgella Perry and Christina Graham for their expert preparation of all my publications, letters, and my thesis while I have been at the Lawrence Berkeley Laboratory and for their equally expert job of rendering all my administrative and bureaucratic dealings as simple and pleasant as possible.

Most of all, more than simple thanks go to my wife Sharon for her perseverance, encouragement, and support.

This research was supported in part by the National Science Foundation and the Energy Research and Development Agency.

I. INTRODUCTION

A. Overview of Three-Wave Interactions

The processes considered in this thesis are representative of a much more general class of phenomena, common to many branches of physics, described as three-wave interactions. We restrict consideration here to those three-wave interactions occurring in an unmagnetized plasma involving the scattering of a transverse wave, i.e., a photon, into another transverse wave and a longitudinal wave, i.e., a plasmon. When the longitudinal wave is an electron plasma wave, the three-wave interaction is called Raman scattering.¹⁻⁴ If the longitudinal wave is an ion acoustic wave, the process is called Brillouin scattering.⁵⁻⁹

All three waves in the interaction need not be normal modes however. We shall show how finite amplitude effects can lead to the production of driven modes as decay products in the three-wave interaction. We shall also show how the simultaneous scattering of monochromatic transverse waves into two other transverse waves accompanied by a growing density disturbance can be viewed as two three-wave interactions which are coupled by a virtual or nonpropagating wave. These last two phenomena are described as modified Brillouin or Raman scattering¹⁰ (also known as strong coupling^{11,12}) and modulational instability¹² (examples of which are filamentation¹³ and self-focusing^{14,15}).

To make these ideas somewhat clearer we shall introduce model equations that represent the three-wave interaction of three normal modes in a homogeneous plasma. For the sake of simplicity we consider the coupling of three waves all propagating in one dimension.

The three interacting normal modes are each assumed to satisfy, in the absence of coupling, a linear partial differential equation of the form

$$(\partial_t^2 - 2iv_j\partial_t + \Omega_j^2 - v_j^2\partial_x^2) a_j(x,t) = 0 \quad (j = 1,2,3) \quad (1)$$

where $\{v_j\}$ represent dissipation, $\{a_j\}$ represent field quantities, and the normal mode frequencies satisfy (in the absence of dissipation) the linear dispersion relations $\omega_j^2 = \Omega_j^2 + v_j^2 k_j^2$ (k_j is the wavenumber of the j th wave). If the waves are allowed to couple, then the set Eq. (1) becomes

$$\begin{aligned} (\partial_t^2 - 2iv_1\partial_t + \Omega_1^2 - v_1^2\partial_x^2) a_1(x,t) &= \beta_1 a_2(x,t) a_3(x,t) \\ (\partial_t^2 - 2iv_2\partial_t + \Omega_2^2 - v_2^2\partial_x^2) a_2(x,t) &= \beta_2 a_1(x,t) a_3^*(x,t) \\ (\partial_t^2 - 2iv_3\partial_t + \Omega_3^2 - v_3^2\partial_x^2) a_3(x,t) &= \beta_3 a_1(x,t) a_2^*(x,t) \end{aligned} \quad (2)$$

The constants β_j are real coupling constants, and $a_1(x,t)$ is taken to be the pump wave. For specific three-wave interactions use of Maxwell's equations, fluid or kinetic equations, and equations of motion for ions and electrons results in the set Eq. (2).^{16,17} We shall explicitly derive the linearized coupled mode equations for the interaction of a transverse wave with another transverse wave and an electron plasma wave in Section II.C.

We assume that the field quantities $a_j(x,t)$ can be written $a_j(x,t) = \tilde{a}_j(x,t) \exp(-i\omega_j t + ik_j x) + \text{c.c.}$ ($j = 1,2,3$), where

the $\tilde{a}_j(x,t)$ are slowly varying quantities. If the three waves satisfy the frequency and wavenumber matching conditions,

$\omega_1 = \omega_2 + \omega_3$ and $k_1 = k_2 + k_3$, then Eqs.(2) become

$$\left[2i\omega_1 \partial_t + 2iv_1 \omega_1 + 2iv_1^2 k_1 \partial_x \right] \tilde{a}_1(x,t) = \beta_1 \tilde{a}_2(x,t) \tilde{a}_3(x,t)$$

$$\left[2i\omega_2 \partial_t + 2iv_2 \omega_2 + 2iv_2^2 k_2 \partial_x \right] \tilde{a}_2(x,t) = \beta_2 \tilde{a}_1(x,t) \tilde{a}_3^*(x,t)$$

$$\left[2i\omega_3 \partial_t + 2iv_3 \omega_3 + 2iv_3^2 k_3 \partial_x \right] \tilde{a}_3(x,t) = \beta_3 \tilde{a}_1(x,t) \tilde{a}_2^*(x,t)$$

(3)

The terms involving $\partial_t^2 \tilde{a}_j$ and $\partial_x^2 \tilde{a}_j$ have been ignored. If we divide each equation by $2i\omega_j$ respectively, and introduce the group velocities $V_j \equiv k_j v_j^2 / \omega_j$ and new coupling constants $\alpha_j \equiv \beta_j / 2\omega_j$, then we obtain the linearized coupled mode equations

$$\left[\partial_t + v_1 + V_1 \partial_x \right] \tilde{a}_1(x,t) = -i\alpha_1 \tilde{a}_2(x,t) \tilde{a}_3(x,t)$$

$$\left[\partial_t + v_2 + V_2 \partial_x \right] \tilde{a}_2(x,t) = -i\alpha_2 \tilde{a}_1(x,t) \tilde{a}_3^*(x,t) \quad (4)$$

$$\left[\partial_t + v_3 + V_3 \partial_x \right] \tilde{a}_3(x,t) = -i\alpha_3 \tilde{a}_1(x,t) \tilde{a}_2^*(x,t)$$

We thus consider all three waves on an equal basis. Much work has been done on these equations in various limits.¹⁸⁻²¹ In the limit that $|a_2|, |a_3| \ll |a_1|$, the coupled set of equations reduces to two equations describing the evolution in space and time of the field quantities $a_2(x,t)$ and $a_3(x,t)$ coupled by the pump whose amplitude is assumed constant.^{11,12,22-24} The research on various

parametric instabilities induced by the coupling of two initially small amplitude waves by a pump wave has been vigorous: the work by Rosenbluth²³ and also by Nishikawa²⁴ has been especially significant. In this thesis examples of three-wave interactions are considered both where the pump-wave amplitude is held fixed, and where changes in the pump-wave amplitude are essential.

The three-wave process described by Eqs. (4) is illustrated in Fig. 1a. The decay of a high frequency pump wave (ω_1) into two lower frequency product waves (ω_2, ω_3) is pictured. Figure 1b shows two three-wave interactions coupled by a virtual wave; this could represent filamentation for example. For the case of three-wave interactions among coherent, normal modes, the coupled mode equations Eqs. (4) lead to certain conservation laws. If there is no dissipation, $\nu_j = 0$, then multiplication of Eqs. (4) by $\tilde{a}_j^* \alpha_j^{-1}$ and addition of the equations taking the complex conjugate yield

$$\left[\partial_t + v_1 \partial_x \right] \alpha_1^{-1} |\tilde{a}_1|^2 + \left[\partial_t + v_2 \partial_x \right] \alpha_2^{-1} |\tilde{a}_2|^2 = 0 \quad (5)$$

$$\left[\partial_t + v_1 \partial_x \right] \alpha_1^{-1} |\tilde{a}_1|^2 + \left[\partial_t + v_3 \partial_x \right] \alpha_3^{-1} |\tilde{a}_3|^2 = 0 .$$

The expressions in Eqs. (5) are statements of the well-known Manley-Rowe relations.²⁵⁻²⁹ Loosely speaking, the sum of the wave actions of the pump with either of the decay products is a constant (wave action $\propto \alpha_j^{-1} |\tilde{a}_j|^2$). Since we have assumed that frequency and wavenumber matching prevail and since the wave energy is equal to the frequency times the action (as we shall explicitly show in Part II), then the relative portion of energy transferred to the decay products is given by ω_2/ω_1 for the wave with frequency ω_2 and ω_3/ω_1 for the wave with frequency ω_3 . Similarly for the wave momentum,

equal to the wavenumber times the action, the relative momentum transfer goes as the ratio of wavenumbers. These results should not be surprising; we know from quantum mechanics that the wave energy is given by $\hbar\omega_j N_j$ and the wave momentum by $\hbar k_j N_j$, where N_j is the number of quanta. Action conservation is just a statement of the conservation of quanta.

B. Thesis Synopsis

This thesis presents studies of nonlinear wave-wave interactions involving intense, coherent radiation in an underdense plasma ($\omega_e < \omega$). We examine the possibilities for heating plasma by utilizing the resonance of the beat wave produced by two electromagnetic waves with an electron plasma wave. The excited plasma wave is allowed to be large in amplitude, and the nonlinear effects of electron trapping are considered in detail. We further examine the stimulated scattering of an intense, coherent electromagnetic wave by longitudinal plasma waves or driven plasma modes at low frequency involving both ions and electrons, which is of much interest in laser-fusion applications. A unified picture of stimulated Brillouin scattering and modulational instability (filamentation or self-focusing) is described. We compare linear and nonlinear theory with computer simulation where possible.

In Part I we provide an overview of the basic plasma phenomena of interest here, viz. three-wave interactions among coherent normal modes or driven modes. If the waves can satisfy certain resonance conditions and if their coupling is sufficiently large, a vigorous transfer of energy can occur. The resonance conditions correspond classically to phase matching both in time and space. Quantum mechanically, frequency and wavenumber matching correspond

to energy and momentum conservation. These ideas are made explicit in Section I. A and Section I.C. The mechanisms leading to the nonlinear energy transfer, or mode coupling, are provided by the nonlinear medium, in this case the plasma. The specific nonlinearities responsible for the mode coupling will be manifest in the general treatment appearing in Section I.C, which is concluded with the derivation of an implicit dispersion relation describing the stimulated scattering of a transverse wave by plasma.

Part II of the thesis treats the scattering of light into a longitudinal electron plasma wave and a scattered transverse wave for the purpose of heating plasma. Section II.A begins by specializing our general formulation to the case of beat heating, i.e., the resonant excitation of an electron plasma wave by two electromagnetic waves (of frequencies ω_0, ω_1 with $\omega_0 > \omega_1$ and wavenumbers $\underline{k}_0, \underline{k}_1$) whose difference frequency ($\Omega \equiv \omega_0 - \omega_1$) and wavenumber ($\underline{\kappa} \equiv \underline{k}_0 - \underline{k}_1$) nearly satisfy the Bohm-Gross dispersion relation for an electron plasma wave. This process is closely related to Raman scattering, but the finite amplitude of the lower frequency electromagnetic wave requires equal treatment of both the lower and the higher frequency electromagnetic wave. The excited plasma wave then damps, either due to collisions, Landau damping, or nonlinearly. The plasma heating is provided by the electron plasma wave.

In order to lay the proper groundwork for the subsequent, extensive use of particle simulation, Section II.B describes a relativistic, electromagnetic, particle code. The code was created in collaboration with A. B. Langdon, Mike Mostrom, and Dwight Nicholson, to study a variety of electromagnetic phenomena in linear

and nonlinear regimes. The code implements an efficient Maxwell's equations solver for the one dimensional propagation of light, that is quite free from numerical instability. Poisson's equation is solved by Fourier transform. Langdon's electrostatic version of the code utilizes the same fast Fourier transform of Poisson's equation and was used to study some of the nonlinear aspects of beat heating.

Section II.C is devoted to the study of the beat heating of opposed lasers. The nonlinear interaction may be considered as an induced decay ($\omega_0 \rightarrow \omega_1 + \Omega$), in which a fraction R of the incident power at frequency ω_0 is converted to frequencies ω_1 and Ω , with the fraction $R\Omega/\omega_0$ appearing as a longitudinal plasma oscillation and, because of damping, ultimately as heat. Theory and simulations are utilized in Section II.C.1 to determine the dependence of the efficiency parameter R on the available parameters: laser intensities, density scale length, and temperature. We find that beat heating in a nonuniform plasma with linear density gradient is largely independent of the electron wave dissipation rate.

We describe the steady-state energy transfer to the plasma, first treating the small amplitude electron plasma wave as a quasi-steadily driven disturbance ignoring convection. Subsection II.C.2 examines the space-time interaction of the two lasers, again assuming that the electron wave is quasi-steadily driven by the ponderomotive force of the two lasers. In Section II.C.3 we relax this assumption and integrate (in space and time) the linearized coupled mode equations describing all three waves on an equal basis.

We continue our study of beat heating in Section II.C.4 by investigating the influence of electron trapping in the plasma wave. The threshold and time scale for trapping are compared to those for the

Raman backscatter, electron-ion decay, and oscillating two-stream instabilities to determine for what parameters trapping is the dominant nonlinear feature in beat heating. In reviewing the beat heating simulations exhibiting trapping, we find that certain unphysical effects, caused by the comparatively short length of the plasma, motivate the construction of a simplified model problem.

As a first step in determining the nonlinear plasma response to resonant excitation by the low frequency beat of two high frequency waves, we solve a model problem. For the sake of simplicity, we assume that the plasma is uniform, and that the excitation of the longitudinal beat-wave is provided by a constant-amplitude ponderomotive potential. In Section II.C.5, we formulate an explicit theoretical prescription for the time-dependent nonlinear plasma response to resonant excitation within the context of our simplified model problem. The time-dependence of this nonlinear response, and its approach to equilibrium, are related to the behavior of a nonlinear normal mode, and in particular to its time-dependent eigenfrequency. We determine the equilibria possible for electron plasma waves with trapping, and the stability of the equilibria. Our analysis is demonstrated in simulation, and comparison is made with theory.

Our discussion of the beat heating of opposed lasers is concluded in Section II.C.6, where we consider the back-reaction of the nonlinear electron plasma wave on the evolution of the transverse waves. We specifically investigate the influence of particle trapping in the beat wave and how trapped particle effects can be removed by plasma inhomogeneity.

Section II.D reviews the idea of cascading: parallel propagating electromagnetic waves can be multiply scattered by an electron plasma wave resonantly excited by the ponderomotive $\underline{v} \times \underline{B}$ force of any two successive electromagnetic waves in the cascade. We discuss the influence of plasma inhomogeneity on cascading and how cascading might occur preferentially over Raman backscatter.

When the induced scattering of light involves a beat wave of low frequency $|\Omega| \ll \omega_i$, both electrons and ions can respond. This occurs in many interesting situations, e.g., in astrophysical plasmas, the ionosphere, laser fusion, and radio-frequency heating. Incident radiation can backscatter from an ion acoustic wave or, at higher intensities, from a driven, low frequency density perturbation (strong coupling). These are both examples of stimulated Brillouin backscattering. If the radiation scatters from a growing density perturbation into two sidebands, modulational instability is occurring. The incident radiation can then filament or self-focus. These scattering instabilities involving ions pose a particular threat to laser-pellet fusion. They have relatively low intensity thresholds and can lead to considerable scattering of the laser light and deformation of the target with perhaps deleterious effects on absorption mechanisms requiring relatively uniform illumination of highly spherically symmetric targets. Part III of the thesis is devoted to an examination of stimulated Brillouin scattering and filamentation in a homogeneous, unmagnetized plasma.

Section III.A presents an introduction to the stimulated scattering of light by low frequency ion modes. We construct a general dispersion relation describing Brillouin and filamentation instabilities in Section II.B. The linear dispersion relation for

filamentation is solved in Section III.C, while Brillouin is considered in Section III.D. We examine Brillouin strong coupling and filamentation from a unified point of view. We conclude with a detailed study of Brillouin absolute instability and the construction of its asymptotic Green's function.

C. Coupling of High Frequency Transverse Waves to Unmagnetized Plasma

Of particular interest in laser fusion, radiation from pulsars, radio frequency heating, and ionospheric scattering is the class of parametric instabilities involving the scattering of light from longitudinal electron and ion waves. The instabilities involving ions characteristically exhibit lower thresholds for onset of instability and lower growth rates than their counterparts involving only electrons.^{11,12,30} Examination here will be restricted to just the scattering of a monochromatic electromagnetic wave from longitudinal density perturbations in unmagnetized plasma. The formulation will be sufficiently general to include induced Thomson scattering, but evaluation of dispersion relations and partial differential equations describing the scattering will be confined to situations where the scattering involves collective plasma behavior: stimulated Raman and Brillouin scattering and filamentation.

The discussion begins with a qualitative picture of the physical mechanism responsible for this class of parametric instability. We assume that the electron and ion motion is nonrelativistic and for the sake of simplicity that radiation with frequency ω_0 and wavenumber \underline{k}_0 is incident upon a uniform, unmagnetized, warm plasma. We relax the assumption of plasma uniformity in Section II.C.

The electrons and ions acquire transverse "quiver" velocities as their lowest order response to the radiation. Of course the electron quiver velocity \tilde{v}_e will be larger than the ion quiver velocity by the mass ratio $m_i/m_e \gg 1$. If there is an electron density perturbation or fluctuation present δn_e , e.g., due to noise, then a coupling to the radiation can occur via the electron current $\delta \underline{j}_e$ produced by the transverse quiver velocity and the density perturbation: $\delta \underline{j}_e = e \delta n_e \tilde{v}_e$, where the electron charge is defined by e . This current will act as an antenna for scattered radiation propagating at the sum and difference frequencies and wavenumbers of the density perturbation and the transverse oscillation velocity: $(\omega_0 + \Omega, \underline{k}_0 + \underline{\kappa})$ and $(\omega_0 - \Omega^*, \underline{k}_0 - \underline{\kappa}^*)$, where the frequency and wavenumber of the density perturbation is given by $(\Omega, \underline{\kappa})$.

The feedback necessary to produce parametric instability is provided by the coupling of the scattered radiation with the incident radiation via the Lorentz force $\underline{v} \times \underline{B}$. The Lorentz force is produced by the cross-product of the transverse oscillation velocities with the transverse magnetic fields at the various existing frequencies and wavenumbers of the transverse fields, namely the incident and scattered radiation. The Lorentz force provides a driver for high frequency and high wavenumber density perturbations $(2\omega_0, 2\underline{k}_0)$, $(2\omega_0 + \Omega, 2\underline{k}_0 + \underline{\kappa})$, and $(2\omega_0 - \Omega^*, 2\underline{k}_0 - \underline{\kappa}^*)$ which contribute to the lowest order nonlinear frequency shifts.³¹ In addition to the high frequency density perturbations however, there will be the low frequency $\underline{v} \times \underline{B}$ beat at $(\Omega, \underline{\kappa})$ which serves to reinforce the original density perturbation and can give rise to instability.

The Lorentz force acts like an external, electrostatic driving field in creating density perturbations. If the beat

frequency and wavenumber nearly satisfy the Bohm-Gross dispersion law for electron plasma waves, $\Omega^2 \approx \omega_e^2(1 + 3\kappa^2\lambda_e^2)$ where ω_e is the electron plasma frequency and λ_e the electron Debye length, then Raman scattering can occur. If $|\Omega| \leq \omega_i$ where ω_i is the ion plasma frequency, both the ions and the electrons will respond to the Lorentz force. Then Brillouin scattering and filamentation can occur. In any case the Lorentz force depends bilinearly on the amplitudes of the incident and scattered radiation. The current producing the scattered radiation depends in turn on the amplitudes of the density perturbation and again on the electromagnetic pump. Thus the scattered light is shifted up and down from the pump frequency and wavenumber by the beat frequency and wavenumber, $(\omega_0 + \Omega, \underline{k}_0 + \underline{\kappa})$ and $(\omega_0 - \Omega^*, \underline{k}_0 - \underline{\kappa}^*)$, respectively and can grow exponentially. If the depletion of the electromagnetic pump wave is ignored, then the pump intensity becomes a parameter governing the "parametric" instability.

No attempt at this point has been made to describe the influence on the scattering of the relative polarization and scattering angle of the scattered radiation and the pump. For particular scattering configurations, e.g., forward, both scattered electromagnetic waves can grow exponentially with comparable amplitudes.^{11,12} The incident laser light appears to develop a modulation with $|\Omega| < \omega_i$ and can eventually break up into many filaments or self-focus.^{13,14,32,33} For $\Omega \approx \omega_e$ and $\underline{\kappa} \approx (\omega_e/c)\hat{k}_0$ multiple Raman scatterings from a single electron plasma wave can occur.^{34,35} If instead radiation is observed to backscatter, it is sufficient to consider only the scattered radiation shifted down by the beat

frequency and wavenumber and describe it as stimulated Brillouin or Raman backscatter.^{11,12}

Several authors have constructed general formalisms describing parametric instabilities.^{11,12,36-39} The most complete work on the normal mode structure is due to Drake, Kaw, Lee, Schmidt, Liu, and Rosenbluth,¹² whose analysis is three dimensional and nonrelativistic, and assumes the plasma to be uniform, isotropic, and unmagnetized. We adopt an approach similar to theirs here, but further simplify by considering only the scattering of parallel, linearly polarized light in two dimensions. Comments on the generalization of this formalism to three dimensions are found in Section III.D.

We formulate our description of the induced scattering of radiation by density perturbations in terms of complex vector potentials. We assume that all radiation is linearly polarized in the y direction and propagates in the x - z plane (see Fig. 2). The real vector potential is written as a sum over the modes present, omitting the multiplicative factor \hat{y} ,

$$A(\underline{r}, t) \equiv A_0 \exp(i\mathbf{k}_0 \cdot \underline{r} - i\omega_0 t) + A_- \exp[i(\mathbf{k}_0 - \mathbf{\kappa}^*) \cdot \underline{r} - (\omega_0 - \Omega^*)t] \\ + A_+ \exp[i(\mathbf{k}_0 + \mathbf{\kappa}) \cdot \underline{r} - i(\omega_0 + \Omega)t] + \text{c.c.} \quad (6)$$

In deriving the dispersion relations describing the various parametric instabilities that can arise here, we assume that $|A_+|, |A_-| \ll |A_0|$ and A_0 is held constant. The vector potential represented in Eq. (6) includes the pump wave and the radiation shifted up and down by the beat frequency and wavenumber. If further scattering occurs to produce radiation at frequencies and wavenumbers $(\omega_0 - 2\Omega^*, \mathbf{k}_0 - 2\mathbf{\kappa}^*)$

and $(\omega_0 + 2\Omega, \underline{k}_0 + 2\underline{\kappa})$ for example, then these modes must be explicitly included in Eq. (6). The beat wavenumber $\underline{\kappa}$ is restricted to lie in the x - z plane.

An examination of the equation of motion for the charges quivering in the electromagnetic fields described in Eq. (6) allows the identification of an effective external potential. The equation of motion for a charged particle of species s in the field of an electromagnetic wave and in an electrostatic field with potential $\phi(\underline{r}, t)$ is given in the nonrelativistic limit by

$$m_s \underline{d}\underline{v}/dt = e_s \underline{v} \times [\nabla \times A\hat{y}]/c - e_s \hat{y} \partial A/c\partial t - e_s \nabla \phi \quad (7)$$

We solve Eq. (7) approximately, expanding in powers of the small parameter $e_s A_0/m_s c^2$. The Lorentz force term can be rewritten in approximate form as the gradient of an effective potential. From the conservation of canonical momentum in the y direction (due to translational invariance), we have $\underline{v} \cdot \hat{y} = -e_s A/m_s c + \text{constant} \equiv \tilde{v}_s + \text{constant}$. For a cold plasma the constant can be set equal to zero for all charges, and the component of the Lorentz force term in the scattering plane becomes

$$\left[e_s (\underline{v} \cdot \hat{y}) \hat{y} \times (\nabla \times A\hat{y})/c \right] = -e_s^2 \nabla A^2 / 2m_s c^2 \quad (8)$$

For a warm plasma canonical y momentum is still conserved. However, the y velocities are given by $\underline{v} \cdot \hat{y} = \tilde{v}_s + v'_y$ where v'_y is the velocity of charge described by an arbitrary thermal distribution of velocities in the absence of external fields. The thermal corrections that result will be discussed when the nonlinear current is evaluated.

From Eq. (8) we can define the effective or ponderomotive potential⁴⁰⁻⁴² driving longitudinal electron density perturbations:

$$\phi_0^e(\underline{r}, t) \equiv e [A(\underline{r}, t)]^2 / 2m_e c^2 . \quad (9)$$

The quiver velocity and the effective potential for the ions are both smaller by the mass ratio m_e/m_i ; and are ignored, $\tilde{v}_i \approx \phi_0^i \approx 0$.

The density perturbation is described by the self-consistent Coulomb potential $\phi(\underline{r}, t) = \tilde{\phi} \exp(i\kappa \cdot \underline{r} - i\Omega t) + \text{c.c.}$ We define the total potential $\phi^S(\underline{r}, t)$ as the sum of the Coulomb potential ϕ and the ponderomotive potential ϕ_0^S due to the Lorentz force according to $\phi^S(\underline{r}, t) \equiv \phi(\underline{r}, t) + \phi_0^S(\underline{r}, t)$. The total and the ponderomotive potentials are represented with the same dominant phase dependence as the Coulomb potential. Poisson's equation becomes

$$\tilde{\phi} = 4\pi\kappa^{-2} \sum_s e_s \tilde{n}_s , \quad (10)$$

where \tilde{n}_s is the amplitude of the number density for species s , with phase dependence $\exp(i\kappa \cdot \underline{r} - i\Omega t)$ factored out. We introduce the linear susceptibilities, $\chi_s(\Omega, \underline{\kappa}) \equiv -4\pi\kappa^{-2} e_s \tilde{n}_s / \tilde{\phi}^S$, and the linear dielectric function, $\epsilon(\Omega, \underline{\kappa}) \equiv 1 + \sum_s \chi_s(\Omega, \underline{\kappa})$, in order to replace \tilde{n}_s in Eq. (10) by a linear function of $\tilde{\phi}^S$.

From Eq. (10) and the definitions of the linear susceptibilities, we obtain

$$\begin{aligned} \tilde{\phi}^e &= [1 + \chi_i(\Omega, \underline{\kappa})] \tilde{\phi}_0^e / \epsilon(\Omega, \underline{\kappa}) = \\ &= e [1 + \chi_i(\Omega, \underline{\kappa})] A^2(\Omega, \underline{\kappa}) / [2m_e c^2 \epsilon(\Omega, \underline{\kappa})] , \end{aligned} \quad (11)$$

where by $A^2(\Omega, \underline{\kappa})$ we mean the sum over all coefficients of terms in A^2 varying with phase $\exp(i\underline{\kappa} \cdot \underline{r} - i\Omega t)$. The linear electron susceptibility describes the accompanying electron charge density perturbation:

$$e\tilde{n}_e = -\chi_e(\Omega, \underline{\kappa}) \kappa^2 \tilde{\phi}^e / 4\pi = -\kappa^2 [\chi_e(1 + \chi_i) / \epsilon]_{\Omega, \underline{\kappa}} eA^2(\Omega, \underline{\kappa}) / (8\pi m_e c^2). \quad (12)$$

The wave equation for the vector potential in Coulomb gauge is

$$(\nabla^2 - c^{-2} \partial_t^2) A = -4\pi J c^{-1}. \quad (13)$$

To evaluate the transverse current $J(\underline{r}, t)$ we adopt the simple fluid model that the electromagnetic fields induce a linear electron current and a lowest order nonlinear contribution^{11,12}

$$\begin{aligned} J(\underline{r}, t) &= e\tilde{v} \left[n_0 + \left\{ \tilde{n}_e \exp(i\underline{\kappa} \cdot \underline{r} - i\Omega t) + \text{c.c.} \right\} \right] \\ &= -\frac{e^2 A}{m_e c} \left[n_0 + \left\{ \tilde{n}_e \exp(i\underline{\kappa} \cdot \underline{r} - i\Omega t) + \text{c.c.} \right\} \right] \end{aligned} \quad (14)$$

where n_0 is the unperturbed number density. Equation (12) is employed to construct the perturbed electron number density. The ion contribution to the current is down by the mass ratio and is consequently ignored.

A treatment including finite temperature effects in the ponderomotive potential and the nonlinear current, based on, for example, an analytic solution of the Vlasov-Poisson-wave equation system expanding systematically in powers of $|eA_0/m_e c^2| \ll 1$, shows that thermal corrections³¹ arise of order $T_e/m_e c^2$, where T_e

is the electron temperature. For plasmas with nonrelativistic thermal velocities $v_s \equiv (T_s/m_s)^{1/2} \ll c$, these corrections can be safely ignored. This is not to say that the plasma is assumed cold when the linear susceptibilities and the dielectric response are evaluated; temperature effects here can be very important.

We define $\Gamma(\Omega, \underline{k}) \equiv [\chi_e(1 + \chi_i)/\epsilon]_{\Omega, \underline{k}}$ and postulate a general kinetic description in order to evaluate the linear plasma response, say the Vlasov or Fokker-Planck equations. We can now systematically manipulate Eqs. (12) and (13) to derive coupled mode equations. We shall examine all couplings that lead to nonlinear contributions to the current of order $|A_0|^3$.

First of all, for the nonlinear correction to the dispersion relation for the pump wave due to the Lorentz force with phase dependence $\exp(i2\underline{k}_0 \cdot \underline{r} - i2\omega_0 t)$, we obtain from Eqs. (12), (13), and (14), considering only the terms with phase dependence $\exp(i\underline{k}_0 \cdot \underline{r} - i\omega_0 t)$ in Eq. (13),

$$\omega_0^2 = \omega_e^2 + k_0^2 c^2 \left[1 + 2\Gamma(2\omega_0, 2\underline{k}_0) e^2 |A_0|^2 / m_e^2 c^4 \right] \quad (15)$$

The amplitude dependence of the electromagnetic wave dispersion relation is, however, of the same order as relativistic effects. If we include both the Lorentz force and relativity following Arons and Max³¹ and if we evaluate the susceptibilities in the high frequency limit ($2\omega_0 \gg \omega_e$, $\omega_0/k_0 \gg v_e$), $\chi_e(\omega, \underline{k}) \approx -\omega_e^2/\omega^2$ and $\chi_i \approx 0$, we obtain

$$\omega_0^2 = k_0^2 c^2 + \omega_e^2 \left\{ 1 + 4e^2 |A_0|^2 (m_e c^2)^{-2} \left[3/4 - k_0^2 c^2 / (4\omega_0^2 - \omega_e^2) \right] \right\}.$$

We henceforth assume that the frequency ω_0 and wavenumber \underline{k}_0 of the pump satisfy the nonlinear dispersion relation. In this way the coupling to the high frequency density disturbance with phase dependence $\exp(i2\underline{k}_0 \cdot \underline{r} - i2\omega_0 t)$ has been absorbed into a nonlinear frequency shift.

For the scattered radiation, we look for couplings which involve large $\Gamma(\Omega, \underline{k})$ and recall its definition and the linearization $|A_+|, |A_-| \ll |A_0|$. In addition to the density oscillation at frequency $2\omega_0$ there are density oscillations driven by the Lorentz force at frequencies $2\omega_0 + \Omega$, $2\omega_0 - \Omega^*$, and Ω .⁴³ For the low frequency beat (Ω), the near vanishing of $\epsilon(\Omega, \underline{k})$ at a resonance, which appears in the denominator of $\Gamma(\Omega, \underline{k})$, characterizes the scattering by a longitudinal normal mode. If $\Omega \approx \kappa c_s$ where $c_s \equiv (T_e/m_i)^{1/2}$, then stimulated Brillouin scattering is said to occur. If $\text{Re } \Omega \approx (\omega_e^2 + 3\kappa^2 v_e^2)^{1/2}$ then stimulated Raman scattering occurs. The linear susceptibilities χ_s , from which ϵ and Γ are constructed, are evaluated in an appendix from a Vlasov model for a Maxwellian plasma. For high frequencies $\gg \omega_s$ and phase velocities $\gg v_s$ Γ is real. Consequently the couplings $2\omega_0 + \Omega$ and $2\omega_0 - \Omega^*$ lead to nonlinear frequency shifts which are of the same order as described in Eq. (15), but only when the parametric instability enters the nonlinear regime, i.e., $|A_+|, |A_-| \sim \mathcal{O}(|A_0|)$.^{31,43}

If we substitute Eq. (14) into Eq. (13) and use Eqs. (11) and (12), we obtain

$$D_{-A_-}^* = -e^2(A_-^*|A_0|^2 + A_+A_0^{*2})\kappa^2 c^2 \Gamma(\Omega, \underline{k}) / (m_e c^2)^2 \quad (16a)$$

and

$$D_+ A_+ = -e^2 (A_+ |A_0|^2 + A_-^* A_0^2) \kappa^2 c^2 \Gamma(\Omega, \underline{\kappa}) / (m_e c^2)^2, \quad (16b)$$

where $D_{\pm} \equiv D(\omega_0 \pm \Omega, \underline{k}_0 \pm \underline{\kappa}) = \mp 2\Omega\omega_0 - \Omega^2 \pm 2\underline{k}_0 \cdot \underline{\kappa} c^2 + \kappa^2 c^2$, and $D(\omega, \underline{k}) \equiv \omega_e^2 + \underline{k}^2 c^2 - \omega^2$. We recognize $D(\omega, \underline{k}) = 0$ as the linear dispersion relation for an electromagnetic wave. Thus D_{\pm} are measures of the mismatch of the scattered waves A_+ and A_- from their linear dispersion relations. In obtaining Eqs.(16), the high frequency couplings at $2\omega_0$, $2\omega_0 + \Omega$, and $2\omega_0 - \Omega^*$ are ignored, since $|\Gamma(\Omega, \underline{\kappa})| \gg |\Gamma(2\omega_0 + \Omega, 2\underline{k}_0 + \underline{\kappa})|$, $|\Gamma(2\omega_0 - \Omega^*, 2\underline{k}_0 - \underline{\kappa}^*)|$, $|\Gamma(2\omega_0, 2\underline{k}_0)| \approx \mathcal{O}(\omega_e^2/4\omega_0^2)$. These couplings lead to nonlinear frequency shifts and not to instability.⁴³

Modulational instability is described by the cross-coupling and simultaneous growth of A_+ and A_- with comparable amplitudes in Eqs. (16). Brillouin or Raman scattering is said to occur when A_- grows with amplitude much larger than A_+ . The scattering of light into two plasmons at the quarter-critical point ($\omega_0 = 2\omega_e$)^{12,44,45} and the parametric decay of light at the critical surface

($\omega_0 = \omega_e$)²⁴ into an electron plasma wave and an ion acoustic wave, or into two electron plasma waves and a purely growing ion density perturbation, have been omitted from our description. This is because we demanded that the incident light scatter into another transverse wave and an electron plasma wave, i.e., $\omega_0 > 2\omega_e$, or into another transverse wave and an ion wave, i.e., $\omega_0 > \omega_e$.

To simplify the notation we introduce the dimensionless amplitudes $a_0 \equiv eA_0/(m_e c^2)$ and a_+, a_- similarly. The maximum transverse quiver velocity \tilde{v}_0 in the electric field of the incident electromagnetic wave is determined by $\tilde{v}_0^2/c^2 = 4a_0^2$ (taking a_0 to be real arbitrarily). We define $\mu^2 \equiv \kappa^2 \tilde{v}_0^2 \Gamma(\Omega, \underline{\kappa})/4$, which

measures the coupling strength in units of frequency squared.

Equations (16) can be rewritten

$$[D_- - \mu^2]a_-^* - \mu^2 a_+ = 0 \quad (17a)$$

$$[D_+ - \mu^2]a_+ - \mu^2 a_-^* = 0 \quad (17b)$$

Setting the determinant of the coefficients equal to zero, the general dispersion relation describing modulation, induced Thomson scattering, and stimulated Brillouin and Raman scattering is obtained:

$$D_+ D_- - (D_+ + D_-)\mu^2 = 0 \quad (18)$$

For stimulated Raman and Brillouin scattering, $|D_-| \ll |D_+|$ and $|a_+|$ is consequently small compared to $|a_-|$, so that Eqs. (17) can be reduced to

$$D_- - \mu^2 = 0 \quad (19)$$

Equations (18) and (19) are implicit dispersion relations describing the parametric instability of the stimulated scattering of light in an unmagnetized, uniform plasma. We shall make use of various aspects of this formalism in the subsequent calculations.

II. BEAT HEATING OF A PLASMA

A. Introduction to the Coupling of Transverse Waves to Electron Plasma Waves

In this section we consider the resonant interaction of two lasers whose difference frequency Ω and wavenumber \underline{k} nearly satisfy the linear dispersion relation for an electron plasma wave $\Omega^2 \approx \omega_e^2 + 3k^2 v_e^2$. This process is an example of stimulated Raman

scattering. In as much as we begin with two electromagnetic waves of frequency ω_0 and ω_1 ($\omega_0 > \omega_1$), corresponding to the vector potentials with amplitudes A_0 and A_1 in Eq. (6), we are not looking at an example of parametric instability and must treat A_0 and A_1 equally. The three-wave interaction in this limit is called beat heating³⁴ or optical mixing.⁴⁶⁻⁵⁰ The mechanism for the coupling of the two high frequency waves ($\omega_0, \omega_1 > \omega_e$) with the electron plasma wave is, however, the same as for the parametric instability of Raman scattering and is described in the Introduction, Section I.C.

We are motivated to study this process by the fact that it affords the opportunity to couple the very intense energy at high frequency in lasers to lower frequency plasma modes where the energy might be absorbed as heat. An important consideration that determines the upper limit on the efficiency of this process is the fact that a heating process making use of three-wave interactions is subject to the Manley-Rowe conditions Eqs. (5). If R is the relative efficiency of the action transfer, then no more than the relative amount of energy $R\omega_e/\omega_0$ can be ultimately absorbed by the plasma.

The resonant interaction between two transverse waves and one longitudinal wave or mode for the purpose of plasma heating or as a diagnostic has been investigated by many. Kroll, Ron, and Rostoker (1964) first proposed optical mixing as a diagnostic tool for determining plasma density and calculated the enhanced scattering cross section due to the induced density perturbation.⁴⁶ Wolff (1971) theoretically studied Raman scattering in semiconductors using cold fluid equations and the conservation of transverse canonical momentum to formulate neatly the nonlinear density perturbation and the nonlinear transverse current.³ Wolff found that the scattering instability could be saturated by a

nonlinear Doppler shift in the electron plasma wave produced by an induced longitudinal drift.

James and Thompson (1967) and Capjack and James (1970) applied the principle of optical mixing to the theoretical study of the heating of ions in magnetized plasma by beating high frequency transverse waves at the ion cyclotron resonance⁴⁷ or by mixing Whistler waves at either the ion cyclotron resonance or in the regime of induced scattering by the ions.⁴⁸ They found a marked sensitivity of the resonant process to detuning influences: finite pump bandwidth, variation in the magnetic field, and plasma inhomogeneity. Because of the small ratio of the ion cyclotron frequency to the pump frequencies, the ultimate efficiency of these schemes suffers greatly. Weyl (1970) considered optical mixing for diagnostic application in cold, underdense, magnetized plasma at the cold electron plasma frequency and the upper hybrid frequency.⁴⁹ Weyl further examined the effects of finite pump bandwidth and plasma inhomogeneity to first approximation. Stansfield, Nodwell, and Meyer (1971) mixed two dye laser beams at an angle of 45° in a plasma jet to observe the resonant density fluctuation enhancement when the beat wave resonantly excited an electron plasma wave.⁵⁰ In all the foregoing studies a low frequency beat wave is driven by two high frequency waves in a uniform plasma. If a magnetic field is present, it also is assumed uniform.

The physics of beat heating and parametric instability in general in a nonuniform plasma is significantly different from the case of uniform plasma. Three of the more significant papers discussing parametric instabilities in a nonuniform plasma are by Perkins and Flick (1971)²³ and by Rosenbluth, Liu, and White (1972).^{51,52} Rosenbluth and Liu (1972) studied beat heating in a

homogeneous plasma considering the case where the beat frequency equals twice the cold electron plasma frequency.⁵³ They also consider beat heating in a warm, inhomogeneous plasma where the difference frequency somewhere equals the Bohm-Gross frequency. However, in both cases the high frequency transverse waves are assumed to have constant amplitude. Beaudry and Martineau (1973) extended Rosenbluth and Liu's calculations to include collisional dissipation in the plasma wave.⁵⁴ Strel'tsov (1973) calculated the parametric amplification of the decay products for Raman backscatter in a very sharp density gradient assuming the higher frequency transverse wave to have fixed amplitude.⁵⁵

Fuchs, Neufeld, Teichman, and Engelhardt (1973) studied beat heating in a nonuniform medium calculating the self-consistent amplitudes of the high frequency pumps.⁵⁶ Their results for the dependence of the action transfer upon pump strength, input ratio, and density scale length agree with Ref. 59. However, Fuchs et al. erroneously infer that the resonance region is proportional to the wavelength of the plasma wave rather than the scale length of the plasma. Schmidt (1973) described the excitation of electron or ion waves due to the beating of opposed transverse waves in homogeneous plasma including the nonlinear electromagnetic frequency shifts due to the ponderomotive force but neglecting the comparable shift due to relativity.⁵⁷ He observed that in order to deposit energy into the low frequency, longitudinal wave, there must be a concomitant energy transfer from the higher frequency transverse wave to the lower. Beaudry (1974) investigated beat heating in the limit that convection dominates dissipation for an inhomogeneous medium finding agreement with Ref. 59 which established that action transfer was insensitive to the details

of the dissipation mechanism, be it Landau damping, collisions, or convection.⁵⁸

In the remaining sections in Part II we will review in detail and extend the results of Kaufman, Cohen, Watson, Mostrom, Nicholson, Max, and Langdon, in chronological order Refs. 34, 59, 60, and 43. The general aim of those papers is to consider the interaction of transverse waves with longitudinal electron plasma waves in their linear regimes. All wave amplitudes are treated equally. The beat heating of two electromagnetic pump waves propagating in opposed and parallel directions in uniform plasma is examined in Refs. 60 and 34 respectively. Beat heating of opposed lasers in a nonuniform plasma is studied analytically and in simulation in Refs. 59 and 43. In Section II.C we extend the study of beat heating of opposed lasers to the regime of nonlinear electron waves. Our detailed examination of beat heating begins with a review of the electromagnetic code⁴³ introduced to study beat heating.

B. Electromagnetic Simulation Code

There is a considerable literature concerning electromagnetic codes.⁶¹ Most algorithms for solution of Maxwell's equations require solving a current-driven wave equation for the vector potential. In our code, we solve for the electromagnetic fields explicitly by integrating Maxwell's equations along their characteristics. Dawson and Langdon⁶² first used this method in 1966.

Charged particles are represented by clouds of infinite cross-sectional area in the plane transverse to the grid. In the one dimension in which spatial variations are followed and particle positions are assigned, particles have finite size. Charge densities are calculated by linear interpolation according to the cloud-in-cell

model.⁶³ In this same dimension, designated "longitudinal", there are components of particle velocity and electric field, and all wave propagation occurs. The electromagnetic waves are linearly polarized in the direction of the single transverse velocity component (see Fig. 2). The self-consistent and external magnetic fields lie in the transverse plane and are perpendicular to the polarization direction. The equations of motion are relativistic. There are versions of the code for which the plasma is assumed periodic or, alternatively, finite.

For the particular configuration we describe (Fig. 3), the two Maxwell curl equations take the form:

$$-\partial B_z / \partial x - c^{-1} \partial E_y / \partial t = 4\pi J_y / c$$

$$\partial E_y / \partial x + c^{-1} \partial B_z / \partial t = 0$$

By adding and subtracting these equations, we obtain

$$(\partial / \partial x) [E_y \pm B_z] \pm c^{-1} (\partial / \partial t) [E_y \pm B_z] = \mp 4\pi J_y / c \quad (20)$$

If we define the right- and left-going electromagnetic field quantities respectively, as $F_{\pm} \equiv E_y \pm B_z$, the two Maxwell equations become

$$\left[(\partial / \partial x) \pm c^{-1} (\partial / \partial t) \right] F_{\pm} = \mp 4\pi J_y / c \quad (21)$$

Equation (21) is integrated along the vacuum characteristics $x \mp ct = \text{const.}$, the current J_y being given by the particle positions and velocities. Gridpoints in the space-time mesh are linked by the vacuum characteristics. Then $\Delta x / \Delta t \equiv c$, and there is no Courant condition in the usual sense. A standard Courant condition for the

stability of the finite-differenced wave equation is $\Delta x/\Delta t \geq c$ where Δx and Δt are otherwise independent. In our case $\Delta x = c\Delta t$, and stability and accuracy depend only on how small Δt is.

Spurious numerical dispersion is minimized because we solve explicitly for the electromagnetic fields and introduce some smoothing in calculating the transverse current (Fig. 4). Transverse currents J_y^+ and J_y^- are calculated from the velocities at half time-step intervals and charge positions at whole time-step intervals and then averaged along the vacuum characteristics to obtain $J_y = (J_y^+ + J_y^-)/2$. Consequently, if we treat the particle motion relativistically there should be no numerical Cerenkov instability.⁶⁴ Furthermore, the parameters for which light waves in a drifting plasma can become unstable, due to finite differencing, are unphysical and can easily be avoided with a reasonable choice of $\omega_e \Delta t$. Only for $\omega_e \Delta t \sim \mathcal{O}(1)$ does numerical instability occur for the largest wavenumbers characteristic of the grid, i.e., $2\pi/\Delta x$; and saturation of the instability occurs at low levels of the associated field amplitude.

The differential equations which the code solves can be summarized as follows: the equations for the fields, given the sources, i.e., charge density and current, are Eq. (21) and the Poisson equation

$$-\partial^2 \phi / \partial x^2 = 4\pi e(n - n_0) \quad (22)$$

where n_0 is the uniform neutralizing charge density. Electrons have charge e . We assume a single species here (with fixed neutralizing background), but generally the code deals with two. The equations for the particle and current densities (before linear interpolation) are

$$n(\mathbf{x}) = \sum_i \delta(\mathbf{x} - \mathbf{x}^i) \quad (23)$$

$$\mathbf{J}_y(\mathbf{x}) = \sum_i e v_y^i \delta(\mathbf{x} - \mathbf{x}^i) .$$

The equation of motion for the particles is

$$(d/dt) \left[m\gamma(1 - v^2/c^2)^{-\frac{1}{2}} \right] = e(\mathbf{E} + \mathbf{v} \times \mathbf{B}/c) . \quad (24)$$

The closed set of equations can be integrated forward in time leap-frog style using a differencing scheme centered in space and time (Fig. 4). The equation of motion (24) is integrated forward in time using a hybrid, fast half-acceleration and rotation method.⁶⁵ Because we are interested in the Fourier transform of the electrostatic potential, we solve Poisson's equation by means of fast Fourier transforms. The differences between the bounded and periodic versions of the code appear in the boundary conditions on the potential ϕ , the particles, and the electrostatic and electromagnetic fields at the system walls. Our simulation of a finite plasma assumes that the walls are radiation transparent and particle reflecting. In the bounded version, the longitudinal field E_x vanishes at the system walls. The magnetostatic, vacuum field contribution to B_z is an arbitrary constant value throughout, in either version of the code. We have found the code quite inexpensive to use; typical computer experiments with 4000 particles have required 0.25 sec of central processing unit time per time-step on the CDC 7600 at the Lawrence Berkeley

Laboratory (this includes all operations: field solving, particle pushing, and diagnostics).

C. Beat Heating of Opposed Lasers

We examine here the nonlinear interaction of two oppositely propagating, linearly polarized electromagnetic waves resonantly exciting an electron plasma wave in an inhomogeneous plasma. We review the work in our publications, Refs. 59 and 43, in Section II.C.1 and include Ref. 60 in Section II.C.2. These papers consider primarily the plasma response in the small amplitude limit. In Section II.C.3 we integrate in space and time the three linearized coupled-mode equations Eqs. (4) and compare the results with those in the preceding section and with the literature.²⁰ In the remaining sections of this chapter nonlinear beat-wave effects are examined. A detailed study of the resonant excitation of nonlinear plasma oscillations appears in Section II.C.5. Finally the back-reaction of electron wave trapping on beat heating is considered in Section II.C.6.

1. Theory of Beat Heating for Small Amplitude Electron Plasma Waves

The theory of beat heating has been discussed at some length in the literature, Refs. 34, 43, 53, 57-60. For the sake of completeness we include the derivation due mostly to Kaufman that appears in Ref. 43, and for convenience we adopt the same notation. We shall, however, make much use of the formalism presented in Section I.C. We begin by recalling that the invariance of the canonical y momentum permits the identification of the electron transverse oscillation velocity: we define $u(\underline{x}, t) \equiv \tilde{v} = -eA(\underline{x}, t)/mc$. We assume that for beat heating the ions form an immobile, charge neutralizing background and drop the subscripts denoting electrons.

We adopt a fluid model for the transverse current

$J = e\vec{v}[n_0(\underline{x}) + \delta n(\underline{x}, t)]$, Eq. (14) generalized to a nonuniform medium.

Then use of the wave equation Eq.(13) for the vector potential and substitution for $A(\underline{x}, t)$ in terms of $u(\underline{x}, t)$ yields

$$\left[\partial_t^2 + \omega_e^2(\underline{x}) - c^2 \nabla^2 \right] u(\underline{x}, t) = -\omega_e^2(0) \left[\delta n(\underline{x}, t) / n_0(0) \right] u(\underline{x}, t) . \quad (25)$$

To make the notation less cumbersome we adopt the convention that $\omega_e \equiv \omega_e(0)$ and $n_0 \equiv n_0(0)$. Corrections to the model for the current and thus to Eq. (25) are of relative order u^2/c^2 and v_e^2/c^2 .³¹ We utilize a WKB representation for the transverse waves, and express the vector potential or in this case the transverse oscillation velocity as

$$\begin{aligned} u(\underline{x}, t) = & u_0(\underline{x}, t) \exp \left[-i\omega_0 t + i \int^{\underline{x}} \underline{k}_0(\underline{x}') \cdot d\underline{x}' \right] + \text{c.c.} \\ & + u_1(\underline{x}, t) \exp \left[-i\omega_1 t + i \int^{\underline{x}} \underline{k}_1(\underline{x}') \cdot d\underline{x}' \right] + \text{c.c.} \end{aligned} \quad (26)$$

where u_0 and u_1 are the slowly varying complex transverse velocity amplitudes of the two electromagnetic waves. The wavenumbers of the two transverse waves satisfy the local dispersion relations

$$k_l^2(\underline{x}) \equiv \left[\omega_l^2 - \omega_e^2(\underline{x}) \right] c^{-2} .$$

The density perturbation is excited by the low frequency beat of the two high frequency waves via the Lorentz force on the electrons. The density perturbation is not assumed small:

$$\delta n(\underline{x}, t) = \tilde{n}(\underline{x}, t) \exp \left[-i\Omega t + i \int^{\underline{x}} \underline{\kappa}(\underline{x}') \cdot d\underline{x}' \right] + \text{c.c.} \quad (27)$$

where $\Omega \equiv \omega_0 - \omega_1$ is the beat frequency, and $\underline{\kappa} \equiv \underline{k}_0 - \underline{k}_1$ is the local beat wavenumber, restricted to lie in the x - z plane perpendicular to the transverse electric field polarizations. The electron plasma wave is resonantly excited if the beat frequency and wavenumber nearly satisfy the Bohm-Gross linear dispersion relation,

$$\Omega^2 = \omega_e^2 + 3\kappa^2 v_e^2.$$

We can ignore the density perturbations at the sum frequencies ($\omega_0 + \omega_1$, $2\omega_0$, and $2\omega_1$) for the following reason. Since they represent high frequency, high phase velocity, nonresonant perturbations, they can be only collisionally damped and are not normal modes. However, if we consistently ignore collisional loss in the high frequency perturbations, the coupling constant $\Gamma \equiv \chi_e(1 + \chi_i)/\epsilon$ is real and small, $\Gamma \approx \mathcal{O}(-\omega_e^2/4\omega_0^2)$. Then the density perturbations at these sum frequencies simply couple back into the electromagnetic waves to produce nonlinear frequency shifts as in Eq. (15). Further consideration of these nonlinear frequency shifts is deferred until later in the section.

We assume that $\tilde{n}(\underline{x}, t)$ is slowly varying on the beat frequency and beat wavenumber time and space scales respectively. If we substitute Eqs.(26) and (27) into Eq. (25) and keep only the resonant, nonlinear coupling terms, i.e., only terms with slow temporal and spatial variation, we obtain

$$(\partial_t + c_0 \cdot \nabla + c_0 \cdot \nabla \ln k_0^{\frac{1}{2}}) u_0(\underline{x}, t) = -(i/2)(\omega_e^2/\omega_0)(\tilde{n}/n_0) u_1 \quad (28)$$

$$(\partial_t + c_1 \cdot \nabla + c_1 \cdot \nabla \ln k_1^{\frac{1}{2}}) u_1(\underline{x}, t) = -(i/2)(\omega_e^2/\omega_1)(\tilde{n}^*/n_0) u_0.$$

Equations (28) describe the mode coupling of the transverse wave amplitudes without any assumption on the amplitude of the density perturbation \tilde{n} . The energy density of each transverse wave is given by $W_\ell \equiv \omega_\ell^{-1} \left[\partial(\omega^2 \epsilon) / \partial \omega \right] (\omega_\ell / c)^2 |A_\ell|^2 / 4\pi = \omega_\ell^2 |A_\ell|^2 / 2\pi c^2 = (m/e)^2 \omega_\ell^2 |u_\ell|^2 / 2\pi$ where $\epsilon(\omega) = 1 - \omega_e^2 / \omega^2$.^{34, 59} The transverse wave actions $W_\ell \omega_\ell^{-1}$ are then proportional to $\omega_\ell |u_\ell|^2$. Multiplying Eqs. (28) by $\omega_0 u_0^*$ and $\omega_1 u_1^*$ and then adding the complex conjugates of these equations, we obtain by analogy to Eq. (5) the conservation law for transverse action (Manley-Rowe or photon conservation):

$$\partial_t (\omega_0 |u_0|^2 + \omega_1 |u_1|^2) + \nabla \cdot (\underline{c}_0 \omega_0 |u_0|^2 + \underline{c}_1 \omega_1 |u_1|^2) = 0. \quad (29)$$

The Manley-Rowe relation is evidently quite generally true: it requires only that the WKB analysis be valid. No assumption has been made on the size of the density perturbation. We have assumed that there is no collisional damping of the electromagnetic waves.

Transverse action is therefore conserved for uniform or weakly nonuniform plasma, and for a linear or nonlinear density perturbation.²⁶⁻²⁹ The conservation of action implies that transverse energy is not conserved. As action is transferred from the higher frequency wave (ω_0) to the lower frequency one (ω_1), the energy difference, of relative size Ω/ω_0 , is deposited in the plasma as a coherent oscillation or as heat. If the energy difference is absorbed as heat, the energy transfer is irreversible. If a coherent oscillation persists, however, the energy transfer can be reversed, and the transition $\omega_1 \rightarrow \omega_0$ can occur. This is observed in simulations and predicted theoretically when the beat wave is small in amplitude and weakly damped, and when the beat wave is large enough in amplitude to trap electrons.

The rate of action transfer is, from Eqs.(28), given by

$$\partial_t \omega_0 |u_0|^2 + \nabla \cdot c_0 \omega_0 |u_0|^2 = -\omega_e^2 \text{Im}(u_0 u_1^* \tilde{n}^* / n_0) \quad (30)$$

On using the Poisson equation for the density and scalar potential amplitudes, $\kappa^2 \tilde{\phi} = 4\pi \tilde{n}e$, the right side of Eq. (30) becomes

$$-\kappa^2 \text{Im}[u_0 u_1^* (e\tilde{\phi}^* / m)] \quad (31)$$

The potential ϕ is the longitudinal response to the ponderomotive potential energy⁴⁰⁻⁴² $\psi(\underline{x}, t) \equiv \left\langle \frac{1}{2} m u^2 \right\rangle(\underline{x}, t)$ of the electrons; the angular brackets represent an average over the rapid temporal variation at ω_0, ω_1 yielding a beat variation

$\psi(\underline{x}, t) = \tilde{\psi}(\underline{x}, t) \exp(-i\Omega t + i \int \underline{\kappa} \cdot d\underline{x}) + \text{c.c.}$, $\tilde{\psi}(\underline{x}, t) = m u_0 u_1^*$. From Eqs. (9), (10), and (11) we obtain for the linear longitudinal response

$$\tilde{\phi}(\underline{x}, t) = (1 + \chi_1) \epsilon^{-1} \tilde{\phi}_0 - \tilde{\phi}_0 \approx (\epsilon^{-1} - 1) \tilde{\phi}_0 = (\epsilon^{-1} - 1) m u_0 u_1^* / e \quad (32)$$

where ϵ is the linear dielectric function, evaluated at $\Omega, \underline{\kappa}$. The ponderomotive potential energy is evidently related to the effective, external potential introduced in Eq. (9) by the expression $\tilde{\psi} = e\tilde{\phi}_0$.

If the space-time variation of (u_0, u_1) is not sufficiently slow we should instead use $\Omega + i\partial_t$ and $\underline{\kappa} - i\nabla$ as the arguments of ϵ . To illustrate this we undertake the following construction.

Suppose the electron plasma wave to be driven at frequency Ω and to exhibit dissipation rate ν . Define the real, linear normal mode frequency Ω_L by $\text{Re } \epsilon(\Omega_L, \underline{\kappa}) = 0$. Then expanding about Ω_L we obtain:

$$\begin{aligned}
\epsilon(\Omega + i\partial_t, \underline{\kappa} - i\nabla) &= \text{Re } \epsilon(\Omega_L, \underline{\kappa}) + i\text{Im } \epsilon(\Omega_L, \underline{\kappa}) \\
&+ \bar{\epsilon} \left[\Omega + i\partial_t + (\partial\omega/\partial\underline{\kappa}) \cdot i\nabla - \Omega_L \right] + \dots \\
&\approx (2\Omega_L/\omega_e^2) \left[\Omega - \Omega_L + i \left(\partial_t + \nu + 3\underline{\kappa} \frac{v_e^2}{\Omega_L} \cdot \nabla \right) \right]
\end{aligned} \tag{33}$$

where $\bar{\epsilon} \equiv \partial \text{Re } \epsilon / \partial \omega$ is evaluated at Ω_L and we have made use of $\text{Re } \epsilon(\Omega_L, \underline{\kappa}) = 0$, $\nu = \text{Im } \epsilon / \bar{\epsilon}$, and for electron plasma waves $\bar{\epsilon} \approx 2\Omega_L/\omega_e^2$ and $\partial\omega/\partial\underline{\kappa} = 3\underline{\kappa} v_e^2/\Omega_L$. This construction requires that $|\Omega - \Omega_L + i[\partial_t + \nu + 3\underline{\kappa}(v_e^2/\Omega_L) \cdot \nabla]| \ll \omega_e$ to justify truncation of the Taylor series where shown in Eq. (33). In Section II.C.5 a similar expansion is examined in more detail for the case of a nonlinear dielectric function where certain of the nonlinear aspects may be incorporated by modifying the form of ϵ , so that ϵ depends on ϕ implicitly.

In the case that Eq. (33) is applicable, i.e., if spatial and temporal variations in the longitudinal response are appreciable, then the formulation making use of Eq. (32) is not the most expedient. The three-wave analysis in Section II.C.3 becomes preferable. The opposite limit, where Eq. (32) is applicable, defines what we mean by the "quasi-steady" longitudinal response.

We now use Eqs. (32) and (31) to express the right side of Eq. (30) as

$$\kappa^2 |u_0|^2 |u_1|^2 \text{Im } \epsilon^{-1}(\Omega, \underline{\kappa}) . \tag{34}$$

We observe that the action transfer depends upon the beat wavenumber as κ^2 , if the variation of $\text{Im } \epsilon^{-1}(\Omega, \kappa)$ with κ is neglected. By orienting the lasers oppositely to one another ($\kappa = k_0 + k_1$), the beat wavenumber and hence the coupling are maximized. All wave propagation then occurs in one dimension, say x (see Fig. 5).

For a uniform medium, the nonlinear equations for $|u_0|^2(x, t)$ and $|u_1|^2(x, t)$ can be solved analytically, as discussed in Ref. 60 included here as Section II.C.2. Numerical solution of the action transfer Equations (29) and (30) for the case of a nonuniform medium using (31) is also discussed in Section II.C.2. For a nonuniform medium, we limit our analytic study here to the steady state ($\partial_t u_0 = \partial_t u_1 = 0$), whence Eqs. (29) and (30) become

$$(d/dx)(k_0 |u_0|^2) = (d/dx)(k_1 |u_1|^2) = \kappa^2 c^{-2} |u_0|^2 |u_1|^2 \text{Im } \epsilon^{-1} \quad (35)$$

where $\epsilon(\Omega, \kappa; x)$ has an explicit x variation through the plasma parameters: density, temperature, possibly non-Maxwellian electron distribution.

In order to understand Eq. (35), we introduce the action flux density, which is merely the action density J_ℓ multiplied by the group velocity $c_\ell \equiv k_\ell c^2 / \omega_\ell$. We express the action flux density in natural units as $S_\ell \equiv (e/mc^2)^2 c_\ell W_\ell / \omega_\ell = (k_\ell / 2\pi) |u_\ell / c|^2$. Then Eq. (35) reads as in Eq. (3) of Ref. 59: $dS_0/dx = dS_1/dx = \bar{\delta} S_0 S_1 \text{Im } \epsilon^{-1}(x)$, with $\bar{\delta} \equiv 2\kappa^2 / k_0 k_1 \approx 8$ for $\Omega \ll \omega_0$. Upon integrating over x , we found the solution

$$\Delta \ln(S_0/S_1) = \bar{\delta} \pi \bar{S} \int_a^b dx \text{Im } \epsilon^{-1}(x) \quad , \quad (36)$$

where $\Delta f \equiv f(x = a) - f(x = b)$, a and b are any two x planes (such as the boundaries of the plasma), and $\tilde{S} \equiv S_0 - S_1$ is the constant action density flux.

In the limit of weak damping ($|\text{Im } \epsilon| \equiv |\epsilon''| \ll 1$), the x integral can be carried out exactly.⁵⁹ We write $\text{Im } \epsilon^{-1}(x) = -\pi \delta[\epsilon'(x)]$, where $\epsilon' \equiv \text{Re } \epsilon$. The integral on the right-hand side of Eq. (36) is then

$$\int_a^b dx \text{Im } \epsilon^{-1}(x) = -\pi \left| \frac{\partial \epsilon'}{\partial x} \right|_{\epsilon'=0}^{-1} \equiv -\pi L_n, \quad (37)$$

defining the effective density scale length L_n . In this limit, the action transfer of Eq. (35) takes place over the infinitesimal region where $\epsilon'(\Omega, \kappa; x) = 0$, i.e., at that position x where the beat frequency Ω matches the Bohm-Gross frequency at the beat wavenumber $\Omega_L(\kappa; x)$.

More realistically with finite ϵ'' , we have

$\text{Im } \epsilon^{-1} = -\epsilon'' / (|\epsilon'(x)|^2 + |\epsilon''|^2)$. It can be shown that $\text{Im } \epsilon^{-1}$ has a half-width of order $\epsilon'' L_n \approx 2\nu L_n / \omega_e$ (see Fig. 5), where ν is the total damping rate of a Langmuir oscillation. Equation (37) remains unaltered, however, in the limit that the half-width is small compared to the plasma length. In order that the WKB representation be valid, the transfer zone width $\nu L_n / \omega_e$ must exceed the wavelengths, i.e., $(\nu / \omega_e) \gg (k_\perp L_n)^{-1}$. (Typical parameters for a θ -pinch, $n_0 \sim 10^{17} \text{ cm}^{-3}$, $T_e \sim 100 \text{ eV}$, $\omega_e / \omega_0 \sim 0.1$, and $L_n \sim 10 \text{ cm}$, satisfy this inequality, since $\nu / \omega_e \geq 10^{-2}$ while $(k_0 L_n)^{-1} \sim 10^{-4}$. For our simulations the resonance zone was of order ten wavelengths long.) If the damping is not weak ($\nu \sim \omega_e$), then $\epsilon(x)$ may not be considered small. However, the integration in Eq. (37) can still be performed for known $\epsilon(x)$.

Since strong damping implies $\text{Im } \epsilon^{-1} = -\mathcal{O}(1)$, we obtain in place of (37)

$$\int dx \operatorname{Im} \epsilon^{-1}(x) = -\mathcal{O}(L) , \quad (38)$$

where L is the length of the plasma. In a real plasma, when $L \sim \mathcal{O}(L_n)$, we have the important result that the action transfer is, in order of magnitude, the same for strong as for weak damping of the longitudinal response. This is true provided $|\epsilon'' L_n| \ll L$, otherwise the action transfer, proportional to the integral in Eq. (38), is incomplete. Thus, for given κ , the dependence on $\kappa \lambda_e$ is weak; and for $\kappa \lambda_e \ll 1$, the dependence vanishes, since the integral is truly independent of ν for the model of a linear gradient.

At this point we return to our earlier examination of the nonresonant $[|\epsilon| \sim \mathcal{O}(1)]$ high-frequency density oscillations, which give rise to nonlinear frequency shifts in the two electromagnetic pumps. Arons and Max³¹ have derived the frequency shift for a single, linearly polarized electromagnetic wave: we recall from Section I.C their result

$$\omega^2 = k^2 c^2 + \omega_e^2 \left\{ 1 - \frac{1}{2} (v_y/c)^2 \left[\frac{3}{4} - (\omega^2 - \omega_e^2)/(4\omega^2 - \omega_e^2) \right] \right\} ,$$

where v_y is the amplitude of the transverse electron velocity, $v_y \equiv eE_y/(m\omega)$. The frequency shift due to relativity only is $-\frac{3}{16} \omega(\omega_p/\omega)^2 (v_y/c)^2$, while that due to $e\vec{v}_y \times \vec{B}_z/c$ (the Lorentz or "ponderomotive" force) is $\frac{1}{4} \omega(\omega_p/\omega)^2 (v_y/c)^2 (\omega^2 - \omega_p^2)/(4\omega^2 - \omega_p^2)$ using Eq.(15). The ponderomotive frequency shift describes the effects of density perturbations at the frequencies $2\omega_0$ and $2\omega_1$. There is an additional ponderomotive frequency shift due to the $\vec{v}_y \times \vec{B}_z$ coupling at $\omega_0 + \omega_1$.

In the steady-state, there can be considerable spatial variation of the amplitude of each of the electromagnetic waves. We can nevertheless set an upper bound on the relative frequency shifts, viz. $|\Delta\omega/\omega| \leq \mathcal{O}\left[\frac{1}{4} (\omega_e/\omega)^2 (v_y^{\text{in}}/c)^2\right]$. To estimate their effect on the action transfer, they should be compared to the quantity $|\epsilon(x)|/|\partial\epsilon(x)/\partial\omega|_{\Omega, \kappa} \geq 0.02 \omega_e$ which represents both the linear dissipation and the mismatch of the electron plasma wave. Since that quantity is more than an order of magnitude larger than the electromagnetic frequency shifts $|\Delta\omega| \leq 0.001 \omega_e$ (for typical simulations $\omega_0/\omega_e \sim \mathcal{O}(5)$ and $2|u_0/c|_{\text{in}} = 2|u_1/c|_{\text{in}} \leq 0.1$), we have neglected those shifts in Eq. (35). An investigation of the nonlinear frequency shift and dissipation of the driven electron plasma wave, and of their influences upon beat heating, is considered in subsequent sections.

In a simulation model, for reasons of economy the slab thickness L may be smaller than L_n , and even smaller than the resonance width $(v/\omega_e)L_n$. In that case appropriate corrections must be made in comparing theory and simulation. A typical simulation for beat heating when the density perturbations are linear is shown in Fig. 6.

Inserting (37) into (36), we have the result (Eq. (5) of Ref. 59):

$$\frac{1}{2} 8\pi k_0 L_n |u_0/c|_{\text{in}}^2 = (1 - R - \rho)^{-1} \ln\left[(1 - R)(\rho + R)/\rho\right], \quad (39)$$

an implicit equation for the relative action transfer $R \equiv \Delta S/S_0^{\text{in}}$, in terms of the input ratio $\rho \equiv S_1^{\text{in}}/S_0^{\text{in}}$ and the input amplitude $|u_0|_{\text{in}}$. (See Fig. 2 of Ref. 59 for a plot, also Fig. 7 here.) This result is remarkable not only in its independence of the damping rate

ν (and thus of the temperature, the collision rate, and the damping mechanism), but also in that its dependence on the power parameter $|u_0|_{in}^2$ and the scale length L_n is only through their product.

To test relation (39), a set of simulation runs was made for the case of equal input actions ($\rho = 1$), corresponding to approximately maximum transfer for a given total power input. For the set reported here, the power was kept sufficiently low that the longitudinal response could be treated as linear. The dependence of action transfer R on the product of scale length and input power is shown in Fig. 7; the simulations and the theory are seen to be in excellent agreement. The action transfer was measured by averaging in time over the decaying oscillations of the instantaneous action transfer rate, which approaches a steady state. The error bars represent the statistically weighted magnitudes of these oscillations.

To verify the theoretical prediction that the dependence on scale length and input power is only through their product, three runs were made, with different scale lengths and powers, but constant product. The action transfers (also shown in Fig. 7) were found to agree, within statistical error.

The damping of the longitudinal response in these simulations was due to resonant particles, i.e., Landau damping. With $\kappa\lambda_e$ chosen between 0.30 and 0.45, the damping rate ν lay between $10^{-2} \omega_e$ and $10^{-1} \omega_e$. The ν -independence of the action transfer was tested by varying $\kappa\lambda_e$, holding $k_0 L_n |u_0|_{in}^2$ fixed. The simulations corroborated this independence.

We have thus used the electromagnetic simulation code to study beat heating of a plasma in the linear regime of the driven density

disturbance. Steady-state theory was found to be useful in understanding the action transfer and plasma heating for small amplitude electron waves. There was good quantitative agreement between simulation and theory.

2. Space-time interaction of opposed transverse waves in a plasma

Bruce I. Cohen

Department of Physics and Lawrence Berkeley Laboratory, University of California, Berkeley, California 94720

(Received 17 August 1973)

The interaction of two opposed, intense electromagnetic waves, whose difference frequency approximates the plasma frequency, is studied. Plasma heating ensues. Energy is transferred to the lower-frequency wave throughout a uniform plasma, but only in a resonance zone in a nonuniform plasma.

The nonlinear interaction of coherent electromagnetic waves (lasers) in an underdense plasma ($\omega_p < \omega$) is of interest because of the potential for heating when the difference frequency of the two waves is near the local plasma frequency.¹⁻⁶ When this is the case, energy is partially transferred from one transverse wave to the other and is partially deposited in the plasma in the form of electrostatic plasma oscillations. In the present note, we extend the work of Kaufman and Cohen⁶ by including the temporal evolution of the interaction.

We examine the transfer of energy between two transverse waves of frequencies ω_0, ω_1 , with $\omega_0 > \omega_1$. The transfer is driven at the beat frequency $\Omega \equiv \omega_0 - \omega_1$ and at the beat wavenumber $K \equiv k_0 + k_1$ (for opposed wave vectors). The plasma is considered to be infinite in extent. We assume that the dissipation rate ν of the plasma wave and the mismatch $\Delta\omega(z) = \Omega - \omega_p(z)$ are small, so the interaction is nearly resonant.

The analysis follows that of Ref. 6, employing the longitudinal dielectric function and using the same notation. Both the temporal and the spatial evolution of the intensities of the electromagnetic waves are studied. The electrostatic potential in response to a vector potential $A(z, t)$ is $\phi(z, t) \propto [\epsilon^{-1} - 1]A^2(z, t) + \text{noise}$. The behavior of the transverse waves will be analyzed over time scales long compared with ν^{-1} ; thus, any potential $\phi(z, t)$ present at either the initiation or termination of the laser pulses can be ignored as a transient whose decay occurs in a time of the order of ν^{-1} . The generalization of Kaufman and Cohen's⁶ nonlinear coupled mode equation for the action fluxes in natural units is

$$(\partial_t + c^{-1}\partial_z)J_0 = (\partial_t - c^{-1}\partial_z)J_1 = -2\Gamma J_0 J_1, \quad (1)$$

where $\Gamma \equiv -4\pi \text{Im} \epsilon^{-1}(\Omega, K)$ and $J_i \equiv k_i |A_i|^2 e^2 / (2\pi m^2 c^4)$. The group velocities of the two electromagnetic waves have been set equal to c , since we assume $\omega \gg \omega_p$. Because $\Gamma > 0$, the higher-frequency wave loses action flux J_0 as it propagates to the right (increasing z). The action flux J_1 of the lower-frequency wave increases as it propagates to the left. The conservation law for action flux, from (1), is $\partial_t(J_0 + J_1) + \partial_z(cJ_0 - cJ_1) = 0$.

For a uniform plasma the solution of (1), subject to conditions that the ω_0 wave is incident from the left and the ω_1 wave from the right with step function profiles $\Theta(ct - z)$ and $\Theta(ct + z)$ respectively, is straightforward. The mismatch $\Delta\omega$ and damping ν are constant. One transforms to new variables $ct - z$ and $ct + z$, the characteristics of the operators of (1). The equations are then solved using the method of Maier *et al.*⁷ In terms of the input action fluxes, J_0^i and J_1^i let $\rho \equiv J_1^i/J_0^i$, $\eta \equiv (ct$

$-z)\Gamma J_0^i$ and $\xi \equiv (ct + z)\Gamma J_0^i$. The solutions for the relative action fluxes are

$$\begin{aligned} \bar{J}_0(t, z) &\equiv J_0(t, z)/J_0^i = e^{-\eta} (e^{-\eta} + e^{\rho\xi} - 1)^{-1}, \\ \bar{J}_1(t, z) &\equiv J_1(t, z)/J_0^i = \rho e^{\rho\xi} (e^{-\eta} + e^{\rho\xi} - 1)^{-1}, \end{aligned} \quad (2)$$

valid for $\eta, \xi \geq 0$. For a cold plasma, $\epsilon = 1 - \omega_p^2/(\Omega^2 + i\Omega\nu_{ei})$, so that $\Gamma \approx 4\pi(\nu_{ei}/\omega_p)[(\nu_{ei}/\omega_p)^2 + (2\Delta\omega/\omega_p)^2]^{-1}$. The energy density deposited in the longitudinal wave, $2\pi(mc^2/e)^2 J_0 J_1 |\epsilon^{-1}(\Omega, K) - 1|^2$, is ultimately available for plasma heating.

We consider the example of CO₂ lasers ($\omega_0 \sim 2 \times 10^{14} \text{sec}^{-1}$) with $\omega_p/\omega_0 = 0.1$, $\nu_{ei}/\omega_p = 2\nu/\omega_p = 0.01$, pulse lengths $\approx 60\nu_{ei}^{-1}$, and $\Delta\omega \approx \nu_{ei}$. Significant transfer of action occurs when the dimensionless space and time variables are of order unity: $\eta, \xi \sim \Gamma J_0^i ct = \omega_0 \nu^{-1} \times \omega_p P^0 / (2.5 \times 10^{16} \text{W/cm}^2) = O(1)$. Hence, appreciable interaction occurs for intensities $P^0 \geq 2 \times 10^{10} \text{W/cm}^2$.

Figure 1(a) shows the solutions (2) for $\rho = 1$. Dimensionless time and space variables $t' = \Gamma J_0^i ct$ and $z' = \Gamma J_0^i z$ are employed. The pulse shape of the ω_1 wave peaks and sharpens as the ω_0 photons are turned around and converted to ω_1 photons. The ω_1 photons "pile up" as the ω_1 wave propagates through the ω_0 wave. Energy transferred to the plasma then grows as the ω_1 wave front progresses to the left. Since the interaction rate depends upon the product of the actions, we have chosen $\rho = 1$ to maximize the action transfer.

Analytic solutions to (1) for a uniform plasma but with linearly varying leading edges for the two pulses are obtained similarly. If we define $J_i' \equiv |\partial_z J_i|$, $\sigma \equiv (ct - z)(\Gamma J_0^i)^{1/2}$, and $\tau \equiv (ct + z)(\Gamma J_0^i)^{1/2}$, the action transfer between the two transverse waves is described by

$$\begin{aligned} \bar{J}_0(t, z) &\equiv J_0(t, z)(\Gamma/J_0^i)^{1/2} = \sigma \exp(-\sigma^2/2) \\ &\quad \times [\exp(-\sigma^2/2) + \exp(\rho\tau^2/2) - 1]^{-1}, \\ \bar{J}_1(t, z) &\equiv J_1(t, z)(\Gamma/J_0^i)^{1/2} = \rho\tau \exp(\rho\tau^2/2) \\ &\quad \times [\exp(-\sigma^2/2) + \exp(\rho\tau^2/2) - 1]^{-1}, \end{aligned} \quad (3)$$

valid for $\sigma, \tau \geq 0$. Again marked amplification and "pile-up" of the ω_1 wave occurs just behind its leading edge [Fig. 1(b)].

We next examine the case of a linear density inhomogeneity. We define the density scale length $L \equiv |d \ln n/dz|^{-1}$. The frequency mismatch now depends upon position: $\Delta\omega(z) \equiv \Omega - \omega_p(z) \approx \Omega z(2L)^{-1}$. It follows that $\Gamma(z) \approx 4\pi\nu_{ei}\Omega[\nu_{ei}^2 + (\Omega z/L)^2]^{-1}$. For a nonuni-

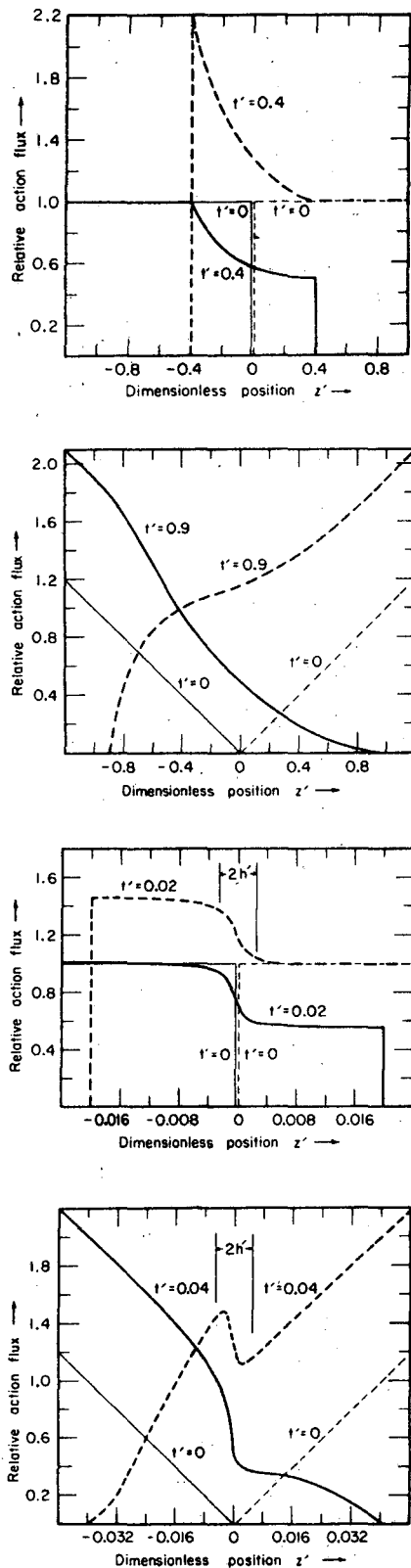


FIG. 1. Dimensionless action fluxes $J_0(t, z)$ ———, and $J_1(t, z)$ ———, as functions of dimensionless time t' and position z' defined below, for input ratio $\rho = 1$. Case (a) shows step-function pulse profiles for a uniform plasma, with $t' = \Gamma J_0^2 ct$ and $z' = \Gamma J_0 z$. Case (b) shows linear pulse profiles for a uniform plasma, with $t' = (\Gamma J_0^2)^{1/2} ct$, and $z' = (\Gamma J_0^2)^{1/2} z$. Case (c) shows step-function pulse profiles for a linear density variation, with $t' = 4\pi J_0^2 ct$ and $z' = 4\pi J_0 z$. Case (d) shows linear pulse profiles for a linear density variation, with $t' = (4\pi J_0^2)^{1/2} ct$ and $z' = (4\pi J_0^2)^{1/2} z$. In (a) and (b) for a uniform plasma, $\Gamma = 4\pi\nu\Omega[\nu^2 + (2\Delta\omega)^2]^{-1}$. In (c) and (d) for a linear variation of the plasma density, $h' = 0.0025$ and 0.005 , respectively in the dimensionless units of z' .

-41-

form plasma, $\Gamma(z)$ is large (coupling is appreciable) only in a narrow zone around $z = 0$ [$\Omega = \omega_p(0)$]. The width of this resonance zone has been defined as $h = 2\pi L\nu_{ei}/\Omega$ by Mostrom *et al.*⁸ We assume that $k_0 h \gg 1$ to permit a WKB analysis.

Again, we follow the evolution of step function and linear initial pulse profiles. Since $\Gamma \propto \nu^{-1}$ at the exact resonance position $z = 0$, while the response width $h \propto \nu$, the total action transfer is only a weak function of the damping ν . In absolute units the action transfer is linear in both the scale length of the plasma and the laser intensity (for $\rho = 1$).⁶ Again, $\rho = 1$ gives the maximum transfer efficiency. Figures 1(c) and 1(d) display the numerical solution of (1) for $\nu/\Omega = 0.01$. Figure 1(c) is the case $h = 0.0025(4\pi J_0^2)^{-1}$, while $h = 0.005(4\pi J_0^2)^{-1/2}$ in Fig. 1(d). Nearly all pulse profile modification occurs within the resonance zone. For the step-function profiles a steady state for the conversion of the ω_0 wave to the ω_1 wave is achieved at times greater than $6h/c$ for the dimensionless parameter $h' \equiv h4\pi J_0^2$ chosen. There is no such steady state in the case of linear pulse profiles, because the unperturbed wave intensities are linearly increasing functions of time.

These solutions to the coupled mode equations (1) are valid as long as the transverse waves overlap within the plasma. For a finite length plasma, the interaction can be very different; for example, the possibility of relaxation oscillation arises.⁹ However, for a nonuniform plasma, the interaction is appreciable only in the resonance zone. In this case the solutions remain valid as long as the region over which the transverse waves overlap contains the resonance region, regardless of the finite extent of the plasma.

The author thanks A. N. Kaufman for his assistance and criticism and is indebted to D. Nicholson, C. Max, M. Mostrom, K. Watson, R. Pyle, W. Kunkel, Y.-R. Shen, and J. Dawson for their discussion and encouragement.

This work was supported by the U. S. Atomic Energy Commission, the U. S. Air Force Office of Scientific Research F44620-C-70-0028, and the National Science Foundation.

- ¹ N. Kroll, A. Ron, and N. Rostoker, *Phys. Rev. Lett.* **13**, 83 (1964).
- ² G. Weyl, *Phys. Fluids* **13**, 1802 (1970).
- ³ B. Cohen, A. Kaufman, and K. Watson, *Phys. Rev. Lett.* **29**, 581 (1972).
- ⁴ M. N. Rosenbluth and C. S. Liu, *Phys. Rev. Lett.* **29**, 701 (1972).
- ⁵ P. S. Lee, Y. C. Lee, C. T. Chang, and D. S. Chu, *Phys. Rev. Lett.* **30**, 538 (1973).
- ⁶ A. N. Kaufman and B. I. Cohen, *Phys. Rev. Lett.* **30**, 1306 (1973).
- ⁷ M. Maier, W. Kaiser, and J. Giordmaine, *Phys. Rev.* **177**, 583 (1969).
- ⁸ M. Mostrom, D. Nicholson, and A. N. Kaufman (to be published).
- ⁹ R. Johnson and J. Marburger, *Phys. Rev. A* **4**, 1175 (1971).

3. Three-wave Analysis of Beat Heating Coupled Mode Equations

This section will describe the three-wave analysis that becomes necessary when in Eq. (32) the space-time variation of (u_0, u_1) is sufficient to demand the inclusion of space and time derivatives in ϵ . The arguments of the warm plasma ϵ become $\Omega + i\partial_t$ and $\kappa - i\partial_x$ in one dimension, Eq. (33). If we assume $|\epsilon| \ll 1$ and make use of Eq. (33), then instead of Eq. (32) we obtain

$$2\Omega_L \omega_e^{-2} \left[\Omega - \Omega_L + i(\partial_t + \nu + 3\kappa v_e^2 \Omega_L^{-1} \partial_x) \right] \tilde{\phi}(x, t) = m u_0 u_1^* / e \quad (40)$$

where Ω_L is the Bohm-Gross frequency $\Omega_L^2 = \omega_e^2 + 3\kappa^2 v_e^2$. Poisson's equation allows us to replace $\tilde{\phi}$ by $4\pi\kappa^{-2} e\tilde{n}$. Then Eqs. (28) and (40) form a complete set of first order partial differential equations describing the three-wave interaction.

In the limit that the temporal or spatial rate of action transfer dominates dissipation and mismatch, then the three linearized coupled mode equations in a homogeneous, underdense ($\omega_e \ll \omega_1, \omega_0$) plasma can be written

$$\begin{aligned} (\partial_t + c_0 \partial_x) u_0(x, t) &= \beta (i\tilde{\phi}) u_1 \\ (\partial_t - c_1 \partial_x) u_1(x, t) &= -\beta (i\tilde{\phi})^* u_0 \\ (\partial_t + 3\kappa v_e^2 \Omega_L^{-1} \partial_x) i\tilde{\phi}(x, t) &= \alpha u_0 u_1^* \end{aligned} \quad (41)$$

where $\beta \equiv \kappa^2 e / (2m\omega_0)$ and $\alpha \equiv m\omega_e^2 / (2e\Omega)$. Analytic solutions for the coupled mode equations in this form have been found.¹⁸⁻²¹ Nozaki and Taniuti obtain a special class of solutions corresponding to the steady propagation of solitary pulses.²⁰ The solutions for the three waves are functions of only $x - \lambda t$ where λ is the constant

propagation speed and is amplitude dependent. Nozaki and Taniuti find solutions whose forms are hyperbolic secants for $u_1(x - \lambda t)$ and $\tilde{\phi}(x - \lambda t)$, and hyperbolic tangent for $u_0(x - \lambda t)$ with only two of the three amplitudes as free parameters. Since the system of equations (41) in general possesses an arbitrary initial configuration $u_0(x, 0)$, $u_1(x, 0)$, and $\tilde{\phi}(x, 0)$, there is no guarantee that the interaction will always evolve into a solitary pulse or pulses (see Fig. 10 and discussion below).

To examine Nozaki and Taniuti's solitary pulses we have recast Eqs. (41) in the form

$$(\partial_t + V_1 \partial_x) a_1 = -i a_2 a_3$$

$$(\partial_t + V_2 \partial_x) a_2 = -i a_3^* a_1$$

$$(\partial_t + V_3 \partial_x) a_3 = -i a_2^* a_1$$

and set $V_1 = -V_2 = V_3 = 1$ arbitrarily. A right-going solitary pulse solution is illustrated in Fig. 8, where we directly numerically integrate the coupled mode equations. In performing the numerical integration we employ the space-time characteristics of the linear, partial differential operators to reduce the differential operators to ordinary, first derivatives which are straightforwardly finite-differenced and integrated by a first order predictor-corrector method.⁶⁷ The steady propagation of pulses conforming to the solutions of Nozaki and Taniuti is verified and pictured in Fig. 8 for value of $\lambda = 1.01$.

If we consider perturbations to the solitary pulse solution corresponding to an excess of energy in one or more of the three waves,

a solitary pulse can evolve if normal convection can carry the excess energy away from the solitary pulse interaction region. In Fig. 9 the initial pulse profile for a_2 corresponds to ten times the solitary pulse amplitude in Fig. 8. The excess energy is convected to the left and out of the system. The residual propagates to the right as part of a solitary pulse in a direction counter to normal convection, resembling the solitary pulse in Fig. 8. For the case of superposed, counter-streaming (colliding) solitary pulses with propagation velocities nearly equal and opposite $\lambda = \pm 1.0$, no return to steady propagation of solitary pulses is observed within the duration of the integration (see Fig. 10). In fact $|a_1|$ and $|a_3|$ in Fig. 10 appear to fragment into three localized components.

In interpreting these numerical experiments we emphasize that in all cases the three-wave interactions are initially localized; but, while some of the wave amplitudes are localized, others are not. The pump wave is present everywhere being proportional to $\tanh(x - \lambda t)$. If there is steady propagation of the interaction as a solitary pulse, then the interaction remains localized in the frame $x - \lambda t = \text{constant}$.

Zakharov and Manokov use the inverse scattering method to construct a prescription for the general solution of Eq. (41) to describe the resonant three-wave interaction of wave packets.²¹ They construct the necessary nonlinear operators in matrix form that render Eq. (41) equivalent to the solution of linear integral and differential equations. For the case of three-wave decay certain general classes of solutions are discussed; however, for specific initial conditions no explicit solutions are constructed in Ref. 21.

Zakharov and Manokov claim that if the pump velocity V_1 satisfies either the condition $V_3 < V_1 < V_2$ or $V_2 < V_1 < V_3$, then the wave envelopes can suffer large changes in their shape and incur spectral broadening due to the nonlinear interaction (nonlinear collision of the three interacting wave packets). However, no significant energy exchange occurs asymptotically at $t = \infty$. They further claim that if the pump velocity satisfies the condition $V_3 < V_2 < V_1$ and one considers collisions of wave packets a_1 with a_2 where initially ($t = -\infty$) $|a_1|, |a_2| \gg |a_3|$, then complete transfer can occur subject to a threshold condition on the energy in the interacting wave packets. If instead a_1 collides with a_3 where initially $|a_1|, |a_3| \gg |a_2|$ or if a_2 collides with a_3 where initially $|a_2|, |a_3| \gg |a_1|$, no final ($t = \infty$) redistribution of energy results.

If we include finite dissipation in Eq. (41) and generalize to a nonuniform medium, then following Rosenbluth^{11,23,52} we obtain the coupled equations

$$\begin{aligned}
 (\partial_t + v_1 + V_1 \partial_x) a_1 &= -i a_2 a_3 \exp(-i\kappa' x^2/2) \\
 (\partial_t + v_2 - V_2 \partial_x) a_2 &= -i a_3^* a_1 \exp(i\kappa' x^2/2) \\
 (\partial_t + v_3 + V_3 \partial_x) a_3 &= -i a_2^* a_1 \exp(i\kappa' x^2/2)
 \end{aligned} \tag{42}$$

The unit of time has been scaled so that the characteristic growth rate γ_0 of Raman backscatter instability in a uniform medium

($|a_1| \gg |a_2|, |a_3|$ and $\kappa' = 0$) is given by $\gamma_0^2 = |2u_0/c|^2 \omega_e \omega_0 \equiv |a_1|^2$. The complex amplitudes a_1 , a_2 , and a_3 correspond to u_0 , u_1 , and $\tilde{\phi}$ respectively.

The quantity $k_0(x) - k_1(x) - [\Omega^2 - \omega_e^2(x)]^{1/2} / (3v_e^2)^{1/2}$ is the difference between the spatially dependent beat wavenumber $\kappa(x) \equiv k_0(x) - k_1(x)$ and the wavenumber $k_p(x)$ satisfying the local dispersion relation for a Langmuir wave: $\Omega^2 = \omega_e^2(x) + 3k_p^2(x)v_e^2$. If we define $\kappa' \equiv (d/dx)\{k_0(x) - k_1(x) - [\Omega^2 - \omega_e^2(x)]^{1/2} / (3v_e^2)^{1/2}\}$, where $x = 0$ is the position of exact frequency and wavenumber matching, then the quantity $\kappa'x^2/2$ measures the spatially dependent phase mismatch of the three-wave coupling, produced by the plasma nonuniformity. The linear dissipation rates of the three waves are given by ν_1, ν_2 , and ν_3 respectively. The group velocities are denoted by V_1, V_2 , and V_3 which are all positive quantities, whose WKB variations are ignored.

For initial conditions corresponding to $|a_2|, |a_3| \ll |a_1|$, integration of Eq. (42) verified the linear parametric backscatter instability growth rate for a uniform plasma ($\kappa' = 0$), which in our units is $\gamma_0 = |a_1|$. For a nonuniform plasma assuming a linear density profile ($\kappa' = \text{constant}$), we obtain convective saturation with a net amplification factor $\exp(\pi\gamma_0^2 / |\kappa'V_1V_2|)$ for the backscattered amplitude provided negligible pump depletion occurs:

$|a_1^0| \gg \exp(\pi\gamma_0^2 / |\kappa'V_1V_2|) |a_2^0|$. A detailed examination of the influence of plasma nonuniformity on parametric instability appears in Ref. 22. In the limit of significant pump depletion, characteristic reversible oscillations of energy from the decay products a_2, a_3 to the pump wave a_1 were observed. We shall refer to this phenomenon as nonlinear oscillations.⁶⁶

The numerical integration of the system of Eqs. (42) corresponding to beat heating is shown in Figs. 11 and 12. In both the warm

and cold plasma cases we have set the input ratio equal to unity, $|a_1| = |a_2| = 1$, and chosen $|a_3| = 0$ initially. In Fig. 11 we assume a cold plasma with dissipation of the Langmuir wave assumed due to Coulomb collisions. The group velocity for the Langmuir wave vanishes, $V_3 = 0$; and we ignore the dissipation of the high frequency waves, $v_1 = v_2 = 0$. We select parameters $v_3 = 0.2$, $V_1 = V_2 = 1$, and $\kappa' = 0$. The results (Fig. 11) are reminiscent of those pictured in Fig. 1 of Section II.C.2, if we average over the nonlinear oscillations.

In our solutions for beat heating in Sections II.C.1 and II.C.2, we assumed that the density perturbation could be expressed in terms of the ponderomotive potential and the linear dielectric function. Our integrations here retain the time derivative and, in subsequent cases, the spatial derivative in the equation for the longitudinal response, Eq. (40). Numerical integrations of the coupled mode equations, retaining ∂_t and ∂_x in the equations for all three modes, Eq. (42), were performed with various dissipation rates. In the limit of rather large dissipation, $|v_3| \gg |\partial_t \ln \phi|$, $|V_3 \partial_x \ln \phi|$, the results of the integrations here conform with those in Section II.C.2. This regime of the nonlinear interaction corresponds to the plasma wave being overdamped on the slow, nonlinear time scale. With increasing plasma wave dissipation, the nonlinear oscillations diminish, and there is improved quantitative agreement with solutions where the small amplitude plasma wave is treated as being quasi-steadily driven.

The results of the integration of Eq. (42) in the warm plasma case are shown in Fig. 12 for parameters $V_1 = V_2 = 5$, $V_3 = 1$, $v_1 = v_2 = 0$, $v_3 = 0.2$, and $\kappa' = 0$. The convection of the Langmuir

wave appears as an asymmetric distortion in space of its amplitude, $a_3(x,t)$ in Fig. 12. The effect of convection can be viewed as a spatially dependent dissipative term $v_{\text{eff}}(x) = V_3 \partial_x$. Then increasing V_3 is similar to increasing the dissipation v_3 . Nonlinear oscillations decrease; however, there is a pulse asymmetry or distortion produced by the sign change in $V_3 \partial_x$ operating on the front as compared to the back of the plasma wave envelope $a_3(x,t)$ (see Fig. 12). The three-wave interaction dominated by convection (Fig. 12) is otherwise qualitatively similar to that dominated by dissipation (Fig. 11), which agrees with the conclusion of Ref. 58.

In this section we have seen how beat heating is influenced by relaxing the assumption that $\phi \approx [\epsilon^{-1}(\Omega, \kappa) - 1] m u_0 u_1^* / e$, and by replacing it with a linearized wave equation for ϕ where $\partial_t \phi$ and $\partial_x \phi$ appear. We have reviewed the case of parametric instability. For the case of mode coupling when there is appreciable energy transfer from the pump to the decay products we have found two phenomena which can occur only when we retain ∂_t and ∂_x in our equations for all three modes: reversible nonlinear oscillations⁶⁶ and the propagation of solitary pulses.^{20,21} We have concluded this section by demonstrating under what circumstances solutions for the three-wave interaction with the terms $\partial_t \phi$ and $\partial_x \phi$ present are similar to those considered earlier without them, i.e., $\partial_t \phi = \partial_x \phi = 0$.

4. Introduction to Nonlinear Beat-Wave Effects

In this section we begin consideration of beat heating in the nonlinear beat-wave regime. We survey competing nonlinear phenomena and establish for what parameters electron trapping is the dominant nonlinear effect.

a. Onset of trapping in beat heating simulations

We have used simulations to investigate beat heating when the electrostatic wave becomes of sufficiently large amplitude to trap electrons. Trapping can cause resonant particles to act as an energy source or sink for the longitudinal wave which is scattering the photons. Consequently the overall efficiency of action transfer, and hence heating, can significantly decrease after the onset of trapping.

Once a large amplitude beat wave is excited, after an interval of time of the order

$$\tau_B \equiv 2\pi/\omega_B = 2\pi(2\kappa^2 e|\tilde{\phi}|/m)^{-\frac{1}{2}} \quad (43)$$

the "bounce period", the trapped particles can return energy and momentum to the longitudinal wave.⁶⁸⁻⁷⁵ If the orbit modification due to the trapping is included in the dielectric function, the dielectric function becomes time dependent; and its imaginary part changes sign on the time scale of the bounce period.⁷³ From Eq. (34), we see that the direction of action transfer consequently reverses (Fig. 13b): energy flows from the lower frequency electromagnetic wave and the electron plasma wave back to the higher frequency electromagnetic wave. This is observed in simulation whenever a significant fraction ($\geq 10\%$) of the particles is trapped.

We offer a theory for beat heating when the electron wave is no longer small in amplitude and when trapping is the principle nonlinearity. For trapping to be important, the longitudinal wave must be of sufficiently large amplitude to reach back into the distribution function and trap an appreciable fraction of particles. If we define a velocity characteristic of the trapping $v_T \equiv (2e|\tilde{\phi}|/m)^{\frac{1}{2}}$,

then the condition for trapping becomes $v_\phi - v_T \leq \mathcal{O}(2v_e)$ where v_ϕ is the phase velocity of the longitudinal wave and v_e is the electron thermal velocity. Moreover the period over which trapping occurs must be shorter than the length of the experiment τ_{exp} or the characteristic time for some ignored effect to become important τ_I (e.g., significant growth of modulational or parametric decay instability²⁴). We can then observe trapping if $\tau_B < \tau_{\text{exp}}, \tau_I$. Our simulations typically last times τ of order $100 \leq \omega_e \tau \leq 400$.

The condition for there to be an appreciable number of trapped particles can be rewritten as

$$v_T = (2e|\tilde{\phi}|/m)^{\frac{1}{2}} \geq v_e |2 - 1/\kappa\lambda_e| \quad (44)$$

Further if we replace the left side of (44) v_T by $2\pi/\kappa\tau_B$, we can neatly summarize all the above conditions on trapping as follows:

$$\tau_B < (2\pi/\kappa v_e) |2 - 1/\kappa\lambda_e|^{-1}, \tau_{\text{exp}}, \tau_I \quad (45)$$

In practice, for parameters of a particular simulation, one can use linear theory to predict $(2e|\tilde{\phi}|/m)^{\frac{1}{2}} v_\phi^{-1}$ or $|\tilde{n}|/n_0$ and to check the criteria above, Eq. (45), to ascertain a priori whether there will be much trapping. If we use Eq. (32) and assume $|\epsilon| \ll 1$, then we can evaluate the scalar potential and write the condition (44) as

$$|u_0 u_1^*| \geq (1/2)(2v_e - \omega_e/\kappa)^2 |\epsilon| \quad .$$

Motivated by Eq. (33), we propose that a suitable model for the linear or nonlinear dielectric function evaluated near a resonance ($\epsilon = 0$) is given by

$$\epsilon = 2(\Delta + i\nu)/\Omega \quad (46)$$

where Δ is the mismatch, ν is the dissipation rate, and the beat frequency Ω satisfies $\Omega \approx \omega_e$. We shall construct the nonlinear dielectric function in the next section. We have defined the mismatch as the difference between the beat frequency Ω and the Bohm-Gross frequency Ω_L : $\Delta \equiv \Omega - \Omega_L$, $\Omega_L \equiv (\omega_e^2 + 3\kappa^2\nu_e^2)^{\frac{1}{2}}$. If we assume that close to a resonance the frequency mismatch is small compared to the dissipation rate ($|\text{Re } \epsilon| \ll |\text{Im } \epsilon|$), then the criterion for appreciable trapping to occur is

$$|u_0 u_1^*| \geq (2\nu_e - \omega_e/\kappa)^2 (\nu/\omega_e) \quad (47)$$

To evaluate the second criterion, that trapping be observed during the experiment, we use Eqs. (10) and (43) to obtain

$$2|\tilde{n}|/n_0 = \omega_B^2/\omega_e^2 \quad (48)$$

From Eqs. (43) and (32), and again evaluating the linear dielectric function near resonance, we express the condition $\tau_B < \tau_{\text{exp}}$ as

$$|u_0 u_1^*| > (\omega_e/\kappa)^2 (\nu/\omega_e) (2\pi/\omega_e \tau_{\text{exp}})^2, \quad (49)$$

where we have made use of $\tau_B \equiv 2\pi/\omega_B \equiv 2\pi/\kappa\nu_T$. If the condition (47) is marginally satisfied then (49) takes on the form

$$\omega_e \tau_{\text{exp}} > 2\pi |1 - 2\kappa\lambda_e|^{-1}.$$

For realistic plasma parameters, e.g., a dense θ -pinch: $n_0 = 10^{17} \text{ cm}^{-3}$, $T_e = \mathcal{O}(50 \text{ eV})$, $\omega_e/\nu = 100$, $\kappa c/\omega_e = 10$, and CO_2 lasers (9.6 μm and 10.6 μm wavelengths, setting $|u_0| = |u_1|$), one obtains from (47)

$$|u_0|^2 \geq (v/\omega_e)v_e^2 = \mathcal{O}(3 \times 10^7 \text{ cm/sec})^2 \quad (50a)$$

and from Eq. (49)

$$(\omega_e \tau_{\text{exp}})^2 > (2\pi)^2 |u_0|^{-2} (v/\omega_e)(\omega_e/\kappa)^2 \quad (50b)$$

If (50a) is marginally satisfied and $\omega_e/\kappa = \mathcal{O}(3v_e)$, then to observe trapping we require $\omega_e \tau_{\text{exp}} > 6\pi$, which is quite easily satisfied in all our simulations.

b. Simulations of nonlinear beat heating: electromagnetic code

We have employed our electromagnetic simulation code to study beat heating when the electron wave traps particles. For the sake of simplicity the plasma was taken to be homogeneous. The simulations were severely limited however, by the finite plasma slab width being only of order five beat wavelengths (see Fig. 14). This leads to a certain number of unphysical effects which will be described in this discussion.

In our comments and observations concerning the simulations, some mention of temperature and heating is made. Temperature is calculated in the code by subtracting the (relativistic) kinetic energy density of the local sloshing motion of the particles from the total kinetic energy density, in the frame of the grid. Heating is defined as the time rate of change of the average local temperature.

In Fig. 13 the temperature and the action flux transfer are plotted as functions of time for a simulation exhibiting trapping (corresponding to Fig. 14). There is strong action transfer and heating at early times while the density disturbance and the distribution function modification are still linear. There then follows a marked decrease in the heating of the plasma at a time τ_B after

initiation of the beat disturbance, accompanying the reversal of action transfer. Meanwhile the velocity distribution function has evolved appreciably with a distended nonmaxwellian tail forming beyond the phase velocity and a plateau occurring near the beat-wave phase velocity (Fig. 14b).

Scattering continues, however, and there is a return of the heating and action transfer to somewhat diminished rates as compared to the early stage of strong beat heating. Beat heating continues as the three-wave interaction evolves into a regime best described as induced Thomson scattering, $\kappa\lambda_e \geq 0.35$.^{11,12,76} Now the beat-wave phase velocity falls much closer into the body of the velocity distribution function at a point where the distribution has negative slope (Fig. 14c). By the considerable modification of the distribution function and from the plot of the electron temperature, we observe that there has been considerable electron heating over a relatively short time: $\Delta T_e/T_e(0) \approx 5$ over $\omega_e \Delta t = 40$.

Figure 15 displays the results of several simulations of beat heating in a uniform, finite plasma slab where the increase in effective thermal velocity squared over the bounce period τ_B is plotted against initial ponderomotive potential in natural units $|u_0 u_1^*|c^{-2}$. We find empirically that $v_e^2(\tau_B) - v_e^2(0)$ is linearly proportional to $|u_0 u_1^*|$. We would be motivated to seek an explanation for this interesting result were it not for certain unphysical simulation effects that occur.

When there is appreciable trapping, particles absorb momentum from the beat-wave and are more readily carried to the right end of the system, where they are either electrostatically returned, or

elastically reflected if they reach the system wall. In a longer system, trapped particles would have a longer time to bounce back and forth in the potential well of the beat-wave, exchanging energy and momentum, before encountering the edge of the plasma. In our simulations after one or two bounce periods a significant fraction of the particles has been reflected from the right wall of the system. Once reflected these particles no longer can resonantly interact with the beat wave, and they artificially symmetrize the distribution function and phase space (Fig. 14c). In a more realistic plasma model strong wave particle interaction persists for a much longer time. Then additional dissipation mechanisms should be considered for finite amplitude beat waves, e.g., the side-band instability.⁷⁷ In the next subsection competing dissipation mechanisms, the electron-ion parametric decay and modulational instability,²⁴ are considered.

c. Competition of beat heating and beat-wave trapping with other effects

We begin by examining under what condition the two electromagnetic waves can propagate across the plasma to induce beat heating without first suffering significant attenuation due to parametric Raman backscatter instability. We shall subsequently investigate nonlinear processes competing with particle trapping by the beat-wave.

In Section II.C.3 we reviewed the result due to Rosenbluth et al.⁵³ describing the parametric amplification of decay products due to Raman backscatter in an inhomogeneous medium. The condition that appreciable pump attenuation occurs due to Raman backscatter in an inhomogeneous medium of scale length L_n is given by

$$L_n = 2\pi\gamma_0^2 / |\kappa' V_1 V_2| \gg 1. \quad ^{78,79} \quad \text{For the plasma parameters}$$

corresponding to a dense θ -pinch with $L = \mathcal{O}(10 \text{ cm})$ and CO_2 lasers, the condition becomes $|u_0|^2 \gg [L_n(\text{cm})]^{-1} (10^9 \text{ cm/sec})^2 = \mathcal{O}(10^{17} \text{ cm}^2/\text{sec}^2)$. Comparison with the threshold for trapping, given by expression (50a), indicates that trapping can occur without there being much attenuation due to Raman backscatter.

Because the ions are fixed in our simulations, there is no possibility for parametric decay, modulational instability,²⁴ or nonlinear Landau damping by ions. In a real plasma these processes will, however, compete with trapping. The thresholds for these processes can be quite low compared to trapping. But since their growth rates scale to a higher power in the small parameter v_T/v_ϕ , there is a regime of beat-wave strengths in which electron trapping occurs first.

To illustrate this, we examine the possible parametric electron-ion decay of the beat-wave. For purposes of discussion we quote the threshold and growth rate derived by Nishikawa²⁴ for the decay of an infinite wavelength Langmuir pump wave into finite wavelength Langmuir and ion acoustic waves. For the actual case of a finite wavelength beat wave acting as the pump, the thresholds for parametric decay or modulational instability are reduced but the growth rates do not change much.⁸⁰

Nishikawa found that the threshold for the decay instability is given by

$$\tilde{v}/v_e = 4(v_e v_i / \omega_e \omega_a)^{\frac{1}{2}}, \quad (51)$$

where \tilde{v} is the magnitude of the longitudinal oscillation velocity, v_s is the dissipation rate for the electron or ion acoustic wave,

and ω_a is the ion acoustic frequency. For the growth rate γ_{ei} of the decay instability, well above threshold, Nishikawa found

$$\gamma_{ei}/\omega_e = (1/4)(\kappa\lambda_e)^{\frac{1}{2}}(\tilde{v}/v_e)(m_e/m_i)^{\frac{1}{2}} . \quad (52)$$

It will be useful in the following to observe that from Eq. (43) and the electron longitudinal equation of motion we obtain $\tilde{v} = v_T^2/v_\phi$. From Eq. (32) and Eq. (43) we recall that $v_T^2 = 2|u_0 u_1^*|/|\epsilon|$. The threshold for trapping Eq. (44) can be rewritten as

$$\tilde{v}/v_e \geq \kappa\lambda_e |2 - (\kappa\lambda_e)^{-1}|^2 . \quad (53)$$

Comparison of Eq. (53) with Eq. (51) reveals that the threshold for decay instability can be very much lower than that for trapping in θ -pinches and laser-pellet plasmas, for example.

If we, however, compare the growth rate of parametric decay Eq. (52) to the electron bounce frequency $\omega_B \equiv \kappa v_T \approx \omega_e \tilde{v}/v_T$, we find that

$$\gamma_{ei}/\omega_B = (1/4)(m_e/m_i)^{\frac{1}{2}}(\kappa\lambda_e)^{\frac{1}{2}}(v_T/v_e) . \quad (54)$$

At threshold for trapping, described by an equality in (44), we obtain by substituting for v_T

$$\gamma_{ei}/\omega_B \rightarrow (1/4)(m_e/m_i)^{\frac{1}{2}}(\kappa\lambda_e)^{\frac{1}{2}}|2 - (\kappa\lambda_e)^{-1}| .$$

For $0.2 < \kappa\lambda_e < 0.4$ and $m_i \geq 1836 m_e$, then $\gamma_{ei}/\omega_B < \mathcal{O}(0.1)$. We conclude that trapping can occur before there is significant growth of the decay instability.

In our simulations trapping and the ensuing deformation of the velocity distribution function are the most important features affecting beat heating. There is also convection in both the linear and nonlinear regimes of beat heating which can produce effective loss and mismatch. To test the importance of convection, we recall the formulation of the coupled mode equations as considered in the previous section, Eqs. (40)-(42). In Eq. (40) the Coulomb potential, or, using Poisson's equation, the density perturbation satisfies a linearized wave equation driven by the ponderomotive force whose left side becomes (in the WKB limit)

$$(\partial_t + \nu + v_g^l \partial_x - i\Delta) \tilde{n}(x,t)$$

where v_g^l is the group velocity for an electron plasma wave, ν is the dissipation rate, and Δ is the frequency mismatch $\Delta \equiv \Omega - \Omega_L$. We can estimate the effect of convection as being of order $v_g^l/L = 3(\kappa^2 \lambda_e^2 / \kappa L) \omega_e = \mathcal{O}(0.01) \omega_e$ compared to $\nu = \mathcal{O}(0.1) \omega_e$ for typical simulations, where we have estimated $\partial_x \sim L^{-1}$ using the length of the plasma L .

We have therefore ignored convection and treat the beat disturbance as a wave driven near resonance with both damping and mismatch functions of time and implicitly of wave amplitude. We shall incorporate these nonlinearities into the slowly time dependent dielectric response of the plasma $\epsilon_{NL}(\Omega, \kappa; t) \equiv \epsilon' + i\epsilon''$. The nonlinear dielectric response is formulated by including the nonlinear, time dependent, complex frequency shift to the linear normal mode frequency due to trapped particles. We construct the nonlinear dielectric function and the nonlinear normal mode frequency in Section II.C.5.

d. Motivation for a model problem

The qualitative dependence of action transfer upon ϵ_{NL} has been verified in the fully electromagnetic simulations discussed so far. The difficulty with a quantitative analysis of ϵ_{NL} in our electromagnetic simulation derives from the finite length of the plasma which is only of order five beat wavelengths (see Fig. 14). In our simulations after a time as short as one or two bounce periods of a representative trapped electron, a large number of accelerated electrons have elastically scattered off the right-hand system boundary. The ensuing artificial symmetrization of the distribution function and the sudden termination of strong wave-particle interaction after wall reflection of an individual electron distort the evolution of nonlinear beat heating in an unphysical way. In addition there is a nonlinear oscillation of the entire plasma slab because of the accumulation of space charge at the slab edges due to the trapping. We have therefore constructed a model problem where we consider the ponderomotive force driving the beat wave as a fixed amplitude external driver in a uniform, infinite, periodic plasma.

For purposes of simplification, we hold the driver steady and simulate the electrostatic ponderomotive driver in a one dimensional, electrostatic particle code describing a periodic, homogeneous, warm electron plasma. Section II.C.5 takes up the theoretical analysis of the model problem generalized to include a time dependent driver amplitude and discusses the simulations. Section II.C.6 considers the consequent back-reaction of the nonlinear dielectric response on beat heating. Electrostatic simulations are performed with the previously fixed amplitude ponderomotive potential $\tilde{\phi}_0$ replaced by $m\omega_0 u_1^*/e$, and we integrate the linearized coupled mode equations (28)

describing u_0 and u_1 in the temporal limit ($\partial_x \rightarrow 0$). We emphasize that, in the model electrostatic simulations to follow, connection with our theory of beat heating is made by using the following expression for the ponderomotive potential:

$$\tilde{\phi}_0(x,t) = (m/e) u_0(x,t) u_1(x,t)^* . \quad (55)$$

Equation (55) is obtained from the relation between the vector potential and the transverse oscillation velocity, and from Eqs. (9) and (26).

5. Resonant Excitation of Nonlinear Plasma Waves

a. Introduction

There has been considerable experimental⁶⁸⁻⁷¹ and theoretical⁷²⁻⁷⁵ attention given the study of the damping and frequency shift of freely propagating, large-amplitude, longitudinal electron plasma oscillations. Relatively little work has been done concerning finite amplitude waves resonantly excited by the modulation of a high frequency wave^{17,81,82} or by the low frequency beat of two high frequency waves.^{34,43} In this section we study the propagation of resonantly excited, longitudinal plasma waves. We formulate the resonant plasma response from the point of view of considering the approach to a self-consistent equilibrium determined by a nonlinearly induced frequency shift. The formalism is based on the construction of a nonlinear normal mode, allowing for the time dependence of the nonlinear eigenfrequency.

b. General formulation of the model problem

For simplicity we consider an initial value problem, and assume the plasma is infinite and uniform. We begin by defining the total potential $\phi^S(x,t)$ to be the sum of the external potential $\phi_0^S(x,t)$ (possibly species-dependent, for example, a ponderomotive potential;⁴⁰⁻⁴² or a true external potential supplied by a grid or a slow-wave structure), and the self-consistent Coulomb potential $\phi(x,t)$: $\phi^S(x,t) = \phi(x,t) + \phi_0^S(x,t)$. (Litvak^{83,84} and S. Johnston⁷⁶ have exploited the utility of the idea of a beat-wave potential to high degree in describing induced scattering.) The unperturbed plasma is assumed to be spatially uniform; all wave forms and perturbed quantities have the same spatial phase dependence:

$\phi^S(x,t) \equiv \phi^S(t) \exp ikx + \text{c.c.}$ Poisson's equation can be written

$$\phi^S(t) - \phi_0^S(t) = 4\pi\kappa^{-2}\rho(t) \quad (56)$$

where $\rho(t)$ is the total charge density summed over species and over linear and nonlinear components, $\rho(t) \equiv \sum_S \rho^S(t) \equiv \sum_S [\rho_L^S(t) + \delta\rho^S(t)]$.

We postulate a relation for the nonlinear susceptibilities: $\rho^S(t) \equiv -[\kappa^2/4\pi] \int_0^\infty d\tau \hat{\chi}^S(\tau) \phi(t - \tau)$, with the wavenumber and amplitude dependence implicit. The kernels for the linear susceptibilities $\hat{\chi}_L^S(\tau)$ are obtained by replacing $\rho^S(t)$ with only its linear part $\rho_L^S(t)$ on the left side. If we separate the dominant time dependence, $\rho^S(t) = \tilde{\rho}^S(t) \exp[-i\Omega t] + \text{c.c.}$, and similarly for the potentials, we obtain

$$\begin{aligned} \tilde{\rho}^s(t) &= -[\kappa^2/4\pi] \int_0^\infty d\tau \hat{\chi}^s(\tau) \exp[i\Omega\tau] \tilde{\phi}(t - \tau) = \\ &-[\kappa^2/4\pi] \int_0^\infty d\tau \hat{\chi}^s(\tau) \exp[i\Omega\tau - \tau(d/dt)] \tilde{\phi}(t), \end{aligned} \quad (57)$$

where we have used the propagator $\exp[-\tau(d/dt)] \tilde{\phi}(t) = \tilde{\phi}(t - \tau)$. The operator (d/dt) within the argument of the exponential in Eq. (57) therefore only acts to the right.

Utilizing the definition of the Laplace transform of the susceptibility $\chi^s(\omega) \equiv \int_0^\infty d\tau \hat{\chi}^s(\tau) \exp[i\omega\tau]$, we sum Eq. (57) over species and substitute for $\rho(t)$ from Eq. (56), which we have rewritten in the form $\tilde{\phi}(t) = [4\pi/\kappa^2] \tilde{\rho}(t)$, to obtain

$$\epsilon(\Omega + id/dt) \tilde{\phi}(t) + \sum_s \chi^s(\Omega + id/dt) \tilde{\phi}_0^s(t) = 0. \quad (58)$$

We have defined the nonlinear dielectric function $\epsilon(\omega) \equiv \sum_s 1 + \chi^s(\omega)$, with its wavenumber and amplitude dependence implicit. For the frequency-like argument ω , we use $\Omega + i(d/dt)$. The differential operator again acts only to the right on $\tilde{\phi}(t)$ and $\tilde{\phi}_0^s(t)$.

If the external ion potential is negligible, which is the case for the $\underline{v} \times \underline{B}$ ponderomotive force (Eq. (8)) considered here, and for the ponderomotive forces considered in Refs. 12, 25, 40, 41, and 42, then Eq. (58) becomes

$$\epsilon(\Omega + id/dt) \tilde{\phi}^e(t) = [1 + \chi^i(\Omega + id/dt)] \tilde{\phi}_0^e(t).$$

If the external potential acts equally on the species, e.g., the potential due to a grid, or if the ion susceptibility is negligible, Eq. (58) gives $\epsilon(\Omega + id/dt) \tilde{\phi}^e(t) = \tilde{\phi}_0^e(t)$.

At this point we digress briefly to consider the concept of a nonlinear normal mode. In the absence of the external potential $\phi_0^s(t) \rightarrow 0$, and for slow time dependence $\Omega^{-1}(d/dt) \rightarrow 0$, Eq. (58) defines a nonlinear normal mode: $\epsilon(\omega_{NL}; \kappa, \tilde{\phi})\tilde{\phi} = 0$, i.e., $\epsilon(\omega_{NL}; \kappa, \tilde{\phi}) = 0$. If we express the nonlinear dielectric response as $\epsilon(\omega; \kappa, \tilde{\phi}) = \epsilon_L(\omega; \kappa) + \delta\epsilon(\omega; \kappa, \tilde{\phi})$, where $\delta\epsilon$ is the nonlinear increment to the dielectric function, then we can determine the complex, nonlinear normal mode frequency $\omega_{NL} \equiv \omega_L + \delta\omega$. The complex, linear normal mode frequency $\omega_L = \Omega_L + i\gamma_L$ is determined by $\epsilon_L(\omega_L, \kappa) = 0$, and $\delta\omega$ is then the complex, nonlinear frequency shift. We can Taylor series expand $\epsilon(\omega_{NL}; \kappa, \tilde{\phi})$ around ω_L to obtain $\epsilon(\omega_{NL}; \kappa, \tilde{\phi}) = \epsilon_L(\omega_L; \kappa) + \delta\epsilon(\omega_L; \kappa, \tilde{\phi}) + \bar{\epsilon}(\omega_L)\delta\omega + \dots = 0$ where $\bar{\epsilon} \equiv \partial\epsilon/\partial\omega$. Assuming $|\delta\omega/\omega_L| \ll 1$ in order to truncate the expansion, we find

$$\delta\omega = -\delta\epsilon/\bar{\epsilon}\Big|_{\omega_L; \kappa, \tilde{\phi}} \quad (59)$$

We return to Eq. (58) and now Taylor series expand ϵ around ω_{NL} to obtain $\epsilon(\omega_{NL} + \Omega - \omega_{NL} + id/dt) = \epsilon(\omega_{NL}) + \bar{\epsilon}(\omega_{NL})[\Omega - \omega_{NL} + i(d/dt)] + \dots$. We consequently find that to lowest order in $|\Omega - \omega_{NL} + i(d/dt)|/|\omega_{NL}| \ll 1$, and for $|\tilde{\phi}_0^i| \ll |\tilde{\phi}_0^e|$,

$$\bar{\epsilon}(\omega_{NL})[\Omega - \omega_{NL} + i(d/dt)] \tilde{\phi}^e(t) = [1 + \chi^i(\Omega + id/dt)] \tilde{\phi}_0^e(t) \quad (60)$$

Equation (60) describes the self-consistent evolution of the nonlinear plasma response $\tilde{\phi}(t)$ to the driver $\tilde{\phi}_0(t)$. The problem of explicitly deducing the nonlinear normal mode frequency ω_{NL} , and of evaluating Eq. (59) from a calculation of the actual orbit modifications induced by the finite wave amplitude, remains.

For $\tilde{\phi}_0^e(t) = 0$ and $|d \ln \tilde{\phi}(t)/dt| \rightarrow 0$, use of the Poisson equation and Eqs. (57) and (59) leads to

$$\delta\omega(t) = \left[4\pi/\kappa^2 \epsilon(\omega_L) \right] \left[\tilde{\rho}(t) - \tilde{\rho}_L(t) \right] / \tilde{\phi}(t) . \quad (61)$$

From Eq. (61), we observe that it is the nonlinear increment to the total charge density perturbation that gives rise directly to the complex frequency shift. We can make some progress in calculating the particle orbit modifications if we can assume that the wave amplitude is nearly constant, $d\tilde{\phi}/dt \approx 0$, i.e., $|d \ln \tilde{\phi}/dt| \ll |\delta\omega|$.^{72,73}

c. Application to the excitation of electron plasma waves

The separation of the linear and nonlinear plasma response is the essence of the subtraction procedure of Morales and O'Neil.⁷³ They appealed to a Vlasov analysis for a specific kinetic model from which they derived the dielectric function ϵ and deduced the temporal or spatial dependence of the free propagation of finite amplitude electron plasma waves. We can adopt for the driven-wave problem, the results of any specific calculation of orbit modifications due to finite wave amplitude for the free-wave problem, provided that in the kinetic description employed, the particle acceleration depends on the gradient of the total potential, $-\left[e_s/m_s \right] \nabla \phi^S(x,t)$. Thus results derived for the complex frequency shift $\delta\omega$, depending on $\tilde{\phi}$ in the problem of freely propagating waves, can be used to describe

the driven-wave problem, if we replace $\tilde{\phi}$ by $\tilde{\phi}^S$ in the particle orbit calculations and in the nonlinear eigenfrequency relation.

To illustrate our theoretical construction, we consider resonantly excited electron plasma waves in the case that trapping constitutes the principal nonlinear effect. If the plasma response is quasi-steady, i.e., if we can set $d/dt \rightarrow 0$ in Eq. (60), then we can utilize the calculation of Morales and O'Neil, for example, to deduce ω_{NL} and $\tilde{\phi}$ self-consistently. (We have dropped the superscript denoting that $\tilde{\phi}$ is the total potential for electrons.) At this point we emphasize the fact that Morales and O'Neil's theory is analytic and perturbative, but not self-consistent. As in most of the analytic theories⁷²⁻⁷⁵ describing trapping, the potential $\tilde{\phi}$ is assumed constant.

Specific application of Morales and O'Neil's theory requires that certain assumptions be valid to justify their perturbation expansion. The perturbation analysis requires that $v_T \Omega / \kappa \ll v_e^2$, i.e., weak nonlinearity, and in order that the wave amplitude be nearly constant $|\gamma_L| / \omega_B \ll 1$, i.e., weak Landau growth or damping relative to the bounce frequency. The two conditions require that $\Omega / \kappa \geq 4v_e$. We have defined the bounce frequency and the trapping velocity: $\omega_B \equiv \kappa v_T \equiv \kappa [2|e\tilde{\phi}|/m_e]^{1/2}$. At this point it is convenient to introduce the real and imaginary parts $\delta\omega(t) \equiv \delta\Omega(t) + i\delta\gamma(t)$ of the complex frequency shift.

To evaluate the right side of Eq. (61) we replace $\tilde{\phi}(t)$ by $\tilde{\phi}(t)$ in Morales and O'Neil's calculation. The unperturbed distribution function $f_0(v)$ is Taylor expanded to second order around Ω/κ to find that $\delta\Omega \propto d^2 f_0 / dv^2$ and $\delta\gamma \propto df_0 / dv$ evaluated at the phase

velocity Ω/κ . The time dependences of $\delta\Omega(t)$ and $\delta\gamma(t)$ are shown in Figs. 1 and 2 of Ref. 73. Morales and O'Neil find that the dissipation $-\left[\gamma_L + \delta\gamma(t)\right]$ has a damped, oscillatory time dependence with frequency ω_B and phase-mixes to zero over a time $\mathcal{O}(5 \text{ to } 10)(2\pi/\omega_B)$. The frequency shift oscillates at $2\omega_B$ and asymptotically approaches a value,

$$\delta\Omega(t \rightarrow \infty) = -1.63 \delta\Omega_0 \quad (62)$$

where $\delta\Omega_0 = \text{Re} \bar{\epsilon}_L^{-1}(\Omega_L) v_T \left[\omega_e^2 / \kappa^2 \right] d^2 f_0 / dv^2$. Asymptotically there is no dissipation, but the resonantly excited wave acquires a finite negative frequency shift proportional to ω_B .

d. Equilibrium response

The vanishing of the total dissipation and the approach of the frequency shift to a steady value determine an equilibrium. By setting $(d/dt) = 0$ in Eq. (60) and defining the relative response $R \equiv \tilde{\Phi}/\tilde{\Phi}_0$, the normalized linear mismatch frequency $\Delta_L \equiv \bar{\epsilon}(\omega_{NL}) \left[\Omega - \Omega_L \right]$, and the normalized nonlinear frequency shift $\delta\Delta(|R|) \equiv \bar{\epsilon}(\omega_{NL}) \delta\Omega(t = \infty)$, we can describe the equilibrium by

$$\left[\Delta_L - \delta\Delta(|R|) \right] R = 1 \quad (63)$$

If we express the response as $R \equiv r \exp(i\theta)$ where $r \equiv |\tilde{\Phi}/\tilde{\Phi}_0|$ and θ is the relative phase, then Eq. (63) becomes

$$\left[\Delta_L - \delta\Delta(r) \right] r = \pm 1 \quad (64)$$

The sign of the right-hand side of Eq. (64) corresponds to a value of $\theta = 0$ or π , which is determined by the sign of $\Delta_L - \delta\Delta(r)$.

Equation (64) implicitly determines the magnitude r of the response. If we attempt to prepare the linear mismatch and wave amplitude in such a manner as to make $\Delta_L - \delta\Delta(r)$ vanish, or a random fluctuation in the response occurs to effect the same, then according to Eq. (64) the response r should diverge. Rather than diverge, however, the response exhibits finite dissipation and time dependence necessarily. The approach to a new equilibrium is then described once again by Eq. (60).

For the case of trapped electrons the nonlinear frequency shift can be modeled $\delta\Delta(r) = -\alpha r^{\frac{1}{2}}$ where Eq. (62) determines α . Then Eq. (64) leads to a cubic equation in the variable $r^{\frac{1}{2}}$ describing the possible equilibria. Presuming the plasma parameters to be fixed, the free parameter governing the nature of the equilibria is the normalized linear mismatch Δ_L . The driver amplitude has been removed by scaling, $r \equiv |\tilde{\phi}/\tilde{\phi}_0|$.

Figure 16 illustrates graphically the nature of the possible equilibria. For $\Delta_L > 0$ there is only one equilibrium possible. Multiple equilibria occur for $\Delta_L < 0$ and $(-\Delta_L)^3 \geq (27/4)\alpha^2$. We conclude that at least one equilibrium solution always exists and is described by Eq. (64) subject to its consistency with earlier assumptions on the weakness of the nonlinearity. We defer discussion of the stability of the equilibrium until after we consider momentum and energy transfer.

e. Energy and momentum conservation laws

To understand the time dependence of the nonlinear frequency shift and dissipation, and consequently to appreciate some of the details of the approach to and departure from equilibrium, we calculate

the energy and momentum exchange between the driving potential and the nonlinear plasma response. The derivation here assumes no particular kinetic model for the plasma. The momentum and energy balance considerations of Morales and O'Neil⁷³ are generalized to the case of an externally driven plasma wave.

For the momentum exchange, we express the time derivative of the momentum density P averaged over the length $\lambda \equiv 2\pi\kappa^{-1}$,

$$\begin{aligned} dP/dt &= \int (dx/\lambda) \left\{ \rho \left[-\partial_x \phi_0(x,t) - \partial_x \phi(x,t) \right] \right\} = \\ & i\kappa\rho(t) \tilde{\phi}^*(t) + \text{c.c.} + \mathcal{O}(|\phi|^4) . \end{aligned} \quad (65)$$

We have used the identity $0 = \int dx \rho \nabla \phi(x,t)$ in obtaining Eq. (65).

The higher order terms in Eq. (65) will be ignored. Using

$$\begin{aligned} \tilde{\rho}^s(t) &= -[\kappa^2/4\pi] \chi^s(\Omega + id/dt) \tilde{\phi}^s(t), \text{ we sum over species to obtain} \\ \tilde{\rho}(t) &= [\kappa^2/4\pi] \left\{ \left[1 - \epsilon(\Omega + id/dt) \right] \tilde{\phi}(t) - \sum_s \chi^s(\Omega + id/dt) \tilde{\phi}_0^s(t) \right\} . \end{aligned}$$

Appropriate to the electron wave case, we ignore ion contributions and expand $\epsilon(\Omega + id/dt)$ around ω_{NL} , as in Eq. (60), in order to express the right side of Eq. (65) as a function of $\tilde{\phi}$.

We can formally express the nonlinear contribution to $\bar{\epsilon}$ in Eq. (60) as follows: $\bar{\epsilon}(\omega_{NL}) \equiv (\partial/\partial\omega)(\epsilon_L + \delta\epsilon)|_{\omega_{NL}} =$
 $\bar{\epsilon}_L(\omega_{NL}) + \partial\delta\epsilon/\partial\omega|_{\omega_{NL}} \approx \left[\bar{\epsilon}_L + \delta\omega(\partial\bar{\epsilon}/\partial\omega) + \partial\delta\epsilon/\partial\omega \right]_{\omega_L} =$

$\bar{\epsilon}_L \left[1 + \partial(\delta\epsilon/\bar{\epsilon}_L)/\partial\omega \right] \equiv \bar{\epsilon}_L [1 + \beta]$, where we have used Eq. (59). We

evaluate $\bar{\epsilon}_L$ and $\beta \equiv \partial(\delta\epsilon/\bar{\epsilon}_L)/\partial\omega$ at ω_L . At this point we intro-

duce an explicit ordering scheme suggested by theory and verified in

our simulations: we assume that $\Omega, \Omega_L \sim \mathcal{O}(1)\omega_e$;

$\omega_B, \delta\Omega, \omega_e \text{ Re } \beta, (\Omega - \Omega_L), (d/dt) \sim \mathcal{O}(\eta)\omega_e$; and $\omega_e \text{ Im } \beta, \gamma_L, \delta\gamma \sim \mathcal{O}(\eta^2)\omega_e$,

where $\eta \ll 1$.

From Eq. (65), we then find that to lowest order in η the momentum exchange is given by

$$dP/dt = \kappa \operatorname{Re} \bar{\epsilon}_L \left[(d/dt) - 2(\gamma_L + \delta\gamma) \right] |\kappa\tilde{\phi}|^2/4\pi \quad (66)$$

Transposing the time derivative of the linear wave momentum, $(d/dt) \kappa \operatorname{Re} \bar{\epsilon}_L |\kappa\tilde{\phi}|^2/4\pi$, to the left side of Eq. (66), we can reduce Eq. (66) to a statement describing the momentum in the resonant particles:

$$(d/dt) \left[P - \kappa \operatorname{Re} \bar{\epsilon}_L |\kappa\tilde{\phi}|^2/4\pi \right] = -2(\gamma_L + \delta\gamma) \kappa \operatorname{Re} \bar{\epsilon}_L |\kappa\tilde{\phi}|^2/4\pi \quad (67)$$

The momentum P can be thought of as the sum over the linear and nonlinear parts of the wave momentum, and the particle momentum in resonant and nonresonant particles exclusive of that attributed to the wave momentum. Thus on the left side of Eq. (67) the linear wave momentum has been subtracted, leaving to lowest order in η the linear and nonlinear changes of the momentum in the resonant particles. We have generalized to the nonlinear case the linear concept that the change in the momentum of the nonresonant particles, exclusive of the wave momentum, is negligible.

For the energy exchange we construct the time derivative of the average kinetic energy density K , integrating by parts and using the continuity equation and Parseval's equality,

$$dK/dt = \int (dx/\lambda) J \left(-\partial_x \Phi \right) = - \int (dx/\lambda) \Phi (d\rho/dt) =$$

$$\left[\kappa^2/4\pi \right] \tilde{\phi}^* \left[-i\Omega + (d/dt) \right] \left[\epsilon(\Omega + id/dt) - 1 \right] \tilde{\phi} + \text{c.c.} + \mathcal{O}(|\tilde{\phi}|^4) \quad (68)$$

where J is the longitudinal current density. In the extensive algebraic manipulation that Eq. (68) leads to, we assume the same ordering scheme used earlier and calculate the kinetic energy in the driven wave frame, i.e., $\Omega = 0$. If we substitute

$$\epsilon(id/dt) \approx \bar{\epsilon}(\omega_{NL}) \left[\Omega - \omega_{NL} + i(d/dt) \right] + (1/2) \bar{\epsilon}(\omega_{NL}) \left[\Omega - \omega_{NL} + i(d/dt) \right]^2$$

and define the linear wave action density $J_{\kappa}(t) = \text{Re } \bar{\epsilon}_L |\kappa\tilde{\phi}(t)|^2/4\pi$,

we find that to $\mathcal{O}(\eta^3)$

$$\begin{aligned} (d/dt) \left\{ K - \left[(\Omega - \Omega_L) J_{\kappa} - |\kappa\tilde{\phi}|^2/4\pi \right] \right\} = \\ - \left[\delta\Omega(d/dt) + 2(d\delta\Omega/dt) \right] J_{\kappa} + \text{Re } \bar{\epsilon}_L (\kappa^2/4\pi) \left[i\tilde{\phi}^*(d^2/dt^2)\tilde{\phi} + \text{c.c.} \right] \end{aligned} \quad (69)$$

In the plasma frame, the linear wave energy of a free wave ($\tilde{\phi} = \tilde{\phi}$) is given by $\left[\partial(\omega \text{Re } \epsilon_L)/\partial\omega \right]_{\Omega_L} |\kappa\tilde{\phi}(t)|^2/4\pi = \Omega_L J_{\kappa}$. Because the driven wave is excited at frequency Ω rather than at Ω_L , we must evaluate $\left[\partial(\omega \text{Re } \epsilon_L)/\partial\omega \right]$ at Ω , which gives $\left[\Omega + (\Omega - \Omega_L) \right] J_{\kappa}$ for the linear wave energy in the plasma frame (in the driven wave frame: $(\Omega - \Omega_L) J_{\kappa}$). Since the field energy is given by $|\kappa\tilde{\phi}|^2/4\pi$, the left side of (69) is the time derivative of the total particle kinetic energy with the kinetic part of the linear wave energy subtracted away. We interpret the residual as the energy exchange rate due to resonant particles, evaluated in the driven wave frame. Then to lowest order in η , we have the expression

$$\begin{aligned} (d/dt) K_R^W = - \left[2(d\delta\Omega/dt) + \delta\Omega(d/dt) \right] J_{\kappa} \\ + \text{Re } \bar{\epsilon}_L (\kappa^2/4\pi) \left[i\tilde{\phi}^*(d^2/dt^2)\tilde{\phi} + \text{c.c.} \right] \end{aligned} \quad (70)$$

where we define $K_R^W \equiv K - [(\Omega - \Omega_L)J_\kappa - |\kappa\tilde{\phi}|^2/4\pi]$ as the average kinetic energy density of the resonant particles in the driven wave frame.

We now introduce a simple model which illustrates some of the physics hidden in Eqs. (67)-(70). Our objective is to gain insight into how the trapped particles can give rise to time dependence in the dissipation and the frequency shift. The model crudely represents the resonant, trapped particles by a clump of density n_T oscillating in the wave frame with velocity $v = v_T \sin \omega_B t$. Effects due to the time dependence of the resonant, but untrapped, particles and due to nonlinear orbit modification of the nonresonant particles are ignored. Furthermore, we make no attempt to include phase-mixing.

The momentum and kinetic energy of the resonant, trapped particles are given by $P_R = n_T m\Omega/\kappa + n_T m v_T \sin \omega_B t$ and $K_R^W = (1/2)n_T m v_T^2 \sin^2 \omega_B t$ in the driven wave frame. Since the depth of the potential well seen by a trapped particle in the wave frame is influenced by the presence of the other trapped particles via Poisson's equation, the potential acquires a time dependence $\tilde{\phi}(t) \approx \phi^{(0)} + \phi^{(1)} \exp - i\omega_B t$.

We substitute into Eqs. (67) and (70) our model equations for the momentum and kinetic energy of the trapped particles in the wave frame and for the time dependent potential amplitude. We obtain to $\mathcal{O}(n^2)$ the momentum,

$$n_T m v_T \omega_B \cos \omega_B t = -2(\gamma_L + \delta\gamma)\kappa \operatorname{Re} \bar{\epsilon}_L |\kappa\phi^{(0)}|^2/4\pi. \quad (71)$$

-71-

We deduce from Eq. (71) that the total dissipation has a time dependence given by $-(\gamma_L + \delta\gamma) \propto \cos \omega_B t$. This is a lower order effect than the time dependence of the nonlinear frequency shift, which is $\mathcal{O}(\eta^3)$.^{72,73} To further examine the time dependence of the wave amplitude, the dissipation, and the frequency shift at frequency ω_B , we substitute the Fourier series $\tilde{\phi}(t) = \phi^{(0)} + \phi^{(1)} \exp -i\omega_B t + \dots$ and $\delta\omega = \delta\omega^{(0)} + \delta\omega^{(1)} \exp -i\omega_B t + \dots$ into Eq. (60). The lowest order time independent part of Eq. (60) is given by $\bar{\epsilon}^{(0)} \Delta\omega^{(0)} \phi^{(0)} = \tilde{\phi}_0$, where $\Delta\omega^{(0)} \equiv \Omega - \Omega_L - \delta\Omega^{(0)}$. Subtracting this from Eq. (60) and collecting terms with $\exp -i\omega_B t$ time dependence, we find to lowest order in η

$$\bar{\epsilon}^{(0)} \Delta\omega^{(0)} \phi^{(1)} - \bar{\epsilon}^{(0)} [\delta\Omega^{(1)} + i\gamma^{(1)}] \phi^{(0)} + \bar{\epsilon}^{(0)} \omega_B \phi^{(1)} = 0 \quad (72)$$

Then both the dissipation and the component of the frequency shift oscillating at ω_B are related to the wave amplitude oscillations:

$$\delta\Omega^{(1)} + i\gamma^{(1)} = [\Delta\omega^{(0)} + \omega_B] \phi^{(1)} / \phi^{(0)} \quad (73)$$

The time dependence of the frequency shift and the dissipation in our simulation concurs with that described in Eqs. (71) and (73), implying that the model time dependence of the velocity of the clump of trapped particles and the potential amplitude are consistent. Furthermore, we can use the equation for the kinetic energy to deduce that the frequency shift can oscillate at $2\omega_B$ as well as at ω_B . Substitution of our models for the time-dependent wave amplitude and the trapped particle velocities into Eq. (70) yields

$$(1/2)n_T m v_T^2 \omega_B \sin(2\omega_B t) = \left\{ -2(d\delta\Omega/dt) + 2\omega_B(\omega_B - \delta\Omega) \right. \\ \left. \times \text{Im} \left[\left[\phi^{(1)} / \phi^{(0)} \right] \exp -i\omega_B t \right] \right\} \text{Re} \bar{\epsilon}_L |\kappa\phi^{(0)}|^2 / 4\pi \quad (74)$$

Equation (74) suggests that the frequency shift $\delta\Omega$ has time dependence at both the bounce frequency ω_B and twice the bounce frequency $2\omega_B$. For the case of a free wave, Morales and O'Neil find that for $v_T v_\phi \ll v_e^2$ and $v_\phi \geq 4v_e$ the time dependence at frequency $2\omega_B$ dominates.⁷³ In the work of O'Neil, Winfrey, and Malmberg⁸⁵ however, the frequency shift of a large amplitude electron plasma wave excited by the weak beam-plasma instability varies at both ω_B and $2\omega_B$, with the former dominant.

We can Fourier analyze Eq. (74) to determine the relative variations of the frequency shift at the frequencies ω_B and $2\omega_B$. In so doing we recall the assumptions that $|\phi^{(1)}/\phi^{(0)}| \sim \mathcal{O}(\eta)$ and that $\delta\Omega, \omega_B \sim \mathcal{O}(\eta)\omega_e$. Then from Eq. (74) we find that to lowest order in η

$$\delta\Omega^{(1)} \sim \mathcal{O}[\delta\Omega^{(0)} - \omega_B] |\phi^{(1)}/\phi^{(0)}| \quad (75)$$

and

$$\delta\Omega^{(2)} \sim \mathcal{O}[(\omega_e/8) L_T m v_T^2 / \omega_e J_K] . \quad (76)$$

In our simulations we find that the oscillation in the frequency shift at ω_B dominates that at $2\omega_B$. The magnitude of $\delta\Omega^{(1)}$ in simulation is consistent with Eq. (75) to within 25%, if we use $\delta\Omega^{(0)}$ from the simulation directly or if we take $\delta\Omega^{(0)} \approx -(3/4)v_\phi^3 d^2 f_0 / dv^2$ as given by Morales and O'Neil's theory.

f. Stability of equilibria

The stability of the nonlinear equilibrium Eq. (64) can be examined by employing Eq. (60) and considering a complex, infinitesimal perturbation to the equilibrium plasma response of the form

$\delta R \equiv (r + \delta r) \exp(i\theta + i\delta\theta) - r \exp(i\theta)$. If we define the dimensionless quantity $\tau \equiv \bar{\epsilon}^{-1} t$ and derivative $\dot{x} \equiv dx/d\tau$ and ignore the nonlinear dissipation perturbed from its equilibrium value of zero, then from Eqs. (60) and (64) we obtain the coupled equations:

$$r^2 \dot{\delta\theta} - \delta r (\pm 1 + \alpha r^{3/2}/2) = 0 \quad (77a)$$

and

$$\dot{\delta r} \pm \delta\theta = 0 \quad (77b)$$

The + and - signs correspond to equilibrium phases $\theta = 0$ and π respectively.

Differentiation of Eqs. (77) with respect to τ and straightforward algebraic manipulation give

$$r^2 (d^2/d\tau^2) \begin{bmatrix} \delta\theta \\ \delta r \end{bmatrix} + (1 \pm \alpha r^{3/2}) \begin{bmatrix} \delta\theta \\ \delta r \end{bmatrix} = 0 \quad (78)$$

The frequency of a stable oscillation or the growth rate of instability is given by $(1 \pm \alpha r^{3/2}/2)^{1/2}/\bar{\epsilon} r$. Recalling that the equilibrium is described by Eq. (64), $\alpha r^{3/2}$ can be replaced by $\pm 1 - \Delta_L r$ wherever convenient.

We observe from Eq. (78) that for $\theta = 0$ the equilibrium is obviously stable, $1 + \alpha r^{3/2}/2 > 0$. For $\theta = \pi$ and $\Delta_L < 0$, multiple equilibria can occur if $(-\Delta_L)^3 \geq 27\alpha^2/4$. The condition for stability in this case, $\alpha r^{3/2} < 2$ or equivalently $\alpha r^{1/2} < -2\Delta_L/3$ using Eq. (78), coincides with the equilibrium response r_1 lying to the left of the minimum of $r[\Delta_L - \delta\Delta(r)]$ in Fig. 16b, given by $\alpha r^{1/2} = -2\Delta_L/3$. Thus we conclude that for a large response, in phase

with the driver, the equilibrium is stable, corresponding to r_0 or r_3 in Fig. 16b.

For sufficiently large, negative linear frequency mismatch, a pair of additional equilibria are possible, corresponding to r_1 and r_2 in Fig. 16b, of which only r_1 is stable.⁴¹ Both r_1 and r_2 have relative phase π with respect to the driver. Our simulations correspond to $\alpha \approx 0.4$ and $\Delta_L \approx -0.33$ which do not satisfy the condition for multiple equilibria. We therefore expect the simulated equilibrium to be stable as it corresponds to r_0 in Fig. 16b.

We point out that one cannot rigorously omit the perturbed nonlinear dissipation. Without going into a detailed derivation we, however, can make some qualitative remarks. From the conservation laws we observe that the nonlinear dissipation is fundamentally related to the nonlinear momentum. The trapped particles have no momenta in the wave frame. The untrapped particles have either positive or negative momenta in the wave frame depending on whether they travel faster or slower than the wave. A perturbation to the wave amplitude and its phase, will alter the separatrix, trapping or detraping particles and consequently producing a small momentum exchange. The momenta of the particles remaining trapped is still zero. However, the momenta of the free particles and the wave itself will be altered since they are wave amplitude dependent.

In conjunction with the momentum exchange there will be a dissipation increment as described by Eq. (67). We expect the unstable equilibrium to remain unstable, the growth rate acquiring a complex increment perhaps. For the "stable" equilibria the influence of positive or negative dissipation may cause the oscillations about the

equilibrium to grow or relax. Our simulations indicate that for the equilibrium labeled r_0 in Fig. 16 the dissipation increment is such that perturbations relax, and the equilibrium is stable.

g. Simulations with constant-amplitude ponderomotive potential

To illustrate and apply our theoretical construction we have performed computer simulations. For the sake of simplicity we have considered a model in which the plasma is unmagnetized, uniform, and periodic. Electron plasma oscillations are excited with a fixed ion background. The computer simulation uses a finite-sized particle code originally furnished by A. B. Langdon and extended by this author and G. Smith. We simulate the entire Maxwellian velocity distribution with a modest number of particles (2500) and mesh points (64) in one dimension.

Many researchers have investigated in simulation the free propagation of electron plasma waves studying the effects due to wave particle resonance.⁸⁶⁻⁹² Particular attention has been paid to the case of finite γ_L/ω_B .^{86-89,92} Resonantly excited ion waves have been recently considered by Book and Sprangle.⁹³ In our simulations we resonantly excite an electron plasma wave of finite wavelength equal to the system length.

We have attempted to simplify our simulation model as much as possible. Because of the discrete Fourier spectrum, excitation of a large amplitude electron wave at the fundamental wave length cannot give rise to the sideband instability;⁷⁷ the spacing of wavenumbers around the fundamental is much too broad to accommodate the spacing of the sidebands $\pm\Delta k \approx \pm\omega_B\omega_e/3kV_e^2$. Furthermore, since the ions are held fixed, parametric decay and modulational instability are

excluded.²⁴ We measure directly in simulation the amplitude and phase of the total electric field amplitude $-ik\tilde{\phi}$ relative to the ponderomotive force $-ik\tilde{\phi}_0$. Then use of Eq. (60) permits identification of the nonlinear dissipation and frequency shift as functions of time (Fig. 18). Comparison of the asymptotic frequency shift with theory, Eq. (62), is made in Fig. 19.

Results of typical simulations are shown in Figs. 17, 18, and 19. For the set of simulations, the electron distribution was initially Maxwellian with parameters $\Omega/kv_e = 3.0$, $\kappa\lambda_e = 0.33$, and $\Omega = \omega_e$. Therefore the linear mismatch derived from the Bohm-Gross dispersion relation is $\Omega - \Omega_L = -0.17 \omega_e$, and the linear dissipation is $-\gamma_L/\omega_e \approx 0.03$. In Figure 17 we observe the characteristics of the large amplitude response (shown here driven in phase with the ponderomotive force), electron phase space, and the velocity distribution all at $\omega_e t = 300$. There is evidence of considerable trapping. Particles are trapped much closer to the separatrix than to the bottom of the potential well, however. The typical orbital period of these particles in the wave frame is of order $6\pi/\omega_B$ and concurs with the observed oscillation period of the nonlinear dissipation in Fig. 18b. We seem to have a preponderance of particles trapped fairly high in the potential well and relatively few down at the bottom; this gives rise to the hole observed in phase space, Fig. 17b.

We recall that from Eqs. (71) and (76) we expect both the nonlinear dissipation and the frequency shift to vary at frequency ω_B for our parameters ($v_\phi = 3 v_e$). We observe in Fig. 18 that $-(\gamma_L + \delta\gamma)$, $\delta\Omega$, and the amplitude and phase of the response all vary at the bounce frequency, but not at the bounce frequency of the deeply

trapped particles. Instead it is the average bounce frequency of the bulk of the particles trapped near the separatrix that determines the time dependence of $-(\gamma_L + \delta\gamma)$ and $\delta\Omega$. To understand this and other features in our simulations, we must appreciate certain conditions of the simulations not anticipated by existing analytic theory.

Rather large amplitude waves have been induced in the simulations, i.e., $v_T v_\phi \approx v_e^2$. Since $v_\phi = 3v_e$ initially, the trapping width v_T is large enough to extend back into the main body of the distribution function to do considerable trapping (Fig. 17c). With only 2500 particles, we do not have good statistics for the particles that become deeply trapped, i.e., the nearly, exactly resonant particles $v \approx v_\phi$. The trapping then of relatively many particles near the separatrix and fewer deeper in the potential well is not so surprising.

The ponderomotive potential amplitude was varied over a range such that $0.2 \leq \kappa v_T / \Omega \leq 0.6$ in order to check the dependence of the nonlinear frequency shift on the total potential amplitude (Fig. 19). The ponderomotive potential was switched on instantaneously and also over rise-times $\omega_e t = 50\pi$ which was of order two or three characteristic bounce periods of the simulated trapped electrons. More rapid phase-mixing and relaxation to equilibrium (in terms of the number of bounce periods $2\pi/\omega_B$) was observed for the slower driver switch-on and for weaker amplitudes, effects similar to those in Kruer's simulations.⁹⁴ The initial conditions and the rise-time of the driver influence the details of the asymptotic state. However, as the slower drive switch-on was not very long compared to a typical bounce period, the asymptotic state was not significantly different from the sudden switch-on case (Fig. 19).

The power law dependence $\delta\Omega(t = \infty) \propto |\tilde{\phi}|^{\frac{1}{2}}$ and magnitude of the frequency shifts seem to roughly agree with the nonlinear normal mode calculation of Morales and O'Neil, although both the ratio $v_{\phi}/v_e = 3.0$ and magnitude of the wave amplitude $v_T v_{\phi} \approx v_e^2$ lie outside the regime where their theory is applicable. The nonlinear frequency shifts are quite appreciable $\delta\Omega = -\mathcal{O}(0.10 \text{ to } 0.25)\omega_e$, and the distribution functions are considerably perturbed acquiring distinct tails at $v > \Omega/\kappa$. The body of the distribution functions remain approximately Maxwellian, however. Furthermore, the wave amplitude and phase in simulation show appreciable variation, although the relative changes are not large. Thus the particle trajectories have slightly different histories as compared with Morales and O'Neil's theoretical description. We therefore conclude that the quantitative agreement of the simulated asymptotic frequency shift with theory (Fig. 19) is quite remarkable.

For the case of resonantly excited, longitudinal waves in a uniform, unmagnetized plasma, we have constructed the nonlinear dielectric response. We have formulated the resonant response in terms of the mismatch between the driving frequency and the time-dependent, complex, nonlinear eigenfrequency of a normal mode. We have used simulations to illustrate our formalism and find that simulations compare remarkably well with nonlinear normal-mode theory in a regime of parameters outside the range where analytic perturbation theory is valid. We have derived energy and momentum conservation laws and used them to explain phenomena observed in the simulations, for example the time dependence of the response.

6. Beat Heating with Trapped Electrons

We return to our discussion of beat heating for large amplitude beat waves. Now that we understand to some extent the role that finite amplitude effects play in determining the resonantly excited response of the plasma when the driving potential has a fixed amplitude, we examine the back-reaction that the nonlinear, time-dependent response has upon the ponderomotive potential. Specifically, we investigate beat heating, relaxing the constraint that the ponderomotive potential has a constant amplitude. We consider the entire system composed of the coupled mode equations describing the transverse wave amplitudes u_0 and u_1 , Eqs. (28); the Poisson equation, Eq. (10); the equation describing the nonlinear dielectric response, given in the temporal limit ($\partial_x = 0$) by Eq. (60); and the constitutive relation between ϕ_0 and $u_0 u_1^*$, Eq. (55). We shall also discuss further simulations and make some remarks on the influence of plasma inhomogeneity on trapping and beat heating.

a. General consideration of the coupled mode equations

We recall Eq. (29) which expresses the conservation of transverse wave action. The equation is rewritten here defining the operators $D_{0,1} \equiv \partial_t \pm c_{0,1} \partial_x$, where $c_\ell \equiv k_\ell c^2 / \omega_\ell$ are the group velocities, and the transverse wave actions $J_\ell \equiv \omega_\ell |u_\ell|^2$: then Eq. (29) becomes

$$D_0 J_0 + D_1 J_1 = 0 \quad . \quad (79)$$

Introducing the phases $\theta_{0,1}$, defined by $u_{0,1} \equiv |u_{0,1}| \exp(-i\theta_{0,1})$, we manipulate Eq. (28) to obtain the relation

$$J_0 D_0 \theta_0 - J_1 D_1 \theta_1 = 0 \quad (80)$$

We can rewrite Eq. (30) describing the rate of action transfer as

$$D_0 J_0 = -D_1 J_1 = -\omega_e^2 \operatorname{Im}(u_0 u_1^* \tilde{n}^*/n_0) \quad (81)$$

and similarly for the phases

$$J_0 D_0 \theta_0 = J_1 D_1 \theta_1 = \omega_e^2 \operatorname{Re}(u_0 u_1^* \tilde{n}^*/2n_0) \quad (82)$$

Equations (81) and (82) are quite general; the plasma is allowed to be weakly nonuniform, and the density disturbance can have quite arbitrary amplitude \tilde{n} excluding, however, higher order couplings.

To understand the energy exchange between the plasma and the transverse waves, we manipulate Eq. (81), recalling the definition of the transverse wave energy density in terms of the wave action in CGS units $W_\ell = \omega_\ell J_\ell \equiv (m/e^2) \omega_\ell^2 |u_\ell|^2 / 2\pi$. We obtain the energy density conservation law:

$$D_0 W_0 + D_1 W_1 + (\Omega/\kappa) 2 \operatorname{Re} \left[\tilde{E}_0(x,t) e \tilde{n}^*(x,t) \right] = 0 \quad (83)$$

where $\tilde{E}_0 \equiv -ik\tilde{\phi}_0 = -ik(m/e)u_0 u_1^*$. This conservation law states that the rate of energy loss or gain by the transverse waves must be equivalent to the rate of work done on the plasma by the ponderomotive force.

We observe from Eq. (83) that no further work is done when \tilde{E}_0 and \tilde{n} have a relative phase of $\pi/2$ or $3\pi/2$, which is equivalent to $\tilde{\phi}$ and $\tilde{\phi}_0$ having relative phase 0 or π . Then as described by Eqs. (81) and (82) there is no action transfer, and the transverse waves acquire nonlinear frequency shifts as the only consequence of the coupling:

$$\delta\omega_{0,1}(x,t) \equiv D_{0,1}\theta_{0,1} = (\omega_{0,1}|u_{0,1}|^2)^{-1} \omega_e^2 \operatorname{Re}(u_0 u_1^* \tilde{n}^* / 2n_0) . \quad (84)$$

b. Quasi-steady nonlinear plasma response

When the temporal and spatial variation of the amplitude of the total potential $\tilde{\phi}$ is sufficiently weak to permit setting $\partial_t = \partial_x = 0$ in evaluating the dielectric function, i.e., $\epsilon(\Omega + i\partial_t, \kappa - i\partial_x)\tilde{\phi} \rightarrow \epsilon(\Omega, \kappa)\tilde{\phi}$, then we describe the plasma response as "quasi-steady". We can then use Eq. (32), $\tilde{\phi} = [\epsilon^{-1}(\Omega, \kappa) - 1]\tilde{\phi}_0^e$, and Poisson's equation to algebraically solve for \tilde{n} and express Eqs. (81) and (82) as

$$D_0\omega_0|u_0|^2 = -D_1\omega_1|u_1|^2 = \kappa^2|u_0|^2|u_1|^2 \operatorname{Im}(\epsilon^{-1} - 1) \quad (85)$$

and

$$\omega_0|u_0|^2 D_0\theta_0 = \omega_1|u_1|^2 D_1\theta_1 = -\kappa^2|u_0|^2|u_1|^2 \operatorname{Re}(\epsilon^{-1} - 1)/2 . \quad (86)$$

The quasi-steady response approximation requires $|\Omega - \omega_{NL}| \gg |\partial_t|$, $(3\kappa v_e^2/\Omega_L)|\partial_x|$, if we use Eqs. (33) and (60) to determine the relative importance of finite ∂_t and ∂_x effects in the dielectric response.

In Section II.C.5 the nonlinear dielectric function was evaluated by expanding about the nonlinear eigenfrequency, Eqs. (59) and (60). We find that in the quasi-steady limit the nonlinear dielectric response evaluated near a resonance is given approximately by

$$\epsilon(\Omega, \kappa) \sim \bar{\epsilon}(\omega_{NL})[\Omega - \omega_{NL}] \equiv \bar{\epsilon}(\omega_{NL})[\Delta + i\gamma] \quad (87)$$

where the mismatch is defined $\Delta \equiv \Omega - \Omega_L - \delta\Omega$, and the dissipation is defined by $\gamma = -\text{Im } \omega_{NL}$. To lowest order of approximation $\bar{\epsilon}$ can be replaced by $\bar{\epsilon}(\omega_{NL}) \approx \bar{\epsilon}_L \approx 2\omega_e^{-1}$ for electron plasma waves assuming $\kappa\lambda_e \ll 1$. For $|\epsilon^{-1}| \gg 1$ and $|\Delta| \gg |\gamma|$ the right sides of Eqs. (85) and (86) can be re-expressed in terms of Δ and γ by use of Eq. (87), obtaining respectively

$$-\kappa^2 |u_0|^2 |u_1|^2 \gamma \omega_e / 2\Delta^2 \quad (88)$$

and

$$-\kappa^2 |u_0|^2 |u_1|^2 \omega_e / 4\Delta \quad (89)$$

From Eq. (88) it is evident that action transfer requires finite dissipation. Since for trapped particles the total dissipation of the electron plasma wave oscillates around zero at the bounce frequency (Fig. 18), the action transfer will also oscillate at the bounce frequency. If the dissipation asymptotically vanishes while the frequency shift approaches a finite value, as was the case for a constant ponderomotive driver (Section II.C.5), then the action transfer will cease; and the transverse waves will acquire nonlinear frequency shifts.

c. Simulations with self-consistent ponderomotive potential and coupled mode equations

To investigate the back-reaction of trapping on the transverse wave action transfer and to determine the actual usefulness of the quasi-steady plasma response approximation, further simulations were performed. The coupled mode equations for the transverse waves, Eqs. (28) with $\nabla = 0$, and the constitutive relation (55) $\tilde{\phi}_0 = (m/e) \tilde{u}_0 \tilde{u}_1^*$

were appended to the one dimensional, electrostatic, particle code discussed in Section II.C.5.

Integration forward in time of the coupled mode equations describing the beat heating of two transverse waves in a uniform, infinite, periodic plasma is performed as an initial value problem. At each time-step, the transverse wave amplitudes are incremented, and the ponderomotive potential is constructed. The particle velocities and positions are then advanced using the electric field constructed from the gradient of the ponderomotive and self-consistent plasma potentials. The self-consistent plasma potential is obtained from the solution of the Poisson equation given the charge density. Finally the Fourier component of the density perturbation at the beat wavenumber is determined from which the coupling of the transverse modes is calculated in Eqs. (28). Simulations in much the same spirit as these have been performed for the case of induced scattering by Litvak et al.^{83,84}

One of the advantages of adding the coupled mode equations to an electrostatic simulation over the direct electromagnetic simulation is that there is then no restriction on the time-step of the integration due to the high frequency waves, which would otherwise require that $\omega_{0,1}\Delta t \ll 1$ in addition to $\omega_e\Delta t \ll 1$. In practice the time-step was restricted to a value $\omega_e\Delta t < 0.2$. For ease in comparing with earlier electrostatic simulations where the ponderomotive potential was held constant, the following plasma parameters were again chosen: $e/m = \Omega = \omega_e = \kappa = 1$ and $\Omega/\kappa = 3v_e$. The range of transverse wave amplitudes considered was $0.1 \leq |\tilde{u}_0(0)| = |\tilde{u}_1(0)| \leq 0.3$ which induced ponderomotive electric fields $0.01 \leq |\tilde{E}_0| \leq 0.09$. The

transverse wave frequencies were chosen arbitrarily, $\omega_0 = 5\omega_e$ and $\omega_1 = 4\omega_e$.

Results typical of simulations exhibiting considerable trapping are displayed in Figs. 20, 21, 22, and 23. The electric field response, longitudinal phase space, and the longitudinal velocity distribution function are shown in Fig. 20 at $\omega_e t = 431$ and $\omega_e t = 784$. At the earlier time the results are in many ways similar to simulations in which the ponderomotive potential amplitude was fixed. There is a large amplitude response driven nearly in phase with the ponderomotive force (Fig. 20a); longitudinal phase space has a hole centered over the bottom of the total potential well (Fig. 20b); and the distribution function has a distended, nonmaxwellian tail for $v \geq \Omega/k$ (Fig. 20c). At the later time the electric field response and the ponderomotive force are both weaker than at the earlier time and not in phase. In addition, there is considerable harmonic structure induced. The total potential well being not so deep as before, the hole in phase space (related closely to the separatrix) is reduced. The distribution function is further perturbed by the scattering.

In Figs. 21a and 21b are plotted the histories of the ponderomotive potential and response amplitudes ϕ_0 and ϕ and phases θ_0 and θ . The response amplitude and phase oscillate on the time scale of the bouncing of the trapped electrons as in earlier simulations. The ponderomotive potential amplitude and phase also oscillate on this time scale due to the back-reaction of the trapping on the transverse waves as illustrated by Eqs. (88) and (89); however, the oscillations are of lesser degree than for the response. The phase of the response relative to the driver oscillates with a considerably larger excursion around zero than was observed in our earlier simulations (Fig. 18).

The general decrease of the amplitude of the ponderomotive potential is due to pump depletion of the higher frequency transverse wave. The general increase of the nonlinear frequency shift and dissipation (Figs. 22a and b) due to the continued deformation of the distribution function fairly steadily reduces the relative amplitude of the response. Beat heating enters the regime of induced scattering.^{83,84} Many particles can satisfy the condition $\Omega \approx \kappa v$, and within a trapping width v_T of $v = \Omega/\kappa$ the distribution function has finite slope (Fig. 20c).

When the frequency shift and nonlinear dissipation become appreciable compared to the plasma frequency ω_e , we can no longer make expansions which require $|\Omega - \omega_{NL} + i(d/dt)|/|\omega_{NL}| \ll 1$; then Eq. (60) is no longer valid. Our construction of the nonlinear frequency shift and dissipation consequently fails when either of the following are appreciable compared to unity: $|\Omega - (\Omega_L + \delta\Omega)|/\omega_e$ or $|\gamma_L + \delta\gamma - i(d \ln \tilde{\phi}/dt)|/\omega_e$.

In Fig. 23 the amplitude and phases of the three interacting waves u_0 , u_1 , and \tilde{n} are plotted as functions of time. The amplitude of the density perturbation $\tilde{n} = (\kappa^2/4\pi e)\tilde{\phi}$ oscillates at the bounce frequency and diminishes due to the increasing dissipation and frequency shift and due to the decrease of the ponderomotive potential. The wave energy in the higher frequency transverse wave depletes by approximately 90%. With a relative action transfer efficiency then of $R = 0.9$, the relative energy transfer to the plasma is given by $R\Omega/\omega_0 \approx (0.9)(0.2) = 0.18$. On the trapped particle bounce time scale, the amplitudes $|u_0|$ and $|u_1|$ vary slightly in accordance with the sign of the dissipation (Fig. 22b) in Eq. (88). The slowly varying

wave phase θ_1 does not significantly vary over the duration of the simulation, but θ_0 varies and fluctuates much more since comparatively much less action is associated with it (see Eqs. (82) and (86)).

The continued appreciable time dependence of the nonlinear phenomena, the extensive trapping and deformation of the distribution function, the relatively large nonlinear frequency shift and dissipation, and the transition of the scattering from resonant ($\Omega = \omega_e$ and $\Omega/k = 3v_e$) to nonresonant (induced scattering) are all features not anticipated in our discussion in Section II.C.5. Nevertheless the simulations seem to be self-consistent using all qualitative and quantitative considerations still at our disposal. Energy and transverse wave action are conserved to within a few percent, Eqs. (83) and (81). Various effects due to particle trapping are observed consistently in the longitudinal electric field response, the nonlinear frequency shift and dissipation, and the back-reaction of the nonlinear response on the action transfer and the beat heating. However, the phase-mixing and relaxation to a quasi-steady state, wherein the longitudinal and transverse waves acquire frequency shifts and no further changes in amplitudes occur, is not observed.

The supposition that beat heating approaches a nonlinear equilibrium as described in Section II.C.5 is predicated on the assumption that the longitudinal plasma distribution function is only weakly perturbed by a weakly nonlinear plasma wave. To compare simulation with an analytic, perturbative, nonlinear theory, a longitudinal plasma wave would have to be excited much farther out on the tail of the distribution function $\Omega/k \geq 4v_e$, with sufficient linear mismatch to guarantee a weak plasma response. We have chosen here to simulate the physically more interesting case where an electron plasma

wave is resonantly excited ($\Omega = \omega_e$ and $\Omega/\kappa = 3v_e$), inducing a large perturbation of the plasma, considerable depletion of the higher frequency laser, and consequently significant momentum and energy transfer to the plasma.

d. Removal of trapping effects by plasma inhomogeneity

For the case of a nonuniform plasma, trapped particles can become untrapped in an electron plasma wave and finite dissipation recovered.^{95,96} The degree of inhomogeneity is characterized by $(\Omega^2/\omega_B^2)(d\chi/dx)$, where $\chi \equiv k^{-1}$ and $k(x) = [\Omega^2 - \omega_e^2(x)]^{1/2}/(3v_e^2)^{1/2}$. Asseo et al.⁹⁵ consider a freely propagating wave. They show, in the limit of a very strong inhomogeneity $(\Omega^2/\omega_B^2)(d\chi/dx) > 1$, that because of the effective acceleration in the wave frame provided by the finite spatial density gradient and consequent spatial dependence of the phase velocity, there are no trapped particles; and linear Landau damping is recovered. They make the same assumption on the weakness of the wave amplitude as do Morales and O'Neil, viz.

$$v_T v_\phi \ll v_e^2.$$

For weak inhomogeneity, $(\Omega^2/\omega_B^2)(d\chi/dx) \ll 1$, trapping occurs; however, the free but nearly resonant particles can exchange energy with the longitudinal wave at a finite, nonlinear rate proportional to the Landau damping or growth rate. Asseo et al. derive a spatial damping coefficient $\delta k(x)$, assuming that the number of trapped particles is constant over the distance the wave has traveled, 0 to x , and also assuming that $|\Delta k/k| \ll 1$, where $\Delta k \equiv \int_0^x dx' (dk/dx')$:

$$\delta\kappa(x) = \begin{cases} (\Omega^2/\omega_B^2)(d\chi/dx)(\gamma_L/v_g) & \text{for } |\Delta k/k| \ll \Omega/\omega_B, \\ (\Omega^2/\omega_B^2)^2(d\chi/dx)^2(\gamma_L\omega_B x/v_g v_\phi) & \text{for } |\Delta k/k| \gg \Omega/\omega_B, \end{cases} \quad (90a)$$

$$(90b)$$

where v_g , the group velocity, is given by $3v_e^2/v_\phi$, and $v_\phi \equiv \Omega/k(x)$ is the spatially dependent phase velocity.

The critical dimensionless parameter $(\Omega^2/\omega_B^2)(d\chi/dx)$ can be recast for purposes of comparison with typical parameters characterizing beat heating. Assuming a linear density gradient, we define the point of exact frequency and wavenumber matching by

$$k(x=0) = [\omega_0^2 - \omega_e^2(0)]^{\frac{1}{2}} c^{-1} + [\omega_1^2 - \omega_e^2(0)]^{\frac{1}{2}} c^{-1} \equiv \kappa(0).$$

We obtain at the point $x=0$

$$(\Omega^2/\omega_B^2)(d\chi/dx) = (v_\phi^2/v_T^2)(6\kappa^2\lambda_e^2)^{-1}(\kappa L_n)^{-1}, \quad (91)$$

where $v_T \equiv \omega_B/\kappa \equiv (2e|\tilde{\phi}|/m)^{\frac{1}{2}}$ and $L_n \equiv [d \ln n_0(x)/dx]_{x=0}^{-1}$.

Expressions equivalent to (91) can be written, recalling from Eq. (48) the relation $v_T^2/v_\phi^2 \approx \omega_B^2/\omega_e^2 = 2|\tilde{n}|/n_0$.

We emphasize that in either the case of weak or strong plasma inhomogeneity there is finite dissipation within the scope of the theory of Asseo et al. Therefore action transfer and heating should persist. The relative action transfer R remains parametrized by $k_0 L_n |u_0/c|^2$ and the input ratio ρ of the electromagnetic wave intensities in Eq. (39). On the other hand, the plasma response and hence v_T, ω_B , and the nonlinear dissipation are determined

self-consistently by the relation $\tilde{\phi}^e \approx \tilde{\phi}_0^e / [\bar{\epsilon}(\Omega - \omega_{NL})]$, Eq. (63).

This relation is parametrized by the ratio v_ϕ/v_e through the nonlinear frequency shift and by the ponderomotive potential amplitude $\tilde{\phi}_0^e = (m/e)u_0u_1^*$. There are a sufficient number of independent parameters to allow, in principle, the achieving of efficient transfer of action and heating of inhomogeneous plasma in a regime where the beat wave is resonantly excited to moderately large amplitude, while dissipation persists.

D. Cascading

We conclude our discussion of the beat heating of plasma by briefly reviewing research on the beat heating and induced cascading of a set of parallel propagating transverse waves all coupled by a single resonantly excited electron plasma wave.^{34,35,97} This heating scheme is another example of stimulated Raman scattering. The mode coupling relies on the same physical mechanisms described in Section I.C.

The cascade is initiated by two lasers propagating parallel to one another, for example, two CO₂ lasers with wavelengths 9.6 μm and 10.6 μm . The cross-coupling of the two lasers to produce a $\underline{v} \times \underline{B}$ ponderomotive force resonantly excites a longitudinal electron plasma wave. The density perturbation can then couple to the transverse oscillation velocity of either of the two lasers producing transverse currents. The transverse currents act as antennas to resonantly excite transverse waves shifted up and down in frequency and wavenumber from the incident laser frequencies and wavenumbers by the beat frequency and wavenumber. The coupling thus induces new transverse waves as well as amplifying or attenuating the pre-existing lasers. The induced

transverse waves can then couple with the existing transverse waves to stimulate further transitions. Thus the stimulated scattering can lead to a transfer of the incident laser energy into the electron plasma wave and into transverse waves at lower and higher frequencies.

We shall be more explicit in our description of cascading and in addition provide a quantum mechanical picture. In this heating scheme the energy is supplied by the two lasers with frequencies ω_L and ω_{L-1} differing by approximately the plasma frequency: $\Omega \equiv \omega_L - \omega_{L-1} \equiv \omega_e + \Delta$ where the mismatch Δ is assumed small. The transverse waves couple via the Lorentz force $\underline{v} \times \underline{B}$ to excite a longitudinal wave with wavenumber $\underline{k}_p = \underline{k}_L - \underline{k}_{L-1}$. For efficient coupling there must be nearly exact phase matching which implies frequency and wavenumber resonance conditions. For $\omega_e \ll \omega_L, \omega_{L-1}$ the beat wavenumber is relatively small, $k_p \approx \omega_e/c$. Since the longitudinal wave is a very long wavelength disturbance, $\omega_e/k_p \approx c \gg v_e$, there is no Landau damping. In practice collisional damping is too weak to effect efficient plasma heating. Nonlinear dissipation is presumed and verified a posteriori.³⁴

The longitudinal wave in turn interacts with each of the two transverse waves (L, L-1) to induce nonlinear currents and produce two more waves at $\underline{k}_{L-2} = \underline{k}_{L-1} - \underline{k}_p$ and $\underline{k}_{L+1} = \underline{k}_{L-1} + \underline{k}_p$ with frequencies $\omega_{L-2} = \omega_L - 2\Omega$ and $\omega_{L+1} = \omega_L + \Omega$. The new transverse waves interact to produce further scattering. The new frequency mismatches $\Delta_\ell \equiv \omega_\ell - (\omega_e^2 + k_\ell^2 c^2)^{\frac{1}{2}}$ are given by the difference of the frequencies of the induced transverse waves $\omega_{L \pm n} = \omega_L \pm n\Omega$ and their corresponding normal mode frequencies given by $(\omega_e^2 + k_\ell^2 c^2)^{\frac{1}{2}}$ where $\underline{k}_{L \pm n} = \underline{k}_L \pm n \underline{k}_p$. When \underline{k}_L and \underline{k}_{L-1} are nearly parallel, the new

mismatches Δ_{ℓ} are also small compared to the plasma frequency ω_e . Otherwise the new mismatches become appreciable, and multiple scattering from the same plasmon is inhibited by progressively larger mismatches Δ_{ℓ} .

In Fig. 24 cascading is diagrammed schematically. In quantum language, a coherent set of photons L undergo stimulated decay into photons $L-1$ already present and plasmons. The plasmons stimulate further transitions upward and downward in frequency by converting photons L into $L+1$ and so on, and by inducing the coherent cascade of photons $L-1$ into $L-2$ and so on to lower frequency. The damping of the plasmons deposits energy irreversibly into the plasma. Because energy and also the number of photons are conserved in these interactions (Manley-Rowe), the process must be preferentially downward, to allow for the plasma heating. In quantum language the heating is described as the irreversible absorption of plasmons by the plasma.

The rate of photon conversion downward in frequency competes with upward spreading. Kaufman, Watson, and Cohen³⁴ have considered under what circumstances the downward cascade rate can be maximized as a function of the input ratio of laser intensities and initial mismatch. For sake of simplicity they assumed the plasma to be uniform and nonrelativistic, $v_e \ll c$. Kaufman³⁴ obtained an analytic solution describing the cascade of the transverse modes in the limit of a steady state. He solved the boundary value problem in which two laser beams with steady intensities are incident on a semi-infinite plasma. His solution, however, required the assumption that all the transverse waves suffered an equal mismatch, $\Delta_{\ell} = \text{constant}$. The neglect of variable mismatch, i.e., the ignoring of the dispersion

of the electromagnetic waves, requires that $\omega_e \ll \omega_L$, which limits the ultimate heating efficiency of the cascade because of the Manley-Rowe relations.

Cohen⁹⁷ and Watson³⁴ independently examined the influence of variable mismatch numerically. Cohen solved the coupled mode equations describing the steady-state cascade as a boundary value problem. Watson investigated the temporal development of the initial value problem in which all transverse wave amplitudes are considered to be uniform in space. For parameters corresponding to CO₂ lasers and a dense θ -pinch, $\omega_L/\omega_e = 10$, the cascade was found to proceed in accordance with Kaufman's theory for the modes separated in frequency by no more than $\pm 3\Omega$ from the incident laser frequencies. Cascading to much lower frequencies was found to be sensitive to the initial choice of Δ . Watson determined that one could choose Δ in such a way as to cause Δ_L to pass through zero at lower frequencies $\omega_L < \omega_L$ and monotonically increase for the higher frequency modes optimizing the downward cascade rate. Mima and Nishikawa³⁵ studied the forward Raman scattering and cascading of a single electromagnetic wave in a very underdense plasma $\omega_e \ll \omega_0$.

By analogy to the earlier derivation of the beat heating by two opposed transverse waves, Eqs. (25)-(28), the equations describing the cascade of parallel propagating transverse waves in inhomogeneous plasma can be derived. For the transverse oscillation velocity one obtains instead of Eq.(26)

$$u(x,t) = \sum_{\ell} u_{\ell}(x,t) \exp\left[-i\omega_{\ell}t + i \int^x k_{\ell}(x')dx'\right] + c.c., \quad (92)$$

where $\omega_{L \pm n} \equiv \omega_L \pm n\Omega$, $k(x) \equiv k_L(x) \pm n k_p(x)$,
 $k_L(x) = [\omega_L^2 - \omega_e^2(x)]^{\frac{1}{2}} c^{-1}$, and $k_p(x) = [\omega_L^2 - \omega_e^2(x)]^{\frac{1}{2}} c^{-1} -$
 $[\omega_{L-1}^2 - \omega_e^2(x)]^{\frac{1}{2}} c^{-1}$. The density perturbation is given similarly to
 Eq. (27) by

$$\delta n(x,t) = \tilde{n}(x,t) \exp \left[-i\Omega t + i \int^x k_p(x') dx' \right] + \text{c.c.} \quad (93)$$

Use of the wave equation, (25), gives the equation describing
 the coupling of the transverse waves

$$\left[\partial_t - i\Delta_\ell(x) + c_\ell \partial_x \right] u_\ell(x,t) =$$

$$-(i/2)(\omega_e^2/\omega_\ell) \left[u_{\ell+1}(\tilde{n}^*/n_0) + u_{\ell-1}(\tilde{n}/n_0) \right] \quad (94)$$

where $c_\ell(x) \equiv k_\ell(x)c^2/\omega_\ell$, $\omega_e^2 = \omega_e^2(x=0)$, and $n_0 = n_0(x=0)$.

We have ignored the WKB variations in $k_\ell(x)$ compared to the spatial
 variation of the amplitudes. From arguments similar to those employed
 in deriving Eqs. (32) and (33) we obtain the equation describing the
 coupling of the density perturbation to the ponderomotive potential

$$\left[\partial_t + \nu - i\Delta(x) + 3(\kappa v_e^2/\Omega_L) \partial_x \right] (\tilde{n}/n_0) = -i(k_p^2/\omega_e) \sum_\ell u_\ell u_{\ell-1}^* \quad (95)$$

where the dissipation rate of the plasma wave is given by ν and
 Ω_L is the Bohm-Gross frequency $\Omega_L^2 \equiv \omega_e^2(1 + 3k_p^2\lambda_e^2)$.

Equation (94) describes explicitly the coupling by the density
 perturbation of any particular transverse wave to both the higher and
 lower frequency adjacent transverse modes. Adjacent transverse modes
 in the cascade then beat together to drive the density oscillation in
 Eq.(95), thus supplying the necessary feedback for the stimulated
 scattering. Kaufman's analytic solution of Eqs. (94) and (95) in the

steady-state limit ($\partial_t = 0$) describes cascading in a uniform plasma assuming that variable mismatch can be ignored and that the dissipation and mismatch of the plasma wave dominate convection:

$|v - i\Delta_L| \gg |(3kv_e^2/\Omega)\partial_x|$. Kaufman obtains a formula for the cascade rate from which the dependence of cascading on the input ratio of the laser intensities and on the plasma wave dissipation rate and mismatch is explicit (Eq. (5) of Ref. 34).

As compared to the case of opposed lasers the coupling to the longitudinal density perturbation (right side of Eq. (95)) is reduced by the factor $k_p^2/(k_L + k_{L-1})^2 \approx \omega_e^2/4\omega_L^2$ for $\omega_e \ll \omega_L$. Thus the intensity threshold for effective forward scatter is likely to be much higher than for backscatter. However, for backscatter there can be no further photon transitions, as the beat wavenumber

$\underline{\kappa} \equiv \underline{k}_L - \underline{k}_{L-1} \approx 2\underline{k}_L$ couples with the lasers to give

$\underline{k}_{L-2} = \underline{k}_{L-1} - \underline{\kappa} \approx -3\underline{k}_L$ and $\underline{k}_{L+1} = \underline{k}_L + \underline{\kappa} \approx 3\underline{k}_L$. Since both these wavenumbers violate the electromagnetic dispersion relation, large mismatches Δ_ρ arise terminating both the cascade of energy to lower frequency and upward spreading as well. The implication is that further decay due to backscatter requires seeding by a third laser beam L-2 exciting a new longitudinal wave with wavenumber:

$\underline{\kappa}' = \underline{k}_{L-1} - \underline{k}_{L-2} \neq \underline{\kappa}$. No energy need be lost on conversion to higher frequency transverse waves, since each transition requires seeding by its own laser beam. This heating mechanism was studied in detail in Ref. 59 and reviewed in Section II.C.1.

We conclude this review of cascading by describing an innovative idea due to W. Kunkel. In Ref. 59 Kaufman and Cohen compare the laser intensity threshold for effective cascading with that for significant

Raman backscatter, finding that in a uniform plasma backscatter has a lower threshold. The backscatter of the two laser beams that act as pumps would of course prohibit efficient cascading. As is reviewed in Section II.C.1, Kaufman and Cohen further determine that beat heating of opposed lasers in a linear density gradient and Raman backscatter occur effectively in a finite length resonance zone proportional to $(v/\omega_e)L_n$ where the density scale length is defined by $L_n \equiv [d \ln n_0(x)/dx]^{-1}$. If the plasma is much larger than the resonance zone, the action transfer is independent of the dissipation mechanism, Eqs. (36) and (37). As is evident from the structure of Eqs. (94) and (95), the same arguments are basically true for cascading as well.

Kunkel points out that in the limit of very large dissipation of the electron plasma wave concomitant with backscatter, the plasma may possibly not contain the entire resonance zone or the electron plasma wave may be nowhere close to resonance within the plasma. The reduction in action transfer or in attenuation of the laser beams due to stimulated backscatter can be exactly calculated from Eq. (36), an estimate of which appears in Eq. (38). The reduction of backscatter when the electron plasma wave is strongly damped, e.g., when $2k_L \lambda_e \geq 0.4$, effectively raises the threshold for appreciable Raman backscatter. However, since the beat wave in cascading is almost always weakly linearly damped $k_p \lambda_e \approx v_e/c \ll 1$, the plasma might quite easily contain the entire resonance zone for cascading. Cascading could then occur at lower laser intensities than the intensity threshold for appreciable backscatter. The question of under what realistic experimental circumstances cascading can preferentially occur over Raman backscatter and effectively heat plasma remains open.

III. FILAMENTATION AND STIMULATED BRILLOUIN SCATTERING

This part of the thesis describes in detail parametric instabilities involving the induced scattering of electromagnetic waves by low frequency ion modes (ω_i). The theory constructed in Section I.C is sufficiently general to describe both collective phenomena, e.g., stimulated Raman and Brillouin scattering and modulational instabilities, and induced Thomson scattering from electrons and ions. We shall limit our discussion here to only the scattering from collective ion modes: Brillouin and filamentation instabilities.

We shall describe Brillouin scattering and filamentation from a unified point of view. The distinction between Brillouin strong coupling and filamentation is examined. We construct in detail the dispersion relations for filamentation and Brillouin. We also consider the absolute instability of Brillouin strong coupling, demonstrating that the asymptotic Green's function for Brillouin instability is described by analytic weak coupling theory derived for all pump intensities within the Brillouin regime. We further show that very strong pump waves can induce growth of the scattered transverse wave at $(\omega_0 + \Omega, \underline{k}_0 + \underline{\kappa})$ comparable to that at $(\omega_0 - \Omega^*, \underline{k}_0 - \underline{\kappa}^*)$. We shall not discuss the nonlinear saturation of Brillouin³⁸ or filamentation.⁹⁸

A. Introduction to the Coupling of Transverse Waves to Ion Modes

An ion acoustic wave can be weakly coupled to transverse waves by means of the ponderomotive force, corresponding to Brillouin weak coupling. The frequency of the ion acoustic wave is given by $\Omega = \kappa c_s + \delta$ where $c_s \equiv (T_e/m_i)^{1/2}$ and δ is a small ($\ll \kappa c_s$) complex-valued frequency shift dependent on the pump wave amplitude.

For a more intense pump wave the ponderomotive force and consequently the coupling to the density perturbation increase. In the limit that the oscillation frequency of the density perturbation is significantly perturbed by the pump, the scattering is defined as Brillouin strong coupling.

Brillouin strong coupling is an example of the stimulated scattering of the pump wave into a transverse wave shifted to lower frequency $\omega_0 - \Omega^*$ with wavenumber $\underline{k}_0 - \underline{\kappa}^*$. Both the scattered transverse wave and the concomitant driven ion mode, or "quasi-mode", grow exponentially in the linear regime of the parametric instability. When the pump wave scatters off a driven ion mode into transverse waves shifted in wavenumber up and down by the wavenumber of the density perturbation, $\underline{k}_0 + \underline{\kappa}$ and $\underline{k}_0 - \underline{\kappa}^*$, with resulting exponential growth of the scattered transverse waves and the density perturbation, the instability is described as filamentation. The density perturbation excited by the scattering is typically a purely growing mode not otherwise present. We consider this as another example of the stimulated scattering of light by a quasi-mode.

B. General Formulation of Brillouin and Filamentation

In Section I.C we derived a very general dispersion relation (18) which implicitly includes Brillouin and filamentation. Equation (18) requires the evaluation of $\Gamma(\Omega, \underline{\kappa}) \equiv [\chi_e(1 + \chi_i)/\epsilon]_{\Omega, \underline{\kappa}}$ for complex beat frequencies Ω and beat wavenumbers $\underline{\kappa}$. In Appendix 1 we show that for Maxwellian velocity distribution functions the electron and ion susceptibilities are given by $\chi_e(\Omega, \underline{\kappa}) \approx 1/\kappa^2 \lambda_e^2$ and $\chi_i(\Omega, \underline{\kappa}) \approx -\omega_i^2/\Omega^2$ where $\lambda_e \equiv v_e/\omega_e$. We have assumed that

$v_i \ll |\Omega/\kappa| \ll v_e$, and that linear Landau damping and collisions are negligible. Then for $\Gamma(\Omega, \underline{\kappa})$ we obtain

$$\Gamma(\Omega, \underline{\kappa}) \approx (\Omega^2 - \omega_i^2) / \left[\Omega^2(1 + \kappa^2 \lambda_e^2) - \kappa^2 c_s^2 \right].$$

If we substitute this form of Γ into Eq. (18) and multiply by $\left[\Omega^2(1 + \kappa^2 \lambda_e^2) - \kappa^2 c_s^2 \right]$, Eq. (18) becomes

$$\begin{aligned} & \left[\Omega^2(1 + \kappa^2 \lambda_e^2) - \kappa^2 c_s^2 \right] \left[(\Omega^2 - \kappa^2 c^2)^2 - 4(\Omega \omega_0 - \underline{\kappa} \cdot \underline{k}_0 c^2)^2 \right] \\ & + (1/2) \omega_i^2 \kappa^2 \tilde{v}_0^2 (\kappa^2 c^2 - \Omega^2) = 0. \end{aligned} \quad (96)$$

Equation (96) describes both filamentation and Brillouin scattering. Analytic solution of (96) for various special cases and numerical solution of the general dispersion relation will be presented.

If we define $\cos \theta \equiv \hat{\kappa} \cdot \hat{k}_0$, then Eq.(96) can be rewritten as

$$\begin{aligned} & \left[\Omega^2(1 + \kappa^2 \lambda_e^2) - \kappa^2 c_s^2 \right] \left[(\Omega^2 - \kappa^2 c^2)^2 - 4(\Omega \omega_0 - \kappa k_0 \cos \theta c^2)^2 \right] \\ & + (1/2) \omega_i^2 \kappa^2 \tilde{v}_0^2 (\kappa^2 c^2 - \Omega^2) = 0. \end{aligned} \quad (97)$$

We note that in Eq. (97) changing both the signs of $\cos \theta$ and Ω , viz. $\Omega \rightarrow -\Omega$ and $\cos \theta \rightarrow -\cos \theta = \cos(\pi - \theta)$, leaves Eq. (97) invariant. We shall therefore solve Eqs. (96) and (97) for $0 < \theta < \pi/2$ realizing that $\Omega(\kappa, \pi - \theta) = -\Omega(\kappa, \theta)$.

C. Filamentation Dispersion Relation

We first consider Eq. (96) in the special case where it describes filamentation. In the limit that $|\kappa \lambda_e| \ll 1$ and $|\Omega| \ll |\kappa c|$, Eq. (96) can be somewhat simplified to give

$$(\Omega^2 - \kappa^2 c_s^2) [(\Omega - \underline{\kappa} \cdot \underline{v}_g)^2 - \kappa^4 c^4 / 4\omega_0^2] - \omega_1^2 (\tilde{v}_0/c)^2 \kappa^4 c^4 / 8\omega_0^2 = 0 \quad (98)$$

where $\underline{v}_g \equiv \underline{k}_0 c^2 / \omega_0$ is the group velocity of the pump wave. Drake et al.¹² derive the same dispersion relation. Since this equation is quartic in Ω and sixth order in κ , we must further simplify the dispersion relation to make analytic progress.

For the formation of filaments whose dimension (see Fig. 2) transverse to the pump propagation direction \hat{k}_0 is quite small compared to its characteristic length of variation in the x direction parallel to \hat{k}_0 , $|\kappa_x / \kappa_z| \ll 1$, we obtain $\Omega = \underline{\kappa} \cdot \underline{v}_g + i\gamma = \kappa_x v_g + i\gamma$. The temporal growth rate γ then satisfies the equation

$$(\gamma^2 + \kappa_z^2 c_s^2)(\kappa_z^4 c^4 + 4\gamma^2 \omega_0^2) - \omega_1^2 \kappa_z^2 \tilde{v}_0^2 / 2 = 0 \quad (99)$$

The expressions $\Omega = \kappa_x v_g + i\gamma$ and Eq. (99) are equivalent to Eq. (98) to lowest order in $|\kappa_x / \kappa_z|$ and $|\kappa_x v_g / \gamma|$, both of which are assumed small. This biquadratic dispersion relation has been obtained also by Drake et al.¹² and Langdon and Lasinski.³³ The biquadratic is readily solved giving

$$\gamma = \pm (\gamma_0^2 - \kappa_z^2 c_s^2)^{\frac{1}{2}} \left[1 + (c_s/c)^2 (2\omega_0 / \kappa_z c)^2 \right]^{-\frac{1}{2}} \quad (100)$$

where $\gamma_0^2 \equiv (1/2) \omega_1^2 (\tilde{v}_0/c)^2$. The following limiting forms are

obtained from Eq. (100): for $|\kappa_z c / 2\omega_0| \ll c_s/c$,

$\gamma \approx \pm \gamma_0 (\kappa_z c / 2\omega_0) (c/c_s)$; and for $|\kappa_z c / 2\omega_0| \gg c_s/c$,

$\gamma \approx \pm (\gamma_0^2 - \kappa_z^2 c_s^2)^{\frac{1}{2}}$. For $\kappa_x = 0$, $\Omega = i\gamma$ which is schematically

diagrammed as a function of κ_z in Fig. 25.

Further discussion of filamentation is relegated to the existing literature and to a forthcoming paper, by C. Max and this author, wherein the Green's function describing the linear, convective growth of filamentation is constructed. Drake et al.¹² and Manheimer and Ott³⁹ consider the temporal problem, whereas Kaw et al.¹³ investigate spatial growth of filamentation. The extensive literature due to researchers in the nonlinear optics field is in general more directed at the nonlinear structure of steady-state or quasi-steady state filamentation or self-focusing.^{14,15,30}

D. Brillouin Scattering

1. Introduction to Brillouin Weak and Strong Coupling

We present a detailed examination of Brillouin weak and strong coupling. Assuming that the scattered wave a_- suffers a much smaller mismatch from its linear dispersion relation than the a_+ scattered wave, i.e., $|D_-/D_+| \ll 1$, the Brillouin dispersion relation can be immediately obtained from Eq. (19). We evaluate the linear susceptibilities in the limit $v_i \ll |\Omega/\kappa| \ll v_e$. If we further assume that $\kappa^2 \lambda_e^2$, $|\Omega|/\omega_0 \ll 1$ then Eq. (19) becomes a dispersion relation describing stimulated Brillouin scattering:

$$D_B(\Omega, \underline{\kappa}) \equiv (\Omega^2 - \kappa^2 c_s^2) \left[\Omega + c^2 (\kappa^2 - 2\underline{\kappa} \cdot \underline{k}_0) / 2\omega_0 \right] + \kappa^2 \tilde{v}_0^2 \omega_i^2 / 8\omega_0 = 0 \quad (101)$$

To justify the assumption that $|D_-| \ll |D_+|$, we require that $|\kappa^2 - 2\underline{\kappa} \cdot \underline{k}_0| \ll |\kappa^2 + 2\underline{\kappa} \cdot \underline{k}_0|$. We continue to assume that the plasma is underdense, $\omega_e < \omega_0$. The dispersion relation Eq. (101) was also obtained by Bodner and Eddleman³⁷ using a fluid equations approach.

In the absence of the electromagnetic pump, $\tilde{v}_0^2 = 0$, there are only free oscillations: ion acoustic waves $\Omega = \pm \kappa c_s$ and freely propagating electromagnetic waves $D_-(\Omega, \kappa) = 0$. In the presence of the pump, the two waves are coupled. The dispersion relation of each wave is altered by the scattering of the radiation by the density perturbation and the accompanying ponderomotive force driving the low frequency density perturbation. In the absence of dissipation, an infinitesimal pump gives rise to a growing ion acoustic oscillation and scattered electromagnetic wave, i.e., $\text{Im } \Omega \ll \text{Re } \Omega \approx \kappa c_s$ for real κ . This constitutes Brillouin weak coupling.

For stronger pump-wave amplitudes the growth rate of the instability and modifications to the oscillation frequency increase. The ponderomotive force becomes comparable to the normal fluid restoring force of an ion acoustic wave. In the strong coupling limit the ponderomotive force is dominant: the oscillation frequency is significantly modified. For $|\Omega| \gg |\kappa c_s|$ we obtain $\Omega^3 \approx -\kappa^2 \tilde{v}_0^2 \omega_i^2 / 8\omega_0$ from Eq. (101). This is similar to filamentation in that the density perturbation is a driven mode, or quasi-mode,¹¹ whose pump-dependent dispersion relation differs dramatically from a plasma normal mode.

2. Generalization of Brillouin Analysis to Three Dimensions

Before proceeding with a detailed, quantitative discussion of two dimensional Brillouin, some comments on the generalization of our theoretical description to include scattering in three dimensions are appropriate. If the scattered radiation propagates in a direction having a component parallel to the pump-wave polarization, then transverse canonical momentum is no longer conserved; our formalism then breaks down. To describe three dimensional Brillouin, Drake et al.,¹² Rosenbluth et al.,¹¹ and Bodner and Eddelman³⁷ consider Maxwell's

equations and fluid equations. They all employ the simple fluid model for the nonlinear current Eq. (14), however, allowing the polarization of the scattered radiation to make an arbitrary angle ψ with the polarization of the incident electromagnetic wave.

In calculating the ponderomotive potential driving the low frequency longitudinal oscillation, the generalization of Eq. (8), one factor of $\cos \psi$ enters due to the $\underline{v} \times \underline{B}$ Lorentz force of the pump and scattered waves. For the component of the total current in the direction parallel to the polarization of the scattered radiation driving the nonlinear wave equation, a second factor of $\cos \psi$ occurs due to the inner product of the pump quiver velocity with the scattered wave polarization direction.

The result then of including the angle of relative polarization is to alter the Brillouin dispersion relation by the replacement of \tilde{v}_0^2 with $\tilde{v}_0^2 \cos^2 \psi$ in Eq. (101). By requiring the pump and the scattered radiation to be polarized perpendicular to the plane defined by their propagation directions, the coupling term in Eq. (101) is maximized $\tilde{v}_0^2 \cos^2 \psi + \tilde{v}_0^2$. For scattering angles such that $\psi \neq 0$ the effective pump strength $\tilde{v}_0^2 \cos^2 \psi$ is reduced.

3. Brillouin Dispersion Relations

We consider first the weak coupling limit of Eq. (101) and define the following variables: $\cos \theta = \hat{\kappa} \cdot \hat{k}_0$; $r_0 \equiv \tilde{v}_0/\omega_0$; the group velocity $v_g \equiv c^2 k_0/\omega_0$; and $\Delta \equiv \kappa c_s + (\kappa^2 - 2\underline{\kappa} \cdot \underline{k}_0)c^2/2\omega_0$, the frequency mismatch of the scattered electromagnetic wave. (The frequency mismatch is obtained from the electromagnetic dispersion relation: $\Delta = (2\omega_0)^{-1} D_-$, with $\Omega = \kappa c_s \ll \omega_0$. If we define $\delta\omega \equiv \Omega - \kappa c_s$ and assume $|\delta\omega/\Omega| \ll 1$, then from Eq. (101) we obtain

$$(1/2) D_B(\Omega, \underline{\kappa}) = \delta\omega^2(\kappa c_s + \Delta/2) + \delta\omega \kappa c_s \Delta + \kappa^2 c_s^2 \omega_0 (r_0/4\lambda_e)^2 . \quad (102)$$

The solution of Eq. (102) is given by

$$\delta\omega(\kappa c_s + \Delta/2) = -\kappa c_s \Delta/2 \pm \left[(\kappa c_s \Delta/2)^2 - \kappa^2 c_s^2 \omega_0 (r_0/4\lambda_e)^2 (\kappa c_s + \Delta/2) \right]^{1/2} . \quad (103)$$

The growth rate, $\text{Im } \delta\omega$, is a maximum, with respect to wavenumber (taken here to be real) for fixed angle, at $\Delta = 0$. This determines the wavenumber $\kappa = 2k_0(\cos \theta - c_s/v_g)$, for which $\Delta = 0$, and thus corresponds to exact wavenumber and frequency matching for the interaction of the three normal modes. From Eq. (103) the maximum growth rate is given by

$$\text{Im } \Omega = \left[2k_0 c_s \omega_0 (\cos \theta - c_s/v_g) \right]^{1/2} (r_0/4\lambda_e) \quad (104)$$

in agreement with Refs. 11, 12, 36, and 37.

Figure 26 schematically displays the dispersion relation $D_B(\Omega, \underline{\kappa}) = 0$ in the weak coupling regime, plotting the normalized frequency $\Omega/2k_0 c_s$ as a function of $\kappa/2k_0$ for fixed angle θ and pump strength. The width of the unstable κ region is found from Eq. (103) to be $2k_0(c_s/v_g)(r_0/4\lambda_e) \left[(\omega_0/k_0 c_s)/(\cos \theta - c_s/v_g) \right]^{1/2}$, for $(r_0/4\lambda_e)^2 (\omega_0/k_0 c_s) \ll |\cos \theta - c_s/v_g|$. In the unstable κ region there are complex conjugate solutions for $\delta\omega$. Both solutions correspond to the three waves being effectively phase-locked at a relative phase $\pi/2$ or $3\pi/2$ in Eq. (3). One value of the relative phase leads to instability and the other to decay. In the stable κ region, $|\Delta| \gg 2\omega_0 (r_0/4\lambda_e)^2$, the three-wave coupling induces a frequency shift which again, depending on the relative phasing of the

three waves, can be either positive or negative. This accounts for the splitting of the oscillation frequency whose dependence on pump-wave intensity, wavenumber, and scattering angle is given by Eq. (103).

To consider the strong coupling limit of Eq. (101) we do not make the assumption that the density perturbation is a weakly growing ion acoustic wave. Equation (101) is a cubic equation in Ω :

$$D_B(\Omega, \kappa, \cos \theta) = \Omega^3 + \Omega^2(\kappa^2 - 2\kappa k_0 \cos \theta)c^2/2\omega_0 - \Omega\kappa^2 c_s^2 + \left[\kappa^2 \tilde{v}_0^2 \omega_i^2 - 4\kappa^2 c_s^2 (\kappa^2 - 2\kappa k_0 \cos \theta)c^2 \right] / 8\omega_0 = 0 \quad (105)$$

The solution for the roots of a cubic equation is standard. Results for Ω as a function of κ for fixed $\cos \theta$ and pump strength in the strong coupling regime are shown in Fig. 27a. For fixed θ the region of κ around $2k_0 \cos \theta$ is restricted in order that we maintain the condition $|D_-/D_+| \ll 1$, which is required in the derivation of the Brillouin dispersion relation Eq. (101).

When the ponderomotive force very much dominates the restoring force associated with a free ion acoustic oscillation (in terms of characteristic frequencies $(\omega_i^2 k_0^2 \tilde{v}_0^2 / 2\omega_0)^{1/3} \gg \kappa c_s$) the following simplification results. We set $k_0 c_s / \omega_0 \rightarrow 0$ in Eq. (105) to obtain

$$D_B(\Omega, \kappa, \cos \theta) = \Omega^3 + \Omega^2(\kappa^2 - 2\kappa k_0 \cos \theta)c^2/2\omega_0 + \kappa^2 \tilde{v}_0^2 \omega_i^2 / 8\omega_0 = 0 \quad (106)$$

The complex frequency of the density perturbation is then completely determined by the scattering of the radiation and the degree of mismatch of the scattered wave from a normal mode, represented by the term involving $\kappa^2 - 2\kappa k_0 \cos \theta$.

For κ and $\cos \theta$ such that $|D_-| \ll |D_+|$, growth is maximized by $\kappa^2 = 2\kappa k_0 \cos \theta = 0$ giving the standard result for strong coupling^{11,12,37}

$$\Omega = \left[(1/2) + i(\sqrt{3}/2) \right] (\cos \theta)^{2/3} (\omega_i^2 k_0^2 \tilde{v}_0^2 / 2\omega_0)^{1/3} \quad (107)$$

For $|\cos \theta| = |\hat{\kappa} \cdot \hat{k}_0| \ll 1$, the Brillouin analysis breaks down, and Eq. (96) must be solved. We note that the largest growth rates for weak and strong coupling Brillouin occur for exact backscatter, $\kappa/2k_0 = \cos \theta = 1$. Figure 27a shows a plot of the normalized frequency Ω/ω_0 , using Eq. (106), as a function of the normalized real wavenumbers $\kappa/2k_0$ for various fixed values of $\cos \theta$ and fixed parameters $(\omega_i^2 k_0^2 \tilde{v}_0^2 / \omega_0^4)^{1/3} = 0.04$ and $k_0 \lambda_e = 0.02$.

We emphasize that Eqs. (101) and (106) give a general description of Brillouin weak and strong coupling. The two regimes of scattering are distinguished by $(r_0/\lambda_e)^2 (\omega_0/2k_0 c_s)$ compared to unity. This is obtained by taking the ratio of the strong coupling frequency in Eq. (107) to $2k_0 c_s$, and then cubing the result, ignoring numerical factors of order unity and the dependence on $\cos \theta$. Strong coupling corresponds to $(r_0/\lambda_e)^2 (\omega_0/2k_0 c_s) \geq 1$; weak coupling occurs for $(r_0/\lambda_e)^2 (\omega_0/2k_0 c_s) \ll 1$. However, to correctly extract weak coupling, one must carefully insure frequency and wavenumber matching, i.e., $\Delta \approx 0$.

Brillouin strong coupling can exhibit a regime of nearly nonoscillatory growth whose parameter dependence closely resembles the growth rate of filamentation in the limit $\tilde{v}_0^2/c^2 \gg \kappa^2 \lambda_e^2$. For $\kappa \geq 2k_0 \cos \theta$ and ω_i/ω_0 , $(\kappa^2 - 2\kappa k_0 \cos \theta)/2k_0^2 \gg \Omega/\omega_0 \gg \kappa c_s/\omega_0$, Eq. (105) becomes $D_B(\Omega, \kappa, \cos \theta) \approx \Omega^2 (\kappa^2 - 2\kappa k_0 \cos \theta) c^2 / 2\omega_0 + \kappa^2 \tilde{v}_0^2 \omega_i^2 / 8\omega_0 = 0$. We must, however, continue to maintain the

inequality $|D_-| \ll |D_+|$, which requires $\kappa^2 - 2\kappa k_0 \cos \theta \approx 0$, to justify the neglect of a_+ compared to a_- and identifies the instability as Brillouin. Solution of the quadratic dispersion relation is readily obtained, $\Omega = \pm i \left[\kappa / (\kappa - 2k_0 \cos \theta) \right]^{\frac{1}{2}} \omega_i k_0 \tilde{v}_0 / \omega_0$. When the right side of the preceding expression becomes comparable to $(\cos^2 \theta \omega_i^2 k_0^2 \tilde{v}_0^2 / 2\omega_0)^{1/3}$, the Ω^3 term in $D_B(\Omega, \kappa, \cos \theta)$ must be retained.

Except for the geometrical coefficient $\left[\kappa / (\kappa - 2k_0 \cos \theta) \right]^{\frac{1}{2}}$, the growth rate for nearly purely growing Brillouin strong coupling is identical in its parameter dependence to that for filamentation in the limit $\tilde{v}_0/c \gg \kappa \lambda_e$, $\omega_0/k_0 \approx c$, $\kappa c / 2\omega_0 \gg c_s/c$, and $|\cos \theta| < 1$, viz. from Eq. (100) $\Omega \approx \pm i \gamma_0 = \pm i \omega_i \tilde{v}_0 / \sqrt{2} c$. Although strong coupling and filamentation have similar growth rates and both are characterized by the coupling of transverse normal modes to a strongly driven longitudinal mode, they differ radically in that for strong coupling the growth of the a_- sideband is dominant and is a maximum for $\kappa \approx 2k_0 \cos \theta$. For filamentation the two sidebands a_-, a_+ have comparable amplitudes; and for the regime of filamentation of interest here, we have the condition $|\cos \theta| \ll 1$.

As the a_- sideband acquires a larger mismatch D_- , Brillouin strong coupling exhibits a smooth transition into modulational instability. The transition is complete for $|D_-/D_+| \approx \mathcal{O}(1)$. In Figure 27b, the numerical solution of Eq. (96) is exhibited plotting Ω/ω_0 vs $\kappa/2k_0$ for various values of θ . For $\kappa \approx 2k_0 \cos \theta$ there is good agreement with the Brillouin strong coupling solutions shown in Fig. 27a. For $\kappa \gg 2k_0 \cos \theta$, filamentation occurs with growth rate

$\Omega \approx i\gamma_0$ corresponding to the limit of $2\omega_0 c_s / c^2 \ll \kappa \ll (\lambda_e)^{-1} \tilde{v}_0 / c$ in Eq. (100) and Fig. 25.

We would like to include the influence of the concomitant growth of the a_+ sideband on Brillouin in such a way as to permit further analysis without resorting to the numerical solution of the complete dispersion relation (96) displayed in Fig. 27b. We can rewrite Eqs. (17) without approximation

$$D_- - \kappa^2 \tilde{v}_0^2 T/4 - (\kappa^2 \tilde{v}_0^2 T/4)^2 / (D_+ - \kappa^2 \tilde{v}_0^2 T/4) = 0. \quad (108)$$

Then defining $\delta(\Omega, \kappa) \equiv D_-(\Omega, \kappa) / D_+(\Omega, \kappa)$ where (Ω, κ) satisfy the Brillouin dispersion relation Eq. (19), $D_- - \kappa^2 \tilde{v}_0^2 T/4 = 0$, the first correction to the Brillouin dispersion relation due to finite δ is included as follows:

$$D_- - \kappa^2 \tilde{v}_0^2 T \left[1 + \delta / (1 - \delta) \right] / 4 = 0. \quad (109)$$

If the solution (Ω, κ) of Eq. (109) is iterated back into δ , then Eq. (109) constitutes a recursive dispersion relation equivalent to the branches of Eq. (18) which correspond to Brillouin.

The dimensionless quantity δ thus characterizes the condition for the existence of the Brillouin instability and the validity and accuracy of its dispersion relation. The mismatch D_- relative to D_+ can increase for a variety of reasons: D_- can cease to be nearly zero because of its dependence on κ and θ , and because of its dependence on pump strength through Ω . As $|\delta|$ approaches order unity filamentation smoothly supercedes Brillouin strong coupling.

By way of an illustration of Brillouin backscattering, a numerical simulation was performed. The electromagnetic code discussed in Section II.B was employed to study Brillouin scattering in

one dimension. A linearly polarized monochromatic wave, $\omega_0 = 1.414 \omega_e$, impinged upon an unmagnetized, finite, warm plasma slab. Electrons were warm ($T_e/m_e c^2 = 0.01$) and singly charged ions cold. There were a modest number of particles, 2000 of each species with $m_i/m_e = 25$. In terms of the parameters used in Eqs. (105) and (106), the dimensionless pump strength was chosen to be $[(\omega_1/\omega_0)^2(k_0^2 r_0^2)/2]^{1/3} = 1.26 \times 10^{-2}$ and the dimensionless sound speed $k_0 c_s/\omega_0 = 1.414 \times 10^{-2}$. This corresponds to a regime marginally between weak and strong coupling.

Because of the discrete Fourier spectrum of wavenumbers in the simulation, only one backscatter mode was excited from noise, $\underline{\kappa} \approx 2\underline{k}_0$. Figures 28 and 29 show the growth of a large amplitude density perturbation in electron and ion phase spaces. From the ion phase space plots a phase velocity nearly equal to the ion sound speed was observed, $\text{Re } \Omega/\kappa \approx c_s = 0.02c$. An accurate measurement of a growth rate was somewhat hopeless because of the very weak growth rate, the early onset of nonlinear features (ion wave breaking) the reflection of particles and waves in our rather short system, and the relatively large noise levels present in the simulation (see Fig. 30). A detailed simulation study of Brillouin instability has been made by Forslund et al.³⁸ in which linear growth rates are carefully measured and the importance of competing nonlinear features are assessed.

4. Absolute Instability of Brillouin

We next consider the asymptotic Green's function analysis for Brillouin. We follow the procedure of Bers and Briggs to ascertain the existence of absolute linear instability^{99,100} as applied to Brillouin weak and strong coupling and extend the work of Jorna³⁶

and Chambers, Bers, and Watson.^{10,101} A δ -function perturbation in space and time is assumed for the space-time dependence of the source in the Laplace-transformed initial-value problem for the linearly unstable coupled modes a_- and δn_s . For the source term we follow Oberman and Auer,¹⁰² allowing discrete particles in a collisionless plasma to produce longitudinal noise. We then construct the Green's functions for the scattered electromagnetic wave and for the electron and ion density perturbations, and analyze the Green's functions asymptotically.

The noise enters the charge density as follows. Poisson's equation is

$$-\nabla^2 \phi(\underline{x}, t) = 4\pi \sum_s e_s \delta n_s(\underline{x}, t) \quad (110)$$

The charge density of species s , $\delta n_s(\underline{x}, t)$, includes the charge density due to noise and the perturbed charge density induced by the longitudinal electric field and the longitudinal component of the ponderomotive force. From Oberman and Auer,¹⁰² the Fourier and Laplace-transformed charge densities are given by

$$\delta \tilde{n}_s(\Omega, \underline{\kappa}) = -\chi_s \kappa^2 \tilde{\phi}^s(\Omega, \underline{\kappa}) / 4\pi e_s + \tilde{S}_n^s(\Omega, \underline{\kappa}) \quad (111)$$

where $\chi_s = \chi_s(\Omega, \underline{\kappa})$ is the linear susceptibility and $S_n^s(\underline{x}, t)$ is the longitudinal charge density due to noise, whose Laplace-transforms in time and Fourier transforms in two spatial dimensions are given by

$$\tilde{S}_n^s(\Omega, \underline{\kappa}) \equiv \int_0^\infty dt' \int d^2 \underline{x}' \exp(i\Omega t' - i\underline{\kappa} \cdot \underline{x}') S_n^s(t', \underline{x}') \quad .$$

Substitution of Eq. (111) for $\delta\tilde{n}_s$ into the Fourier and Laplace-transformed Eq. (110) and use of $\epsilon(\Omega, \underline{\kappa}) \equiv 1 + \sum_s \chi_s(\Omega, \underline{\kappa})$, $\phi^s = \phi + \phi_0^s$, and $|\phi_0^i| \ll |\phi_0^e|$ yield

$$\begin{aligned} \epsilon(\Omega, \underline{\kappa}) \tilde{\phi}^e(\Omega, \underline{\kappa}) &= \left[1 + \chi_1(\Omega, \underline{\kappa}) \right] \tilde{\phi}_0^e(\Omega, \underline{\kappa}) \\ &+ 4\pi\kappa^{-2} e \left[\tilde{S}_n^e(\Omega, \underline{\kappa}) - \tilde{S}_n^i(\Omega, \underline{\kappa}) \right] \end{aligned} \quad (112)$$

In Eq. (112) we solve for $\tilde{\phi}^e$ and substitute the result into Eq. (111) to obtain

$$\delta\tilde{n}_e = -\kappa^2 \chi_e (1 + \chi_1) \epsilon^{-1} \tilde{\phi}_0^e / 4\pi e + (1 + \chi_1) \epsilon^{-1} \tilde{S}_n^e + \chi_e \epsilon^{-1} \tilde{S}_n^i, \quad (113)$$

where the frequency and wavenumber dependence $(\Omega, \underline{\kappa})$ in the susceptibilities and the transformed amplitudes is implicit.

Substituting the electron charge density into the fluid model for the nonlinear transverse current $\mathbf{J} = e\tilde{\mathbf{v}}_e [n_0 + \delta n_e(\underline{x}, t)]$, Eq. (14), and Fourier and Laplace-transforming give

$$\begin{aligned} \tilde{\mathbf{J}}^*(\omega_0 - \Omega^*, \underline{k}_0 - \underline{\kappa}^*) &= -en_0 c \tilde{\mathbf{a}}_-^* - ec \tilde{\mathbf{a}}_0^* \delta\tilde{n}_e(\omega, \underline{\kappa}) \\ &- ec \tilde{\mathbf{a}}_0^* \delta\tilde{n}_e^*(2\omega_0 - \Omega^*, 2\underline{k}_0 - \underline{\kappa}^*) \end{aligned}$$

where $(m_e c^2/e) \tilde{\mathbf{a}}_- = (m_e c^2/e) \tilde{\mathbf{a}}(\omega_0 - \Omega^*, \underline{k}_0 - \underline{\kappa}^*)$ and $(m_e c^2/e) \tilde{\mathbf{a}}_0 = (m_e c^2/e) \tilde{\mathbf{a}}(\omega_0, \underline{k}_0)$ are the Fourier and Laplace-transformed amplitudes of the perturbed and pump-wave vector potentials, respectively. The term $-ec \tilde{\mathbf{a}}_0^* \delta\tilde{n}_e^*(2\omega_0 - 2\Omega^*, 2\underline{k}_0 - 2\underline{\kappa}^*)$ is higher order in $\tilde{\mathbf{a}}_0$ and \tilde{S}_n^s and has been ignored. For $\text{Re}(2\omega_0 - \Omega^*) \gg \omega_e$, the longitudinal noise $\tilde{S}_n^s(2\omega_0 - \Omega^*)$ does not incur the increased plasma shielding that low frequency noise $\tilde{S}_n^s(\Omega)$ can, and therefore

-111-

its contribution is ignored.¹⁰² The electron charge density induced by the ponderomotive potential with phase dependence $(2\omega_0 - \Omega^*, 2\underline{k}_0 - \underline{\kappa}^*)$ is proportional to $|2\underline{k}_0 - \underline{\kappa}^*|^2 \chi_e (1 + \chi_1) \epsilon^{-1}$ and is likewise small compared to the low frequency induced charge density: $|\chi_e/\epsilon| \sim \omega_e^2/4\omega_0^2 \ll 1$ and for backscatter $|2\underline{k}_0 - \underline{\kappa}^*|^2 \ll |\underline{\kappa}|^2$.

The ponderomotive potential given by Eq. (9) can be Fourier and Laplace-transformed to give

$$\tilde{\phi}_0^e(\Omega, \underline{\kappa}) = (m_e c^2/e) \tilde{a}_0 \tilde{a}_-^* .$$

Substitution of the above expression into Eq. (113) determines $\tilde{n}_e(\Omega, \underline{\kappa})$ as a function of $\tilde{a}_0 \tilde{a}_1^*$ and \tilde{S}_n^s . We then substitute for the charge density in Eq. (114) to express the nonlinear current likewise as a function of \tilde{a}_1 , \tilde{a}_0 , and \tilde{S}_n^s . We Fourier and Laplace-transform the electromagnetic wave equation, Eq. (13), to close the set of equations. Recalling the definitions $D_- \equiv \kappa^2 c^2 - 2\underline{k}_0 \cdot \underline{\kappa} c^2 - \Omega^2 + 2\Omega\omega_0$ and $\Gamma(\Omega, \underline{\kappa}) \equiv \chi_e(\Omega, \underline{\kappa}) [1 + \chi_1(\Omega, \underline{\kappa})] / \epsilon(\Omega, \underline{\kappa})$, the transformed wave equation including the effects due to longitudinal noise is

$$\begin{aligned} & [D_- - \kappa^2 c^2 |\tilde{a}_0|^2 \Gamma(\Omega, \underline{\kappa})] \tilde{a}_-^* = \\ & - \omega_e^2 \epsilon^{-1}(\Omega, \underline{\kappa}) \tilde{a}_0^* \left\{ [1 + \chi_1(\Omega, \underline{\kappa})] \tilde{S}_n^e(\Omega, \underline{\kappa})/n_0 + \chi_e(\Omega, \underline{\kappa}) \tilde{S}_n^i(\Omega, \underline{\kappa})/n_0 \right\} . \end{aligned} \quad (115)$$

For $|\kappa\lambda_e| \ll 1$, $v_i \ll |\Omega/\kappa| \ll v_e$, and $|\Omega^2/\omega_i^2| \ll 1$, the linear susceptibilities are $\chi_e \approx 1/\kappa^2 \lambda_e^2$ and $\chi_i \approx -\omega_i^2/\Omega^2$. Then the dielectric response $\Gamma(\Omega, \underline{\kappa})$ can be expressed as

$$\Gamma(\Omega, \underline{\kappa}) \approx -\omega_i^2/(\Omega^2 - \kappa^2 c_s^2) .$$

Equation (115) becomes

$$\begin{aligned} & [(\Omega^2 - \kappa^2 c_s^2) D_- + \kappa^2 c_s^2 \omega_i^2 |\bar{a}_0|^2] \bar{a}_-^* = 2\omega_0 D_B(\Omega, \underline{\kappa}) \bar{a}_-^* = \\ & \omega_e^2 \bar{a}_0^* \left[\Omega^2 \tilde{S}_n^i(\Omega, \underline{\kappa})/n_0 - \kappa^2 c_s^2 \tilde{S}_n^e(\Omega, \underline{\kappa})/n_0 \right], \end{aligned}$$

where $D_B(\Omega, \underline{\kappa})$ is defined in Eq. (101). The dispersion relation for Brillouin scattering is determined by $D_B(\Omega, \underline{\kappa}) = 0$.

We can now exhibit equations for \bar{a}_-^* , $\delta \tilde{n}_e$, and $\delta \tilde{n}_i$. From Eq. (116) we find that

$$\begin{aligned} \bar{a}_-^*(\omega_0 - \Omega^*, k_0 - \underline{\kappa}^*) & \equiv \bar{a}_-^* = \\ \omega_e^2 \left[2\omega_0 D_B(\Omega, \underline{\kappa}) \right]^{-1} \bar{a}_0^* & \left[\Omega^2 \tilde{S}_n^i(\Omega, \underline{\kappa})/n_0 - \kappa^2 c_s^2 \tilde{S}_n^e(\Omega, \underline{\kappa})/n_0 \right] \end{aligned} \quad (117a)$$

and from Eq. (113)

$$\begin{aligned} \delta \tilde{n}_e(\Omega, \underline{\kappa}) & = \kappa^2 c_s^2 \omega_i^2 (\Omega^2 - \kappa^2 c_s^2)^{-1} \left[2\omega_0 D_B(\Omega, \underline{\kappa}) \right]^{-1} \\ & \times |\bar{a}_0|^2 \left[\Omega^2 \tilde{S}_n^i(\Omega, \underline{\kappa})/n_0 - \kappa^2 c_s^2 \tilde{S}_n^e(\Omega, \underline{\kappa})/n_0 \right] \\ & - \kappa^2 c_s^2 (\Omega^2 - \kappa^2 c_s^2)^{-1} \tilde{S}_n^e(\Omega, \underline{\kappa})/n_0. \end{aligned} \quad (117b)$$

Use of Eqs. (110) and (111) with $\phi_0^i \approx 0$ gives an expression for $\delta \tilde{n}_i(\Omega, \underline{\kappa})$ of form similar to Eq. (117b).

To construct the Green's functions for the scattered electromagnetic wave $a_-(\underline{x}, t)$ and for the perturbed electron charge density $\delta n_e(\underline{x}, t)$, we multiply Eq. (117a) by $\exp[i(\omega_0 - \Omega)t - i(\underline{k}_0 - \underline{\kappa}) \cdot \underline{x}]$ and Eq. (117b) by $\exp(-i\Omega t + i\underline{\kappa} \cdot \underline{x})$ and perform the inverse Laplace

and Fourier transforms. We consider the Green's functions with sources due to ion or electron noise separately, asserting that the ion noise and electron noise due to discreteness are independent. We replace $\delta n_s(\underline{x}, t)$ by a Dirac δ -function in space and time whose Fourier and Laplace transform is unity. The Green's functions $G_a^s(\underline{x}, t)$ for $a(\underline{x}, t)$, due to initiation by longitudinal electron or ion noise respectively, are

$$\begin{aligned} \begin{bmatrix} G_a^e(\underline{x}, t) \\ G_a^i(\underline{x}, t) \end{bmatrix} &= (2\pi)^{-3} \int_{C_\Omega} d\Omega \int_{C_{\underline{\kappa}}} d^2\kappa \frac{\omega_e^2 a_0^{*n_0} - 1}{D_B(\Omega, \underline{\kappa})} \\ &\times \exp[i(\omega_0 - \Omega)t - i(\underline{k}_0 - \underline{\kappa}) \cdot \underline{x}] \begin{bmatrix} -k^2 c_s^2 \\ \Omega^2 \end{bmatrix} \end{aligned} \quad (118)$$

where C_Ω is the Laplace or Bromwich contour and $C_{\underline{\kappa}}$, before deformation, is the real $\kappa_x - \kappa_z$ plane. The corresponding Green's functions for the electron and ion density perturbations can be similarly constructed.

The Green's functions for $a(\underline{x}, t)$, Eq. (118), and also for the density perturbations can be written as follows, where we have performed the Ω -integration by depressing the C_Ω contour down as far as possible and deforming the contour around the highest poles of the integrand:

$$\begin{aligned} G_a^s(\underline{x}, t) &= -i \sum_j (2\pi)^{-2} \int_{C_{\underline{\kappa}}} d^2\kappa \frac{I_a^s(\Omega_{\underline{\kappa}; j}, \underline{\kappa})}{\partial D_B(\Omega, \underline{\kappa}) / \partial \Omega |_{\Omega_{\underline{\kappa}; j}}} \\ &\times \exp[i(\omega_0 - \Omega_{\underline{\kappa}; j})t - i(\underline{k}_0 - \underline{\kappa}) \cdot \underline{x}] + \text{c.c.} \end{aligned} \quad (119)$$

$I_a^s(\Omega_{\underline{\kappa};j}, \underline{\kappa})$ absorbs all the constant coefficients and the remaining Ω and $\underline{\kappa}$ dependence of the integrand. The superscripts s denote the species of the noise source. $\Omega_{\underline{\kappa};j}$ is determined by $D_B(\Omega, \underline{\kappa}) = 0$, and \sum_j denotes the sum over the various branches of the dispersion relation $D_B(\Omega, \underline{\kappa}) = 0$. We take only the roots for which $\text{Re } \Omega_{\underline{\kappa};j} > 0$, since we add the complex conjugate on the right side of Eq. (119).

In calculating the Green's functions for $\delta n_s(\underline{x}, t)$, there are additional poles of the integrand due to terms appearing in the denominator like $\Omega^2 - \kappa^2 c_s^2$, for example. Since for these poles $\text{Im } \Omega = \text{Im}(\pm \kappa c_s) = 0$, they do not lead to instability; however, they remind us of the presence of the low frequency normal modes that can also be initiated by longitudinal noise, i.e., ion acoustic waves.

In performing the remaining $\underline{\kappa}$ -integration in Eq. (119), the C_Ω contour can be deformed as long as the zeroes $\underline{\kappa}_\Omega$ of $D_B(\Omega, \underline{\kappa}) = 0$ remain on their respective sides of the contours $C_\underline{\kappa}$ in the complex κ_x - and κ_z -planes.¹⁰⁰ Since $\Omega_{\underline{\kappa}} t$ will lead to a rapid phase variation $\exp(-i \text{Re } \Omega_{\underline{\kappa}} t)$ and perhaps to an exponential growth $\exp(\text{Im } \Omega_{\underline{\kappa}} t)$, the dominant contribution to the integral in the complex κ -space will arise from the saddle or stationary phase points described by $\partial \Omega_{\underline{\kappa}} / \partial \underline{\kappa} = 0$. Provided that $\partial D_B(\Omega, \underline{\kappa}) / \partial \Omega|_{\underline{\kappa}} \neq 0$, the saddle point condition is equivalent to the simultaneous conditions $D_B(\Omega, \underline{\kappa}) = 0$ and $\partial D_B(\Omega, \underline{\kappa}) / \partial \underline{\kappa} = 0$. This corresponds to two roots of the dispersion relation pinching together.

If the pinching roots come from opposite sides of the $C_\underline{\kappa}$ contours, then no further contour deformations can be performed at the pinch point. The C_Ω contour can be depressed elsewhere in the complex Ω -plane but $C_\underline{\kappa}$ is trapped at $\underline{\kappa}_p$ by causality requirements

between the pinching roots $\underline{\kappa}_\Omega = \underline{\kappa}_p$. If $\text{Im } \Omega_{\underline{\kappa}} > 0$ at the pinch point, then the instability grows in time everywhere in space (absolute instability¹⁰⁰) with asymptotic Green's functions:

$$G_a^s(\underline{x}, t) \propto$$

$$\frac{I_a^s(\Omega_p, \underline{\kappa}_p; \underline{x}, t) \exp[i(\omega_0 - \Omega_p)t - i(\underline{k}_0 - \underline{\kappa}_p) \cdot \underline{x}]}{\partial D_B(\Omega, \underline{\kappa}) / \partial \Omega |_{\Omega_p, \underline{\kappa}_p}} + \text{c. c.}$$

and similarly

$$G_n^s(\underline{x}, t) \propto \frac{I_n^s(\Omega_p, \underline{\kappa}_p; \underline{x}, t) \exp(-i\Omega_p t + i\underline{\kappa}_p \cdot \underline{x})}{\partial D_B(\Omega, \underline{\kappa}) / \partial \Omega |_{\Omega_p, \underline{\kappa}_p}} + \text{c. c.},$$

where Ω_p and $\underline{\kappa}_p$ are the pinch-point frequency and wavenumber with largest positive $\text{Im } \Omega_p$. The functions I_a^s and I_n^s incorporate the different frequency- and wavenumber-dependent factors remaining in polynomial form in the numerators and denominators of the respective Green's functions' integrands. They also include the dependence on Ω_p , $\underline{\kappa}_p$, \underline{x} , and t , as the result of the saddle-point integration:

$$\int d^2 \underline{k}' \exp[-i\underline{\Omega}'' : \underline{k}' \underline{k}' t + i \underline{k}' \cdot \underline{x}]$$

where $\underline{\Omega}'' \equiv \partial^2 \Omega / \partial \underline{k} \partial \underline{k} |_{\Omega_p, \underline{\kappa}_p}$

To analyze the nature of the absolute instability of stimulated Brillouin scattering in all regimes of pump strength, the pinch conditions can be directly applied to Eq. (101) or (105). The pinch conditions become

$$D_B(\Omega, \kappa, \cos \theta) = 0 \quad (120a)$$

$$\partial D_B(\Omega, \kappa, \cos \theta) / \partial \kappa = 0 \quad (120b)$$

$$-\kappa^{-1} \sin \theta \partial D_B(\Omega, \kappa, \cos \theta) / \partial \cos \theta = 0 \quad (120c)$$

Equation (120c) gives $2\kappa \sin \theta (\kappa^2 c_s^2 - \Omega^2) = 0$, which has non-trivial solutions for $\theta = 0, \pi$ and $\kappa \neq 0$. The other solutions to Eq. (112c), $\Omega = \pm \kappa c_s$, merely describe free ion acoustic oscillations and are inconsistent with Eq. (120a). The $\theta = 0$ solution corresponds to Brillouin backscatter. Setting $\cos \theta = 1$ reduces Eqs. (120a) and (120b) to a one dimensional description.

The asymptotic behavior for modes where $\theta \neq 0$ is constructed from the simultaneous solution of Eqs. (120a) and (120b) as functions of Ω and κ and with fixed parameter $\cos \theta$. These modes can grow in time as well. However, as they do not represent simultaneous solution of the entire set of Eqs. (120), these modes will have weaker growth rates; i.e., their growth rates have not been maximized with respect to scattering angle θ . This is corroborated by Eqs. (104) and (107) which show that the growth rates of Brillouin weak and strong coupling are maximized for exact backscatter, $\theta = 0$.

The pinch-point solutions for complex Ω describe the temporal growth, if $\text{Im } \Omega > 0$, and oscillation, if $\text{Re } \Omega \neq 0$, of the low frequency density perturbation. The scattered electromagnetic wave has shifted complex frequency $\omega_0 - \Omega^*$. A finite imaginary part of κ will produce a spatial growth or attenuation of the amplitudes of the density perturbation and the scattered electromagnetic wave: in fact, both grow in space in the direction of the backscatter.

-117-

To explicitly determine the pinch-point frequencies and wave-numbers for Brillouin, Eq. (105) is substituted into Eqs. (120a) and (120b) with $\cos \theta = 1$. We then solve numerically. Since the ratio $\left[(\omega_1/\omega_0)^2 (k_0 r_0)^2 / 2 \right]^{1/3} / (k_0 c_s / \omega_0)$ determines the distinction between the weak and strong coupling regimes of the Brillouin dispersion relation, we set $k_0 c_s / \omega_0 = 0.01$ for convenience and vary $P \equiv \left[(\omega_1/\omega_0)^2 (k_0 r_0)^2 / 2 \right]^{1/3}$ as a free parameter. Figure 30 shows a plot of $\text{Re } \Omega/\omega_0$ and $\text{Im } \Omega/\omega_0$ vs $(\omega_1/\omega_0)^2 (k_0 r_0)^2 / 2$, while Fig. 31 plots $\text{Re } \kappa/2k_0$, $\text{Im } \kappa/2k_0$, and $\text{Re } \Omega/\text{Re } \kappa c_s$ vs $(\omega_1/\omega_0)^2 (k_0 r_0)^2 / 2$. By slowly increasing the pump strength from $P^3 \ll (k_0 c_s / \omega_0)^3 = 10^{-6}$ to $P^3 \gg (k_0 c_s / \omega_0)^3 = 10^{-6}$, the continuous transition from weak to strong coupling should be exhibited, if it exists. Before commenting on the results, we digress to solve Eqs. (120a) and (120b) algebraically for weak coupling.

We can write Eq. (101) as

$$D_B(\Omega, \kappa, \cos \theta) = \left[\Omega + c^2 (\kappa^2 - 2\kappa k_0 \cos \theta) / 2\omega_0 \right] (\Omega^2 - \kappa^2 c_s^2) + \omega_1^2 \kappa^2 \tilde{v}_0^2 / 8\omega_0 = 0 \quad (121)$$

If we make an expansion $\Omega = \kappa_0 c_s + \delta\omega$ and $\kappa = \kappa_0 + \delta\kappa$, where $\kappa_0/2k_0 = \cos \theta - c_s/v_g$ is the wavenumber for exact frequency and wavenumber matching, and assume that appropriate for weak coupling $|\delta\kappa/\kappa_0|, |\delta\omega/\kappa_0 c_s| \ll 1$, then from Eq. (121) we find that

$$D_B(\delta\omega, \delta\kappa, \cos \theta) \approx \left[\delta\omega + c^2 \delta\kappa (\kappa_0 - k_0 \cos \theta) / \omega_0 \right] (\delta\omega - \delta\kappa c_s) + \omega_1^2 \kappa_0^2 \tilde{v}_0^2 (16\kappa_0 c_s \omega_0)^{-1} = 0 \quad (122)$$

To obtain the pinch point describing the absolute instability of weak coupling Brillouin, we set $\theta = 0$ in accordance with Eq. (120c) to obtain $\kappa_0 = 2k_0(1 - c_s/v_g)$ and

$$D_B(\delta\omega, \delta\kappa) \equiv \left[\delta\omega + \delta\kappa(\kappa_0 - k_0)c^2/\omega_0 \right] (\delta\omega - c_s\delta\kappa) + \gamma_0^2 \quad (123)$$

where $\gamma_0^2 \equiv \omega_1\omega_0(\kappa_0 r_0)^2(16\kappa_0\lambda_e)^{-1}$ and $\omega_a \equiv 2k_0c_s$. Then Eq. (120b) becomes

$$\begin{aligned} \partial D_B(\delta\omega, \delta\kappa)/\partial\delta\kappa &= \left[(\kappa_0 - k_0)c^2/\omega_0 \right] (\delta\omega - c_s\delta\kappa) \\ &\quad - c_s \left[\delta\omega + c^2(\kappa_0 - k_0)\delta\kappa/\omega_0 \right] . \end{aligned} \quad (124)$$

If we define $c_1 \equiv c^2(\kappa_0 - k_0)/\omega_0$, the magnitude of the group velocity of the backscattered electromagnetic wave, then the simultaneous solutions of Eqs. (123) and (124), determining the pinch point, are

$$\delta\omega_s = \pm i2v_0(c_1 c_s)^{\frac{1}{2}}/(c_1 + c_s) \approx \pm i2\gamma_0(c_s/c_1)^{\frac{1}{2}} \quad (125a)$$

and

$$\delta\kappa_s = (\kappa_s - \kappa_1)/2 \approx \pm i\gamma_0/(c_1 c_s)^{\frac{1}{2}} , \quad (125b)$$

where $\kappa_1 \equiv \delta\omega_s/c_1$ and $\kappa_s \equiv \delta\omega_s/c_s$.¹⁰³ The ratio $k_0 c_s/\omega_0$ has been assumed small throughout. The generalization of these results to include dissipation is found in the literature.^{11,103}

The weak coupling pinch-point solutions Eqs. (125) are plotted for purposes of reference in Figs. 30 and 31 as dashed lines. The lower limit of pump strength in these figures corresponds to $(\omega_1/\omega_0)^2(k_0 r_0)^2/2 = (k_0 c_s/\omega_0)^3 = 10^{-6}$, which, according to the normal mode analysis, is the upper limit of the weak coupling regime. One observes that the weak coupling analytic formulae describe Brillouin

-119-

absolute instability to an excellent approximation over a broad range of pump strengths $(\omega_1/\omega_0)^2(k_0 r_0)^2/2 > (k_0 c_s/\omega_0)^3$ well into the strong coupling regime of normal modes. The weak coupling formulae represent valid pinch-point solutions for the general Brillouin dispersion relation, Eq. (101) or (105) provided $|\delta\omega_s/\kappa c_s| \ll 1$. The condition $(\omega_1/\omega_0)^2(k_0 r_0)^2/2 \ll (k_0 c_s/\omega_0)^3$ applies to the linear dispersion relation describing the normal mode spectrum, i.e., the complex frequency $\Omega_{\underline{k}}$ as a function of real \underline{k} . In terms of a condition on the pump strength \tilde{v}_0^2/c^2 , the weak coupling pinch point formulae require that

$$(\tilde{v}_0/c)^2(\omega_1/2k_0 c_s)^2 \ll 1,$$

while the weak coupling linear normal mode dispersion relation demands that

$$(\tilde{v}_0/c)^2(\omega_1/2k_0 c_s)^2(v_g/c_s) \ll 1,$$

where numerical factors of order unity and dependence on $\kappa/2k_0$ have been dropped. Comparison of the two conditions demonstrates that the weak coupling formulae describe absolute Brillouin instability for pump-wave amplitudes $(\tilde{v}_0/c)^2$ allowed to be larger by $v_g/c_s = c^2 k_0/\omega_0 c_s$ than those for which the linear dispersion relation of Brillouin $\Omega_{\underline{k}}$ becomes strongly modified.

In Figs. 30 and 31, only for pump strengths $(\omega_1/\omega_0)^2(k_0^2 r_0^2/2) \geq 10^{-3}$ do the pinch-point solutions diverge from the weak coupling formulae. In this regime of pump strengths finite $\delta \equiv D_-/D_+$ corrections to the Brillouin dispersion relation become necessary. We recall from Eq. (109) that replacement of $(\tilde{v}_0/c)^2$

by $(\tilde{v}_0/c)^2 [1 + \delta/(1 - \delta)]$, in the Brillouin dispersion relation where δ is to be evaluated for complex Ω and $\underline{\kappa}$, provides an implied recursion relation for including the effects of the A_+ sideband in Brillouin. In Fig. 32 $|\delta|$ evaluated at the pinch-point frequency and wavenumber is plotted as a function of $(\omega_i/\omega_0)^2 (k_0^2 r_0^2/2)$. We conclude from Figs. 30, 31, and 32 that the absolute instability of Brillouin is adequately described by the weak coupling formulae for all pump strengths, except for those so intense as to drive both A_+ and A_- sidebands to comparable amplitude and therefore necessitate solution for the general filamentation and Brillouin pinch-point frequencies and wavenumbers using Eq. (96).

A final but necessary demonstration of the Brillouin pinch-point behavior for large and small pump strengths is furnished in Figs. 33 and 34. Level contours of $|D_B(\Omega, \kappa, \theta = 0)|$ in the complex κ plane for parameter Ω are plotted using Eq. (105). $\text{Re } \Omega$ is held constant at its pinch-point value for given pump strength, and $\text{Im } \Omega$ is varied from slightly below the pinch point, through it, and then above. Roots of the dispersion relation appear as a nesting of concentric contours. Figure 34 shows the coalescing and retreat of pinching roots for weak coupling $(\omega_i^2/\omega_0^2)(k_0^2 r_0^2/2) = 10^{-7} \ll (k_0 c_s/\omega_0)^3 = 10^{-6}$. The identical topological behavior occurs in Fig. 34 for $(\omega_i^2/\omega_0^2)(k_0^2 r_0^2/2) = 10^{-2} \gg (k_0 c_s/\omega_0)^3 = 10^{-6}$.

5. Plasma and Laser Parameters for Brillouin Strong Coupling and Filamentation

For existing laser-plasma experiments, e.g., laser-pellet experiments using neodymium glass lasers and laser heated θ -pinch experiments using CO_2 gas lasers, we consider what pump intensities

are necessary to induce strong coupling and filamentation. Table I exhibits parameters typical of these experiments. P^0 is the laser power intensity in watts/cm². For strong coupling we use Eq. (107) to obtain

$$\Omega_{\underline{k}}(\underline{k} = 2\underline{k}_0) \approx (-\omega_1^2 k_0^2 \tilde{v}_0^2 / 2\omega_0)^{1/3} =$$

$$(-1)^{1/3} \begin{cases} 0.3 \times 10^{13} (P^0 / 10^{16} \text{ W/cm}^2)^{1/3} \text{ sec}^{-1} & \text{CO}_2\text{-gas} \\ 0.5 \times 10^{14} (P^0 / 10^{18} \text{ W/cm}^2)^{1/3} \text{ sec}^{-1} & \text{Nd-glass} \end{cases}$$

Using Table I and comparing $\Omega_{\underline{k}}(\underline{k} = 2\underline{k}_0)$ to $\omega_a = 2k_0 c_s$, we determine the effective power densities for the occurrence of strong coupling Brillouin scattering in a homogeneous plasma. For $\Omega_{\underline{k}} > \omega_a$ we find that $P^0 \geq 10^{13} \text{ W/cm}^2$ for CO_2 and 10^{17} W/cm^2 for Nd.

In the limit $(kc/2\omega_0) \gg (c_s/c)$, and $|\cos \theta| \ll 1$, filamentation occurs for $(\tilde{v}_0/c) > \kappa \lambda_e$ corresponding to $P^0 > 2\kappa^2 \lambda_e^2 \times (10^{16} \text{ W/cm}^2 \text{ for } \text{CO}_2, 10^{18} \text{ W/cm}^2 \text{ for Nd})$. In the absence of dissipation, the thresholds for the growth of long wavelength filaments therefore can be quite low. Of course the size of the laser beam and the plasma target determine limits on the wavelengths. The lifetimes of the laser pulse and the plasma target set further limitations on how strong the filamentation growth rates must be to be significant.

Table I. Laser-plasma Experimental Parameters

	$n_0(\text{cm}^{-3})$	$\omega_e(\text{sec}^{-1})$	$\omega_1(\text{sec}^{-1})$	$\omega_0(\text{sec}^{-1})$	$k_0\lambda_e$	$\tilde{\nu}_0^2/c^2$
CO ₂ -gas	10^{17}	3×10^{13}	5×10^{11}	2×10^{14}	0.1-0.3	$P^0/1.2 \times 10^{16} \text{ W/cm}^2$
Nd-glass	10^{20}	6×10^{14}	1×10^{13}	2×10^{15}	0.1-0.3	$P^0/1.2 \times 10^{18} \text{ W/cm}^2$

APPENDIX I: LINEAR SUSCEPTIBILITIES

To derive the limiting forms for the linear susceptibilities we consider the Vlasov equation as a model kinetic equation:

$$\partial_t f_s(x, v; t) + v \partial_x f_s(x, v; t) - (e_s/m_s) \partial_x \phi \partial_v f_s(x, v; t) = 0 \quad (\text{A.1})$$

where $f_s(x, v; t)$ is the normalized distribution function. Then use of $n_s = n_0 \int dv f_s(x, v; t)$, the Poisson equation $-\partial^2 \phi / \partial x^2 = 4\pi \sum_s n_s e_s$, and the definitions of the Fourier transformed linear susceptibilities $\chi_s(\omega, k) \equiv -4\pi k^{-2} e_s \tilde{n}_s / \tilde{\phi}$ in terms of the Fourier amplitudes \tilde{n}_s and $\tilde{\phi}$ yields

$$\chi_s(\omega, k) = -\omega_s^2 / k^2 \int dv f'_s(v) / (v - u) \quad (\text{A.2})$$

where $\omega_s^2 \equiv 4\pi n_0 e_s^2 / m_s$, $f'_s(v) \equiv \partial f_s^0(v) / \partial v$, $u \equiv \omega/k$, and f_s^0 is the velocity-dependent, time and space-independent, unperturbed distribution function.

There are two cases of particular interest when evaluating Eq. (A.2). For $|\text{Im}(\omega/k)| \ll |\text{Re}(\omega/k)|$ we utilize the Landau prescription in evaluating the Hilbert transform:

$$\lim_{\text{Im } u \rightarrow 0^\pm} \frac{1}{v - u} = P\left[1/(v - u)\right] \mp i\pi\delta(v - u) \quad (\text{A.3})$$

where $P(\)$ indicates the principal value of the implied integral. For the case that $|\text{Im}(\omega/k)| \geq |\text{Re } \omega/k|$ and $|\text{Im}(\omega/k)| > 0$, there is no difficulty in evaluating Eq.(A.2) directly; there is no singularity on or near the contour of integration.

If we consider Maxwellian velocity distribution functions for the separate species $f_s^0(v) = (2\pi v_s^2)^{-1/2} \exp(-v^2/2v_s^2)$ where $v_s \equiv (T_s/m_s)^{1/2}$ is the species thermal velocity, then asymptotic

forms for the susceptibilities can be straightforwardly derived.

Numerical tables have also been compiled.¹⁰⁴ If we define

$\eta \equiv v/\sqrt{2} v_s$ and $\xi \equiv \omega/\sqrt{2} kv_s$, then the Fried-Conte function¹⁰⁴

$Z_s(\omega/k)$ can be defined as follows:

$$Z_s(\omega/k) \equiv 1/\sqrt{2} v_s \left[\pi^{-\frac{1}{2}} \int_{-\infty}^{\infty} d\eta \exp(-\eta^2)/(\eta - \xi) \right] \quad (\text{A.4})$$

$$\equiv z_s(\xi)/\sqrt{2} v_s .$$

In evaluating the susceptibilities, the following identity is useful:

$$\pi^{-\frac{1}{2}} \int_{-\infty}^{\infty} d\eta (-2\eta) \exp(-\eta^2)/(\eta - \xi) = dz_s/d\xi \equiv z'_s(\xi). \quad \text{The suscepti-}$$

bilities take the form $\chi_s(\omega, k) = -\omega_s^2 Z'_s(\omega/k)/k^2$ where

$$Z'_s(\omega/k) \equiv dZ_s(\omega/k)/d(\omega/k).$$

For the case that $\omega/kv_s = \sqrt{2} \xi$ is nearly real, then using Eqs. (A.2), (A.3), and (A.4) one obtains

$$\text{Im } z_s = \pi^{-\frac{1}{2}} \exp(-\xi^2), \quad \text{Im } z'_s = -2\pi^{\frac{1}{2}} \xi \exp(-\xi^2) \quad (\text{A.5a})$$

and asymptotically

$$\lim_{\xi \rightarrow 0} \text{Re } z_s = -2\xi(1 - 2/3\xi^2 + \dots), \quad (\text{A.5b})$$

$$\lim_{\xi \rightarrow \infty} \text{Re } z_s = -\xi^{-1}(1 + \xi^{-2}/2 + \dots) ,$$

and

$$\lim_{\xi \rightarrow 0} \text{Re } z'_s = -2 + 4\xi^2 + \dots , \quad (\text{A.5c})$$

$$\lim_{\xi \rightarrow \infty} \text{Re } z'_s = \xi^{-2}(1 + 3\xi^{-2}/2 + \dots) .$$

For $\omega/kv_s = \sqrt{2} \xi$ complex then the results (A.5b) and (A.5c) describe the complex asymptotic forms of the Fried-Conte functions if one drops the designation "Re" on the left sides of the equations. Weakly damped electron plasma oscillations correspond to $\omega \approx \omega_e \gg \omega_i$ and $|\omega/k| \gg v_e$. Then the ion susceptibility is negligible, and the electron susceptibility is given by

$$\chi_e \approx -\omega_e^2 / (\omega^2 - 3k^2 v_e^2) + i(\pi/2)^{1/2} (\omega_e/kv_e)^3 \exp(-\omega^2/2k^2 v_e^2).$$

For ion modes in the limit that $\omega_i \gg |\omega|$ and $v_e \gg (\omega/k) \gg v_i$, then to lowest order of approximation the susceptibilities are given by

$$\chi_e \approx 1/k^2 \lambda_e^2 \quad \text{and} \quad \chi_i \approx -\omega_i^2 / \omega^2.$$

APPENDIX 2: ELECTROMAGNETIC CODE

```
PROGRAM EM1(INPUT,OUTPUT,TAPE2=INPUT,TAPE3,TAPE4)
C ONE-DIMENSIONAL ELECTROMAGNETIC PLASMA SIMULATION CODE.
C RELATIVISTIC ELECTRONS, NON-RELATIVISTIC IONS.
C WRITTEN BY A. BRUCE LANGOON, LIVERMORE, 1972.
C BEAUTIFIED BY B. COHEN, M. MOSTROM, AND D. NICHOLSON BERKELEY MARCH, 1973
C
COMMON/CFIELD/NG,L,AEL,DX,CGSHL, JYM(257),RZ(257),RHOO(257),
. RHQ(257),PHI(257),EX(257),JYP(257),EYL(257),EYR(257),EY(257)
REAL L, JYM, JYP
C
COMMON/1/X(2000),VX(2000),VY(2000)
COMMON/CNTRL/IT,DT,TIME,IEX,IJY,IEYL,IEYR,
. PLOTS,NTH,ITHL,IEY,IBZ,
. IRHO,IRHOS,IPHI,IXVX,IXVY
COMMON/SAVE/ H(8,301),HH(301),KAY(8),NKAYS,ITH,NT,NF,NL
LOGICAL PLOTS,IFT
COMMON/THERMAL / ITERM
COMMON/UNITS/PNMIC2I,RNM2C2I,RMIC2I,FM2C2I,M2C2EV
COMMON/BDRY/MCAT,ICOLL,EYRM,EYLM,EYRC,EYRN,EYLC,EYLN
COMMON /PLMP/ WPMPR,WPML,EPMPR,EPML
REAL LP,VR(2),M1C2,M2C2
INTEGER TITLE(9)
C
COMMON/2/EXE(301),EYE(301),EYLE(301),EYRE(301),KE1(301),
. KE2(301),PIX(302),PIY(302),PZX(302),PZY(302),NM1,NM2
REAL KE1, KE2, NM1, NM2
REAL M1, M2, KE, KO
NAMelist /IN/ N1,N2,NT,NG,MCDE,V10,V20,X11,X21,
. W1,W2,WCI,QM1,QM2,KO,DT,PLOTS,IRHO,IRHOS,IPHI,
. IXVX,IXVY,IEX,IEY,IBZ,IJY,IEYL,IEYR,IFT/6*40,.TRUE./
. ,TEMP1,TEMP2,WPMPR,WPML,EPMPR,EPML,MCAT,ITERM,NF,NL
C DEFAULT INPUT PARAMETERS.
DATA W1,W2,WCI,QM1,QM2/1.,1.,0.,-1.,-1./
DATA V10,V20,X11,X21,MCDE,KO/0.,-0.,2*0.0 ,1,1./
DATA NG,N1,N2,NT,DT/32,128,128,400,.1/
DATA PLOTS,IRHO,IRHOS,IPHI,IXVX,IXVY/.TRUE.,40,0,40,20,20/
DATA IEX,IEY,IBZ,IJY,IEYL,IEYR,IFT/6*40,.TRUE./
DATA SCALE,SCAL2,HW/0.1E+50,0.1E+50,0./
DATA TEMP1,TEMP2/0.,0./
DATA WPMPR,WPML,EPMPR,EPML,MCAT/4*0.0,3/
DATA ITERM,NF,NL/20,64,24/
DATA NKAYS,KAY/8,2,3,4,5,6,7,8,9/
DATA IT,TIME,ITH,ITHL,NTH/0,0.,0,0,300/
DATA TITLE/9*0/
READ(2,IN)
WRITE(3,IN)
CALL HISTRY
ICLL=0
ITTH=1
EYRC=EYRN=EYLC=EYLN=EYPM=EYLM=0.
ENMAX=0.0
ENMAXR=0.0
ENMAXL=0.0
ELCSS=0.
TWCPI=8.*ATAN(1.)
CGSHL=L*TWCPI/KO
C MOAT INTRODUCED
DX=L/NG
T1=WCI*DT/2.
NP=N1+N2
Q1=W1*W1*(NG-MCAT)/(N1*QM1*NG)
```

```

M1=Q1/CM1
NM1=N1*M1
IF(N2.EQ.0)Q2=0.0
IF(N2.NE.0) Q2=W2*W2*(NG-MOAT)/(N2*QM2*NG)
M2=Q2/CM2
T2=0.
IF(M2.GT.0.) T2=M1*T1/M2
NM2=N2*M2
C MIC2EV=.5110041E06 ELECTRON VOLTS.
M2C2EV=M2/M1*.5110041E06
C SCALING IN UNITS OF REST MASS ENERGY DENSITY
MIC2=M1*(DX/CT)**2
M2C2=M2*(DX/CT)**2
RMIC2I=1./(MIC2)
PNMIC2I=1./(N1*MIC2)
IF(N2.NE.0) RM2C2I=1./(M2C2)
IF(N2.NE.0) RNM2C2I=1./(N2*M2C2)
C * * * * *
C DENSITY AND VELOCITY LOADING
C MOAT INTRODUCED
C MOAT MUST BE AN INTEGER GREATER THAN 2
DMOAT=MOAT*DX
LP=L-DMOAT
N11=N1+1
C QUIET START FOR DENSITY
C SCALE IS IN UNITS OF LP-----CONVERT TO ABSOLUTE UNITS OF LENGTH
C DENSITY PROFILE
C SCALE MUST EXCEED .5
SCALE=SCALE*LP/DX
SCAL2=.5*(DX/SCAL2)**2/LP**2
BB= SCALE
XMIN=FLOAT(MOAT)/2.0
XMAX=NG-FLCAT(MOAT)/2.0
CALL DENSE(BB,SCAL2,HW,X,N1,N2,XMIN,XMAX)
DO 10 I=1,N1
VY(I)=0.
VX(I)=V10
10 CONTINUE
CALL CREATOR(VX,VY,V10,1,N1, TEMP1,36HLONGITUDINAL VELOCITY DIST
. RIBUTION 1,34HTRANSVERSE VELOCITY DISTRIBUTION 1)
CALL SPEAR(X,1,N1)
IF(N11.GT.NP)GC TO 17
DO 11 I=N11,NP
VY(I)=0.0
11 VX(I)=V20
CALL CREATOR(VX,VY,V20,N11,NP, TEMP2,36HLONGITUDINAL VELOCITY DI
. STRIBUTION 2,34HTRANSVERSE VELOCITY DISTRIBUTION 2)
CALL SPEAR(X,N11,NP)
17 CONTINUE
NG1=NG+1
DO 12 J=1,NG1
12 EYL(J)=EYR(J)=JYM(J)=JYP(J)=RHOC(J)=0.0
C THIS WILL ZERO RADIATION FIELDS AT T=0.
C DC NOT NEED CURRENT AT T=-DT/2 NOW.
CALL SETRHO(1,N1,Q1)
CALL SETRHO(N11,NP,Q2)
C AT THIS POINT THE NET DENSITY IS EXACTLY ZERO. IF YOU WANT TO
C TWIDDLE THE DENSITY, YOU MUST DO IT AFTER THIS POINT. *****
DO 13 I=1,N1
X(I)=X(I)+X11*CGS(TWOP[*MODE*X(I)]/NG)
13 CONTINUE
C * * * * *

```



```
CALL FIELDS(EXE(1),EYLE(1),EYRE(1),EYF(1),BZE)  
CALL SETV(1,N1,Q1,M1,DT,T1,PIX(1),PIY(1))  
CALL SETV(N1,NP,Q2,M2,DT,T2,P2X(1),P2Y(1))
```

C

```
WRITE(4,949)  
949 FORMAT(4X,* TIME*,5X,* EXE*,13X,* EYLE*,12X,*EYRE*,13X,* EYE*,  
.14X,* KE*,* ICOLL*,9X,* EYLM(1)*,7X,* EYPM(NG1)*//)  
C BEGIN TIME STEP LOOP.  
100 CONTINUE  
CALL ACCEL(1,N1,Q1,M1,DT,T1,PIX(ITH+2),PIY(ITH+2),KE1(ITH ),KE,  
.IT)  
CALL ACCEL(N1,NP,Q2,M2,DT,T2,P2X(ITH+2),P2Y(ITH+2),KE2(ITH ),  
.KE,IT)  
KE=KE/NM1  
WRITE(4,950) TIME,EXE(ITH+1),EYLE(ITH+1),EYRE(ITH+1),EYE(ITH+1),KE  
.ICOLL,EYLM,EYRM
```

950 FORMAT(F8.2,5E16.8,I5,2E16.8)

C ACCUMULATES RADIATED ENERGY LOSS

```
ELOSS=EY(NG1)*EZ(NG1)-EY(1)*BZ(1)+ELOSS  
TOTAL=EXE(ITH+1)+EYE(ITH+1)+KE+BZE  
TOTAL=TOTAL+ELOSS*DX*RNMIC21/CGSHL  
WRITE(4,951) TOTAL
```

951 FORMAT(* TOTAL ENERGY(FIELD+KINETIC+LOSS) NORMALIZED TO NMC2 *,
.E16.8)

VL=VU=0.

CALL PLCTXV(1,N1,VL,VU,L, 9HELECTRONS,1)

VL=VU=0.0

CALL PLOTXV(1,N1,VL,VU,L, 9HELECTRONS,2)

VMU=0.

CALL PLTVXY(1,N1,VMU, 9HELECTRONS)

VL=VU=0.

CALL PLCTXV(N1,NP,VL,VU,L, 4HIONS,1)

VL=VU=0.0

CALL PLCTXV(N1,NP,VL,VU,L, 4HIONS,2)

VMU=0.

CALL PLTVXY(N1,NP,VMU, 4HIONS)

IF(IT.EQ.NT) GO TO 101

IF(ITH.EQ.NTH) CALL HISTRY

IT=IT+1

C PARTICLE DENSITY AND VELOCITY DISTRIBUTION PLCTS

IF((IT/ITHERM)*ITHERM.NE.IT) GO TO 99

ITTH=ITTH+1

GN=FLOAT(NG)

ENCODE(9C,500,TITLE) TIME

500 FORMAT(*ELECTRON DENSITY (NO. OF PTCLS. VS. X/DX) AT TIME=*,
.F10.4)

CALL FCFV(1,N1,0.,GN,X,10H POSITION ,TITLE)

TTT=TIME+.5*DT

ENCODE(9D,8,TITLE) TTT

8 FORMAT(*ELECTRON VELOCITY DISTRIBUTION (NO. OF PTCLS. VS. V/C)
. AT TIME=*,F10.4)

VR(1)=VR(2)=0.

CALL RANGEY(VX,VR,N1)

VM=AMAX1(ABS(VR(1)),ABS(VR(2)))

CALL FCFV(1,N1,-VM,VM,VX,10HX-VELOCITY,TITLE)

VR(1)=VR(2)=0.

CALL RANGEY(VY,VR,N1)

VM=AMAX1(ABS(VR(1)),ABS(VR(2)))

CALL FCFV(1,N1,-VM,VM,VY,10HY-VELOCITY,TITLE)

99 CONTINUE

TIME=IT*DT

ITH=IT-ITHL

```

CALL MCVE(1,N1,C1)
CALL MCVE(N11,N2,Q2)
CALL FIELDS( EX2(I TH+1),EYLE(I TH+1),EYRE(I TH+1),EYE(I TH+1),BZE)
GO TO 100

```

C

C END OF RUN.

```

101 CONTINUE
CALL HISTRY
CALL EXIT
END

```

SUBROUTINE SMEAR(X,IL,IU)

C THIS SUBROUTINE RANDOMIZES A VECTOR ARRAY BY RANDOM PAIR EXCHANGE

```

DIMENSION X(1)
NUM=IU-IL+1
DO 70 I=IL,IU
II=NUM*РАНF(0)+IL

```

```

XX=X(I)
X(I)=X(II)
X(II)=XX

```

70 CONTINUE

RETURN

END

SUBROUTINE DENSE(SCALE,C,HW,X,N1,N2,XMIN,XMAX)

DIMENSION X(1)

INTEGER TITLE(9)

COMMON/BDRY/MCAT,ICOLL,EYRM,EYLM,EYRC,EYRN,EYLC,EYLN

COMMON/CFIELD/NG,L,AEL,DX,CGSHL, JYM(257),BZ(257),RH00(257),

RHO(257),PHI(257),EX(257),JYP(257),EYL(257),EYR(257),EY(257)

FDENS(X)=(N/(XMAX-XMIN))*(1.+ (X-0.5*XMAX+0.5*XMIN)/SCALE

-C*(X-.5*XMAX+.5*XMIN)**2)*ANORM

ANCRH=1./(1.-(XMAX-XMIN)**2*C/12.)

DATA TITLE/9*0/

N=NN=N1

J=1

NSTEPS=100000

DELTA=(XMAX-XMIN)/NSTEPS

AINT=0.5

50 CONTINUE

DO 100 I=1,NSTEPS

AINT=AINT + FDENS(DELTA*I) * DELTA

IF(AINT.GT.FLOAT(J))X(J)=XMIN + DELTA*I

IF(AINT.GT.FLCAT(J))J=J+1

IF(J.GT.NN) GC TC 250

100 CONTINUE

DO 150 I=J,NN

X(I)=X(I-1) + 10.0* DELTA

150 CONTINUE

250 IF(N2.EQ.0) GC TC 350

IF(NN.GT.N1) GO TO 350

AINT=FLOAT(N1)+0.5

J=N1+1

N=N2

NN=N1+N2

IF(N1.EQ.N2) GC TO 60

GO TO 50

60 DO 65 I=J,NN

65 X(I)=X(I-N1)

350 CONTINUE

GN=FLOAT(NG)

ENCODE(90,400,TITLE)

400 FORMAT(*DENSITY PROFILE (NO. OF PTCLS. VS. X) AT T=0*)

CALL FCFV(1,N1,0.,GN,X,10H POSITION ,TITLE)

```
RETURN
END
SUBROUTINE CREATCR(VX,VY,VO,IL,IU,TEMP,TITLE1,TITLE2)
C WE USE THE VX ARRAY AS A DUMMY ARRAY FOR TOTAL P AND TOTAL V
C NSTEPS IS THE AVERAGE NUMBER OF INTEGRATION STEPS PER PARTICLE
DIMENSION VX(1),VY(1)
INTEGER TITLE1(4),TITLE2(4)
INTEGER TITLE(9),XLAB
F(J)=EXP(-SQRT(1.0+CP2+J**2)/T)*DP**2*C
G(J)=EXP(-.5*DP2+J/T)*DP**2*C
IF(IL.GE.IU.OR.TEMP.EQ.0.) RETURN
T=TEMP
NFCUR=(IU-IL+1)/4
NFCUR=NFCUR*4
ANI=NFCUR+1
N=IU-IL+1
PI=ATAN(1.)*4.
C NSTEPS = 200
C VELOCITIES ARE IN UNITS OF C AND MOMENTA IN MC
FMAX=4.0*SQRT(T+4.0*T**2)
DP=PMAX/(N*NSTEPS)
CP2=DP**2
IF(T.GT.0.002) C=.25*N*EXP(1.0/T)/(T+T*T)
IF(T.LE.0.002) C=.25*N/(T+T*T)
J=1
I=1
AINT=0.0
50 CONTINUE
IF(T.GT.0.002) AINT=AINT+J*F(J)
IF(T.LE.0.002) AINT=AINT+J*G(J)
I4=4*I+IL-4
IF(AINT.GT.1) VX(I4)=J*DP
IF(AINT.GT.1) I=I+1
IF(4*I.GT.NFCUR*CR.J*DP.GT.PMAX) GO TO 100
J=J+1
GO TO 50
100 CONTINUE
IF(4*I.GT.N) GO TO 170
I4=4*I+IL-4
DO 150 K=I4,IU
150 VX(K)=0.0
170 CONTINUE
DO 180 I=IL,IU
180 VX(I)=VX(I)/SQRT(1.0+VX(I)**2)
NFL=NFCUR-4
DO 200 J=1,NFL,4
I=J-1+IL
THETA=RANF(0)*PI*.5
PX=VX(I)
VX(I)=PX*COS(THETA)
VY(I)=PX*SIN(THETA)
VX(I+1)=-VX(I)
VY(I+1)=-VY(I)
VX(I+2)=-VX(I)
VY(I+2)=VX(I)
VY(I+3)=-VX(I)
200 VX(I+3)=VY(I)
IF(NFCUR.EC.N) GO TO 202
ILNF=IL+NFCUR
DO 201 J=ILNF,IU
201 VX(J)=VY(J)=0.0
202 CONTINUE
```

```

VYMAX=PMAX/SQRT(1.0+PMAX**2)
VXMAX=(V0+VYMAX)/(1.+V0*VYMAX)
GM=SQRT(1.-V0*V0)
DO 300 I=IL,IU
  VY(I)=GM*VY(I)/(1.+V0*VX(I))
  VX(I)=(VX(I)+V0)/(1.+V0*VX(I))
300 CONTINUE
  XLAB=10HX-VELOCITY
  ENCODE(90,8,TITLE) TITLE1,XLAB
  8 FORMAT(4A10,*(N3. OF PTCLS. VS. *,A10,*/C) AT TIME = 0*)
  CALL FCFV(IL,IL,-VXMAX,VXMAX,VX,XLAB,TITLE)
  XLAB=10HY-VELOCITY
  ENCODE(90,8,TITLE) TITLE2,XLAB
  CALL FCFV(IL,IL,-VYMAX,VYMAX,VY,XLAB,TITLE)
  RETURN
  END

```

```

SUBROUTINE FOFV(IL,IU,VXMIN,VXMAX,VV,XLAB,TITLE)
C BUNCHES PTCLS. INTO BINS OF WIDTH (VXMAX-VXMIN)/NBINS
C AND PLOTS NO. OF PTCLS. VS. POSITION OF BIN CENTER.
  DIMENSION BIN(101),VXBIN(101)
  DIMENSION VV(1)
  INTEGER TITLE(9),XLAB
  NRINS=100
  BINMAX=0.0
  DO 100 J=1,NBINS
    BIN(J)=0.
    VXBIN(J)=VXMIN+(VXMAX-VXMIN)*(FLOAT(J)-0.5)/FLOAT(NBINS)
100 CONTINUE
  DO 200 I=IL,IU
    XXX=NBINS*(VV(I)-VXMIN)/(VXMAX-VXMIN)
    JJ=XXX+1
    IF(JJ.GT.NBINS.OR.JJ.LT.1)GO TO 200
    BIN(JJ)=BIN(JJ)+1.
    IF(BIN(JJ).GT.BINMAX)BINMAX=BIN(JJ)
200 CONTINUE
  CALL PPLT(VXBIN,BIN,VXMIN,VXMAX,0.,BINMAX,NBINS,XLAB,TITLE)
  RETURN
  END

```

```

SUBROUTINE PPLT(X,Y,XMIN,XMAX,YMIN,YMAX,NUM,XLAB,TITLE)

```

C PPLT0020
C PPLT0030
C THIS SUBROUTINE, GIVEN A SET OF N X-Y COORDINATES, WILL PLOT THEM PPLT0040
C ON A 51 BY 101 XY GRID-----THE X ANY Y ARRAYS ARE UNAFFECTED
C BY THIS ROUTINE AND OUT OF RANGE POINTS ARE IGNORED
C PPLT0090
C PPLT0100

```

  INTEGER TITLE(9),XLAB
  DIMENSION X(1), Y(1), XGRID(11), YGRID(11), GRID(101)
  DIMENSION BLA(37)
  DATA (BLA(I),I=1,37)/1H ,1H*,1H2,1H3,1H4,1H5,1H6,1H7,1H8,1H9,
  * 1HA,1HB,1HC,1HD,1HE,1HF,1HG,1HH,1HI,1HJ,1HK,1HL,1HM,1HN,1HO,1HP,
  * 1HQ,1HR,1HS,1HT,1HU,1HV,1HW,1HX,1PY,1HZ,1HS/
  INTEGER BLA,GRID
  WRITE(3,10) TITLE

```

```

10 FORMAT(1H1,2X,5A10)
20 T1 = (XMAX - XMIN) / 10.
  T2 = (YMAX - YMIN) / 10.
  XGRID(1) = XMIN
  YGRID(1) = YMAX
  DO 25 I = 2, 11
    XGRID(I) = XGRID(I - 1) + T1
    YGRID(I) = YGRID(I - 1) - T2
25

```

PPLT0280
PPLT0290
PPLT0300
PPLT0310
PPLT0320
PPLT0330
PPLT0340

```

IF(YMAX.EC.0) YMAX=1.0E-08
IF( ABS(YGRID(11) /YMAX).LT.1.0E-10) YGRID(11)=0.0
L = 1
M = 1
DO 65 K = 1, 10
DO 50 I = 1, 101
50 GRID(I)=1
A=M
Q = (YMAX * (51. - A) + YMIN * (A - 1.))/ 50.
DO 53 IL = 1, NUM
IF (ABS(Q - Y(IL)) - (YMAX - YMIN) / 100.) 41, 53, 53
41 IXP = 100. * (X(IL) - XMIN) / (XMAX - XMIN) + 1.5
51 IF(IXP.GE.1 .AND. IXP.LE.101) GRID(IXP)=GRID(IXP)+1
53 CONTINUE
52 DO 54 J1=1,101
J2=MIND(GRID(J1),37)
54 GRIC(J1)=8LA(J2)
WRITE (3,75) YGRID(L),(GRID(I), I = 1, 101)
N = M + 1
M = N + 3
DO 60 J = N, M
DO 55 I = 1, 101
55 GRID(I)=1
A=J
Q = (YMAX * (51. - A) + YMIN * (A - 1.))/ 50.
DO 57 IL = 1, NUM
IF (ABS(Q - Y(IL)) - (YMAX - YMIN) / 100.) 46, 57, 57
46 IXP = 100. * (X(IL) - XMIN) / (XMAX - XMIN) + 1.5
56 IF(IXP.GE.1 .AND. IXP.LE.101) GRID(IXP)=GRID(IXP)+1
57 CCNTINUE
DO 59 J1=1,101
J2=MIND(GRID(J1),37)
59 GRID(J1)=8LA(J2)
60 WRITE (3,76) GRID
M = M + 1
65 L = L + 1
DO 66 I = 1, 101
66 GRID(I)=1
DO 72 IL = 1, NUM
IF (ABS(YMIN - Y(IL)) - (YMAX - YMIN) / 100.) 69, 72, 72
69 IXP = 100. * (X(IL) - XMIN) / (XMAX - XMIN) + 1.5
70 IF(IXP.GE.1 .AND. IXP.LE.101) GRID(IXP)=GRID(IXP)+1
72 CONTINUE
71 DO 73 J1=1,101
J2=MIND(GRID(J1),37)
73 GRIC(J1)=8LA(J2)
WRITE (3,75) YGRID(11),(GRIC(I), I = 1, 101)
75 FORMAT (10X, E9.2, 1X, 101A1)
76 FORMAT (20X, 101A1)
WRITE (3,85) (XGRID(I), I = 1, 11)
85 FORMAT (16X, 11( E9.2, 1X))
WRITE(3,90) XLAB
90 FORMAT(/60X,A10)
RETURN
END
SURROUTINE HISTRY
C PLOT ENERGIES ETC. VS. TIME.
COMMON/CNTRL/IT,CT,TIME,IX, IJY,IEYL,IEYR,
.PLOTS,NTH,ITHL,IEY,IBZ,
.IRHO,IRHOS,IPHI,IXVX,IXVY
COMMON/SAVE/ R(8,301),HH(301),KAY(8),NKAYS,ITH,NT,NF,NL
LOGICAL PLOTS,IFT

```

PPLT0410
PPLT0420
PPLT0430
PPLT0440

PPLT0470
PPLT0480
PPLT0490
PPLT0500

PPLT0520

PPLT0540
PPLT0550
PPLT0560
PPLT0570

PPLT0600
PPLT0610
PPLT0620
PPLT0630

PPLT0650

PPLT0670
PPLT0680
PPLT0690

PPLT0710
PPLT0720
PPLT0730

PPLT0750

PPLT0780
PPLT0810

PPLT0830
PPLT0840

I

```

C      COMMON/THERMAL/ITHERM
C
C      COMMON/2/EXE(301),EYE(301),EYLE(301),EYRE(301),KE1(301),
C      KE2(301),PIX(302),PIY(302),P2X(302),P2Y(302),NM1,NM2
C      REAL KE1, KE2, NM1, NM2
C      DIMENSION TIM(301),TIMTH(100)
C      IF( IT.EQ.0 ) GO TO 10
C      TL=ITHL*DT
C      MTH=IT-ITHL+1
C      DO 1 I=1,MTH
C      1 TIM(I)=(I-1)*CT+TL
C
C      PLCT FIELD ENERGIES.
C      CALL PLTHST(22)FIELD ENERGY EXE(NMC2),EXE,TIM,MTH,TL,TIME,1,0)
C      CALL PLTHST(23)FIELD ENERGY EYLE(NMC2),EYLE,TIM,MTH,TL,TIME,1,0)
C      CALL PLTHST(23)FIELD ENERGY EYRE(NMC2),EYRE,TIM,MTH,TL,TIME,1,0)
C      CALL PLTHST(22)FIELD ENERGY EYE(NMC2),EYE,TIM,MTH,TL,TIME,1,0)
C
C      PLOT AVERAGE DRIFT MOMENTUM PER PTCL IN UNITS OF MC IE PLOT GAMMA*V/C
C      PLOT IS LABELED TL TO TIME WHEREAS MOMENTUM VALUES
C      ARE ACTUALLY KNOWN FROM TL-DT/2 TO TIME-DT/2.
C      PIXL=PIX(MTH)
C      PIYL=PIY(MTH)
C      IF(NM2.NE.0.0) P2XL=P2X(MTH)
C      IF(NM2.NE.0.0) P2YL=P2Y(MTH)
C      CALL PLTHST(27)AVERAGE PTCL1 XMOMENTUM(MC),PIX,TIM,MTH,TL,TIME
C      ,0,0)
C      CALL PLTHST(27)AVERAGE PTCL1 YMOMENTUM(MC),PIY,TIM,MTH,TL,TIME
C      ,0,0)
C      IF(NM2.NE.0.0)
C      .CALL PLTHST(27)AVERAGE PTCL2 XMOMENTUM(MC),P2X,TIM,MTH,TL,TIME
C      ,0,0)
C      IF(NM2.NE.0.0)
C      .CALL PLTHST(27)AVERAGE PTCL2 YMOMENTUM(MC),P2Y,TIM,MTH,TL,TIME
C      ,0,0)
C
C      PLOT ES MODE ENERGIES
C      DO 499 K=1,AKAYS
C      DO 500 I=1,MTH
C      HH(I)=H(K,I)
C      500 CONTINUE
C      KAY1=KAY(K)-1
C      CALL PLTHST(20)ES MODE ENERGY(NMC2),HH,TIM,MTH,TL,TIME,1,KAY1)
C      499 CONTINUE
C      IF(IT.NE.NT)GO TO 700
C
C      PLOT THERMAL ENERGIES.
C      NPTH=IT/ITHERM+1
C      DO 200 I=1,NPTH
C      TIMTH(I)=(I-1)*ITHERM*DT
C      200 CONTINUE
C      CALL PLTHST(21)THERMAL ENERGY(EV.) 1,KE1,TIMTH,NPTH,0.,TIME,1,0)
C      IF(NM2.NE.0.0)
C      .CALL PLTHST(21)THERMAL ENERGY(EV.) 2,KE2,TIMTH,NPTH,0.,TIME,1,0)
C
C      700 CONTINUE
C      ITHL=IT
C
C      LAST VALUES NOW ARE FIRST VALUES FOR NEXT TIME INTERVAL.
C      PIX(1)=PIXL
C      PIY(1)=PIYL
C      IF(NM2.NE.0.0)P2X(1)=P2XL
C      IF(NM2.NE.0.0)P2Y(1)=P2YL
C      PIX(2)=PIX(MTH+1)

```

```
PIY(2)=PLY(MTH+1)
IF(NM2.NE.0.0)P2X(2)=P2X(MTH+1)
IF(NM2.NE.0.0)P2Y(2)=P2Y(MTH+1)
DC 33 K=1,NKAYS
33 H(K,1)=H(K,MTH)
EXE(1)=EXE(MTH)
EYLF(1)=EYLE(MTH)
EYRE(1)=EYRE(MTH)
EYE(1)=EYE(MTH)
DO 2 I=2,MTH
PIX(I+1)=PIY(I+1)=P2X(I+1)=P2Y(I+1)=0.0
DO 22 K=1,NKAYS
22 H(K,I)=0.
2 EXE(I)=EYLE(I)=EYRE(I)=EYE(I)=0.
RETURN
```

C
C AT T=0 JUST ZERO ARRAYS.

```
10 MTH=NTH+1
DO 11 I=1,MTH
KE1(I)=KE2(I)=PIX(I+1)=PIY(I+1)=P2X(I+1)=P2Y(I+1)=0.
11 EXE(I)=EYLE(I)=EYRE(I)=EYE(I)=0.
PIX(1)=PIY(1)=P2X(1)=P2Y(1)=0.
RETURN
END
```

C
C SUBROUTINE FIELDS(EXE,EYLE,EYRE,EYE,BZE)

```
C SOLVES FOR PHI AND EX, COMPUTES FIELD ENERGY, ETC.
COMMON/CFIELD/NG,L,AEL,DX,CGSHL, JYM(257),BZ(257),RHOO(257),
. RHQ(257),PHI(257),EX(257),JYP(257),EYL(257),EYR(257),EY(257)
COMMON/BDRY/MOAT,ICLL,EYRM,EYLM,EYRC,EYRN,EYLC,EYLN
COMMON /PUMP/ WPMR,WPML,EPMP,EPML
REAL L, JYP, JYP
COMMON/SAVE/ H(3,301),HH(301),KAY(8),NKAYS,ITH,NT,NF,NL
COMMON/CNTRL/IT,DT,TIME,IEX,IJY,IEYL,IEYR,
. PLOTS,NTH,ITHL,IEY,IEZ,
. IRHO,IRHOS,IPHI,IXVX,IXVY
LOGICAL PLOTS,IFT
COMMON/UNITS/RM1C2I,RM2C2I,RM1C2I,RM2C2I,M2C2EV
INTEGER TITLE(5),XLAB
```

```
C
DIMENSION EYRK(257),EYLK(257),XJ(101),GIVEN(2)
REAL RHOK(1), PHIK(1), SCRACH(1)
EQUIVALENCE (RHC,RHCK), (PHI,PHIK), (EX,SCRACH)
REAL KOX2, KSO(128), LI, S(128)
DATA TITLE/9*0/
```

C
C FIRST TIME STEP DUTIES.

```
DATA NG2/0/
IJ=ITH+1
IF( NG2.NE.0 ) GO TO 2
NG2=NG/2
NGL=NG+1
HOX=0.5*DX
LI=1.0/L
HOXI=0.5/DX
TEM=.25*CGSHL*DT
```

C SET UP RATIO PHIK/RHOK.

```
PI=4.0*ATAN(1.0)
DO 1 K=1,NG2
KOX2=(PI/NG)*K
S(K)=1.0
1 KSO(K)=+CGSHL/((2.0*SIN(KOX2)/DX)**2)*S(K)**2
IF(NF.LE.0) GO TO 2
```

```

ITFML=0
HDT=0.5*DT
NF2=NF/2
NPTS=NL
-----
NPTS=MIN0(NPTS,101)
DO 77 J=1,NPTS
77 XJ(J)=FLOAT(J)-1
   XLAB=10H MODE NG.
   XRIGHT=NPTS
2 CONTINUE
-----
C
C TRANSFORM CHARGE DENSITY.
C APERIODIC BOUNDARY CONDITIONS
PHC(1)=RHC(NG1)=0.
CALL PLCTF(RHC,14HCHARGE DENSITY,IRHO)
DO 10 J=1,NG
RHCK(J)=RHC(J)*FCX
10 SCRACH(J)=0.
   CALL CPFT (RHCK,SCRACH,NG,1,1)
   CALL RPFT2(RHCK,SCRACH,NG,1)
   RHOK(1)=0.
-----
C
C CALCULATE PHIK AND FIELD ENERGY.
ESES=0.
PHIK(1)=0.
-----
C
C COMPUTE THE ENERGY IN A PARTICULAR FOURIER MODE
DO 15 KN=1,NKAYS
K=KAY(KN)
IF(KAY(KN).EQ.1) H(KN,IJ)=0.0
IF(KAY(KN).EQ.1) GO TO 15
IF(KAY(KN).EQ.NG2+1) GO TO 13
KK=NG+2-K
FK=KSQ(K-1)*RHCK(K)
FKK=KSQ(K-1)*RHCK(KK)
H(KN,IJ)=(RHOK(K)*FK + RHOK(KK)*FKK)/L*RNMIC2I
GO TO 15
13 H(KN,IJ)=.5*KSQ(K-1)*RHOK(K)**2/L*RNMIC2I
15 CONTINUE
-----
C
C
DO 20 K=2,NG2
KK=NG+2-K
PHIK(K)=KSQ(K-1)*RHCK(K)
PHIK(KK)=KSQ(K-1)*RHCK(KK)
ESES=ESES+RHCK(K)*PHIK(K)+RHCK(KK)*PHIK(KK)
RHCK(K)=S(K-1)*RHCK(K)
20 RHCK(KK)=S(K-1)*RHCK(KK)
   PHIK(NG2+1)=KSQ(NG2)*RHOK(NG2+1)
   EXE=(2.0*ESES+FHCK(NG2+1)*PHIK(NG2+1))/(2.0*L)*RNMIC2I
   RHOK(NG2+1)=S(NG2)*RHOK(NG2+1)
-----
C
C INVERSE TRANSFORM PHI.
DO 30 K=1,NG
RHO(K)=RHCK(K)*LI
30 PHI(K)=PHIK(K)*LI
CALL RPFTI2(PHI,FHC,NG,1)
CALL CPFT (PHI,FHC,NG,1,-1)
C PERIODIC EIGENFUNCTIONS
RHC(1)=RHO(NG1)=C.
PHI(NG1)=PHI(1)

```



```
C IMPOSE BOUNDARY CONDITION OF ZERO ES FIELD AT J=1 AND J=NG1
DELPHI=HDXI*(PHI(NG1)-PHI(2))
DO 31 J=1,NG1
31 PHI(J)=PHI(J)+DELPHI*(J-1)
CALL PLOTFF(RHG,16HSMOOTHED DENSITY,IPHOS)
CALL PLOTFF(PHI,18HELECTRIC POTENTIAL,IPHI)

C
C CENTERED DIFFERENCE ACROSS 2 CELLS.
DO 101 J=2,NG
101 EX(J)=(PHI(J-1)-PHI(J+1))*HDXI
C BOUNDARY CONDITIONS EX(1)=EX(NG1)=0
EX(1)=EX(NG1)=0.
CALL PLOTFF(EX,11HEX, IEX)

C
C MAXWELL EQUATION SOLVER FOR RADIATION FIELDS
CALL PLOTFF(JYP,11HJYP, IJY)
C INPUT EXTERNAL RADIATION FIELDS HERE
EYL(NG1)=EPMPL*SIN(TIME*WPMPL)
EYR(1)=EPMPR*SIN(TIME*WPMPR)
C ADD HALF OF CURRENT, FORMED FROM X(T) AND VY(T+DT/2).
DO 50 J=1,NG1
EYL(J)=EYL(J)-TEM*JYM(J)
50 EYR(J)=EYR(J)-TEM*JYM(J)
C LET C=DX/DT. THEN EYL IS JUST MOVED ONE CELL TO LEFT
C AND EYR ONE CELL TO RIGHT.
DO 51 J=1,NG
EYL(J)=EYL(J+1)
JJ=NG1-J
51 EYR(JJ+1)=EYR(JJ)
C AGAIN INPUT EXTERNAL RADIATION FIELDS
EYR(1)=EPMPR*SIN((TIME+DT)*WPMPR)
EYL(NG1)=EPMPL*SIN((TIME+DT)*WPMPL)
C ADD OTHER HALF OF CURRENT, FORMED FROM X(T+DT) AND VY(T+DT/2).
DO 52 J=1,NG1
EYL(J)=EYL(J)-TEM*JYP(J)
52 EYR(J)=EYR(J)-TEM*JYP(J)
CALL PLOTFF(EYL,16HLEFT-GOING FIELD,IEYL)
CALL PLOTFF(EYR,17HRIGHT-GOING FIELD,IEYR)
C * * * * *
C CALCULATE PUMP TRANSMISSION
EYRC=EYRC
EYLC=EYLC
EYRC=EYRN
EYLC=EYLN
EYRN=ABS(EYR(NG1))
EYLN=ABS(EYL(1))
IF(EYRC.GE.EYRC.AND.EYRC.GE.EYRN) EYRM=EYRC
IF(EYLC.GE.EYLC.AND.EYLC.GE.EYLN) EYLM=EYLC
C * * * * *
DO 60 J=1,NG1
EY(J)=EYR(J)+EYL(J)
60 BZ(J)=EYR(J)-EYL(J)
CALL PLOTFF(EY,11HEY, IEY)
CALL PLOTFF(BZ,11HBZ, IBZ)

C
C CALCULATE RADIATION FIELD ENERGIES.
EYLES=EYRES=EYES=0.
BZES=0.
DO 70 J=2,NG
EYLES=EYLES+EYL(J)**2
EYRES=EYRES+EYR(J)**2
BZES=BZES+BZ(J)**2
```



```

70 EYES =EYES +EY (J)**2
   EYLES=EYLES+0.5*(EYL(1)**2+EYL(NG1)**2)
   EYRES=EYRES+0.5*(EYR(1)**2+EYR(NG1)**2)
   EYFS=EYES+0.5*(EY(1)**2+EY(NG1)**2)
C   LEFT AND RIGHT GOING FIELD ENERGIES.
   EYLE=EYLES*DX/CGSHL*RNMIC2I
   EYRE=EYRES*DX/CGSHL*RNMIC2I
C   EY ENERGY.
   EYE=EYES*DX/(2.*CGSHL)*RNMIC2I
   BZE=BZES*DX/(2.*CGSHL)*RNMIC2I
C
C   FOURIER ANALYZE EYR(X=L) AND EYL(X=0) OVER NF VALUES OF TIME (0 TO
C   NF-1, NF TO 2NF-1, ETC.). SUM OVER FREQ. MODES GIVES ENERGY DENSITY
C   (IN UNITS OF NMIC2/L) AVERAGED OVER AN INTERVAL NF*DT
   IF(NF.LE.0) GC TO 80
   ITEM=IT-ITEML+1
   EYRK(ITEM)=EYR(NG1)*HDT
   EYLK(ITEM)=EYL(1)*HDT
   IF(ITEM.LT.NF) GC TO 80
   CALL CPFT(EYRK,EYLK,NF,1,1)
   CALL RPFT2(EYRK,EYLK,NF,1)
   EYRK(1)=EYLK(1)=0.0
   DO 75 M=2,NF2
   MM=NF+2-M
   EYRK(M)=(EYRK(M)**2+EYRK(MM)**2)*(2.0/CGSHL)*L*RNMIC2I/(NF*DT)**2
75  EYLK(M)=(EYLK(M)**2+EYLK(MM)**2)*(2.0/CGSHL)*L*RNMIC2I/(NF*DT)**2
   EYRK(NF2+1)=EYRK(NF2+1)**2*(1.0/CGSHL)*L*RNMIC2I/(NF*DT)**2
   EYLK(NF2+1)=EYLK(NF2+1)**2*(1.0/CGSHL)*L*RNMIC2I/(NF*DT)**2
   DO 79 M=1,NPTS
79  EYRK(M)=ALOG10(EYRK(M)+1.0E-20)
   EYLK(M)=ALOG10(EYLK(M)+1.0E-20)
   CALL RANGEY(EYRK,GIVEN,NPTS)
   YBOT=GIVEN(1)-5.
   GIVEN(2)=AMAX1(GIVEN(2),YBOT)
   DO 76 M=1,NPTS
76  EYRK(M)=AMAX1(EYRK(M),GIVEN(2))
   TEML=ITEML*DT
   ENCODE(90,78,TITLE) TEML,TIME
78  FORMAT(*RIGHT-GOING FIELD MODE ENERGY DENSITY(NMIC2/L), X=L, FFT
   . OVER T=*,F10.4,* TO *,F10.4)
   CALL PPLT(XJ,EYRK,1.,XRIGHT,GIVEN(2),GIVEN(1),NPTS,XLAB,TITLE)
   CALL RANGEY(EYLK,GIVEN,NPTS)
   YBOT=GIVEN(1)-5.
   GIVEN(2)=AMAX1(GIVEN(2),YBOT)
   DO 97 M=1,NPTS
97  EYLK(M)=AMAX1(EYLK(M),GIVEN(2))
   TITLE(1)=10HLEFT -GOIN
   TITLE(6)=10HX=C, FFT 0
   CALL PPLT(XJ,EYLK,1.,XRIGHT,GIVEN(2),GIVEN(1),NPTS,XLAB,TITLE)
   ITEML=IT+1
80 CONTINUE
C
C   ELECTRIC FIELD HAS NOT BEEN RENORMALIZED YET.
   AEL=1.
   RETURN
   END
C   SUBROUTINE ACCEL(IL,IU,Q,M,DT,TT,PX,PY,THERMT,KE,IT)
C   ADVANCES VELOCITY ONE TIME STEP, COMPUTES MOMENTUM AND KINETIC ENERGY
   REAL KE, M
   COMMON/CFIELD/NG,L,AEL,DX,CGSHL, JYM(257),BZ(257),RHOD(257),
   . RHC(257),PHI(257),EX(257),JYP(257),EYL(257),EYR(257),EY(257)
   REAL L,JYP,JYP,MC2,NRKE,NONREL

```

```

COMMON/1/X(2000),VX(2000),VY(2000)
COMMON/REL/GAMMA(2000)
COMMON/THERMAL/ITHEFM
COMMON/UNITS/RM1C2I,RM2C2I,FM1C2I,FM2C2I,M2C2EV
REAL AX(1),AY(1),TZ(1),THERMX1(257),THERMX2(257),VXOSC(257),
.V2SX(257),N(257),VYOSC(257)
EQUIVALENCE (AX,EX), (AY,EY), (TZ,BZ), (THERMX1,THERMX2,V2SX,PHI)
EQUIVALENCE (VXOSC,JYM), (VYOSC,JYP), (N,RHO)
REAL M2C2EV

```

C

```

IF(IL.GT.IU)RETURN
NG1=NG+1
DO 100 J=1,NG1
THERMX1(J)=N(J)=VXOSC(J)=VYOSC(J)=0.0

```

100 CONTINUE

C RENORMALIZE ACCELERATION IF NEED BE.

```

AE=(Q/M)*(DT*DT/DX)/2.
IF(AE.EQ.AEL) GO TO 2
TEM=AE/AEL
DO 1 J=1,NG1
AX(J)=AX(J)*TEM
AY(J)=AY(J)*TEM
1 TZ(J)=TZ(J)*TEM
AEL=AE

```

2 CONTINUE

```

IF(IL.EQ.1) KE=0.
IF(ABS(Q/M).LT.0.1) GO TO 5

```

C

C LINEAR, MOMENTUM CONSERVING, INCLUDING ALL MAGNETIC FIELDS,

C RELATIVISTIC ELECTRONS.

```

RELKE=NRKE=0.0
DO 250 I=IL,IU
J=X(I)
XX=X(I)-J
T=TT+TZ(J+1)+XX*( TZ(J+2)-TZ(J+1) )
AAX=AX(J+1)+XX*( AX(J+2)-AX(J+1) )
AAY=AY(J+1)+XX*( AY(J+2)-AY(J+1) )

```

C HALF ACCEL. TWO-STEP ROT. METHOD WITH QUICK ROT. SCHEME.

```

GVXX=VX(I)*GAMMA(I)+AAX
GVYY=VY(I)*GAMMA(I)+AAY
GVZ=GVXX*GVXX+GVYY*GVYY
GAMMA2=1.+GVZ
GAMMA1=SQRT(GAMMA2)
T=TAN(T/GAMMA1)
S=(T+T)/(1.+T*T)
RELKE=RELKE+(GAMMA1-1.)*M
NRKE=NRKE+0.5*M *GVZ/GAMMA2
GVXX=GVXX+T*GVYY
GVYY=GVYY-S*GVXX
GVX=GVXX+T*GVYY+AAX
GVY=GVYY+AAY
GVZ=GVX*GVX+GVY*GVY
GAMMA(I)=SQRT(1.+GVZ)
VX(I)=GVX/GAMMA(I)
VY(I)=GVY/GAMMA(I)
PX=PX+GVX
PY=PY+GVY
K=X(I)+.5
N(K+1)=N(K+1)+1.
VXOSC(K+1)=VXOSC(K+1)+VX(I)
VYOSC(K+1)=VYOSC(K+1)+VY(I)

```

250 CONTINUE



```

      KE=AMAX1(RELKE,NRKE)
      C DPIFT MOM./UNIT MASS IN UNITS OF C.
      PX=PX/(IU-IL+1)
      PY=PY/(IU-IL+1)
      IF(ITHERM.LE.0) GO TO 3
      IF((I1/ITHERM)*ITHERM.NE.IT) GO TO 3
      DO 300 J=1,N61
      IF(N(J).LE.0.) GO TO 300
      VXOSC(J)=VXOSC(J)/N(J)
      VYOSC(J)=VYOSC(J)/N(J)
300  CONTINUE
      DO 350 I=IL,IU
      K=X(I)+.5
      GG=1./SQRT(1.-VXOSC(K+1)*VXOSC(K+1)-VYOSC(K+1)*VYOSC(K+1))
      C RELATIVISTIC CALCULATION
      PXTHERM=VX(I)*GAPMA(I)
      PYTHERM=VY(I)*GAPMA(I)
      PXSQ=GG*VXOSC(K+1)*GG*VXOSC(K+1)
      PYSQ=GG*VYOSC(K+1)*GG*VYOSC(K+1)
      C RELATIVE KE DEFINED AS KE(AVG. MOTION+JIGGLE)-KE(AVG. MOTION)
      RELT=SQRT(1.+PXTHERM*PXTHERM+PYTHERM*PYTHERM)-SQRT(1.+PXSQ+PYSQ)
      RELT=.5110041806*RELT
      C NONRELATIVISTICALLY CORRECT
      C
      C NONRELATIVISTIC CALCULATION
      VXTHERM=VX(I)-VXOSC(K+1)
      VYTHERM=VY(I)-VYOSC(K+1)
      NONREL=0.5*.5110041806*(VXTHERM*VXTHERM+VYTHERM*VYTHERM)
      TEMPP=AMAX1(RELT,NONREL)
      THERMT=THERMT+TEMPP/(IU-IL+1)
      THERMX1(K+1)=THERMX1(K+1)+TEMPP/N(K+1)
350  CONTINUE
      CALL PLCTF(THERMX1,18HREL. TE(EV.) VS. X,ITHERM)
      GO TO 3
5    CONTINUE
      C
      C LINEAR, MOMENTUM CONSERVING, INCLUDING ALL MAGNETIC FIELDS,
      C NON-RELATIVISTIC ICNS.
      VIXS=VIYS=VZS=0.
      DO 251 I=IL,IU
      J=X(I)
      XX=X(I)-J
      T=TT+TZ(J+1)+XX*(TZ(J+2)-TZ(J+1))
      T=TAN(T)
      S=(T+T)/(1.+T*T)
      AAX=AX(J+1)+XX*( AX(J+2)-AX(J+1) )
      AAY=AY(J+1)+XX*( AY(J+2)-AY(J+1) )
      C HALF ACCEL. TWO-STEP ROT. METHOD WITH(BUNEMAN) QUICK ROT. SCHEME.
      VXX=VX(I)+AAX
      VYY=VY(I)+AAY
      VZS=VZS+VXX*VXX+VYY*VYY
      VXX=VXX+T*VYY
      VYY=VYY-S*VXX
      VX(I)=VXX+T*VYY+AAX
      VY(I)=VYY+AAY
      K=X(I)+.5
      N(K+1)=N(K+1)+1.
      VXOSC(K+1)=VXOSC(K+1)+VX(I)
      VYOSC(K+1)=VYOSC(K+1)+VY(I)
      VZSX(K+1)=VZSX(K+1)+VX(I)*VX(I)+VY(I)*VY(I)
      VIXS=VIXS+VX(I)
251  VIYS=VIYS+VY(I)

```

```
C
IF((THERM.LE.0) GO TO 4
IF((IT/I THERM)*I THERM.NE.IT) GO TO 4
THERMT=0.
DC 400 J=1,NG1
IF(N(J).LE.0.) GO TO 400
V2SOSC=(VXOSC(J)+VXOSC(J)+VYOSC(J)+VYOSC(J))/N(J)
THERMX2(J)=0.5*M2C2EV*(V2SX(J)-V2SOSC)
THERMT=THERMT+THERMX2(J)/(IU-IL+1)
THERMX2(J)=THERMX2(J)/N(J)
400 CONTINUE
CALL PLOT6(THERMX2,13HTI(EV.) VS. X,I THERM)
4 CONTINUE
KE=KE+0.5*M*V2S
C DRIFT MOM./UNIT MASS IN UNITS OF C.
PX=VIXS/(IU-IL+1)
PY=VIYS/(IU-IL+1)
3 CONTINUE
RETURN
END
SUBROUTINE SETV(IL,IU,Q,M,DT,TT,PX,PY)
C CONVERTS PARTICLE VELOCITIES AT T=0 TO COMPUTER NORMALIZATION AT
C T=-DT/2.
COMMON/CFIELD/NG,L,AEL,DX,CGSHL, JYM(257),RZ(257),RHOO(257),
. RHQ(257),PHI(257),EX(257),JYP(257),EYL(257),EYR(257),EY(257)
REAL L, JYM, JYP, M
COMMON/1/X(2000),VX(2000),VY(2000)
COMMON/REL/GAMMA(2000)
C
IF(IL.GT.IU)RETURN
T=TT
DTDX=DT/DX
C ROTATE V THRU ANGLE +0.5*WC*DT, NON-RELATIVISTIC.
IF(T.EQ.0.) GO TO 2
T=TAN(T)
C=1.0/SQRT(1.0+T*T)
S=C*T
DO 1 I=IL,IU
VXX=VX(I)
VX(I)=C*VXX-S*VY(I)
1 VY(I)=S*VXX+C*VY(I)
2 CONTINUE
C NORMALIZE VX AND VY.
DO 3 I=IL,IU
VY(I)=VY(I)*DTDX
3 VX(I)=VX(I)*DTDX
C ONLY ELECTRONS RELATIVISTIC.
IF(ABS(Q/M).LT.0.2) GO TO 4
DO 99 I=IL,IU
V2=VX(I)*VX(I)+VY(I)*VY(I)
GAMMA(I)=1./SQRT(1.-V2)
99 CONTINUE
4 CONTINUE
C ELECTRIC IMPULSE TO GO BACK 1/2 TIME STEP.
DATA DUM1,DUM2,DUM3/0.,0.,1/
CALL ACCEL(IL,IU,-0.5*Q,M,DT,0.,PX,PY,DUM1,DUM2,DUM3)
RETURN
END
SUBROUTINE MOVE(IL,IU,Q)
C ADVANCES POSITION ONE TIME STEP AND
C ACCUMULATES CHARGE AND CURRENT DENSITIES.
COMMON/CNTRL/IT,CT,TIME,IFX,IJY,IEYL,IEYR,
```

II

```

• PLOTS, NTH, ITHL, IEY, IPZ,
• IRHO, IRHOS, IPHI, IXVX, IVXVY
COMMON/CFIELD/NG, L, AEL, DX, CGSHL, JYM(257), BZ(257), RHOO(257),
• RHO(257), PHI(257), EX(257), JYP(257), EYL(257), EYR(257), EY(257)
LOGICAL PLOTS
REAL L, JYM, JYP, JY
COMMON/L/X(2000), VX(2000), VY(2000)
COMMON/BDRY/MOAT, ICOLL, EYRM, EYLM, EYPC, EYPN, EYLC, EYLN
IF(IL.GT.IU)RETURN
QDX=Q/OX
QDT=Q/DT
C IF IS FIRST GRUP OF PARTICLES, THEN
C CLEAR CUT OLD CHARGE AND CURRENT DENSITIES.
IF(IL.NE.1) GO TO 10
NG1=NG+1
XN=NG
DO 41 J=1, NG1
RHO(J)=RHOO(J)
41 JYM(J)=JYP(J)=0.
10 CONTINUE
C
C LINEAR
DO 201 I=IL, IU
C LINEAR WEIGHTING USING OLD POSITIONS.
J=X(I)
XX=X(I)-J
JY=QDT*VY(I)
DJY=XX*JY
JYM(J+1)=JYM(J+1)-DJY+JY
JYP(J+2)=JYP(J+2)+DJY
X(I)=X(I)+VX(I)
C APERIODIC BOUNARY CONDITIONS
IF(X(I).GE.1.) GO TO 202
ICOLL=ICOLL+1
X(I)=X(I)+2*(1.-X(I))
VX(I)=-VX(I)
202 CONTINUE
IF(X(I).LE.(XN-1.)) GO TO 203
ICOLL=ICOLL+1
X(I)=X(I)+(XN-1.-X(I))*2
VX(I)=-VX(I)
203 CONTINUE
C LINEAR WEIGHTING USING NEW POSITIONS.
J=X(I)
XX=X(I)-J
DJY=XX*JY
JYP(J+1)=JYP(J+1)-DJY+JY
JYP(J+2)=JYP(J+2)+DJY
CRHO=QDX*XX
RHO(J+1)=RHO(J+1)-CRHO+QDX
RHO(J+2)=RHO(J+2)+DRHO
201 CONTINUE
RETURN
C
END
SUBROUTINE SETPHC(IL, IU, Q)
C ACCUMULATES SETPHC(IL, IU, Q) POSITIONS NORMALIZED IN DENSE
COMMON/CFIELD/NG, L, AEL, DX, CGSHL, JYM(257), BZ(257), RHOO(257),
• RHO(257), PHI(257), EX(257), JYP(257), EYL(257), EYR(257), EY(257)
REAL L, JYM, JYP
COMMON/L/X(2000), VX(2000), VY(2000)
C

```

```
IF(IL.GT.IU)RETURN
CDX=0/DX
XN=NG
C IF IS FIRST GROUP OF PARTICLES, THEN CLEAR CUT RHO.
IF( IL.NE.1 ) GO TO 2
DO 1 J=1,NG
1 RHO(J)=RHO0(J)=0.0
RHO(NG+1)=RHO0(NG+1)=0.0
2 CONTINUE
C
C LINEAR
DO 201 I=IL,IU
C APERIODIC BOUNDARY CONDITIONS
IF(X(I).GE.1.) GO TO 202
X(I)=X(I)+2*(1.-X(I))
202 CONTINUE
IF(X(I).LE.(XN-1.)) GO TO 203
X(I)=X(I)+(XN-1.-X(I))*2
203 CONTINUE
J=X(I)
DRHO=QDX*( X(I)-J )
RHO(J+1)=RHO(J+1)-DRHO+QDX
201 RHO(J+2)=RHO(J+2)+DFHJ
NG1=NG+1
DO 300 J=1,NG1
RHO0(J)=RHO0(J) - RHO(J)
RHO(J) = 0.0
300 CONTINUE
RETURN
END
SUBROUTINE PLOT(F,LABEL,INTRVL)
C PLOT FIELD AT CERTAIN TIMES.
DIMENSION LABEL(2),GIVEN(2),XJ(257)
COMMON/CFIELD/NG,L,AEL,DX,COSHL, JYM(257),BZ(257),PHO0(257),
RHO(257),PHI(257),EX(257),JYP(257),EYL(257),EYR(257),EY(257)
REAL L, JYM, JYP, F(1)
COMMON/CNTPL/IT,CT,TIME,IEY,IJY,IEYL,IEYR,
PLOTS,NTH,ITHL,IEY,IBZ,
IRHO,IRHOS,IPHI,IXVX,IXVY
LOGICAL PLOTS
INTEGER TITLE(9),XLAB
DATA XJ(2)/0/
DATA TITLE/9*0/
C
IF( INTRVL.LE.0 ) RETURN
IF( (IT/INTRVL)*INTRVL.NE.IT ) RETURN
IF( .NOT.PLOTS ) RETURN
C
IF( XJ(2).EQ.DX ) GO TO 2
NPTS=NG+1
XLEFT=0.
XRIGHT=L
XLAB=10H POSITION
DO 1 J=1,NPTS
1 XJ(J)=(J-1)*DX
2 CONTINUE
C
CALL RANGEY(F,GIVEN,NPTS)
ENCODE(90,3,TITLE) LABEL,TIME
3 FORMAT(2A10,* AT TIME=*,F10.4)
CALL PPLT(XJ,F,XLEFT,XRIGHT,GIVEN(2),GIVEN(1),NPTS,XLAB,TITLE)
RETURN
```

H

```

      END
      SUBROUTINE PLOTXV(IL,IU,VL,VU,L,LABEL,MARKER)
C   PLOT X-VX SPACE AT CERTAIN TIMES IF MARKER IS 1   OR   PLOT X-VY SPACE
C   AT CERTAIN TIMES IF MARKER IS 2.
      REAL L, JYP, JYV
      COMMON/1/X(2000),VX(2000),VY(2000)
      COMMON/CNTRL/IT,DT,TIME,IEY,IEYL,IEYR,
      .PLOTS,NTH,ITHL,IEY,IBZ,
      .IRHC,IRHOS,IPHI,IXVX,IVXVY
      LOGICAL PLOTS
      INTEGER TITLE(9),XLAB
      DIMENSION GIVEN( 2),LABEL(2)
      DATA TITLE/9*0/
C
      IF(IL.GT.IU)RETURN
      IF( IXVX.LE.0 ) RETURN
      IF( (IT/IXVX)*IXVX.NE.IT ) RETURN
      IF( .NOT.PLOTS ) RETURN
C
      IF(IL.GT.1) CALL SWAP(X,VX,VY,IL)
      NPTS=IU-IL+1
      GIVEN(2)=VL
      GIVEN(1)=VU
C   SET VELOCITY RANGE ETC. IF NEED BE
      IF(VL.LT.VU) GO TO 1
      CALL RANGEY(VX,GIVEN,NPTS)
1   CONTINUE
      XRIGHT=L
      XLAB=10H POSITION
      TIM=TIME+0.5*DT
      IF(MARKER.EQ.2)GO TO 10
      ENCODE(90,3,TITLE) TIM,LABEL
3   FORMAT(* VX VS. X, TIME=*,F10.4,5X,2A10)
      CALL PPLT(X,VX,0.,XRIGHT,GIVEN(2),GIVEN(1),NPTS,XLAB,TITLE)
      GO TO 11
10  CALL RANGEY(VY,GIVEN,NPTS)
      ENCODE(90,5,TITLE) TIM,LABEL
5   FORMAT(* VY VS. X, TIME=*,F10.4,5X,2A10)
      CALL PPLT(X,VY,0.,XRIGHT,GIVEN(2),GIVEN(1),NPTS,XLAB,TITLE)
11  IF(IL.GT.1)CALL SWAP(X,VX,VY,IL)
      RETURN
      END
      SUBROUTINE PLTVXY(IL,IU,VMU,LABEL)
C   PLOT VX-VY PHASE SPACE AT CERTAIN TIMES.
      COMMON/1/X(2000),VX(2000),VY(2000)
      COMMON/CNTRL/IT,DT,TIME,IEY,IEYL,IEYR,
      .PLOTS,NTH,ITHL,IEY,IBZ,
      .IRHC,IRHOS,IPHI,IXVX,IVXVY
      LOGICAL PLOTS
      INTEGER TITLE(9),XLAB
      DIMENSION GIVEN( 2),LABEL(2)
      DATA TITLE/9*0/
C
      IF(IL.GT.IU)RETURN
      IF(IVXVY.LE.0) RETURN
      IF( (IT/IVXVY)*IVXVY.NE.IT) RETURN
      IF( .NOT.PLOTS) RETURN
C
      IF(IL.GT.1) CALL SWAP(X,VX,VY,IL)
      NPTS=IU-IL+1
C   SET VELOCITY RANGE ETC., IF NEED BE
      IF(VMU.NE.0.) GO TO 1

```



```
CALL RANGEY(VX,GIVEN,NPTS)
VMU=AMAX1( ABS(GIVEN(1)),ABS(GIVEN(2)) )
XRIGHT=GIVEN(1)=VMU
XLEFT=GIVEN(2)=-VMU
CALL RANGEY(VY,GIVEN,NPTS)
VMU=AMAX1( ABS(GIVEN(1)),ABS(GIVEN(2)) )
YTOP=GIVEN(1)=VMU
YBOT=GIVEN(2)=-VMU
1 CONTINUE
TIM=TIME+0.5*DT
XLAB=10H VX
ENCODE(90,3,TITLE) TIM,LABEL
3 FORMAT(* VY VS. VX, TIME=*,F10.4,5X,2A10)
CALL PPLT(VX,VY,XLEFT,XRIGHT,YBOT,YTOP,NPTS,XLAB,TITLE)
IF(IL.GT.1) CALL SWAP(X,VX,VY,IL)
RETURN
END
SUBROUTINE SWAP(XX,V1,V2,NN)
DIMENSION XX(1),V1(1),V2(1)
INTEGER NN
NN=NN-1
DO 10 I=1,NN
S1=XX(I)
S2=V1(I)
S3=V2(I)
XX(I)=XX(I+NN)
V1(I)=V1(I+NN)
V2(I)=V2(I+NN)
XX(I+NN)=S1
V1(I+NN)=S2
V2(I+NN)=S3
10 CONTINUE
NN=NN+1
RETURN
END
SUBROUTINE PLTHST(LABEL,REC,TIM,MTH,TL,TU,LINLOG,MODEN)
C PLOT TIME HISTORY, LINEAR OR LOG.
DIMENSION GIVEN( 2),LABEL(3),REC(MTH),TIM(MTH)
INTEGER TITLE(5),XLAB
DATA TITLE/9*0/
NPTS=MTH
XLAB=10H TIME
CALL RANGEY(REC,GIVEN,NPTS)
IF(LINLOG.EQ.0) GO TO 2
YBOT=1.0E-5*GIVEN(1)
DUM=REC(MTH)
DO 3 I=1,MTH
REC(I)=AMAX1(REC(I),YBOT)
REC(I)=ALOG10(REC(I))
3 CONTINUE
CALL RANGEY(REC,GIVEN,NPTS)
IF(MODEN.NE.0) GO TO 5
ENCODE(90,200,TITLE) LABEL,TL,TU
200 FORMAT(* LOG10 OF *,3A10,* TIME=*,F10.4,* TO *,F10.4)
GO TO 6
5 ENCODE(90,300,TITLE) LABEL,MODEN,TL,TU
300 FORMAT(* LOG10 OF *,3A10,*, MODE NO.*,I3,* TIME=*,F10.4,* TO *
.,F10.4)
6 CALL PPLT(TIM,REC,TL,TU,GIVEN(2),GIVEN(1),NPTS,XLAB,TITLE)
REC(MTH)=DUM
GO TO 102
2 CCNTINUE
```

□

```

IF(MODEN.NE.0) GO TO 7
ENCODE(90,100,TITLE) LABEL,TL,TU
100 FORMAT(3A10,* TIME=*,F10.4,* TO *,F10.4)
GO TO 8
7 ENCODE(90,400,TITLE) LABEL,MODEN,TL,TU
400 FORMAT(3A10,*, MODE NO.*,13,* TIME=*,F10.4,* TO *,F10.4)
8 CALL PPLT(TIM,REC,TL,TU,GIVEN(2),GIVEN(1),NPTS,XLAB,TITLE)
102 CONTINUE
RETURN
END
SUBROUTINE RANGEY(Y,GIVEN,NP)
REAL Y(1),GIVEN(2)
YMX=Y(1)
YMN=Y(1)
INCY=1
DO 1 IP=1,NP,INCY
YMX=AMAX1(YMX,Y(IP))
1 YMN=AMIN1(YMN,Y(IP))
IF(YMX.LE.YMN) YMX=YMN+1.
GIVEN(1)=YMX
GIVEN(2)=YMN
RETURN
END
SUBROUTINE RPFT2(A,B,N,INCP)
REAL A(1), B(1)
C REAL DATA, PERIODIC, FOURIER TRANSFORM, TWO AT A TIME. RPFT2 2
C RPFT2 3
C INTERFACE TO COMPLEX PERIODIC FOURIER TRANSFORM, TO DO PAIRS OF RPFT2 4
C TRANSFORMS OF REAL SEQUENCES. RPFT2 5
C RPFT2 6
C THE TWO SEQUENCES ARE ELEMENTS 0, INC, 2*INC... (N-1)*INC OF ARRAYS A,B. RPFT2 7
C RPFT2 8
C AFTER A COMPLEX PERIODIC FOURIER TRANSFORM, WITH A AND B AS THE RPFT2 9
C REAL AND IMAGINARY PARTS, RPFT2 SEPARATES THE TRANSFORMS OF A AND B RPFT2 10
C AND PACKS THEM, TIMES 2, BACK INTO ARRAYS A AND B. RPFT2 11
C THUS, THE CONTENTS OF A AND B ARE REPLACED BY TWICE THEIR TRANSFORMS RPFT2 12
C BY THE CALLS RPFT2 13
C CPFT (A, B, N, INC, SIGN) RPFT2 14
C RPFT2(A, B, N, INC) RPFT2 15
C TWICE THE REAL PARTS OF THE FIRST HALF OF THE COMPLEX FOURIER RPFT2 16
C COEFFICIENTS OF A (COSINE COEF.) ARE IN A(0), A(1)...A(N/2), IF RPFT2 17
C INC=1. TWICE THE IMAGINARY PARTS (SINE COEF.) ARE STORED IN RPFT2 18
C REVERSE ORDER, IN A(N-1), A(N-2)...A(N/2+1). LIKEWISE FOR B. RPFT2 19
C RPFT2 20
C NO PARAMETER *SIGN* IS PROVIDED FOR THE PURPOSE OF CHANGING THE SIGN RPFT2 21
C OF THE SINE COEFFICIENTS. THIS MAY BE DONE WITH PARAMETER *SIGN* OF RPFT2 22
C THE FOURIER TRANSFORM, CPFT. RPFT2 23
C RPFT2 24
C TIME REQUIRED IS LESS THAN 1/10 OF THAT FOR CPFT. RPFT2 25
C RPFT2 26
C SHOULD BE RE-CODED IN ASSEMBLY LANGUAGE. RPFT2 27
C RPFT2 28
C WRITTEN BY A. BRUCE LANGDON, LRL LIVERMOPE, MAY 1971. RPFT2 29
C RPFT2 30
C RPFT2 31
REAL IP, IM RPFT2 32
INC=INCP RPFT2 33
NINC=N*INC RPFT2 34
A(1)=A(1)+A(1) RPFT2 35
B(1)=B(1)+B(1) RPFT2 36
LP=INC RPFT2 37
LM=NINC-LP RPFT2 38
IF( LP.GE.LM ) GO TO 2 RPFT2 39
RPFT2 40

```

```

1      RP=A(LP+1)
      RM=A(LM+1)
      IP=P(LP+1)
      IM=B(LM+1)
      A(LP+1)=RM+RP
      B(LM+1)=RM-RP
      B(LP+1)=IP+IM
      A(LM+1)=IP-IM
      LP=LP+INC
      LM=NINC-LP
      IF( LP.LT.LM ) GO TO 1
2      IF( LP.GT.NINC ) RETURN
      A(LP+1)=A(LP+1)+A(LP+1)
      B(LP+1)=B(LP+1)+B(LP+1)
      RETURN
      END
      SUBROUTINE RPFTI2(A,B,N,INCP)
      REAL A(1), B(1)
C     REAL DATA, PERIODIC, FOURIER TRANSFORM INVERSE, TWO AT A TIME.
C
C     INTERFACE TO COMPLEX PERIODIC FOURIER TRANSFORM, TO DO PAIRS OF
C     TRANSFORMS OF REAL SEQUENCES.
C
C     UNPACKS THE COSINE AND SINE COEFFICIENTS OF A AND B AND COMBINES
C     THEM SO THAT A + I B IS THE COMPLEX PERIODIC FOURIER TRANSFORM OF
C     THE ORIGINAL SEQUENCES. RPFTI2 REVERSES THE EFFECT OF RPFT2, EXCEPT
C     THAT A AND B ARE DOUBLED.
C     THE CALLS
C     RPFTI2(A, B, N, INC)
C     CPFT (A, B, N, INC, -SIGN)
C     INVERT THE TRANSFORM DONE EARLIER, EXCEPT THAT THE ARRAYS HAVE BEEN
C     MULTIPLIED BY 2*N.
C
C     SHOULD BE RE-CODED IN ASSEMBLY LANGUAGE.
C
C     WRITTEN BY A. BRUCE LANGDON, LRL LIVERMORE, MAY 1971.
C
      INC=INCP
      NINC=N*INC
      LP=INC
      LM=NINC-LP
      IF( LP.GE.LM ) RETURN
3      CA=A(LP+1)
      SB=B(LM+1)
      CB=B(LP+1)
      SA=A(LM+1)
      A(LP+1)=CA-SB
      A(LM+1)=CA+SB
      B(LP+1)=CB+SA
      B(LM+1)=CB-SA
      LP=LP+INC
      LM=NINC-LP
      IF( LP.LT.LM ) GO TO 3
      RETURN
      END
      SUBROUTINE CPFT(P, I, N, INCP, SIGNP)
C     FORTRAN TRANSLITERATION OF SINGLETON'S 6600 ASSEMBLY CODED FFT.
C     DIFFERS FROM SINGLETON'S ORIGINAL IN THAT THERE IS A SPECIAL LOOP
C     FOR ANGLE=PI/2. THIS SHOULD BE FASTER ON MACHINES WHOSE FLOATING
C     POINT ARITHMETIC IS MUCH SLOWER THAN INDEXING (NOT TRUE ON CDC 6600).
C     SEE COMMENTS IN OTHER VERSION.
C     A. BRUCE LANGDON, M DIVISION, L.L.L., 1971.

```

```

RPFT2 41
RPFT2 42
RPFT2 43
RPFT2 44
RPFT2 45
RPFT2 46
RPFT2 47
RPFT2 48
RPFT2 49
RPFT2 50
RPFT2 51
RPFT2 52
RPFT2 53
RPFT2 54
RPFT2 55
RPFT2 56
RPFTI2 2
RPFTI2 3
RPFTI2 4
RPFTI2 5
RPFTI2 6
RPFTI2 7
RPFTI2 8
RPFTI2 9
RPFTI210
RPFTI211
RPFTI212
RPFTI213
RPFTI214
RPFTI215
RPFTI216
RPFTI217
RPFTI218
RPFTI219
RPFTI220
RPFTI221
RPFTI222
RPFTI223
RPFTI224
RPFTI225
RPFTI226
RPFTI227
RPFTI228
RPFTI229
RPFTI230
RPFTI231
RPFTI232
RPFTI233
RPFTI234
RPFTI235
RPFTI236
RPFTI237
RPFTI238
RPFTI239
RPFTI240
CPFTPI22
CPFTPI23
CPFTPI24
CPFTPI25
CPFTPI26
CPFTPI27
CPFTPI28

```

I

	REAL R(1), I(1)	CPFTPI29
	INTEGER SIGNP, SPAN, RC	CPFTPI10
	REAL SINES(15), IO, I1	CPFTPI11
	DATA SINES(1)/0./	CPFTPI12
	IF(SINES(1).EC.1.) GO TO 1	CPFTPI13
	SINES(1)=1.	CPFTPI14
	T=ATAN(1.)	CPFTPI15
	DC 2 IS=2,15	CPFTPI16
	SINES(IS)=SIN(T)	CPFTPI17
2	T=T/2.	CPFTPI18
1	CCONTINUE	CPFTPI19
	IF(N.EQ.1) RETURN	CPFTPI20
	INC=INCP	CPFTPI21
	SGN=ISIGN(1, SIGNP)	CPFTPI22
	SPAN=NINC=N*INC	CPFTPI23
	IT=N/2	CPFTPI24
	CO 3 IS=1,15	CPFTPI25
	IF(IT.EQ.1) GO TO 12	CPFTPI26
3	IT=IT/2	CPFTPI27
10	T=S+(SO*C-CO*S)	CPFTPI28
	C=C-(CO*C+SO*S)	CPFTPI29
	S=T	CPFTPI30
11	K1=K0+SPAN	CPFTPI31
	RO=R(K0+1)	CPFTPI32
	R1=R(K1+1)	CPFTPI33
	IO=I(K0+1)	CPFTPI34
	I1=I(K1+1)	CPFTPI35
	R(K0+1)=RO+R1	CPFTPI36
	I(K0+1)=IO+I1	CPFTPI37
	RO=RO-R1	CPFTPI38
	IO=IO-I1	CPFTPI39
	R(K1+1)=C*RO-S*IO	CPFTPI40
	I(K1+1)=S*RO+C*IO	CPFTPI41
	KO=K1+SPAN	CPFTPI42
	IF(KO.LT.NINC) GO TO 11	CPFTPI43
	K1=KO-NINC	CPFTPI44
	C=-C	CPFTPI45
	KO=SPAN-K1	CPFTPI46
	IF(K1.LT.KO) GO TO 11	CPFTPI47
	KO=KO+INC	CPFTPI48
	K1=SPAN-KO	CPFTPI49
	IF(KO.LT.K1) GO TO 10	CPFTPI50
12	CONTINUE	CPFTPI51
	SPAN=SPAN/2	CPFTPI52
	KO=0	CPFTPI53
13	K1=K0+SPAN	CPFTPI54
	RO=R(K0+1)	CPFTPI55
	R1=R(K1+1)	CPFTPI56
	IO=I(K0+1)	CPFTPI57
	I1=I(K1+1)	CPFTPI58
	R(K0+1)=RO+R1	CPFTPI59
	I(K0+1)=IO+I1	CPFTPI60
	R(K1+1)=RO-R1	CPFTPI61
	I(K1+1)=IO-I1	CPFTPI62
	KO=K1+SPAN	CPFTPI63
	IF(KO.LT.NINC) GO TO 13	CPFTPI64
	IF(SPAN.EC.INC) GO TO 29	CPFTPI65
	KO=SPAN/2	CPFTPI66
14	K1=K0+SPAN	CPFTPI67
	RO=R(K0+1)	CPFTPI68
	R1=R(K1+1)	CPFTPI69
		CPFTPI70

	IO=I(KO+1)	CPFTPI71
	I1=I(K1+1)	CPFTPI72
	R(KO+1)=RO+R1	CPFTPI73
	I(KO+1)=I0+I1	CPFTPI74
	R(K1+1)=SGN*(I1-I0)	CPFTPI75
	I(K1+1)=SGN*(RO-R1)	CPFTPI76
	KO=K1+SPAN	CPFTPI77
	IF(KO.LT.NINC) GO TO 14	CPFTPI78
	K1=INC+INC	CPFTPI79
	IF(SPAN.EC.K1) GO TO 12	CPFTPI80
	CO=2.*SINES(I1)**2	CPFTPI81
	IS=IS-1	CPFTPI82
	SO=S=SIGN(SINES(IS),SGN)	CPFTPI83
	C=1.-CO	CPFTPI84
	KO=INC	CPFTPI85
	GO TO 11	CPFTPI86
20	N1=NINC-INC	CPFTPI87
	N2=NINC/2	CPFTPI88
	IJ=JI=RC=0	CPFTPI89
	IF(N2.EQ.INC) RETURN	CPFTPI90
	GO TO 22	CPFTPI92
21	IJ=N1-IJ	CPFTPI93
	JI=N1-JI	CPFTPI94
	T=R(IJ+1)	CPFTPI95
	R(IJ+1)=R(JI+1)	CPFTPI96
	R(JI+1)=T	CPFTPI97
	T=I(IJ+1)	CPFTPI98
	I(IJ+1)=I(JI+1)	CPFTPI99
	I(JI+1)=T	CPFTPI100
	IF(IJ.GT.N2 ; GO TO 21	CPFTPI01
22	IJ=IJ+INC	CPFTPI02
	JI=JI+N2	CPFTPI03
	T=R(IJ+1)	CPFTPI04
	R(IJ+1)=R(JI+1)	CPFTPI05
	R(JI+1)=T	CPFTPI06
	T=I(IJ+1)	CPFTPI07
	I(IJ+1)=I(JI+1)	CPFTPI08
	I(JI+1)=T	CPFTPI09
	IT=N2	CPFTPI10
23	IT=IT/2	CPFTPI11
	RC=RC-IT	CPFTPI12
	IF(RC.GE.0) GO TO 23	CPFTPI13
	JI=RC=RC+2*IT	CPFTPI14
	IJ=IJ+INC	CPFTPI15
	IF(IJ.LT.JI) GO TO 21	CPFTPI16
	IF(IJ.LT.N2) GO TO 22	CPFTPI17
	RETURN	CPFTPI18
	END	CPFTPI19
		CPFTPI20

LIST OF SYMBOLS

<u>Symbol</u>	<u>Description</u>	<u>Page where defined on first use</u>
Latin Alphabet		
a_j	Complex field quantities	2
a_0, a_+, a_-	Dimensionless vector potentials	19
\tilde{a}_j	Slowly varying or Fourier amplitudes	2,110
A, A_0, A_+, A_-, A_ℓ	Vector potentials	13,31
\underline{B}	Magnetic field	9
\underline{B}_0	External magnetic field	25
c	Speed of light	12
\underline{c}_ℓ	Group velocities	34
c_s	Sound speed	18
$C_{\underline{k}}$	κ -space contour	113
C_Ω	Bromwich or Laplace contour	113
c.c.	Complex conjugate	
$D(\omega, k)$	Dispersion relation for electromagnetic waves	19
D_+, D_-	Dispersion relation for electromagnetic sidebands	19
$D_B(\Omega, \underline{\kappa})$	Brillouin dispersion relation	100
D_0, D_1	Partial differential operators	79
e, e_s	Electron charge, species charge	11,14
\underline{E}	Electric field	25
$f_0(v), f(v)$	Perturbed and unperturbed velocity distribution functions	64,123
F_\pm	Electromagnetic field quantities: $F_\pm \equiv E_y \pm B_z$	25

<u>Symbol</u>	<u>Description</u>	<u>Page where defined on first use</u>
$G_a^s(\underline{x}, t)$	Green's function for $a(\underline{x}, t)$ due to density noise in species s	113
$G_n^s(\underline{x}, t)$	Green's function for number density due to density noise in species s	113
h	Resonance zone	40
\hbar	Planck's constant modulo 2π	5
$I_a^s(\omega, \underline{k})$	Multiplicative factors in Green's function integrand	113
$I_n^s(\omega, \underline{k})$	Multiplicative factors in Green's function integrand	115
in	Subscript or superscript denoting input or boundary value	37
$J, J(\underline{x}, t), \tilde{J}$	Transverse current and amplitude	16, 110
J	Longitudinal current	69
$J_y; J_y^+, J_y^-$	Simulation transverse currents	26
J_k	Transverse wave action density	80
J_ℓ^i, J_ℓ^r	Input action density and spatial derivative	40
\underline{k}	Wavenumber	19
k_j	Wavenumber mode j	2
$\underline{k}_0, \underline{k}_1$	Electromagnetic pump-wave wavenumbers	6
$k_p(\underline{x})$	WKB wavenumber for electron plasma wave	93
K	Kinetic energy density	68
K_R^W	Kinetic energy density of resonant particles in waveframe	70
L	Plasma system length	36
L_n	Plasma density scale length	35

<u>Symbol</u>	<u>Description</u>	<u>Page where defined on first use</u>
m, m_e	Electron mass	11
m_i	Ion mass	11
n_0	Unperturbed number density	16
n_s, \tilde{n}_s	Number density in species s and its amplitude	123,15
N_j	Number of quanta in mode j	5
P	Average momentum density	67
P	Pump parameter	117
P^0	Laser power (watts/cm ²)	121
$P(\)$	Principal value integral	123
P_R	Momentum density in resonant particles	70
\underline{r}	Field position	15
r	Magnitude of response: $r \equiv \tilde{\phi}^e / \phi_0^e $	66
r_j	Equilibrium response magnitude	66
R	Relative action transfer	7
R	Complex response amplitude, $R \equiv \tilde{\phi}^e / \phi_0^e$	65
s	Species index	14
$S_{\ell}, S_{\ell}^{\text{in}}$	Action flux density, input action	34,37
\tilde{S}	Action flux density difference: $\tilde{S} \equiv S_0 - S_1$	35
S_n^s, \tilde{S}_n^s	Number density source term for species s and Fourier-Laplace transform	109
t	Time	2
T_s	Temperature of species s	16
$u(\underline{x}, t)$	Transverse electron fluid velocity	28
u_{ℓ}	Transverse electron fluid velocity for mode ℓ	31

<u>Symbol</u>	<u>Description</u>	<u>Page where defined on first use</u>
\underline{v}	Particle velocity	9
\underline{v}_g	Electromagnetic wave group velocity	99
v_g^{\parallel}, v_g	Longitudinal wave group velocity	57,88
v_j	Characteristic wave velocity	2
v_s	Thermal velocity species s	17
v_T	Trapping velocity	49
v_{ϕ}	Phase velocity	76
\tilde{v}	Oscillation velocity	55
\tilde{v}^s	Transverse oscillation velocity for species s	11,14
\tilde{v}_0	Maximum electron transverse velocity in pump wave field	19
V_j	Mode j group velocity	3
W_{ℓ}	Wave energy density in mode j	31
x, \underline{x}	Field or particle position coordinate	2
y	Position coordinate	13
z	Position coordinate	13
z_s	Related plasma dispersion function: $z_s \equiv \sqrt{2} v_s Z_s$	124
Z_s	Plasma dispersion function	124
Z'_s	Derivative of plasma dispersion function	124

<u>Symbol</u>	<u>Description</u>	<u>Page where defined on first use</u>
Greek Alphabet		
α	Coupling constant	42,66
α_j	Coupling constant mode j	3
β	Coupling constant	42
β_j	Coupling constant mode j	2
γ	Dissipation or growth rate	82
γ_{ei}	Electron-ion parametric decay growth rate	56
γ_L	Linear growth or damping rate	62
γ_0	Growth rates for Raman, filamentation, or Brillouin	45,99,118
$\Gamma(\omega, \underline{k})$	Coupling strength: $\Gamma(\omega, \underline{k}) \equiv \chi_e(1 + \chi_i)\epsilon^{-1}$	17
Γ	Coupling constant: $\Gamma \equiv -4\pi \text{Im } \epsilon^{-1}(\Omega, \underline{k})$	40
$\delta(\omega, \underline{k})$	Mismatch ratio: $\delta \equiv D_-/D_+$	107
$\delta j, \delta j_e$	Transverse electron current perturbation	11
δn_s	Number density perturbation	11
$\delta \tilde{n}_s$	Laplace and Fourier transformed δn_s	109
$\delta(x)$	Dirac δ -function	27
$\delta \epsilon$	Nonlinear dielectric function perturbation	62
$\delta \kappa$	Attenuation length	88
$\delta \rho^s, \delta \tilde{\rho}^s$	Nonlinear charge density by species and amplitude	60
$\delta \omega$	Complex, nonlinear frequency shift	62
$\delta \Omega, \delta \Omega_0$	Real part of $\delta \omega$ and related function	65

Symbol	Description	Page where defined on first use
$\epsilon(\omega, \underline{k})$	Dielectric function	15
ϵ'	Real part of ϵ	35
ϵ''	Imaginary part of ϵ	35
ϵ_L	Linear part of ϵ	62
ϵ_{NL}	Nonlinear dielectric function	57
$\bar{\epsilon}, \bar{\bar{\epsilon}}$	First and second frequency derivatives of ϵ	33, 69
η	Characteristic, $\eta \equiv (ct - z)\Gamma J_0^1$	40
η	Small quantity	67
θ	Relative phase of response w.r.t. driver	65
θ	Angle of $\underline{\kappa}$ w.r.t. to \underline{k}_0	98
θ_l	Phase of mode l	79
Θ	Heaviside unit-step function	40
κ	Wavenumber for density perturbation	6
κ_p	Pinch-point wavenumber	115
$\kappa_0, \kappa_1, \kappa_s$	Characteristic wavenumbers related to Brillouin	117, 118
κ'	Spatial derivative of wavenumber mismatch	46
λ_s	Debye length for species s	12
\star	Inverse wavenumber	87
μ	Coupling strength: $\mu^2 \equiv \kappa^2 \bar{v}_0^2 \Gamma(\Omega, \underline{\kappa})/4$	19
ν	Dissipation rate	33
ν_{eff}	Effective dissipation rate	48
ν_{ei}	Electron-ion collision frequency	40
ν_j	Dissipation rate for mode j	2
ν_s	Dissipation rate for electron wave or ion sound wave	55

Symbol	Description	Page where defined on first use
ξ	Characteristic, $\xi \equiv (ct + z)\Gamma J_0^i$	40
ξ	Dimensionless phase velocity: $\xi \equiv \omega/\sqrt{2} kv_s$	124
ρ	Wave action flux density input ratio	37
$\rho(t)$	Total charge density	60
$\rho^s(t), \tilde{\rho}^s$	Charge density species s and Fourier amplitude	60
$\rho_L^s, \tilde{\rho}_L^s$	Linear part of species charge density and Fourier amplitude	60
σ	Characteristic, $\sigma \equiv (ct - z)(\Gamma J_0^i)^{1/2}$	40
τ	Characteristic, $\tau \equiv (ct + z)(\Gamma J_0^i)^{1/2}$	40
τ	Time	50
τ_B	Bounce period	49
τ_{exp}	Duration of experiment (secs.)	50
τ_I	Characteristic time for ignored effect	50
$\phi, \tilde{\phi}$	Coulomb potential and Fourier amplitude	15
$\phi_0^s, \tilde{\phi}_0^s$	Effective, ponderomotive potential and Fourier amplitude, species s	15
$\phi^s, \tilde{\phi}^s$	Total potential and Fourier transform, species s	15
$\chi_s(\omega, \underline{k})$	Susceptibility for species s	15
$\hat{\chi}^s, \chi^s(\omega, \underline{k})$	Susceptibility kernel and nonlinear susceptibility	60,61
$\psi, \tilde{\psi}$	Ponderomotive potential energy and amplitude	32
ψ	Polarization angle	102

<u>Symbol</u>	<u>Description</u>	<u>Page where defined on first use</u>
ω	Frequency	5
ω_a	Ion acoustic frequency	121
ω_B	Bounce frequency	49
ω_j	Mode frequency	2
ω_L, ω_{NL}	Linear and nonlinear eigenmode frequencies	62
ω_p	Plasma frequency	40
ω_s	Plasma frequency for species s	12
$\omega_{0,1}$	Transverse wave frequencies	6
Ω	Beat frequency	6
Ω_j	Characteristic frequency in normal mode dispersion relation	2
Ω_L	Real part of ω_L	32
Ω_p	Pinch-point frequency	115

REFERENCES

1. C. V. Raman, Indian J. Phys. 2, 387 (1928).
2. C. V. Raman and U. S. Krishan, Nature 121, 501 (1928).
3. P. A. Wolff, in Proceedings 2nd International Conference on Light Scattering in Solids (Paris, 1971).
4. N. Bloembergen and Y. R. Shen, Phys. Rev. 141, 29 (1966).
5. L. Brillouin, Ann. Phys. (Paris) 17, 88 (1922).
6. Y. R. Shen and N. Bloembergen, Phys. Rev. 137, 1787 (1965).
7. N. M. Kroll, J. Appl. Phys. 36, 34 (1965).
8. I. S. Danilkin, Sov. Phys. Tech. Phys. 10, 524 (1965).
9. S. E. Bodner and J. L. Eddleman, Phys. Rev. A5, 355 (1972).
10. D. C. Watson, Ph.D. Thesis, Massachusetts Institute of Technology (1975).
11. C. S. Liu, M. N. Rosenbluth, and R. B. White, Phys. Fluids 17, 1211 (1974).
12. J. Drake, P. Kaw, Y. C. Lee, G. Schmidt, C. S. Liu, and M. N. Rosenbluth, Phys. Fluids 17, 778 (1974).
13. P. Kaw, G. Schmidt, and T. Wilcox, Phys. Fluids 16, 1522 (1973).
14. R. Y. Chiao, E. Garmire, and C. Townes, Phys. Rev. Lett. 13, 479 (1964).
15. L. Gorbunov, Zh. Eksp. Teor. Fiz. 65, 900 (1973) (Sov. Phys.-JETP 38, 490 (1974)).
16. V. N. Tsytovich, Nonlinear Effects in Plasma (Plenum Press, New York, 1970).
17. R. C. Davidson, Methods in Nonlinear Plasma Theory (Academic Press, New York, 1972).
18. L. Stenflo, Z. Physik 243, 341 (1971).

19. P. K. C. Wang, *J. Math. Phys.* 14, 911 (1973).
20. K. Nozaki and T. Taniuti, *J. Phys. Soc. Japan* 34, 796 (1973).
21. V. E. Zakharov and S. V. Manokov, *Zh. Eksp. Teor. Fiz. Pis. Red.* 18, 413 (1973) [*Sov. Phys.-JETP Letters* 18, 243 (1973)].
22. D. R. Nicholson, Ph.D. Thesis, University of California, Berkeley (1975).
23. M. N. Rosenbluth, *Phys. Rev. Lett.* 29, 565 (1972).
24. K. Nishikawa, *J. Phys. Soc. Japan* 24, 916 (1968) and *J. Phys. Soc. Japan* 24, 1152 (1968).
25. W. H. Louisell, *Coupled Mode and Parametric Electronics* (Wiley, New York, 1960).
26. J. Dougherty, *J. Plasma Phys.* 4, 761 (1970).
27. J. Galloway and H. Kim, *J. Plasma Phys.* 6, 53 (1971).
28. L. Altshul and V. Karpman, *Zh. Eksp. Teor. Fiz.* 47, 1544 (1964) [*Sov. Phys.-JETP* 20, 1043 (1965)].
29. D. Melrose, *Plasma Phys.* 14, 1035 (1972).
30. M. Rabinovich and S. M. Fainshtein, *Zh. Eksp. Teor. Fiz.* 60, 1696 (1971) [*Sov. Phys.-JETP* 33, 918 (1971)].
31. J. Arons and C. E. Max, *Phys. Fluids* 17, 1983 (1974).
32. S. A. Akhmanov, A. P. Sukhorukov, and R. V. Khokhlov, *Usp. Fiz. Nauk* 93, 19 (1967) [*Sov. Phys.-Usp.* 10, 609 (1968)].
33. A. B. Langdon and B. F. Lasinski, *Phys. Rev. Lett.* 34, 934 (1975).
34. B. I. Cohen, A. N. Kaufman, and K. M. Watson, *Phys. Rev. Lett.* 29, 581 (1972).
35. K. Mima and K. Nishikawa, in *Proceedings of the Fourth Anomalous Absorption Conference*, Lawrence Livermore Laboratory, Livermore, California (1974), p. A.7.

36. S. Jorna, *Phys. Fluids* 17, 765 (1974).
37. S. Bodner and J. Eddleman, Lawrence Livermore Report UCRL-73378 (1971) (unpublished).
38. D. W. Forslund, J. M. Kindel, and E. L. Lindman, *Phys. Rev. Lett.* 29, 249 (1972); *Phys. Rev. Lett.* 30, 739 (1973); and *Phys. Fluids* 18, 1002 (1975).
39. W. Manheimer and E. Ott, *Phys. Fluids* 17, 1413 (1974).
40. A. V. Gaponov and M. A. Miller, *Zh. Eksp. Teor. Fiz.* 34, 242 (1958) (*Sov. Phys.-JETP* 7, 168 (1958)).
41. L. Landau and E. Lifshitz, *Mechanics* (Pergamon Press, New York, 1969).
42. G. Schmidt, *Physics of High Temperature Plasmas* (Academic Press, New York, 1966), sec. 2-9.
43. B. Cohen, M. Mostrom, D. Nicholson, A. Kaufman, C. Max, and A. B. Langdon, *Phys. Fluids* 18, 470 (1975).
44. M. V. Goldman, *Ann. Phys. (New York)* 38, 95 (1966).
45. E. A. Jackson, *Phys. Rev.* 153, 235 (1967).
46. N. M. Kroll, A. Ron, and N. Rostoker, *Phys. Rev. Letters* 13, 85 (1964).
47. C. R. James and W. B. Thompson, *Can. J. Phys.* 45, 1771 (1967).
48. C. E. Capjack and C. R. James, *Can. J. Phys.* 48, 1386 (1970).
49. G. Weyl, *Phys. Fluids* 13, 1802 (1970).
50. B. Stansfield, R. Nodwell, and J. Meyer, *Phys. Rev. Lett.* 26, 1219 (1971).
51. F. W. Perkins and J. Flick, *Phys. Fluids* 14, 2012 (1971).
52. M. N. Rosenbluth, R. B. White, and C. S. Liu, *Phys. Rev. Lett.* 31, 1190 (1973).
53. M. N. Rosenbluth and C. S. Liu, *Phys. Rev. Lett.* 29, 701 (1972).

54. G. Beaudry and J. Martineau, Phys. Letters 43A, 331 (1973).
55. V. N. Strel'tsov, Zh. Eksp. Teor. Fiz. Pis. Red. 18, 532 (1973)
(Sov. Phys.-JETP Letters 18, 314 (1973)).
56. V. Fuchs, C. Neufeld, J. Teichman, and A. G. Engelhardt, Phys. Rev. Lett. 31, 1110 (1973).
57. G. Schmidt, Phys. Fluids 16, 1676 (1973).
58. G. Beaudry, J. Appl. Phys. 45, 3836 (1974).
59. A. Kaufman and B. Cohen, Phys. Rev. Lett. 30, 1306 (1973).
60. B. Cohen, Phys. Fluids 17, 496 (1974).
61. I. Haber, C. E. Wagner, J. Boris, and J. Dawson, in Proceedings of the Fourth Conference on Numerical Simulation of Plasmas (Government Printing Office, Washington, D.C., 1973), p. 126;
R. L. Morse and C. Nielsen, Phys. Fluids 14, 830 (1971); A. B. Langdon, B. F. Lasinski, and W. L. Kruer, in Proceedings of the Sixth Conference on Numerical Simulation of Plasmas, Conference Report 73-0710 (Lawrence Berkeley Laboratory, Berkeley, California, 1973), p. 56.
62. A. B. Langdon, Ph.D. Thesis, Princeton University (1969).
63. D. Fuss and C. K. Birdsall, J. Compt. Phys. 3, 494 (1969).
64. J. Boris and R. Lee, J. Compt. Phys. 12, 13 (1973); I. Haber, R. Lee, H. Klein, and J. Boris, in Proceedings of the Sixth Conference on Numerical Simulation of Plasmas, Conference Report 73-0710 (Lawrence Berkeley Laboratory, Berkeley, California, 1973), p. 46; B. Godfrey, J. Compt. Phys. 15, 504 (1974).
65. O. Buneman, J. Compt. Phys. 1, 517 (1967); J. Boris, in Proceedings of the Fourth Conference on Numerical Simulation of Plasmas (Government Printing Office, Washington, D. C., 1973), p. 3.

66. R. Z. Galeev and A. A. Sagdeev, Nonlinear Plasma Theory edited by T. M. O'Neil and D. L. Book (Benjamin, New York, 1969) p. 19.
67. ———, Modern Computing Methods, National Physical Laboratory Notes on Applied Science No. 16 (Her Majesty's Stationery Office, London, 1961), Ch. 11.
68. J. H. Malmberg and C. B. Wharton, Phys. Rev. Lett. 19, 775 (1967).
69. P. Vidmar, J. H. Malmberg, and T. P. Starke, Phys. Rev. Lett. 34, 646 (1975).
70. N. Sato, H. Ikezi, Y. Yamashita, and N. Takahashi, Phys. Rev. Lett. 20, 837 (1968).
71. H. Sugai and E. Märk, Phys. Rev. Lett. 34, 127 (1975).
72. T. M. O'Neil, Phys. Fluids 14, 2255 (1965).
73. G. J. Morales and T. M. O'Neil, Phys. Rev. Lett. 28, 417 (1972).
74. W. Manheimer and R. Flynn, Phys. Fluids 14, 2393 (1971).
75. R. L. Dewar, Phys. Fluids 15, 712 (1972).
76. R. S. Johnston, Ph.D. Thesis, Princeton University (1974).
77. W.L. Kruer, J. M. Dawson, and R. N. Sudan, Phys. Rev. Lett. 23, 838 (1969).
78. M. Mstrom, A. Kaufman, and D. Nicholson, Bull. Am. Phys. Soc. 17, 1065 (1972).
79. M. Mstrom, Ph.D. Thesis, University of California, Berkeley (1975).
80. J. Harte, Ph.D. Thesis, University of California, Davis (1975).
81. B. B. Kadomtsev and V. I. Karpman, Usp. Fiz. Nauk 103, 193 (1971) (Sov. Phys.-Usp. 14, 40 (1971)).
82. K. Nishikawa, H. Hojo, K. Mima, and H. Ikezi, Phys. Rev. Lett. 33, 148 (1974).

83. A. G. Litvak and V. Trakhtengerts, Zh. Eksp. Teor. Fiz. 60, 1702 (1971) (Sov. Phys.-JETP 33, 921 (1971)).
84. A. G. Litvak, V. Petrukhina, and V. Trakhtengerts, Zh. Eksp. Teor. Fiz. Pis. Red. 18, 190 (1973) (Sov. Phys.-JETP Letters 18, 111 (1973)).
85. T. M. O'Neil, J. H. Winfrey, and J. H. Malmberg, Phys. Fluids 14, 1204 (1971).
86. V. Bailey and J. Denavit, Phys. Fluids 13, 451 (1970).
87. R. Sugihara and T. Kamimura, J. Phys. Soc. Japan 33, 206 (1972).
88. A. Lee and G. Pocobelli, Phys. Fluids 15, 2351 (1972) and Phys. Fluids 16, 1964 (1973).
89. J. Canosa and J. Gazdag, Phys. Fluids 17, 2030 (1974).
90. S-T. Tsai, J. Plasma Phys. 11, 213 (1974).
91. Y. Matsuda, Ph.D. Thesis, Stanford University (1974).
92. R. Sugihara and T. Taniuti, Suppl. Prog. Theor. Phys. 55, 151 (1974).
93. D. L. Book and P. Sprangle, Bull. Amer. Phys. Soc. 19, 882 (1974).
94. W. Kruer and J. Dawson, Phys. Fluids 13, 2747 (1970).
95. E. Asseo, G. Laval, R. Pellat, R. Welti, and A. Roux, J. Plasma Phys. 8, 341 (1972).
96. V. I. Karpman and D. R. Shklyar, Zh. Eksp. Teor. Fiz. 62, 944 (1972) (Sov. Phys.-JETP 35, 500 (1972)).
97. B. Cohen and A. Kaufman, Bull. Amer. Phys. Soc. 17, 1059 (1972).
98. K. Estabrook and E. Valeo, in Proceedings of the Fifth Annual Anomalous Absorption Conference (University of California, Los Angeles, California, 1975), p. F.6; B. F. Lasinski and A. B. Langdon, in Proceedings of the Fifth Annual Anomalous Absorption

- Conference (University of California, Los Angeles, California, 1975) p. F7.
99. R. J. Briggs, Electron-Stream Interaction with Plasmas (M.I.T. Press, Cambridge, Mass., 1964), Ch. 2.
100. A. Bers, "Theory of Absolute and Convective Instabilities" in G. Auer and F. Cap, International Congress on Waves and Instabilities in Plasma (Innsbruck, Austria, April 1973). pp. B1-B52.
101. F. Chambers, Ph.D. Thesis, Massachusetts Institute of Technology (1975).
102. C. Oberman and G. Auer, Phys. Fluids 17, 1980 (1974).
103. B. Fried, G. Schmidt, and R. Gould in Proceedings of the Sixth Conference on Nuclear Fusion and Plasma Physics (Vienna, 1973) p. 477.
104. B. D. Fried and S. Conte, The Plasma Dispersion Function (Academic Press, New York, 1961).

FIGURE CAPTIONS

- Fig. 1. (a) Stimulated scattering of a higher frequency transverse wave occurs into a lower frequency transverse wave and a longitudinal plasma oscillation.
- (b) Simultaneous three-wave interactions occur coupled by a common driven longitudinal density perturbation. The process is generally described as modulation.
- Fig. 2. Coordinate system for two dimensional scattering in the x - z plane with electric field polarizations in the y -direction. θ is defined as the angle between real wavenumbers \underline{k} and \underline{k}_0 .
- (a) Three-wave coupling, e.g., Raman or Brillouin scattering.
- (b) Forward scattering or four-wave coupling, e.g., filamentation.
- Fig. 3. The one and one-half dimensions (x, v_x, v_y) of the code are pictured schematically. Wave propagation and density variation occur parallel to x . Transverse waves are linearly polarized in the y -direction. Magnetic fields are parallel to z . The three-wave interaction is diagrammed.
- Fig. 4. The equations describing transverse waves and particle dynamics are integrated forward in time using a time-centered, leap-frog technique. Currents are calculated from charge locations measured over consecutive time-steps and from velocities at the half time-steps $[J_y = (J_y^+ + J_y^-)/2]$.
- Fig. 5. Beat heating in an inhomogeneous medium. Because of the resonance condition, there arises a resonance region h . The density gradient, described by the scale length

$L_n \equiv (d \ln n_0 / dz)^{-1}$, is parallel to the propagation direction of waves.

Fig. 6. Beat heating in a finite, inhomogeneous medium:

(a) the right- and left-going electromagnetic waves before onset of beating;

(b) (x, v_x) phase space after a fairly large amplitude electron plasma wave has been established.

Fig. 7. Relative energy or action depletion R of the high frequency wave vs dimensionless parameter (scale length \times pump strength)

$4\pi k_0 L_n |u_0|^2 / c^2$ for beat heating in an inhomogeneous medium with input ratio $J_1^{\text{in}} / J_0^{\text{in}} = 1$. The data points for

$4\pi k_0 L_n |u_0|^2 / c^2 = 0.5$ represent three parameter choices:

∇ : $4|u_0/c|^2 = 0.008$ and $k_0 L_n = 18.3$; \square : $4|u_0/c|^2 = 0.010$ and $k_0 L_n = 15.2$; and Δ : $4|u_0/c|^2 = 0.012$ and $k_0 L_n = 13.7$.

Fig. 8. Steady propagation of a stationary pulse-like three-wave interaction for parameters $V_1 = V_3 = -V_2 = 1$:

$a_1(x, t) = -0.1 \tanh(0.1\xi)$, $a_2(x, t) = 0.00499 \operatorname{sech}(0.1\xi)$, and $a_3(x, t) = 0.1 \operatorname{sech}(0.1\xi)$ where $\xi \equiv x - 1.01t$.

Fig. 9. Perturbed pulse propagation for parameters $V_1 = V_3 = -V_2 = 1$,

and initial conditions $a_1(x, 0) = -0.1 \tanh(0.1x)$, $a_2(x, 0) = 0.0499 \operatorname{sech}(0.1x)$, and $a_3(x, 0) = 0.1 \operatorname{sech}(0.1x)$.

Fig. 10. Propagation of superposed right- and left-going solitary pulse solutions showing break-up for parameters

$V_1 = V_3 = -V_2 = 1$, and initial conditions: $a_1(x, 0) = -0.1 [\tanh(0.1\xi) + \tanh(0.1\eta)]$, $a_2(x, 0) = 0.00499 \operatorname{sech}(0.1\xi) - 2.01 \operatorname{sech}(0.1\eta)$, and $a_3(x, 0) = 0.1 [\operatorname{sech}(0.1\xi) + \operatorname{sech}(0.1\eta)]$ where $\xi = x + x_0$ and $\eta \equiv x - x_0$; $\pm x_0$ denote the initial locations of the left- and right-going pulses respectively.

Fig. 11. Beat heating in a cold, uniform plasma with initial conditions $a_1(x,0) = \theta(-x)$, $a_2(x,0) = \theta(x)$, and $a_3(x,0) = 0$, where θ is the unit-step function. We have chosen parameters $V_1 = V_2 = 1$, $v_3 = 0.2$, and $V_3 = v_1 = v_2 = v_3 = \kappa' = 0$.

Fig. 12. Beat heating in a warm, uniform plasma, with initial conditions $a_1(x,0) = \theta(-x)$, $a_2(x,0) = \theta(x)$, and $a_3(x,0) = 0$. We have chosen parameters $V_1 = V_2 = 5$, $V_3 = 1$, $v_3 = 0.2$, and $v_1 = v_2 = \kappa' = 0$.

Fig. 13. (a) Temperature (eV) is plotted as a function of time. There is a temporary halt in the heating at around the first "bounce period" τ_B after the onset of beat heating.
 (b) The relative action transfer is plotted as a function of time for a simulation exhibiting trapping (corresponding to Fig. 14).

Fig. 14. Phase space (x, v_x) and the velocity distribution function $f(v_x)$, for beat heating in a finite homogeneous plasma with trapping, for parameters: $|u_1| \approx |u_0| = 0.03c$, $v_e(0) = 0.042c$, and $\omega_0 = 5.0\omega_e$.
 (a) At $\omega_e t = 6$; $|\delta n/n_0| = 0.3$, $\Delta S/S_0 = 0.25$, and $T_e/T_e(0) = 1.0$. The action transfer rate is large, since the beat wave is still in a linear regime.
 (b) At $\omega_e t = 25$; $|\delta n/n_0| = 0.7$, $\Delta S/S_0 = 0.11$, and $T_e/T_e(0) = 3.3$. The density disturbance has become large in amplitude. Trapping has significantly reduced the action transfer rate.
 (c) At $\omega_e t = 40$; $|\delta n/n_0| = 0.4$, $\Delta S/S_0 = 0.1$, and $T_e/T_e(0) = 4.7$. There has been significant plasma heating.

Beat heating is no longer resonant but continues in a regime described as induced Thomson scattering.

Fig. 15. Heating $v_e^2(\tau_B) - v_e^2(0)$ is plotted against input laser intensity $\tilde{v}_0^0 \tilde{v}_1^0$ (we have chosen equal intensities $\tilde{v}_0^0 = \tilde{v}_1^0$). The period of time over which the heating is measured is defined as the average "bounce period" τ_B after the onset of beating. The fixed parameters and initial conditions for these simulations are $\kappa c/\omega_e = 8.36$, $\omega_0/\omega_e = 5.0$, and $\kappa\lambda(0) = 0.35$.

Fig. 16. Plotted is $[\Delta_L - \delta\Delta(r)]r$, for $\delta\Delta = -\alpha r^{\frac{1}{2}}$, with Δ_L as a parameter. Equilibria described by Eq. (64) occur at intersections with ± 1 .

(a) Equilibrium occurs only at r_0 for $\Delta_L > 0$.

(b) For $\Delta_L = \Delta_1, \Delta_2$, where $\Delta_2 < \Delta_1 < 0$, multiple equilibria occur for Δ_2 but not for Δ_1 .

Fig. 17. (a) Total electric field E and driving electric field E_0 , in natural units vs κx ;
 (b) Longitudinal phase space, $\kappa v/\omega_e$ vs κx ;
 (c) Electron velocity distribution function $f(v)$ in arbitrary units vs $\kappa v/\omega_e$; all at $\omega_e t = 300$.

Fig. 18. (a) Relative response magnitude r and relative phase θ , $r \exp i\theta \equiv \tilde{\Phi}/\tilde{\Phi}_0$ vs $\omega_e t$.
 (b) Frequency shift and nonlinear dissipation normalized to ω_e vs $\omega_e t$.

Fig. 19. Asymptotic frequency shift normalized to ω_e vs normalized wave amplitude $|e\tilde{\Phi}(t = \infty)|/(m\omega_e^2/2\kappa^2) = \omega_B^2/\omega_e^2$ for slow driver switch-on over $\omega_e t = 50\pi(0)$ and for sudden switch-on

(●). The solid line indicates the theoretical result of Morales and O'Neil.

Fig. 20. Simulation of resonant response of a Maxwellian electron plasma (thermal speed v_e) to a ponderomotive plane wave driving force, of frequency Ω (chosen to equal ω_e) and phase velocity $v_\phi \equiv \Omega/\kappa$ (chosen to equal $3v_e$), induced by the $\underline{v} \times \underline{B}$ coupling of two opposed lasers with oscillation velocity amplitudes u_0 and u_1 (chosen initially equal to $0.2v_\phi$). Initially the linear normal mode frequency is $\Omega_L = 1.17\omega_e$, and the linear Landau damping $-\gamma_L$ is $0.03\omega_e$. The frequencies of the transverse waves are chosen to be $\omega_0 = 5\omega_e$ and $\omega_1 \equiv \omega_0 - \Omega = 4\omega_e$. For a typical simulation, we exhibit at $\omega_e t = 431, 784$:

- (a) The driving field E_0 and the total field E as functions of x , in natural units;
- (b) Longitudinal electron phase space;
- (c) The velocity distribution, in arbitrary units.

Fig. 21. For the same simulation as in Fig. 20, we show, as functions of time:

- (a) The magnitude $\phi^e(t)$ and $\phi_0^e(t)$ of the total and ponderomotive potentials;
- (b) Their respective phases θ and θ_0 :

$$\phi^e(x, t) = \phi^e(t) \cos(\Omega t - \kappa x + \theta) \text{ and}$$

$$\phi_0^e(x, t) = \phi_0^e(t) \cos(\Omega t - \kappa x + \theta_0).$$

Fig. 22. For the same simulation as in Fig. 20, we show, as functions of time:

(a) The deduced frequency shift $\delta\Omega$;

(b) The nonlinear damping γ_{NL} .

Fig. 23. For the same simulation as in Fig. 20, we show, as functions of time:

(a) Coupled mode amplitudes $|u_0|/v_\phi$, $|u_1|/v_\phi$, and $|\tilde{n}|/n_0$;

(b) Their respective phases θ_0 , θ_1 , and θ_n .

Fig. 24. Two lasers in channels L and L-1 initiate the multiple scattering of photons $(\omega_\ell, \underline{k}_\ell)$ by a single plasmon $(\Omega, \underline{k}_p)$, leading to the generation of photons in both lower and higher frequency channels.

Fig. 25. A schematic sketch of $\text{Re } \Omega/\omega_i$ — and $\text{Im } \Omega/\omega_i$ --- vs $\kappa\lambda_e$ for filamentation, with $\underline{\kappa} \cdot \underline{k}_0 = 0$.

Fig. 26. Weak coupling Brillouin scattering: $\text{Re } \Omega/2k_0c_s$ — and $\text{Im } \Omega/2k_0c_s$ --- vs $\kappa/2k_0$.

Fig. 27. (a) Strong coupling Brillouin dispersion relation: $\text{Re } \Omega/\omega_0$ — and $\text{Im } \Omega/\omega_0$ --- vs $\kappa/2k_0$, for $\cos \theta = 0.25, 0.50, 0.75, \text{ and } 1.0$, with parameters $k_0\lambda_e = 0.02$, $\tilde{v}_0/c = 0.2$, $\omega_e/\omega_0 = 0.2$, and $m_i/m_e = 25$.

(b) Combined filamentation and strong coupling Brillouin dispersion relations: $\text{Re } \Omega/\omega_0$ — and $\text{Im } \Omega/\omega_0$ --- vs $\kappa/2k_0$ for $\cos \theta = 0.0, 0.25, 0.50, 0.75, \text{ and } 1.0$ and same parameters.

Fig. 28. Longitudinal phase space (x, v_x) for Brillouin backscatter: electrons at

(a) $\omega_e t = 47.5$ and

(b) $\omega_e t = 90.0$;

ions at

(c) $\omega_e t = 47.5$ and

(d) $\omega_e t = 90.0$

Fig. 29. Electrostatic energy density, $W/n_0 m_e c^2$ vs time, $\omega_e t$, for the $\kappa = 2k_0$ mode.

Fig. 30. Brillouin pinch-point frequency, $\text{Re } \Omega_p/\omega_0$ —, and growth rate $\text{Im } \Omega_p/\omega_0$ --- vs. dimensionless pump strength $(\omega_i/\omega_0)^2(k_0 r_0)^2/2$. The pump strengths exceed $(k_0 c_s/\omega_0)^3 = 10^{-6}$, and thus are in the regime of strong coupling normal modes. Results derived using the weak coupling approximation are shown by —. . —.

Fig. 31. Brillouin pinch-point solutions for $\text{Re } \kappa_p/2k_0$ —, $\text{Im } \kappa_p/2k_0$ ---, and $\text{Re } \Omega/\text{Re } \kappa_p c_s$ — vs $(\omega_i/\omega_0)^2(k_0 r_0)^2/2$. Analytic approximation for weak coupling is shown by — . . —.

Fig. 32. The ratio of mismatches $|D_-/D_+|$ vs pump strength $(\omega_i/\omega_0)^2(k_0 r_0)^2/2$, evaluated at the pinch-point frequency and wavenumber for Brillouin backscatter ($\theta = 0$) and for parameters $\omega_e \ll \omega_0$ and $k_0 c_s/\omega_0 = 10^{-2}$.

Fig. 33. Contours of equal $|D_B|$ vs $\text{Re } \kappa/2k_0$ (abscissa) and $\text{Im } \kappa/2k_0$ (ordinate) for a strong pump, $(\omega_i/\omega_0)^2(k_0 r_0)^2/2 = 10^{-7}$, $(k_0 c_s/\omega_0)^3 = 10^{-6}$, and $\omega_e \ll \omega_0$. $\text{Re } \Omega$ is set equal to the pinch-point frequency.

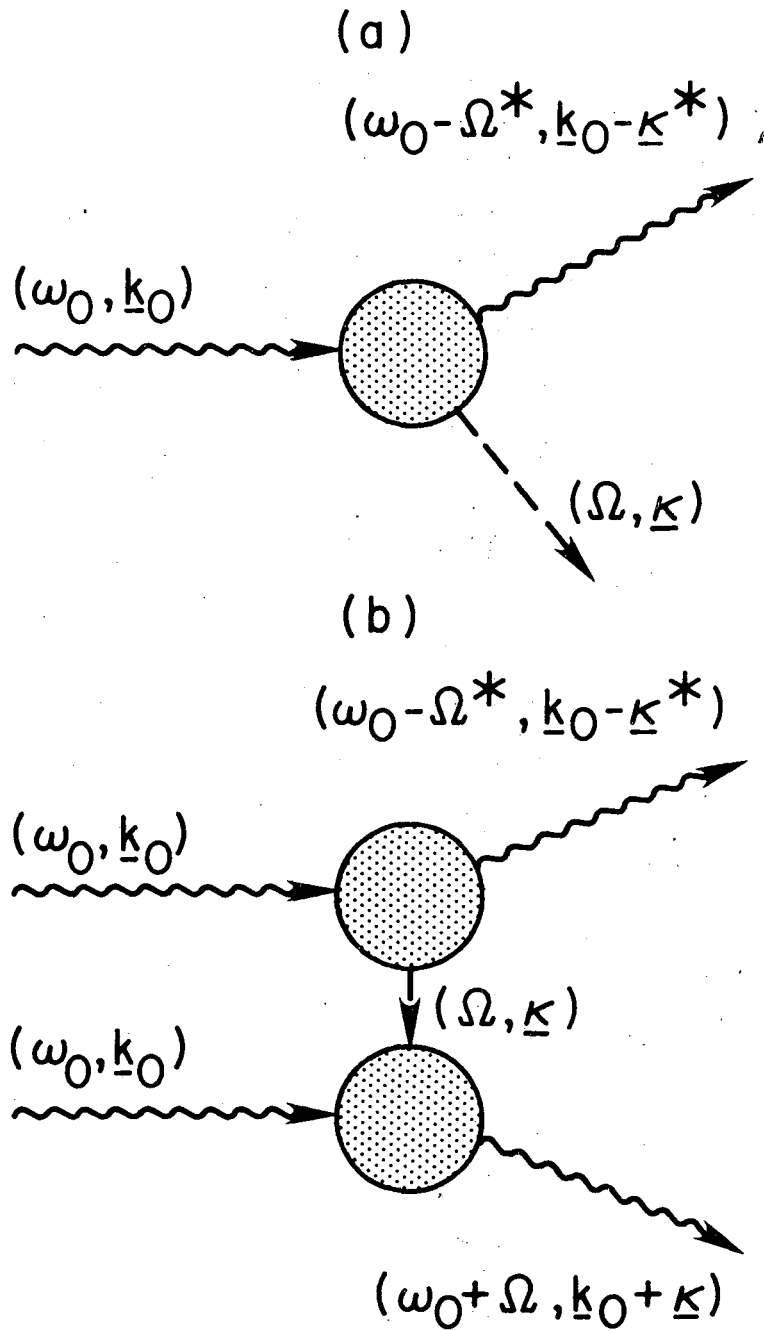
(a) $\text{Im } \Omega$ less than the pinch-point growth rate.

(b) $\text{Im } \Omega$ equal to the pinch-point growth rate.

(c) $\text{Im } \Omega$ greater than the pinch-point growth rate.

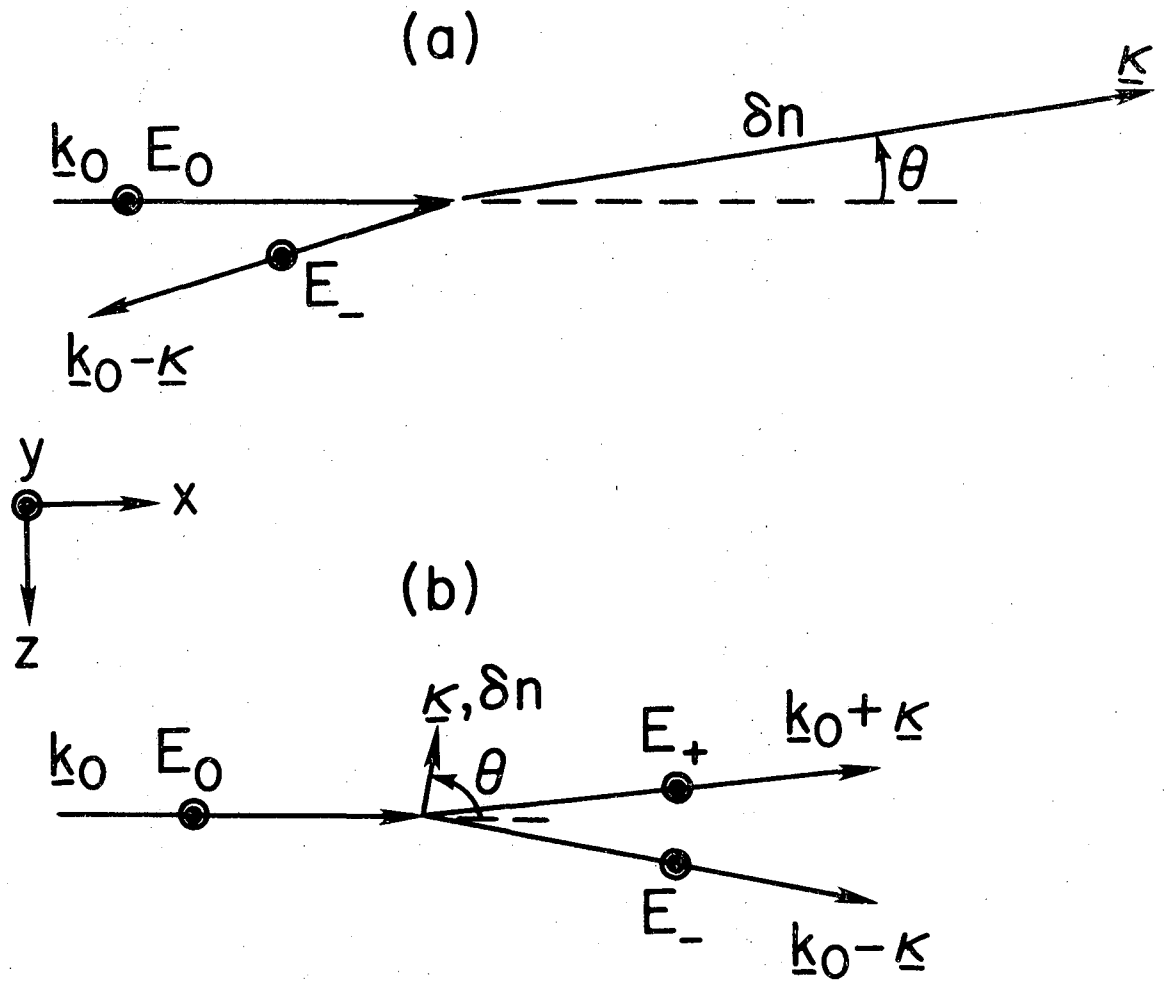
Fig. 34. Contours of equal $|D_B|$ vs $\text{Re } \kappa/2k_0$ (abscissa) and $\text{Im } \kappa/2k_0$ (ordinate) for a weak pump, $(\omega_1/\omega_0)^2(k_0 r_0)^2/2 = 10^{-3}$, $(k_0 c_s/\omega_0)^3 = 10^{-6}$, and $\omega_e \ll \omega_0$. $\text{Re } \Omega$ is set equal to the pinch-point frequency.

- (a) $\text{Im } \Omega$ less than the pinch-point growth rate.
- (b) $\text{Im } \Omega$ equal to the pinch-point growth rate.
- (c) $\text{Im } \Omega$ greater than the pinch-point growth rate.



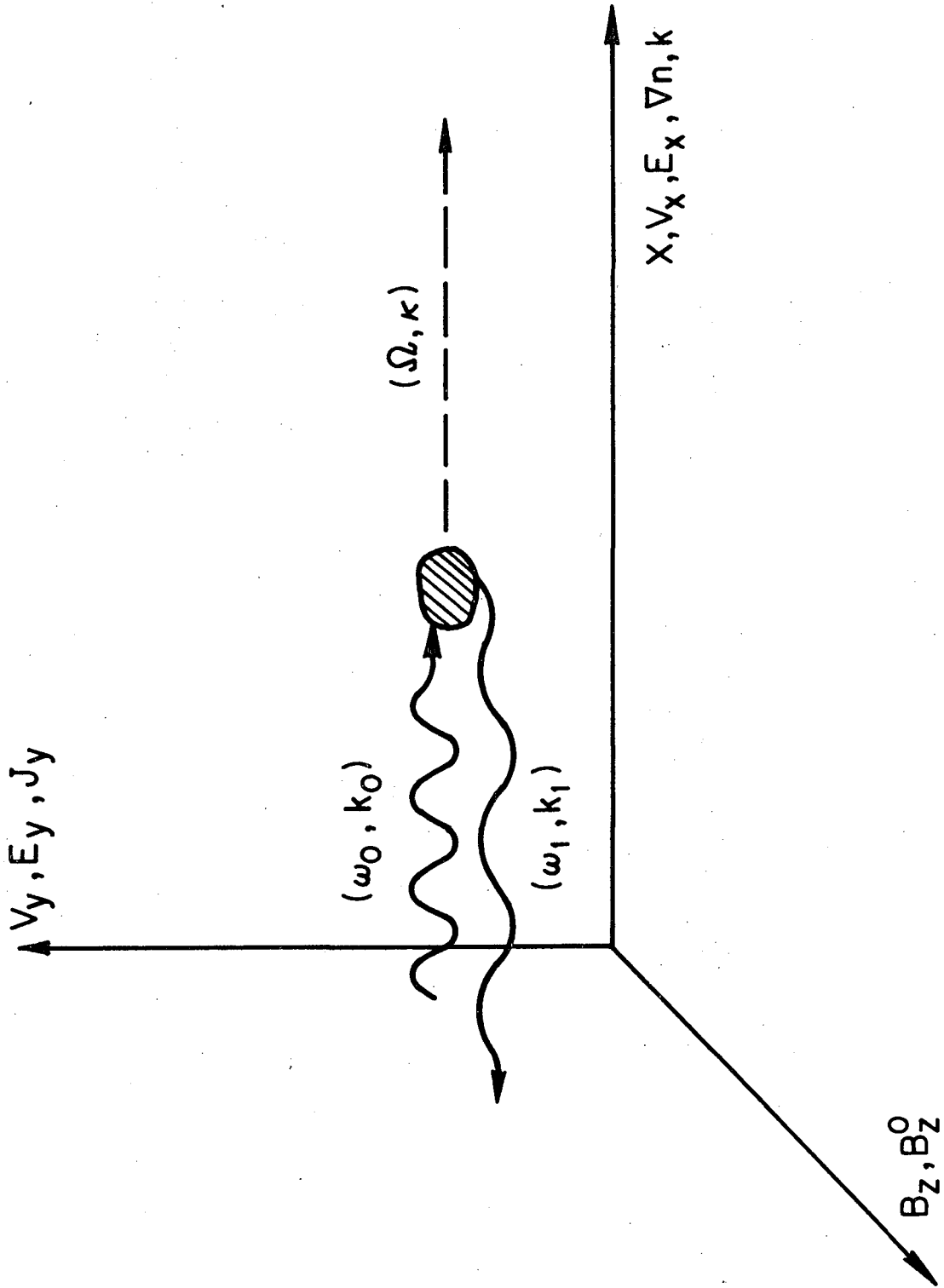
XBL 759-3980

Fig. 1



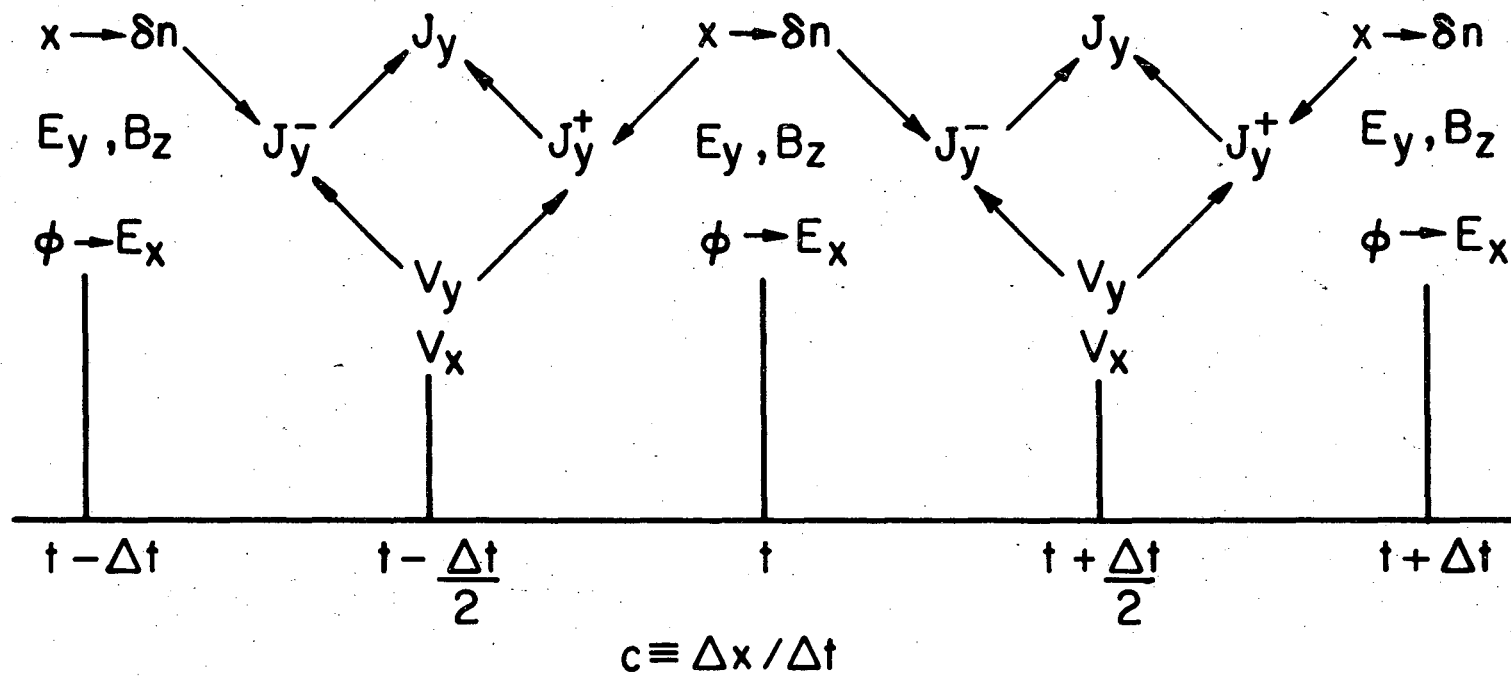
XBL 759-3960

Fig. 2



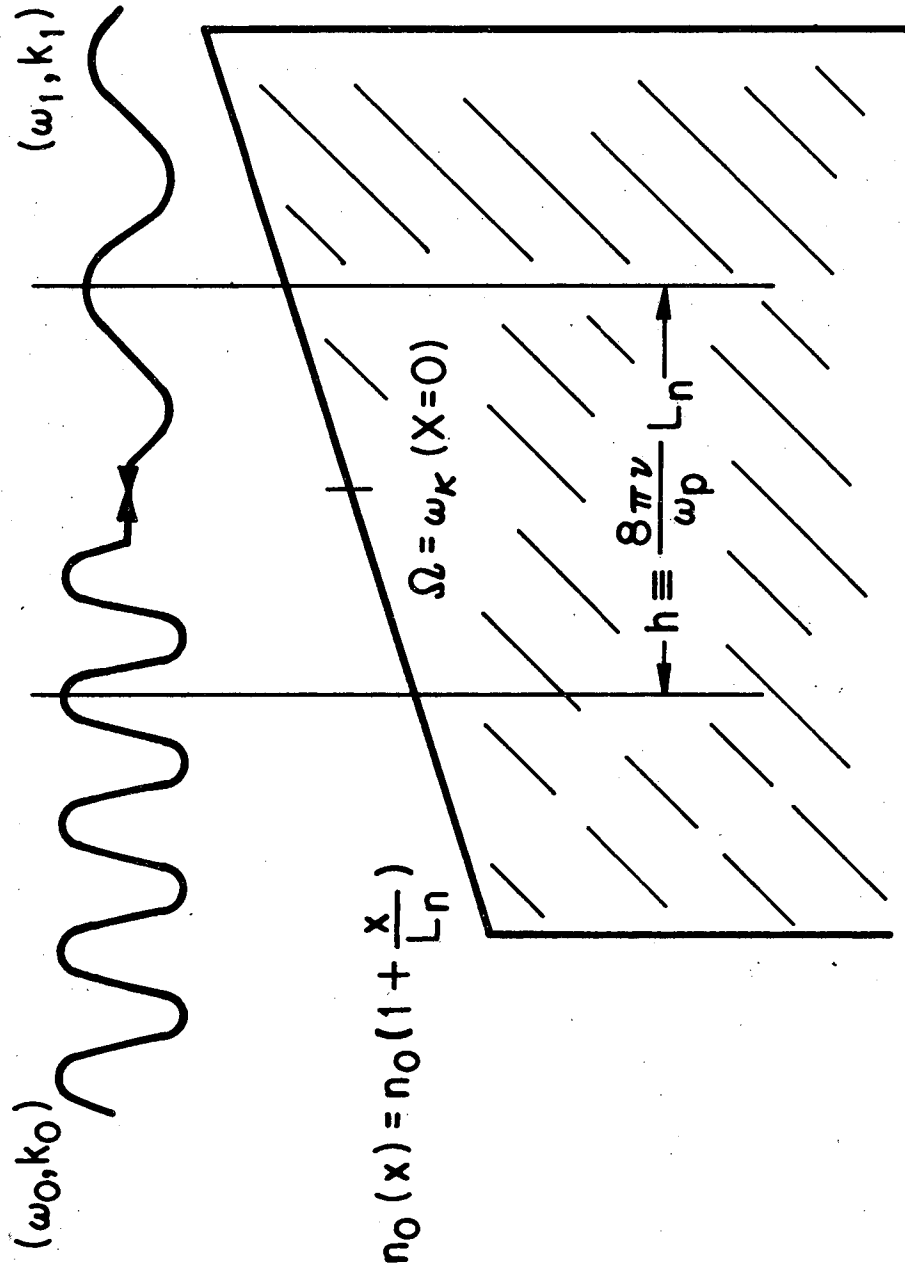
XBL745-3027

Fig. 3



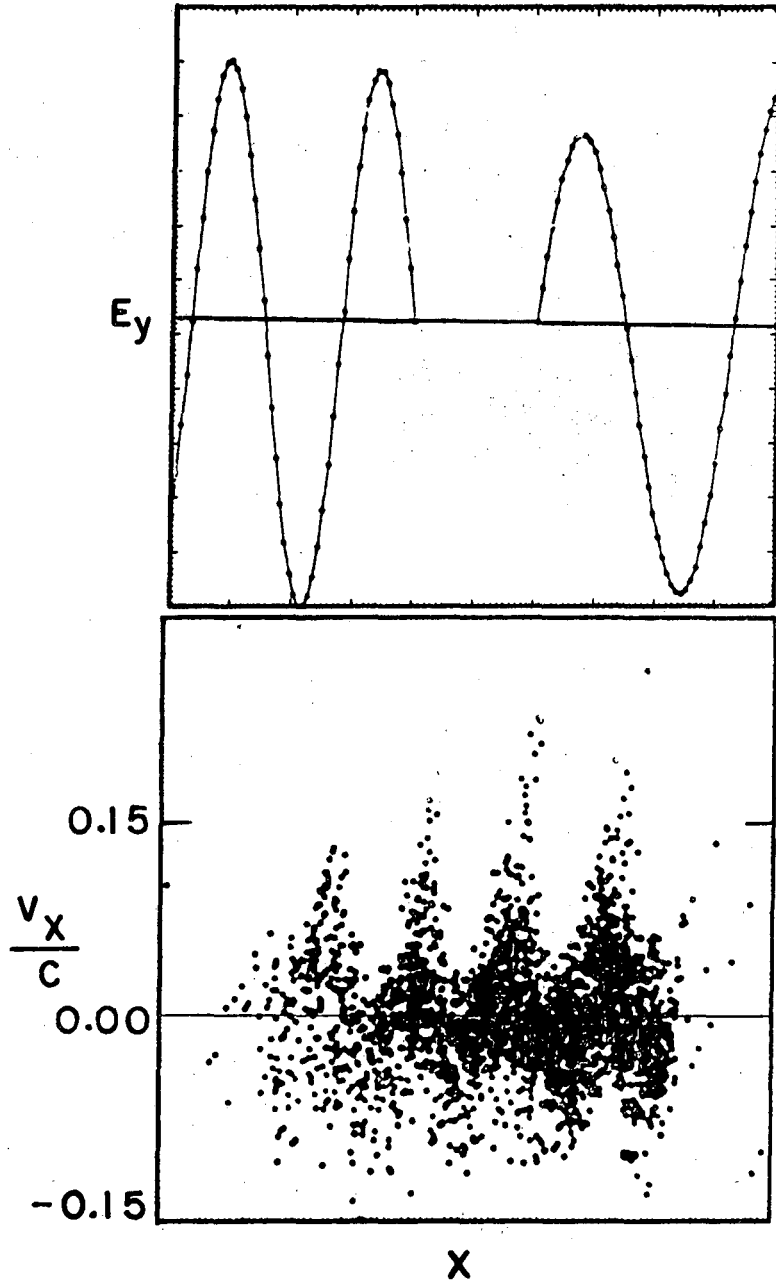
XBL745 - 3029

Fig. 4



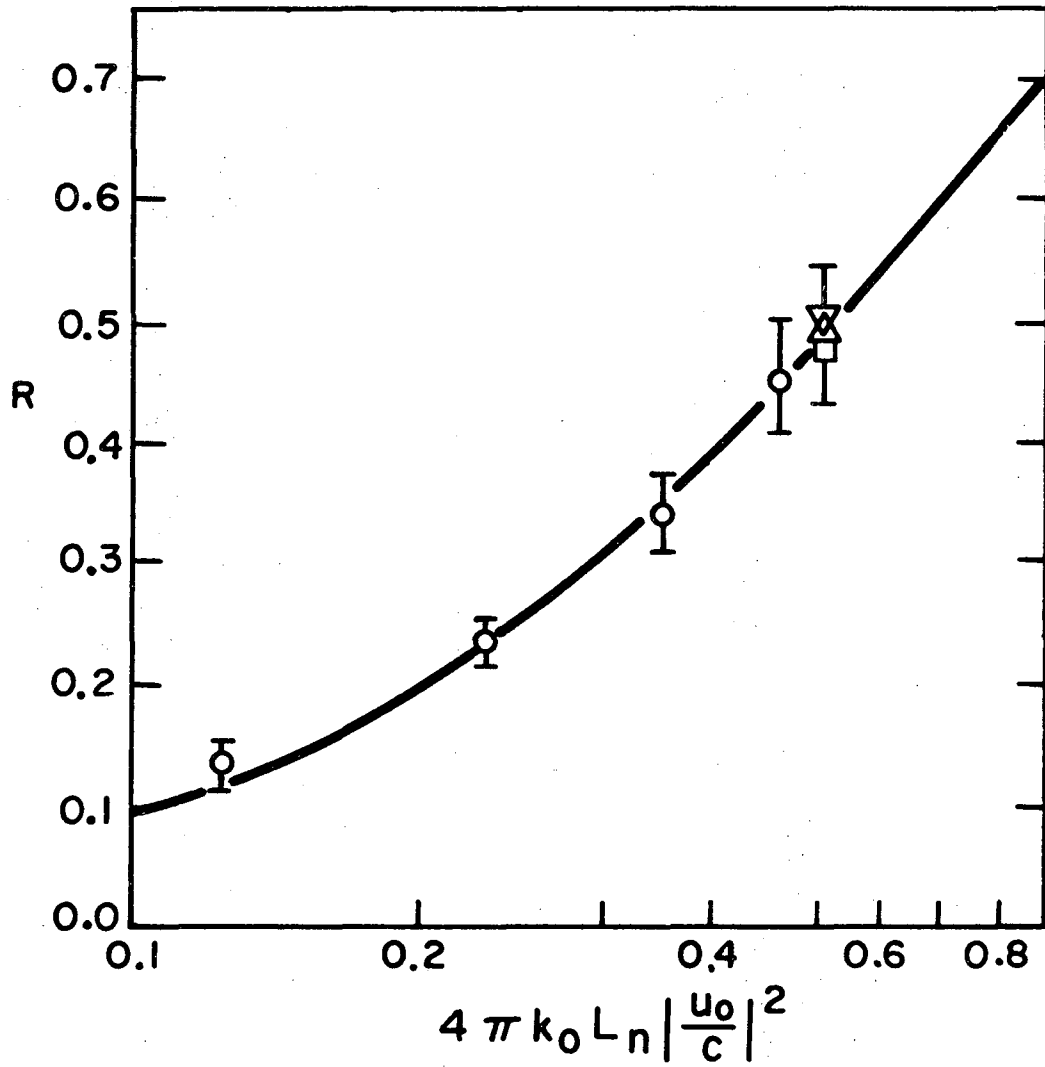
XBL745-3028

Fig. 5



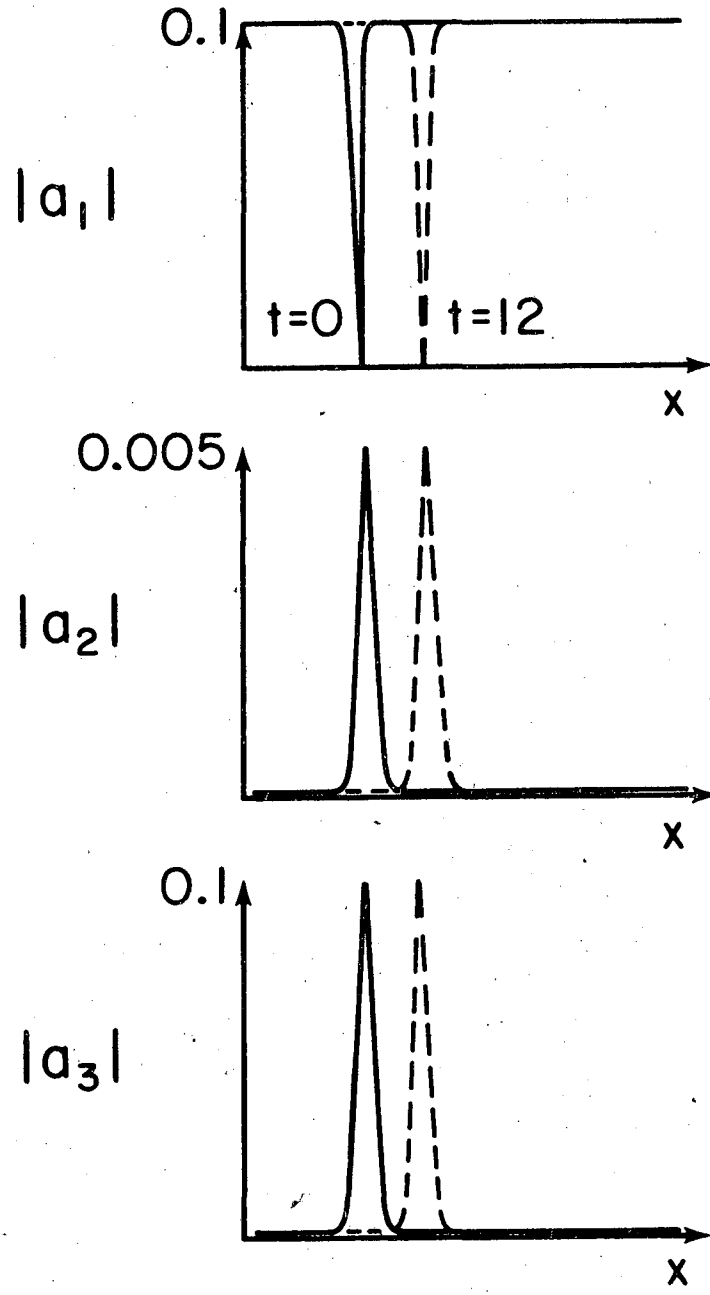
XBL745-3023

Fig. 6



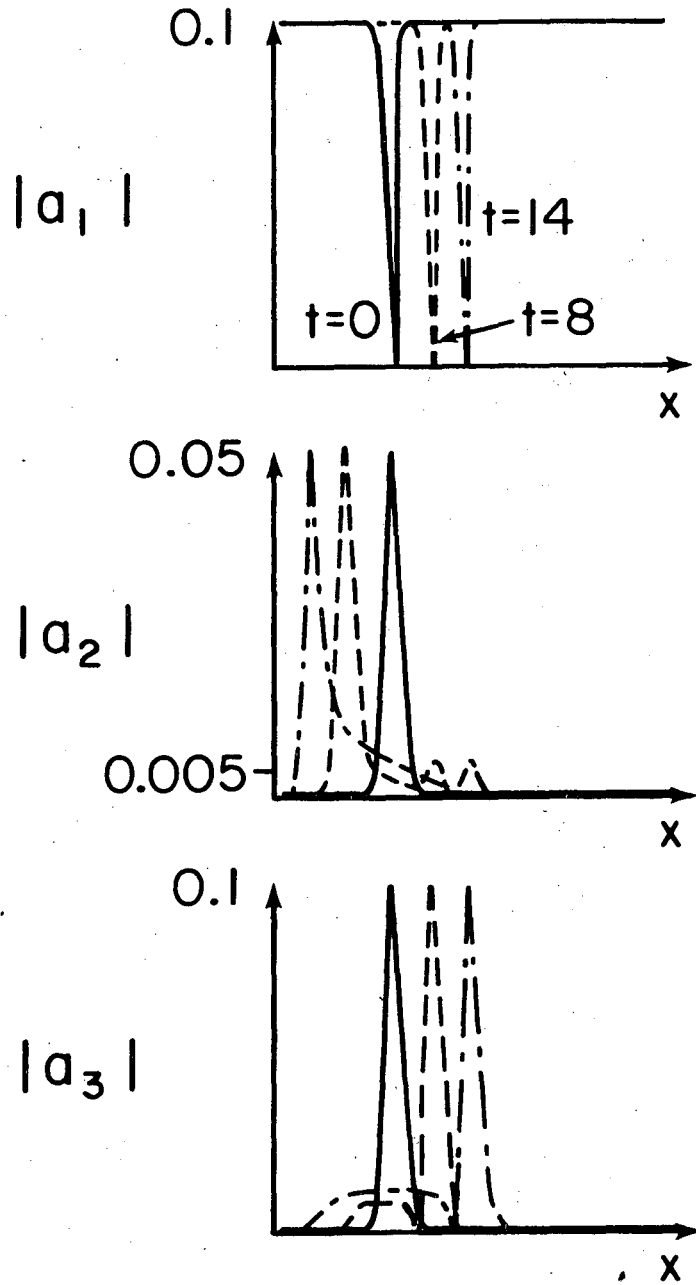
XBL745-3021

Fig. 7



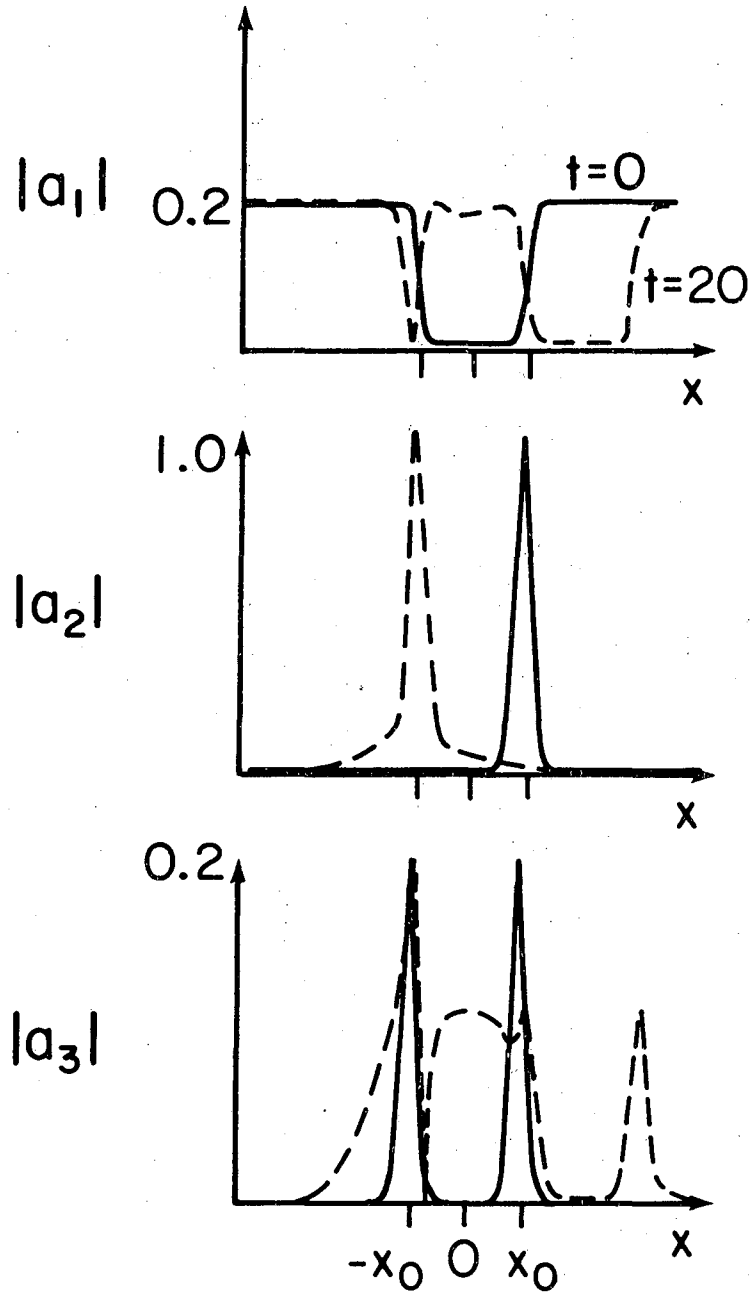
XBL 759-3985

Fig. 8



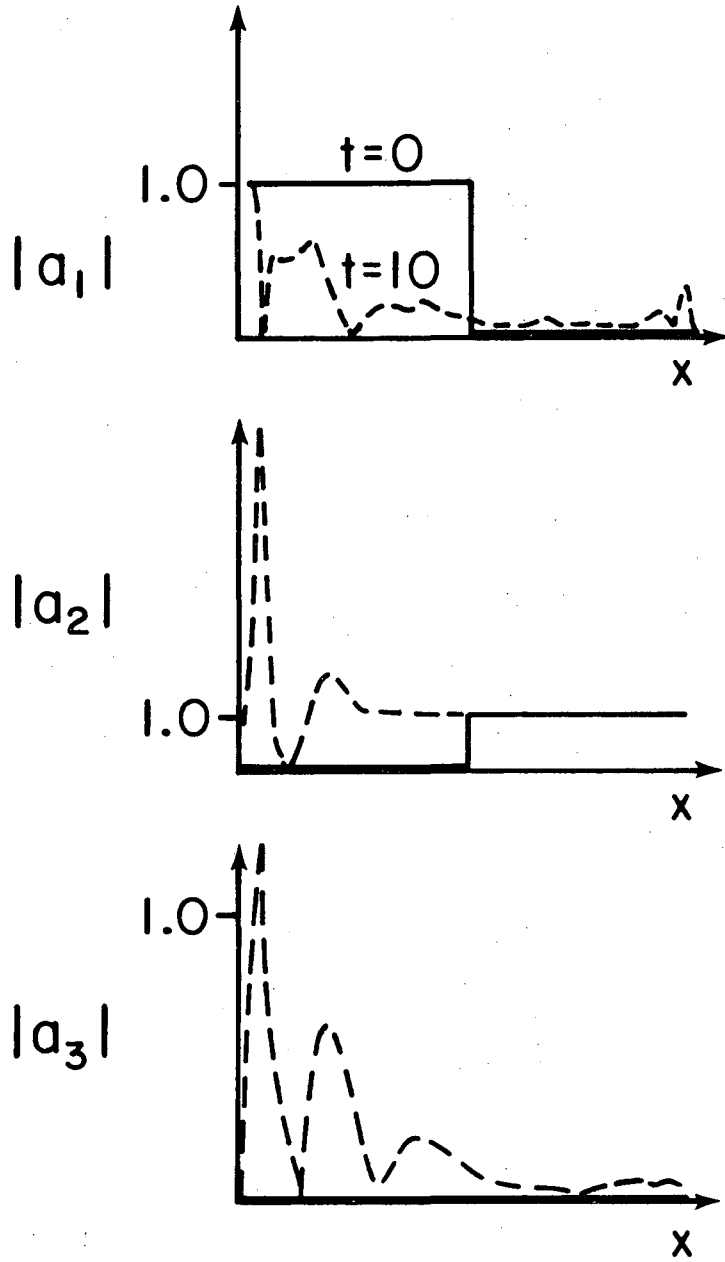
XBL759-3984

Fig. 9



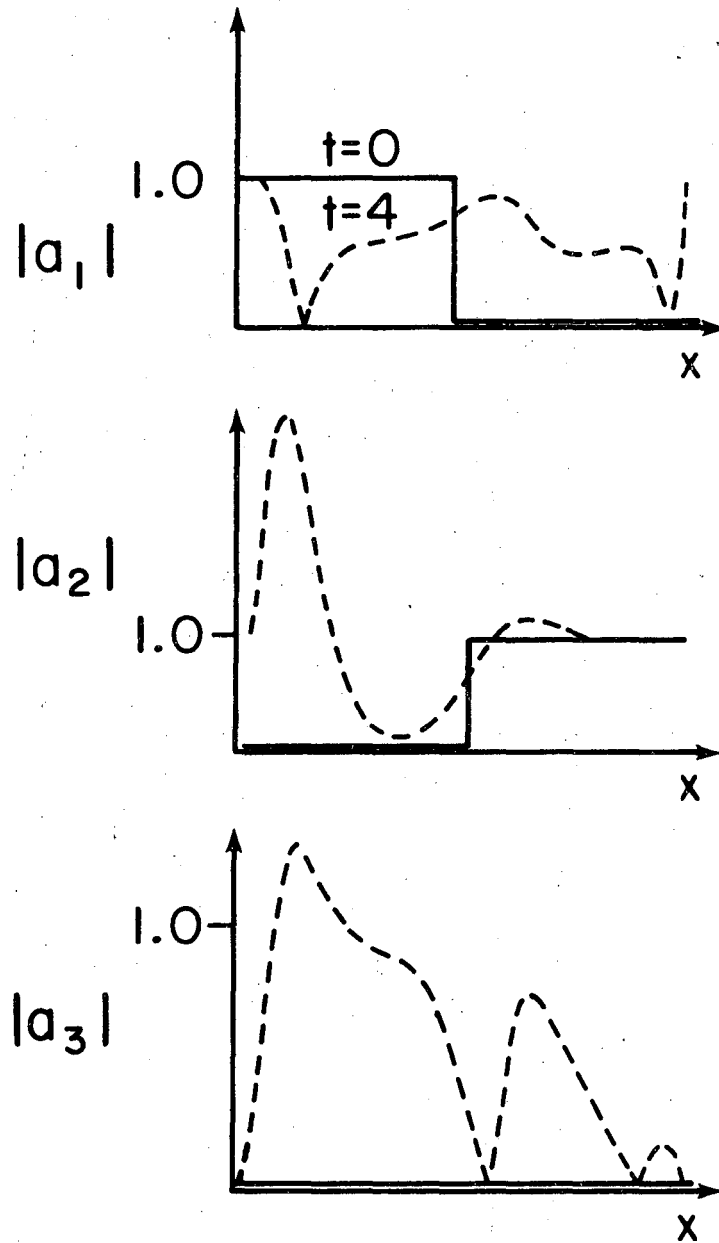
XBL759-3983

Fig. 10



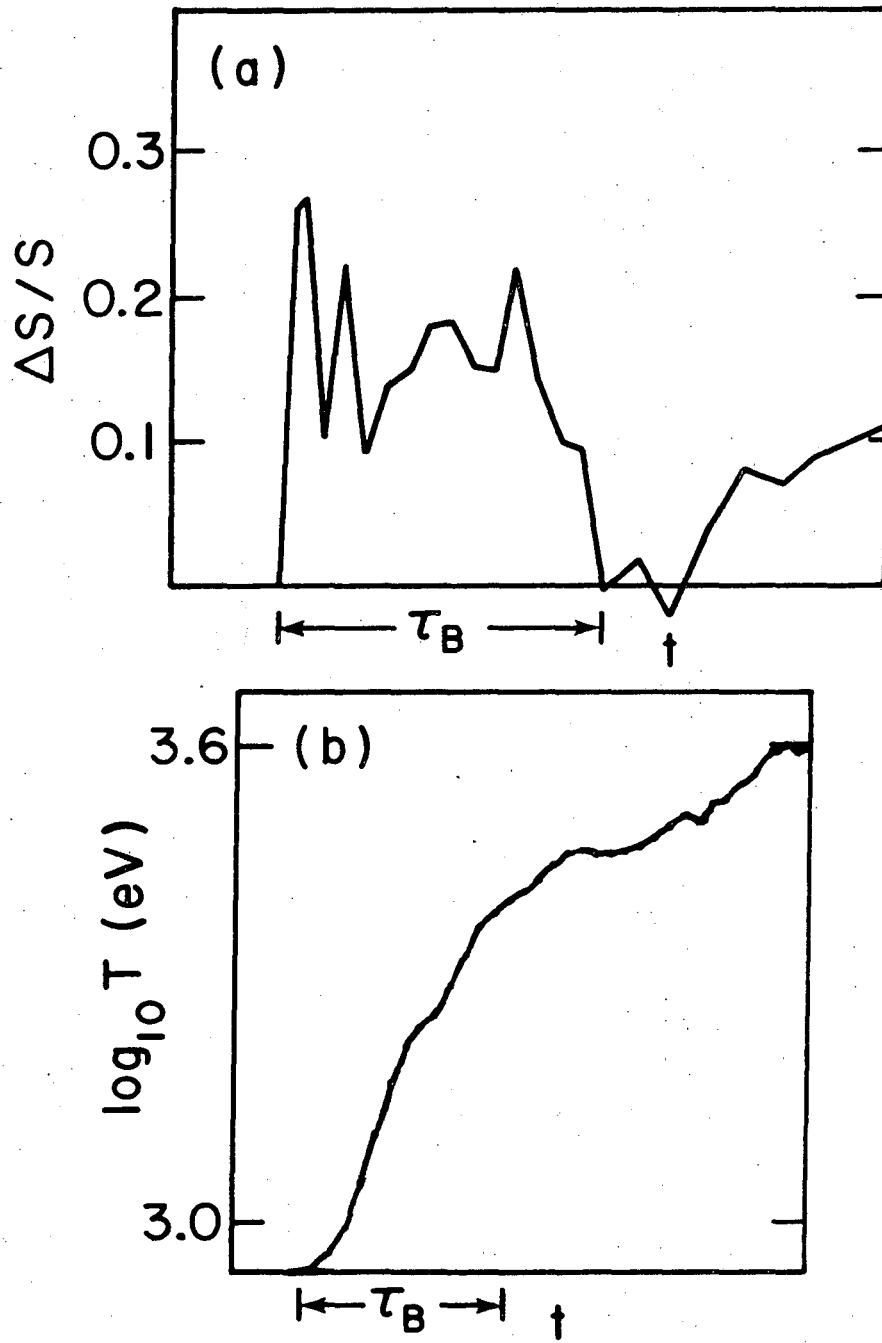
XBL 759-3982

Fig. 11



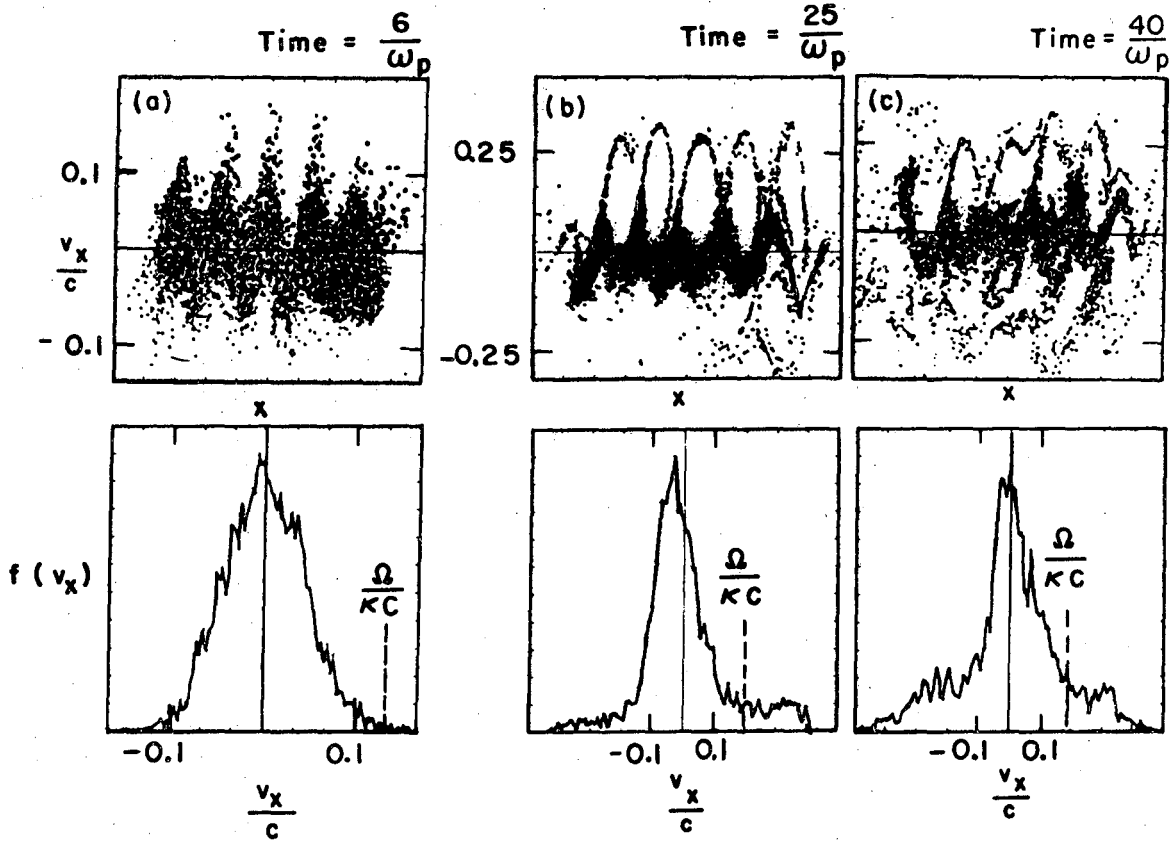
XBL 759-3981

Fig. 12



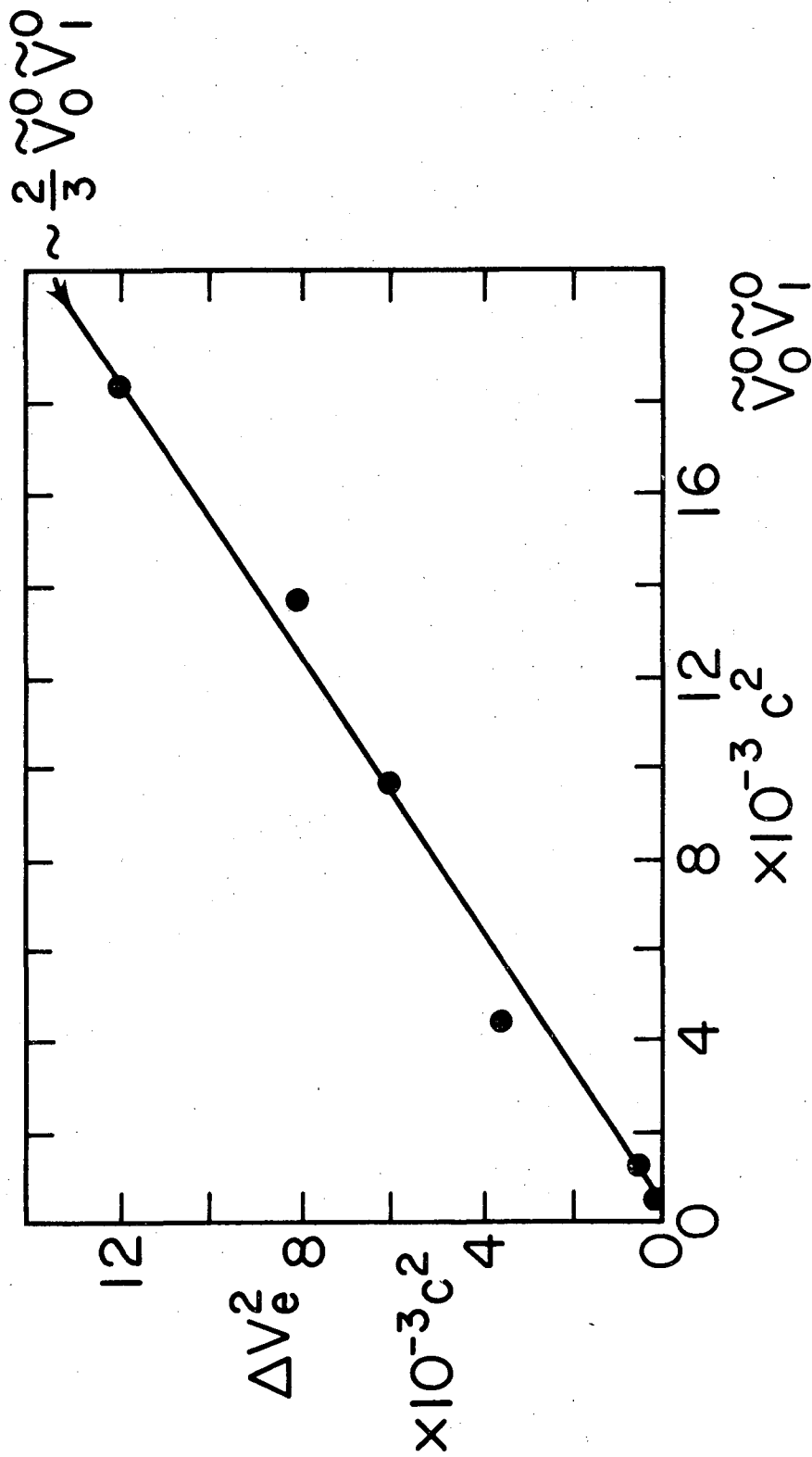
XBL 759-3964

Fig. 13



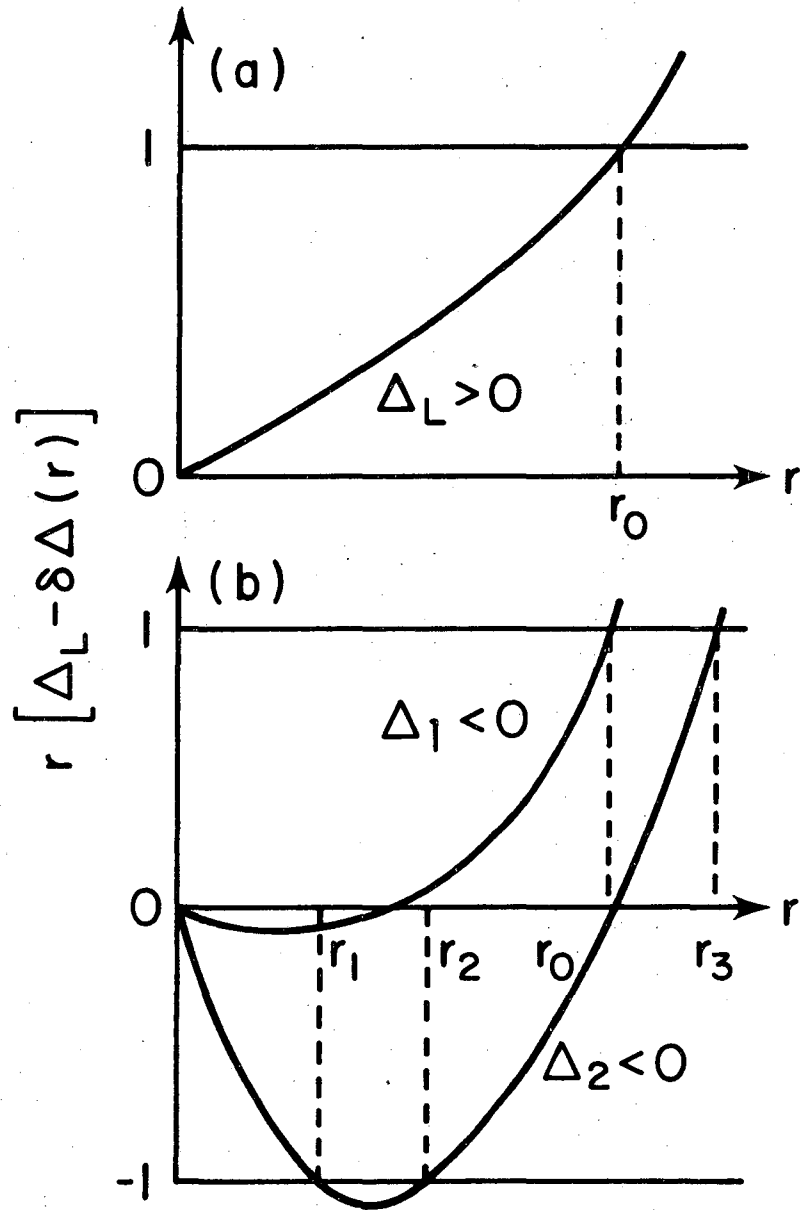
XBL 746-1055

Fig. 14



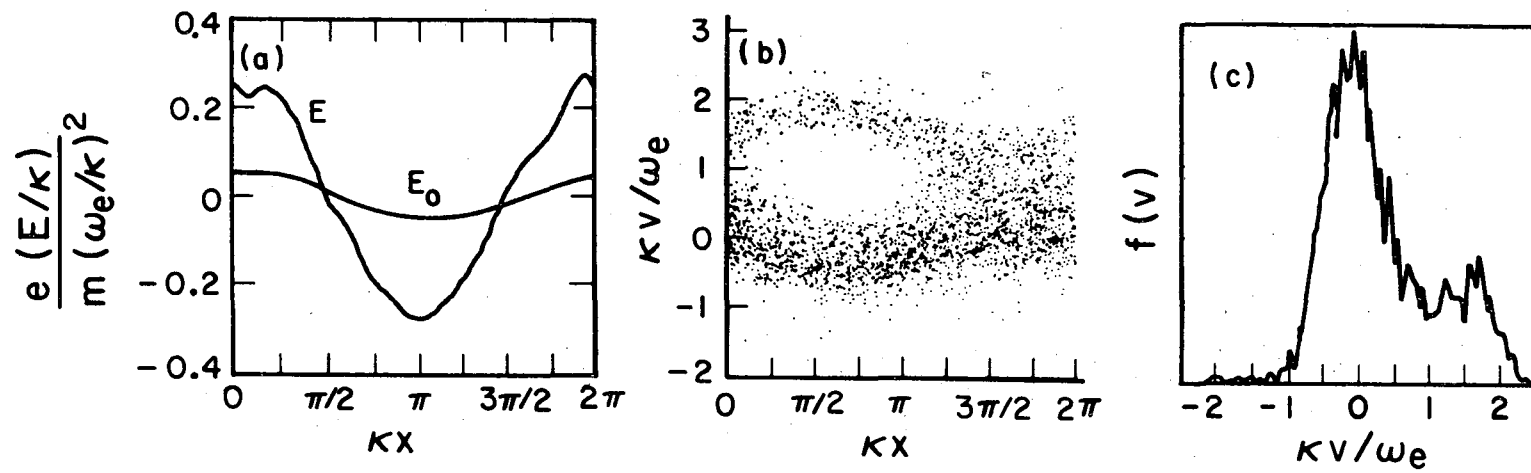
XBL 759-4139

Fig. 15



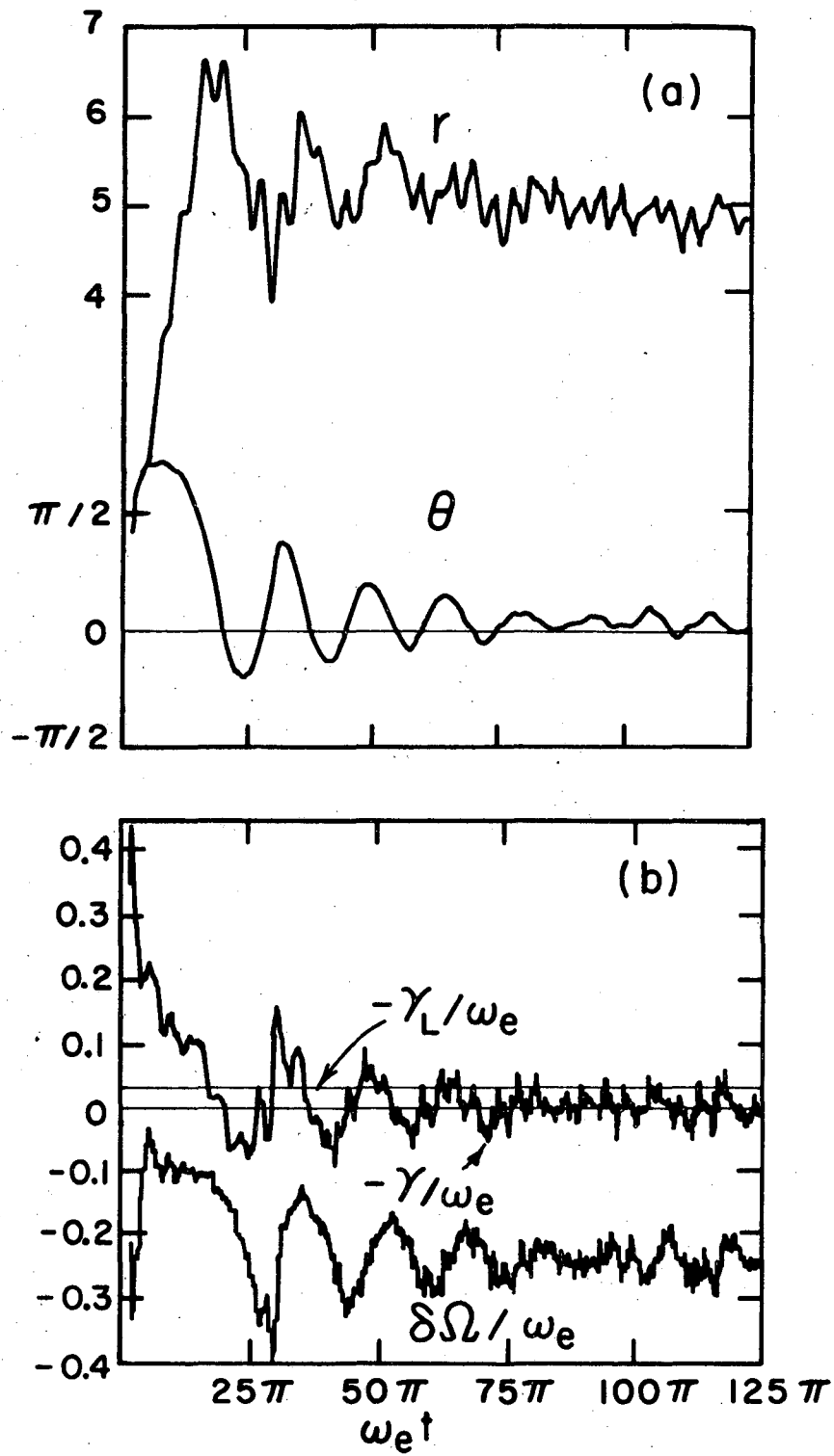
XBL 759 - 3977

Fig. 16



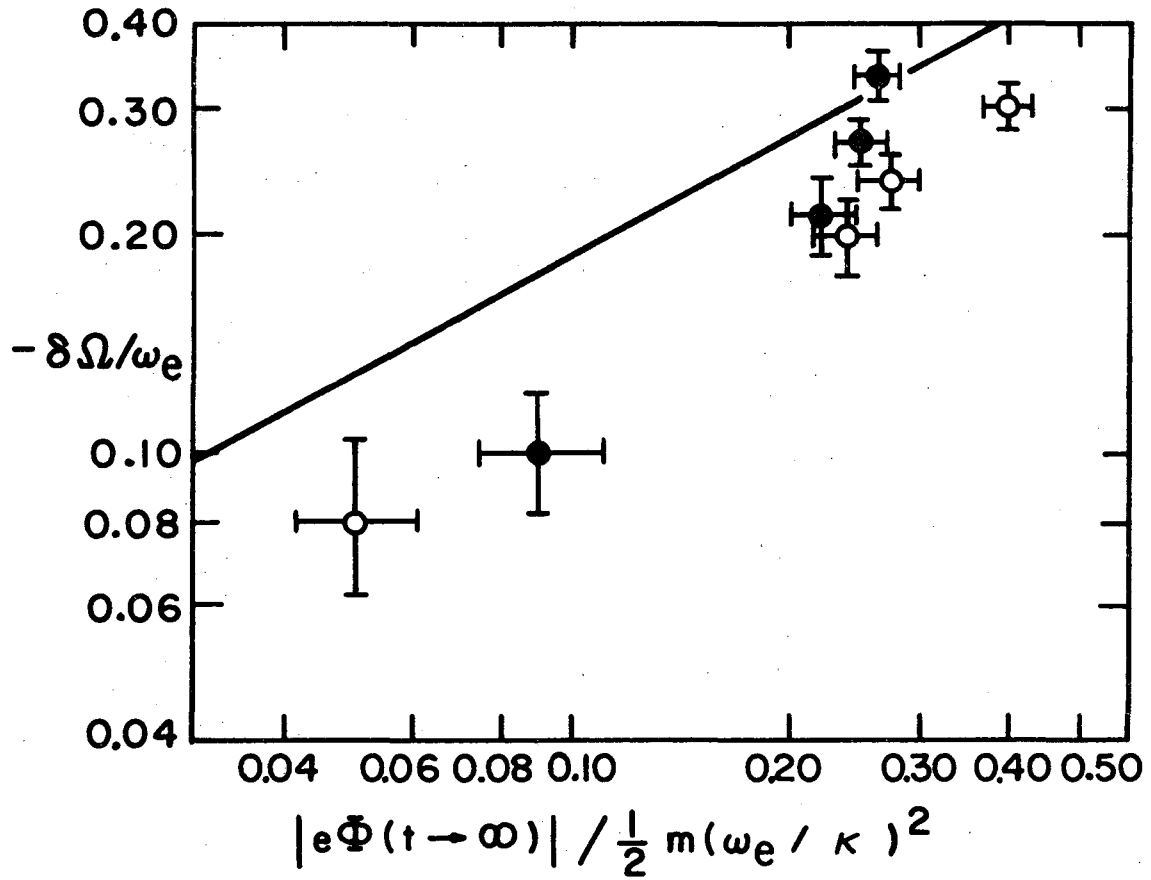
XBL753-2588

Fig. 17



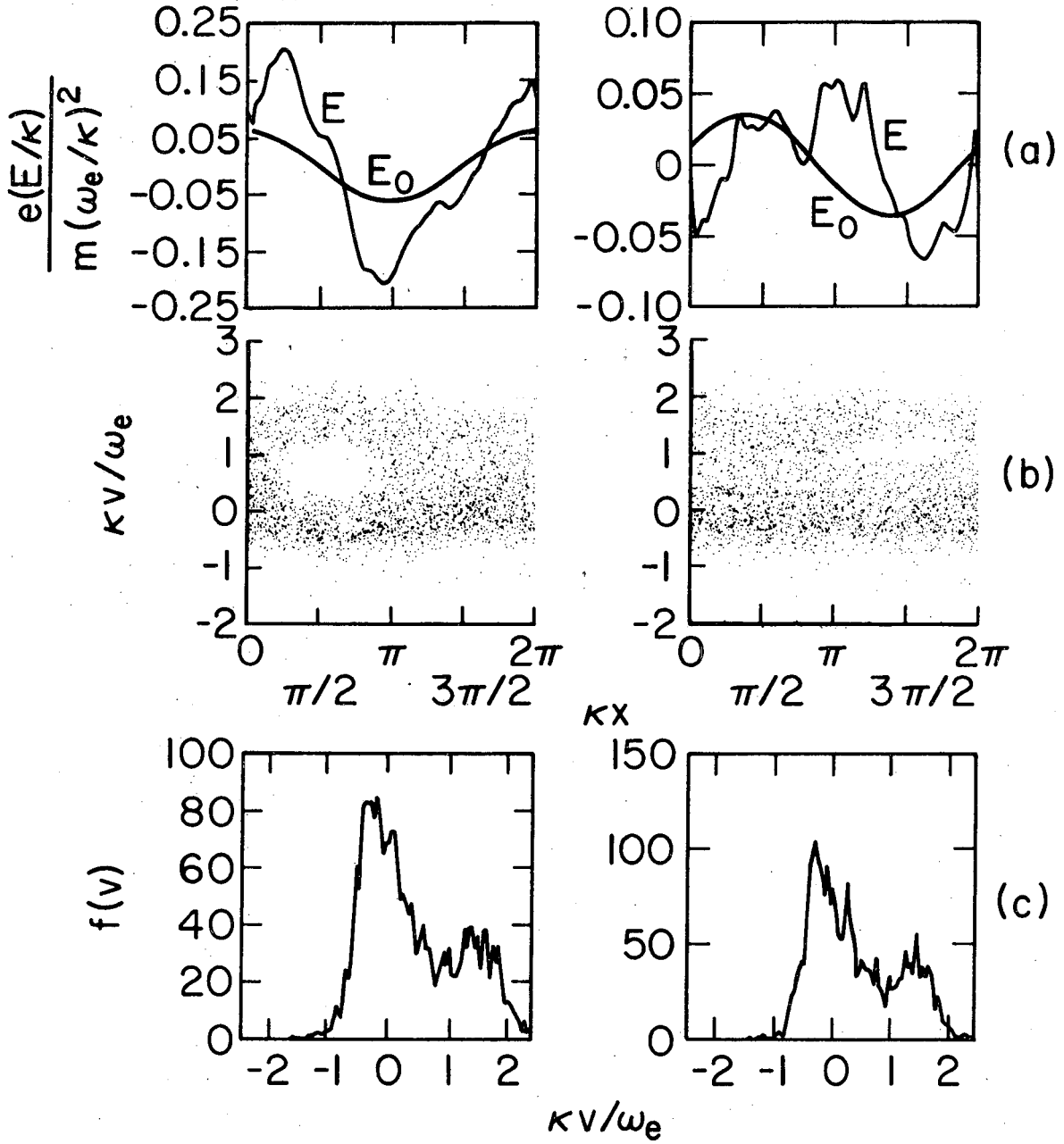
XBL753-2587

Fig. 18



XBL753-2589

Fig. 19



XBL 759-3965

Fig. 20

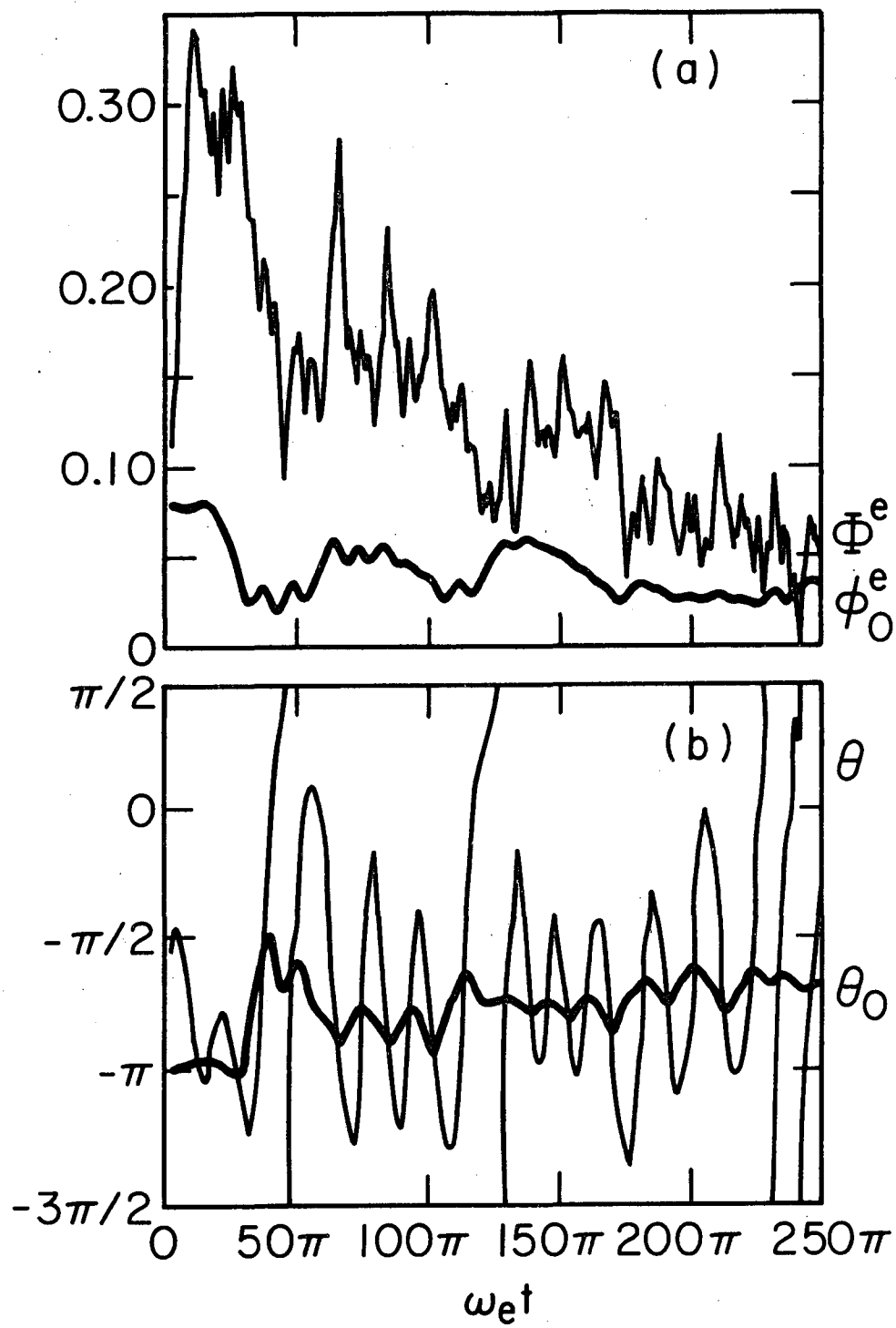
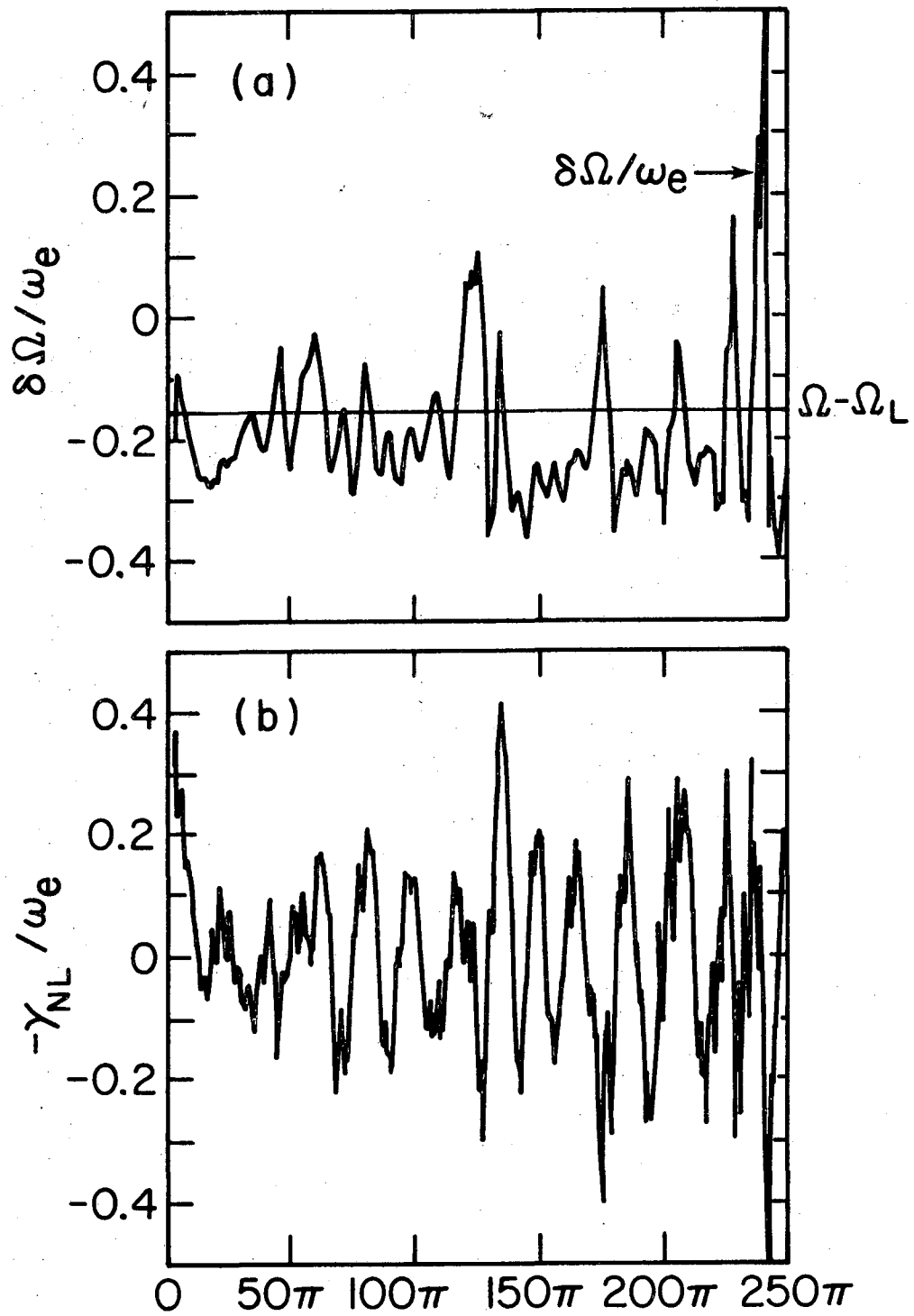
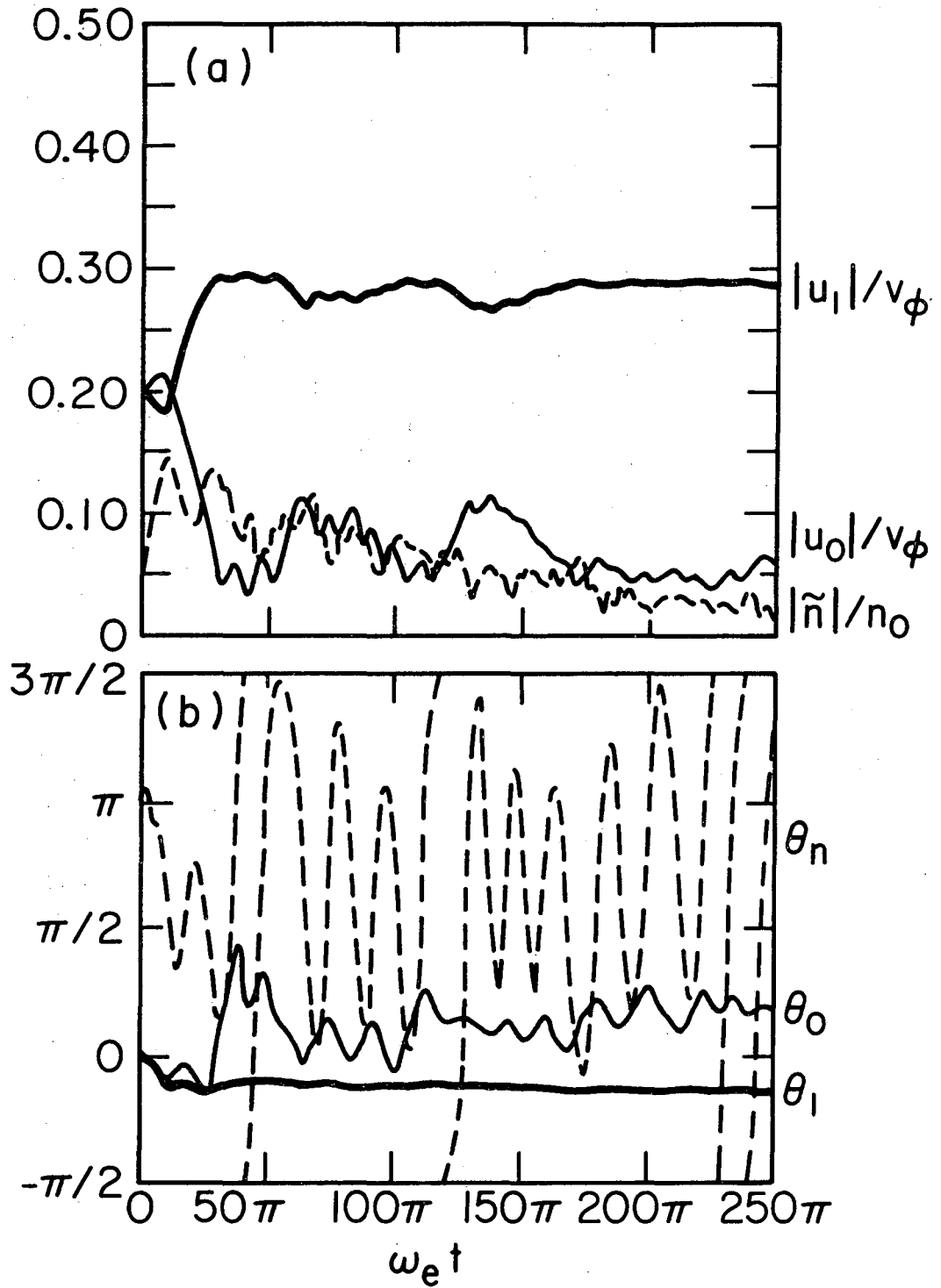


Fig. 21



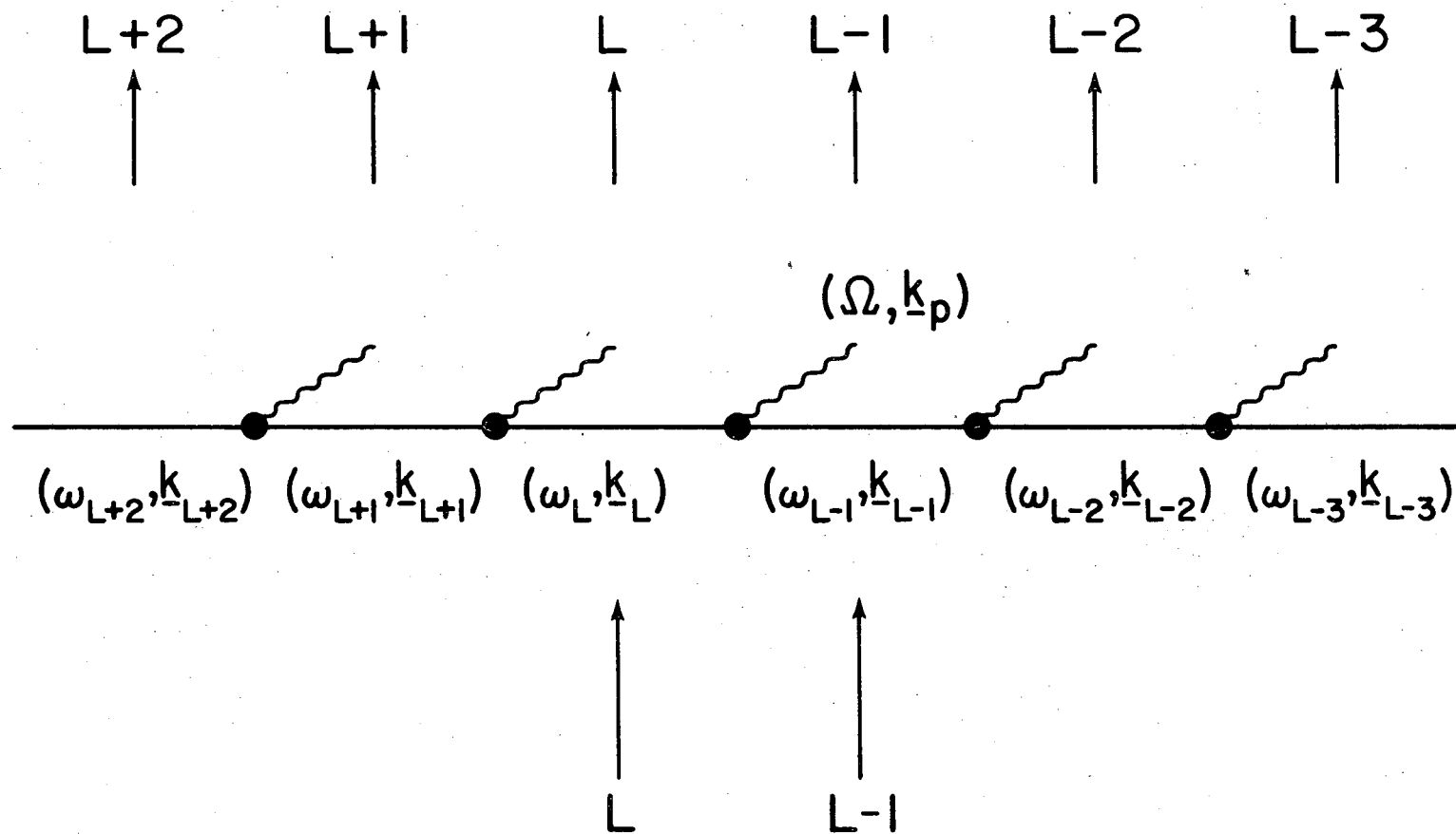
XBL759-3978

Fig. 22



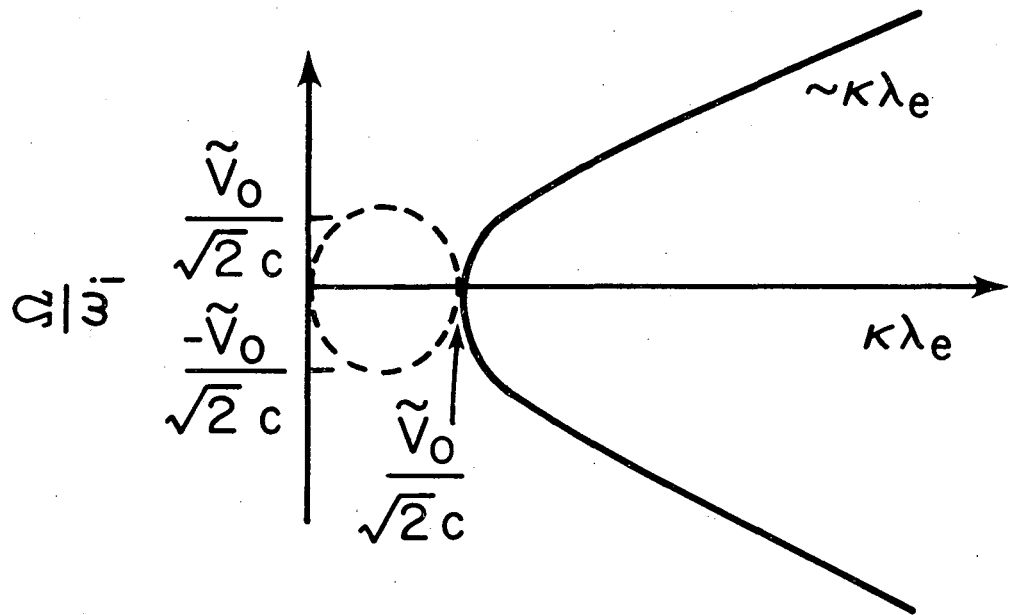
XBL 759-3976

Fig. 23



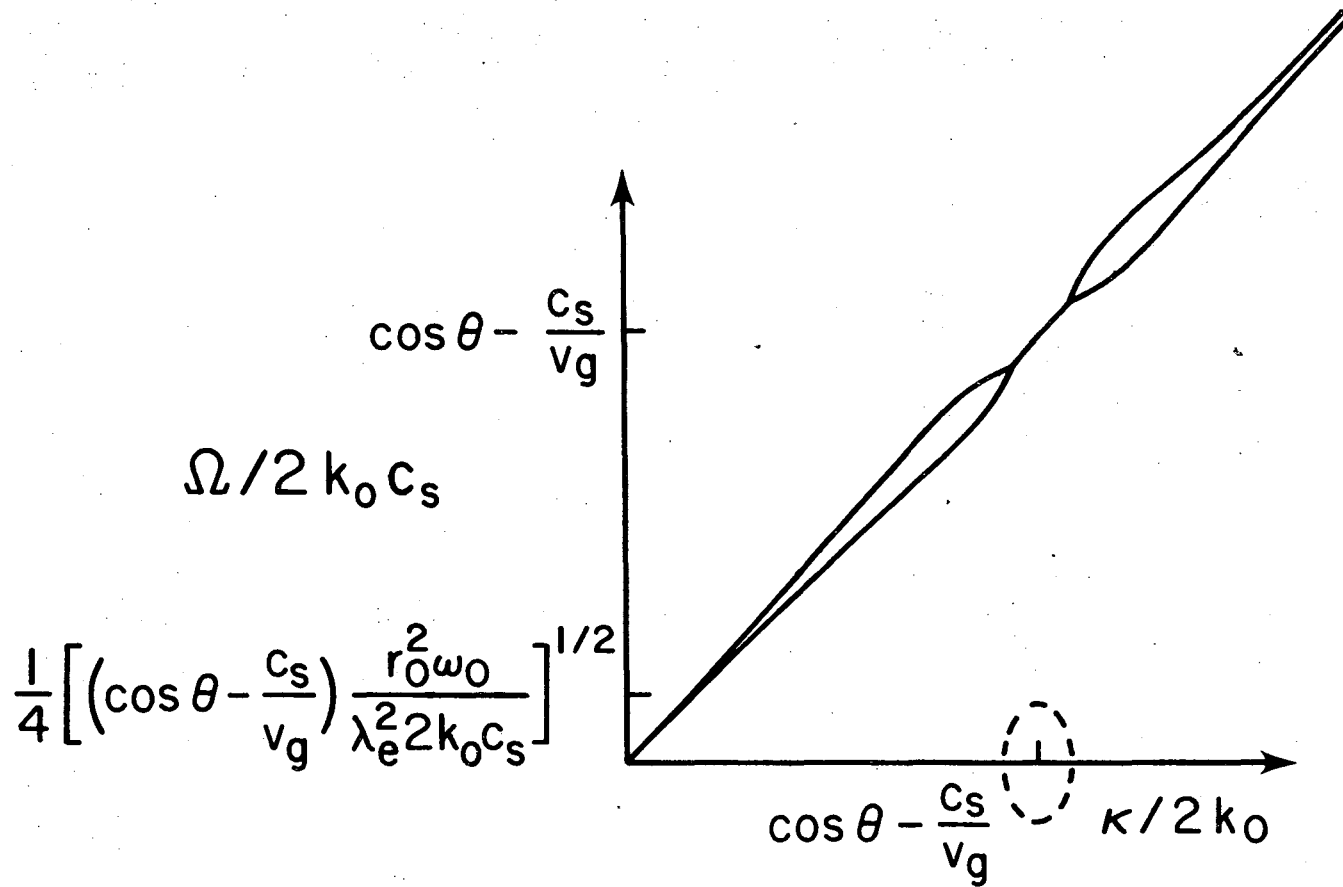
XBL 759-3975

Fig. 24



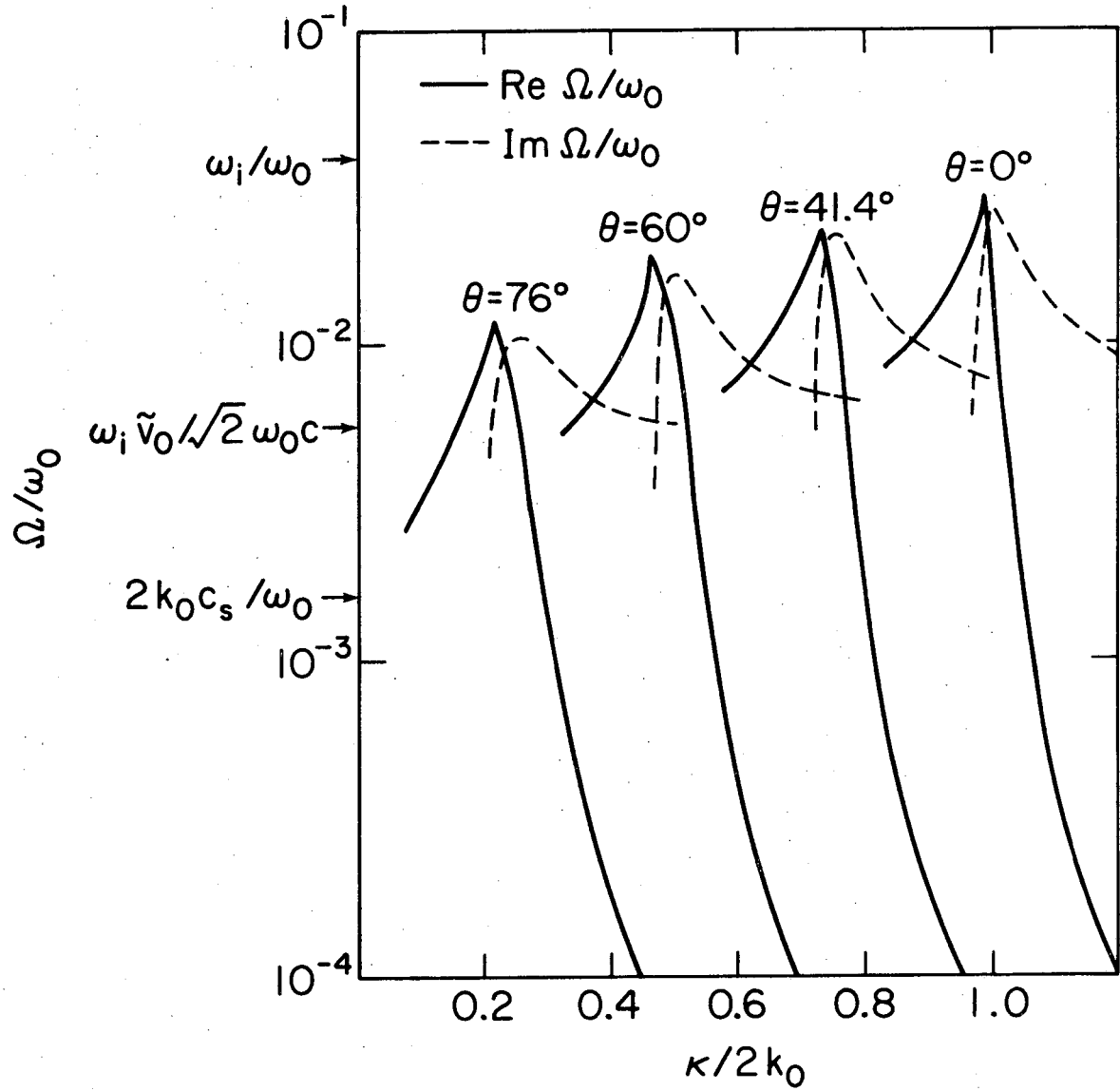
XBL 759-3974

Fig. 25



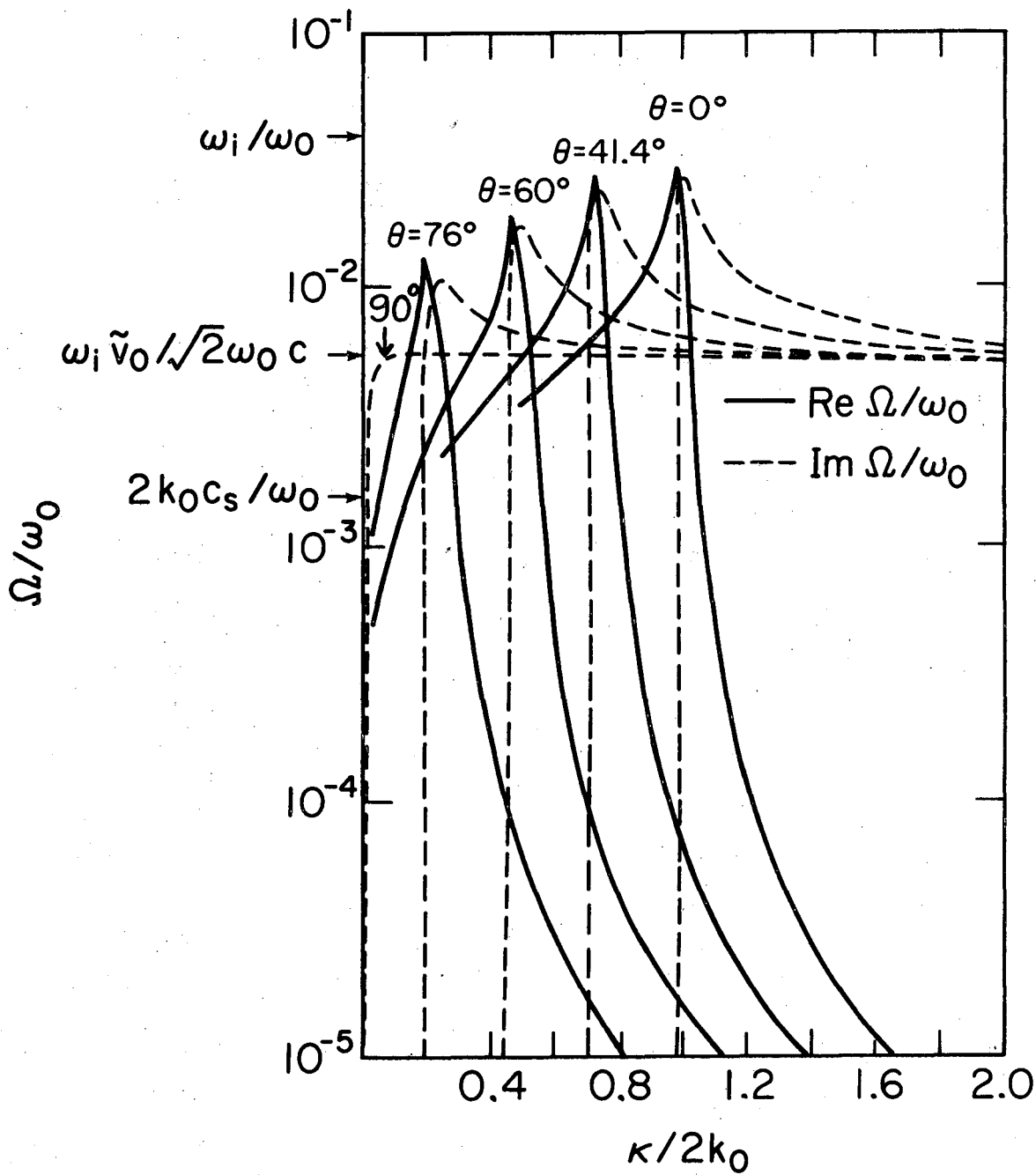
XBL 759-3973

Fig. 26



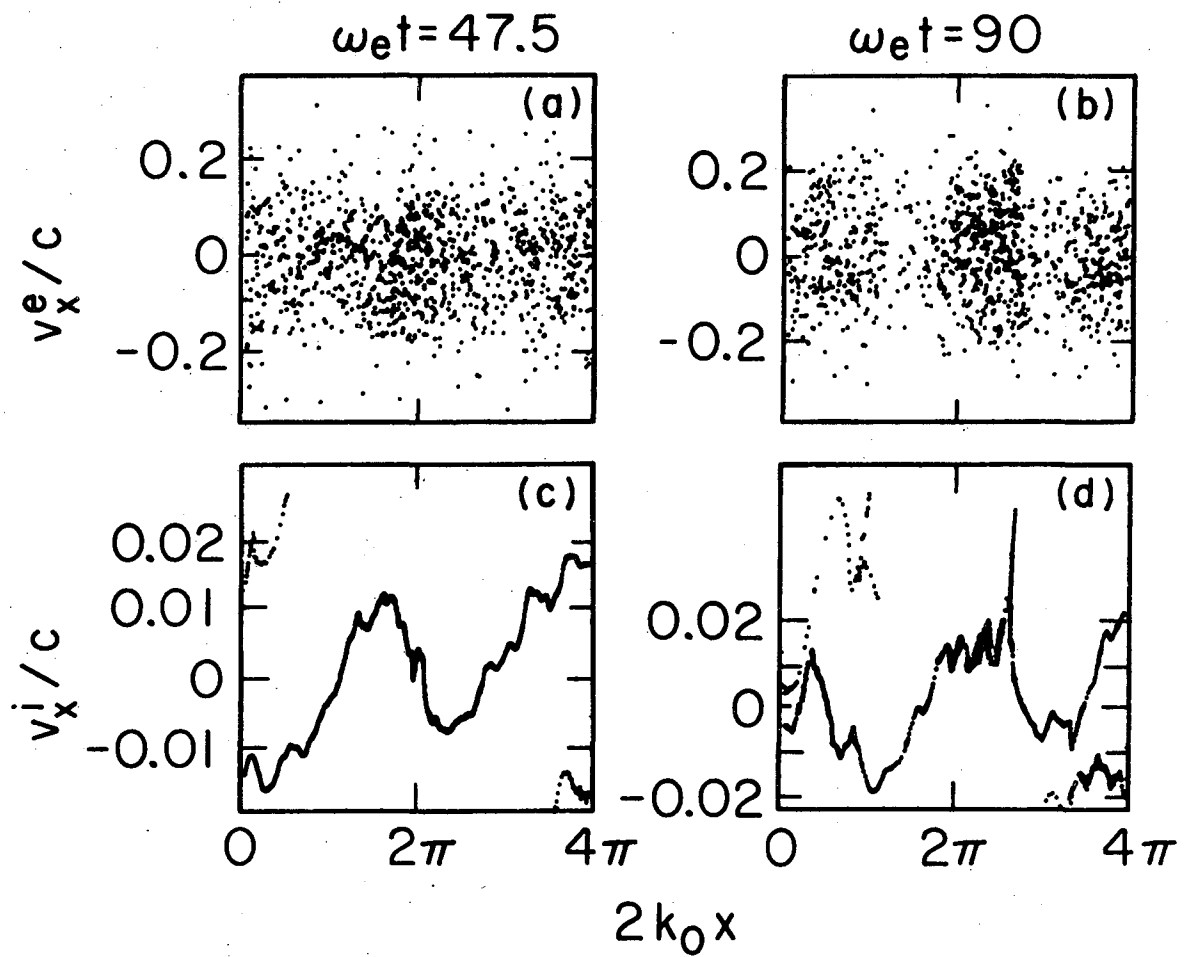
XBL759-3972

Fig. 27(a)



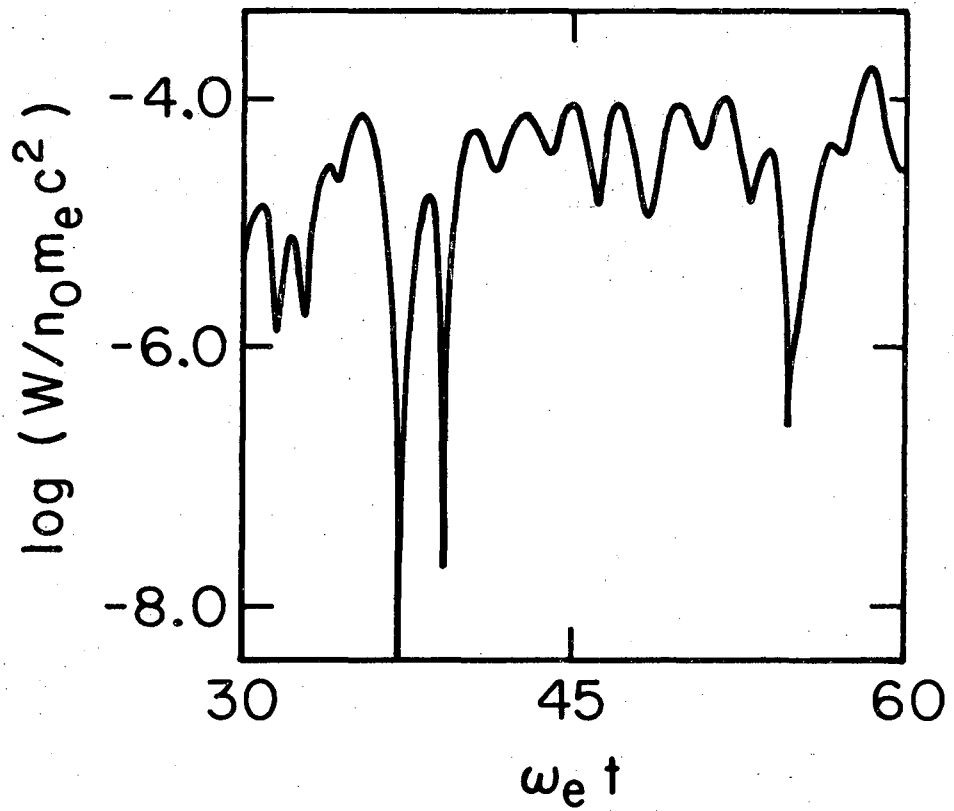
XBL 759-3971

Fig. 27(b)



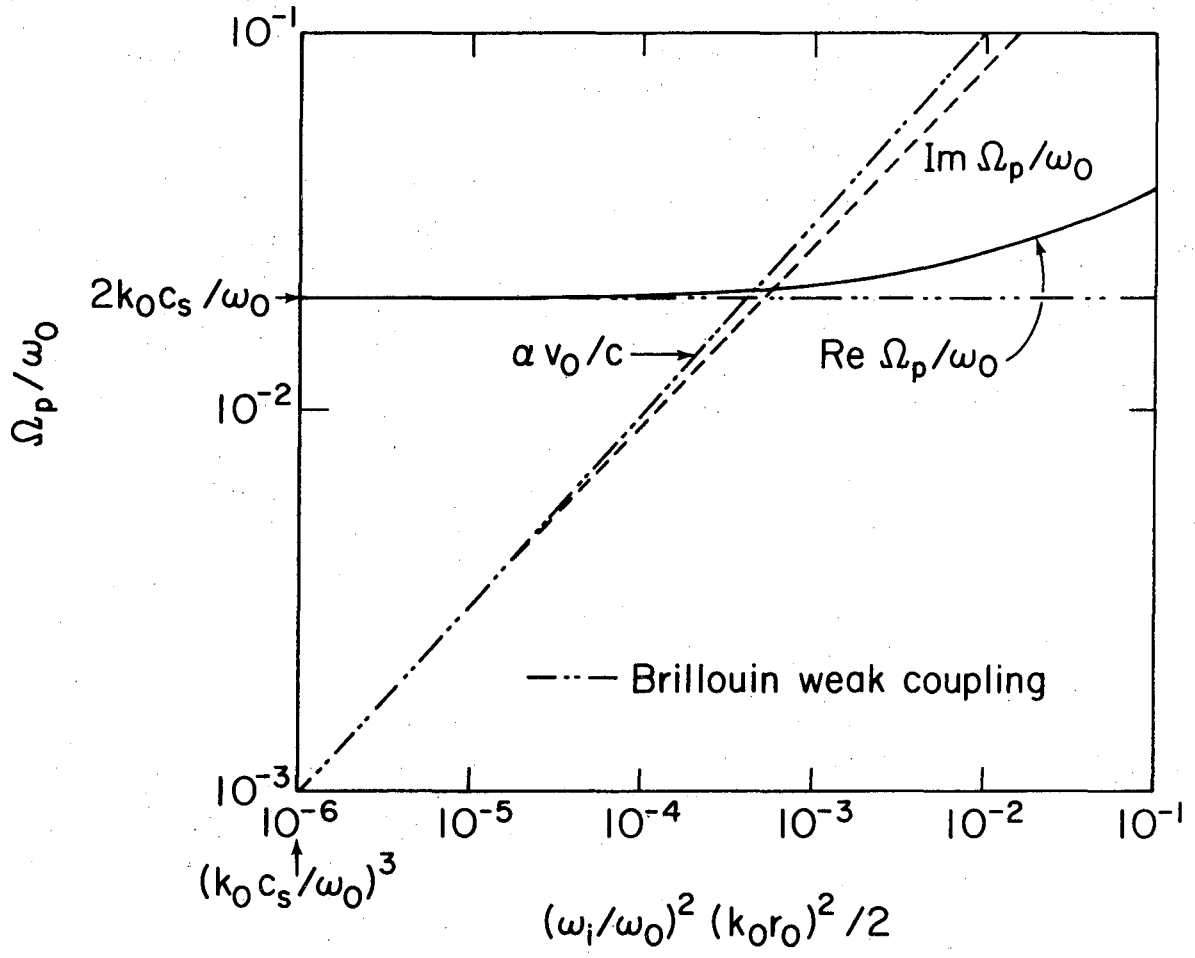
XBL 759-3970

Fig. 28



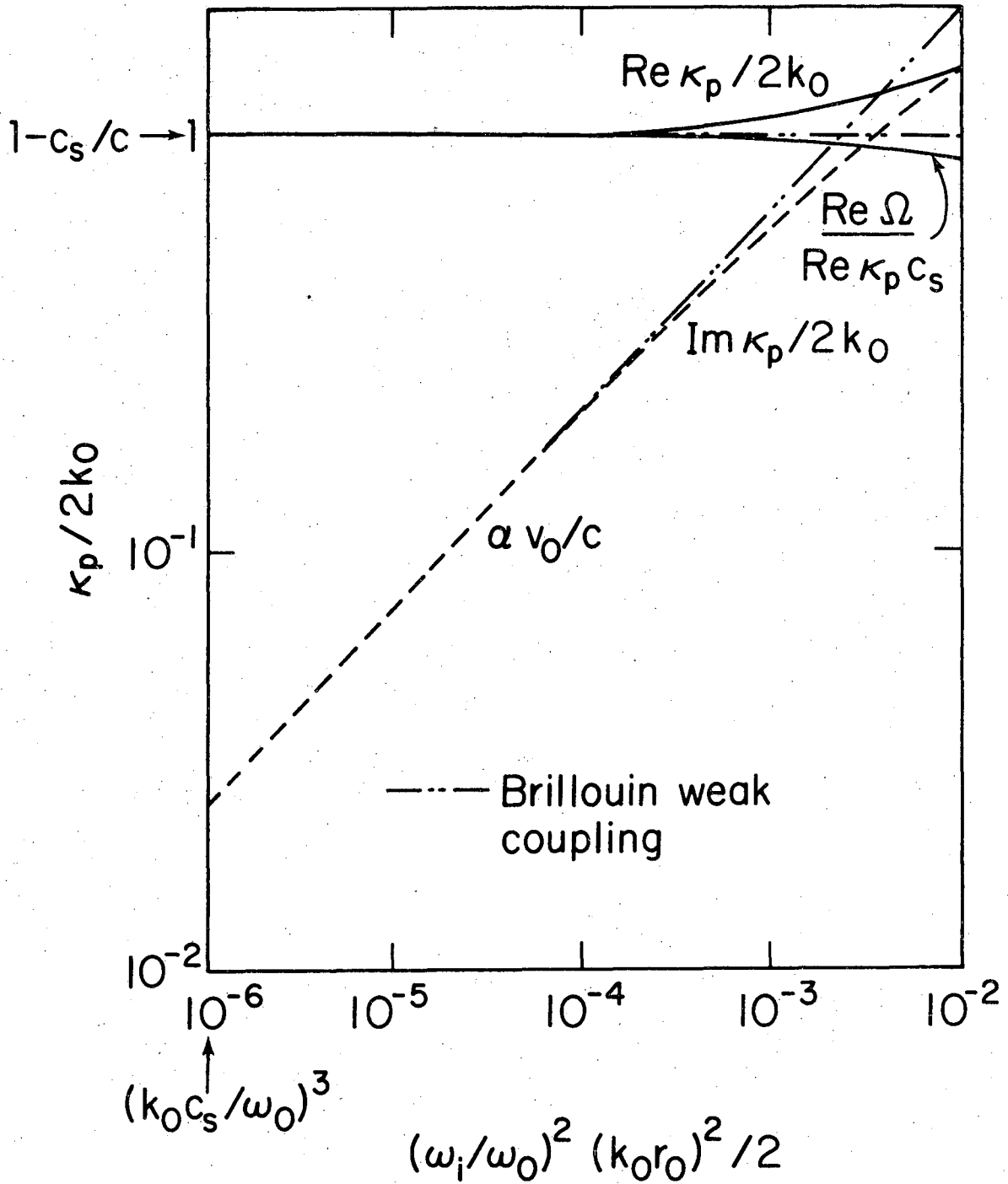
XBL 759-3969

Fig. 29



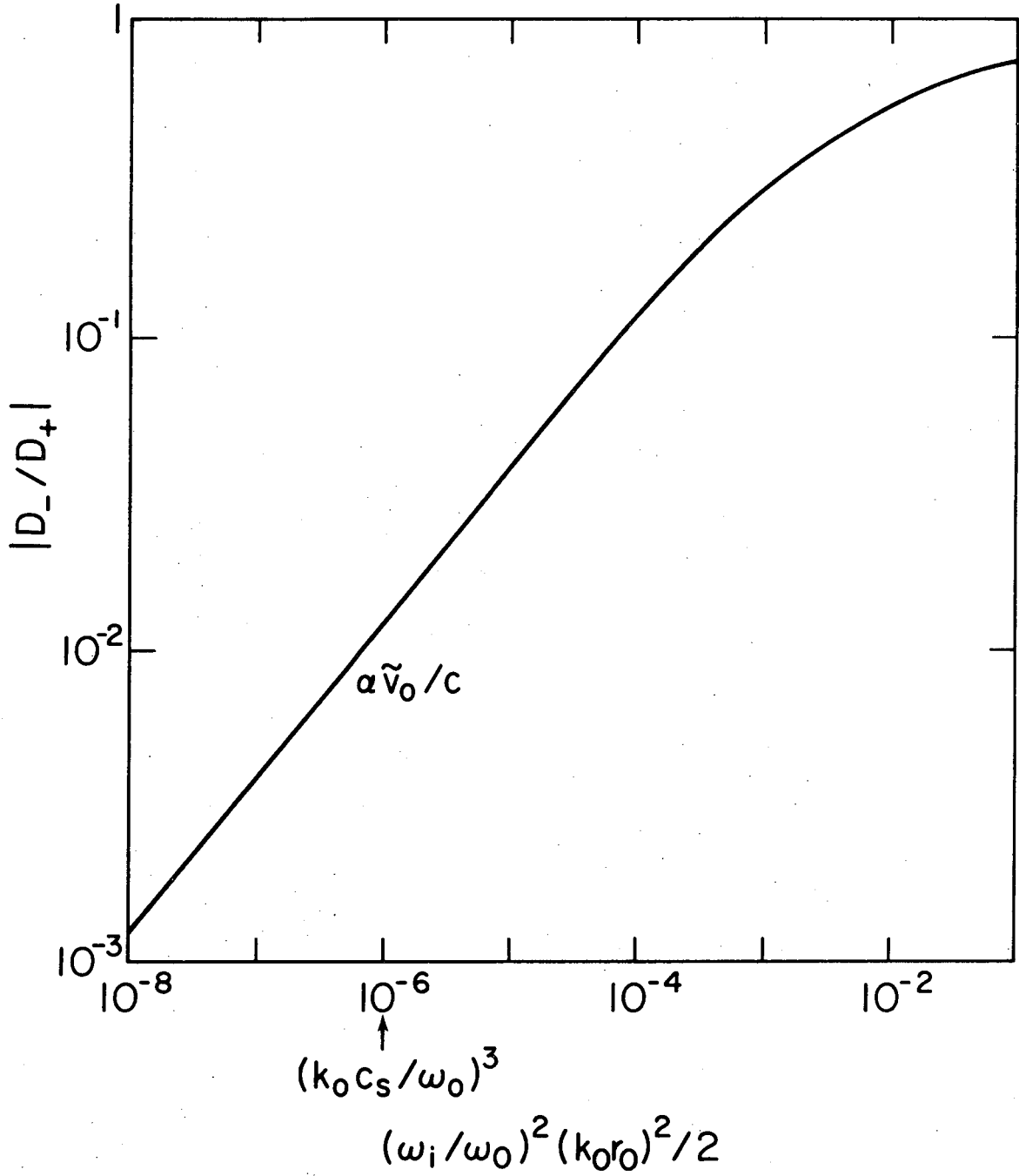
XBL 759-3968

Fig. 30



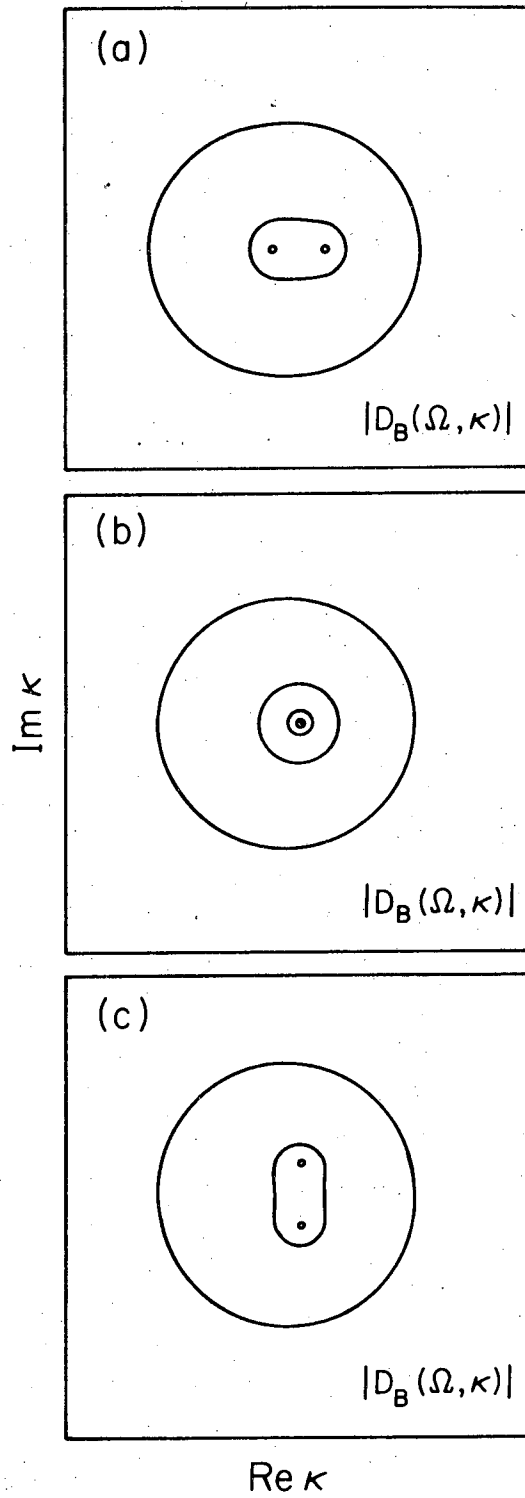
XBL 759-3967

Fig. 31



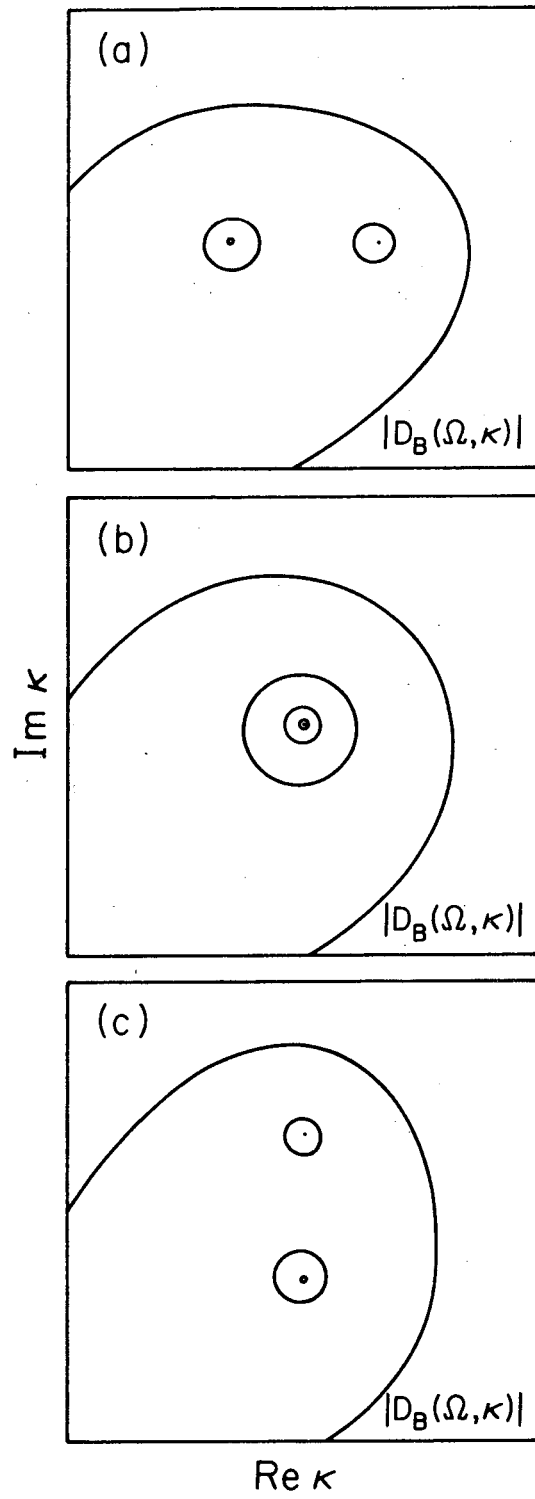
XBL 759-3966

Fig. 32



XBL 759-3962

Fig. 33



XBL 759-3961

Fig. 34

—LEGAL NOTICE—

This report was prepared as an account of work sponsored by the United States Government. Neither the United States nor the United States Energy Research and Development Administration, nor any of their employees, nor any of their contractors, subcontractors, or their employees, makes any warranty, express or implied, or assumes any legal liability or responsibility for the accuracy, completeness or usefulness of any information, apparatus, product or process disclosed, or represents that its use would not infringe privately owned rights.

TECHNICAL INFORMATION DIVISION
LAWRENCE BERKELEY LABORATORY
UNIVERSITY OF CALIFORNIA
BERKELEY, CALIFORNIA 94720